ABSTRACT

Title of Document: ON THE CYCLOPOLYMERIZATION OF 1,6-HEPTADIENES, AND THEIR ROLE AS POLY(METHYLENECYCLOALKANE)S IN STEREOENGINEERING AND BLOCK COPOLYMERS

Kaitlyn E. Crawford, Doctor of Philosophy, 2015

Directed By: Professor Lawrence R. Sita
Department of Chemistry and Biochemistry

The research presented herein, addresses key issues of homogeneous Group 4 single-site coordination polymerization (CP) catalysts for the production of polyolefins and polyolefin-like materials. Specifically, this research moves beyond the 'one-catalyst one-material' paradigm to afford an array of amorphous polyolefin materials with high T_g from a single monomer. The multitude of microstructurally distinct materials available from a single starting olefin is attributed to stereoengineering: a technique, which reduces stereoblock length in a highly controlled fashion while retaining regioselectivity. The precatalysts employed in this work are previously reported Group 4 C_S-symmetric or C_1-symmetric pentamethylmonocyclopentadienyl amidinate complexes with the general formula $\{(\eta^5\text{-}C_5R_5)M[N(R^1)C(R^2)N(R^3)]\text{-}(Me_2)\}$ (M = Zr, Hf, R = alkyl, Me = methyl), which are activated by cocatalysts such as N,N-dimethylanilinium

tetrakis(pentafluorophenyl)-borate ([$PhNMe_2H$][$B(C_6F_5)_4$]). Living CP of 1,6-heptadiene and stereoengineering of the subsequent poly(methylenecycloalkane)s with the above complexes reveal a variety of stereochemically controlled, yet amorphous, poly(methylene-1,3-cyclohexane) (PMCH) materials with T_g values as high as 101 °C. Similar polymerization techniques have been applied, for the first time with Sita group complexes, towards the CP of the heteroatom-olefins such as diallyldimethylsilane (DAS). The controlled CP and stereoengineering of DAS resulted in amorphous poly(3,5-methylene-1,1-dimethyl-1-silacyclohexane) materials with T_g values as high as 127 °C. The living character and tunable stereoblock lengths of PMCH provided the opportunity to explore the high T_g polyolefin as the 'hard' domain (A segment) in pure polyolefin AB block copolymers, BCPs. Specifically, amorphous AB diblock copolymers were synthesized using poly(1-hexene) as the 'soft' B block to afford a series of microphase-separated morphologies without the deleterious effects of crystallization. Microphase-separated morphologies for were also observed for ABA triblock copolymers using atactic polypropylene as the 'soft' segment (B block) and primary component. The latter BCPs were found to exhibit thermoplastic elastomeric properties. The work described in this document provides a foundation for the further expansion of the currently-limited pool of monomers to include heteroatom-olefins for CP with the aforementioned Group 4 transition metal complexes. Moreover, the formation of well-defined pure polyolefin block copolymers serve as an important contribution to the development of new polyolefin architectures.

ON THE CYCLOPOLYMERIZATION OF 1,6-HEPTADIENES, AND THEIR ROLE AS POLY(METHYLENECYCLOALKANE)S IN STEREOENGINEERING AND BLOCK COPOLYMERS

By

Kaitlyn E. Crawford

Thesis submitted to the Faculty of the Graduate School of the
University of Maryland, College Park, in partial fulfillment
of the requirements for the degree of
Doctor of Philosophy
2015

Advisory Committee:
Lawrence R. Sita, Chair
Philip DeShong
Robert Briber
Efrain Rodriguez
Zhihong Nie

Acknowledgements

I would like to express my utmost appreciation to my advisor Professor Lawrence R. Sita for his tremendous support and mentorship over the past four years. I would like to thank him for encouraging my research and allowing me to grow as a scientific researcher.

I would also like to thank my committee members and faculty of the department of Chemistry and Biochemistry at the University of Maryland. Specifically, I would like to express my gratitude for the guidance graciously provided to me by Professors Philip DeShong, Jeffrey Davis, Robert Briber, Efrain Rodriguez, Zhihong Nie, and Mohamad Al-Sheikhly.

The Sita group members, both past and present, have made this endeavor enjoyable. The fruitful discussions, collaborations and friendship will be forever remembered. Specifically, I would like to acknowledge Dr. Brenden Yonke, Dr. Jia Wei, Dr. Jonathan Reeds, Dr. Catherine Blakley, Wonsoek Hwang, Wesley Farrell, Andrew Keane, Tessy Thomas, Kerry DeMella, Kyle Reddick, Samantha Nowak, Leila Dunham, and Katie Pohinda. I would like to extend a special thanks to Kyle Augustine for the opportunity for me to provide research mentorship during his undergraduate studies.

Finally, to my family and friends, you have been the string that has held everything together. You have been there from the beginning with unwavering support and encouragement. Thank you for always being there. I would like to especially acknowledge my husband Kausik, my parents Kevin and Alicia, my

siblings Phillip, Emily, Oliver and Marjorie, and my dearest of friends Anna Sberegaeva and Travis Johnson.

Table of Contents

List of Tables

List of Figures

List of Schemes

List of Abbreviations

ADMET: Acyclic Diene Metathesis Electron Transfer
AFM: Atomic Force Microscopy
Chi (X): Flory's interaction parameter
DAF: Diallylfluorene
DAS: Diallyldimethylsilane
DSC: Differential Scanning Calorimetry
GC: Gas Chromatography
HT-SEC: High Temperature-Size Exclusion Chromatography
LCP: Living Coordination Polymerization
M_n: Number average molecular weight
M_w: Weight average molecular weight
MAO: Methylaluminoxane
MMAO: Modified methylaluminoxane
MPS: Diallylmethylphenylsilane
N: Degree of polymerization
NaK: Sodium/ potassium amalgam
NMR: Nuclear Magnetic Resonance
PDI ($Đ$): Polydisperisty
PhCl: Chlorobenzene
PMCH: Poly(methylene-1,3-cyclohexane)
PMCO: Poly(methylene-1,3-cyclooctane)
PMCP: Poly(methylene-1,3-cyclopentane)
TEM: Transmission Electron Microscopy
TGA: Thermal Gravimetric Analysis
THF: Tetrahydrofuran
SAXS: Small Angle X-ray Scattering
SEC: Size Exclusion Chromatography
WAXD: Wide Angle X-ray Diffraction

Chapter 1

Introduction

1.1. Focus

Sita catalysts were applied for the cyclopolymerization of various non-conjugated dienes. Select non-conjugated dienes that were found to be successful for living polymerization were further utilized as a designated block segment for the preliminary study of phase separation in polyolefin block copolymers. The subsequent Chapters discuss the results of this work in parallel with an introduction to specific topics and literature that are relevant to the research work. While each of the chapters focus on a specific challenges, an overall commonality is the use of 1,6-heptadiene (1,6-HD). This monomer was found to be the most successful of the various non-conjugated dienes investigated for living cyclopolymerization *via* Sita catalysts and will be discussed as: a homopolymer (Chapter 2), substituted non-conjugated dienes (Chapter 3), a homopolymer under the influence of degenerative methyl group transfer polymerization (Chapter 4), a diblock copolymer with poly(1-hexene) (Chapter 5), and as the A-segment in an ABA triblock copolymer with polypropylene as the mid-segment for potential use as a thermoplastic elastomer (Chapter 6). Chapter 1 of this report encompasses a brief history of coordination polymerization, an introduction on the origin of regio- and stereo-selectivity with single-site catalysts as it is understood today, cyclopolymerization, Sita catalysts, degenerative methyl group transfer using Sita catalysts, and block copolymers.

1.2. Initial Breakthrough

The lives of mankind have been changed forever by the development of plastic. In particular, the development and subsequent commercialization of polyolefins have revolutionized nearly every industrial process known. Polyolefins play a key role in myriad applications ranging from manufacturing and automobile industries, to their use in consumer goods such as appliances, hardware, packaging, containers, protective coatings etc. To date, the two most important polyolefins are polyethylene (PE) and polypropylene (PP) with annual consumption expected to reach nearly 170 million tons by 2018.[1]

The most common method of olefin polymerization is through transition metal-mediated coordination polymerization (CP). The term was first described in 1956 by the Dow Chemical Co.[2, 3] based on the original work seen a few years earlier by Karl Ziegler[4, 5] and Giulio Natta.[6] In this regard, Ziegler was the first to successfully polymerize low-density polyethylene (LDPE) using the heterogeneous complex $TiCl_4/AlEt_3$ (where Et = ethyl).[4] Shortly thereafter, Natta employed $TiCl_3/AlEt_3$ for the first ever polymerization of crystalline PP.[6, 7] Zeigler-Natta (ZN) catalysts are still the most common method of olefin polymerization used by industry today, and are considered one of the most important achievements in advancement of polymer technology.[3] The mechanism by which ZN polymerization occurs has not been well understood for a long time due to the limited methods of mechanistic analysis available for heterogeneous catalysts. To date, the most widely accepted mechanism for ZN polymerization, proposed by Arlman[8] and Cossee[9], involves two steps. The first is coordination of an olefin monomer to an active metal-site. The

second is migratory insertion through the formation of a four-membered ring with the polymer chain (tethered to the metal center), the coordinated monomer, and the active metal center. The proposed mechanism presented by Arlman and Cossee has been redrawn in Scheme 1.1.

Scheme 1.1: Heterogeneous CP mechanism proposed by Arlman and Cossee.[8, 10]

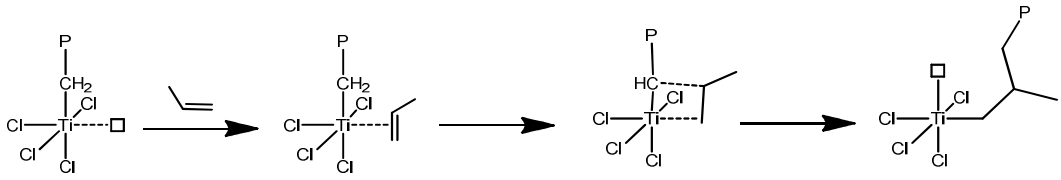

Monomers such as propene are prochiral resulting in stereogenic centers throughout the polymer backbone, *vide infara*. Depending on the direction of insertion, the pendant alkyl group will either be on the same side as the previous pendant group or on the opposite side. The mechanism of polymerization, and environmental conditions such as solvent and temperature play a key role in stereoselectivity during olefin polymerization. Small fluctuations in the stereoregularity of a polyolefin greatly influence the bulk properties of the material. For example, PP that is highly stereoregular is a hard, crystalline material with a high melting temperature (ca. 165 °C); whereas PP that is highly stereoirregular is a soft, amorphous material with limited use in industrial applications. It was determined that if the olefin polymerization mechanism can be better understood, then steps can be taken to more easily control the stereoselectivity of a given polymerization system. One method to better understand how stereoselectivity occurs is through the use of homogeneous single-site catalysts.

1.3. Metallocene Precatalysts

A metallocene is a bis(cyclopentadienyl) (Cp) organometallic complex with the formula Cp_2MX_2 (where M = transition metal and X = ligand). In general, the neutral transition metal complex (in this example Cp_2MX_2) is commonly referred to as the precatalyst, which becomes active for polymerization after the introduction of a cocatalyst such as a boron or aluminum based main group metal alkyl. The first homogeneous, single-site metallocene catalysts (where M = Ti, Zr or Hf and X = Cl or alkyl) were discovered by Natta and Breslow in 1957.[11] Unfortunately, these complexes have poor activity in the presence of triethylaluminum ($AlEt_3$; the most well-known cocatalyst at the time) for the polymerization of ethene. Further, the complex did not show any activity for the polymerization of propene. A major breakthrough for improved activity came in the late 1970s when the use of partially hydrolyzed AlR_3 cocatalysts (primarily methylaluminoxane; MAO) greatly improved the activity of ethylene polymerization and showed some activity towards propene.[12] Although MAO is still the most predominant cocatalyst used today for olefin polymerization, the mechanism by which MAO activates the precatalyst is still under debate.[44f] However, it generally agreed that the Lewis acidic MAO abstracts the chlorides from the precatalyst, replaces them with alkyls and then further removes an alkyl to give a cationic active species, Scheme 1.2. Stereocontrol is not observed under these conditions, except minimally under cold conditions ($\leq$ -45 °C).[13]

Scheme 1.2: Activation of metallocene precatalysts with MAO.

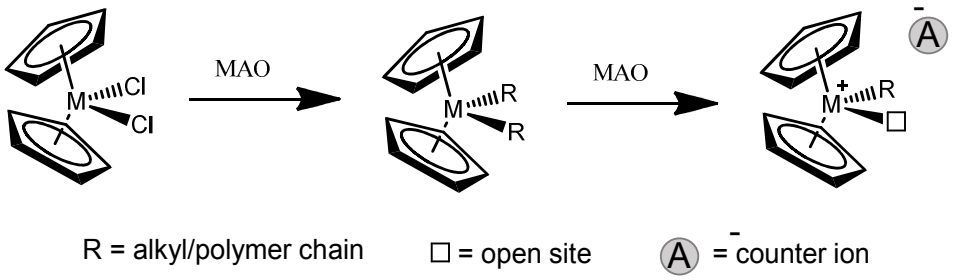

The revolution in terms of understanding the mechanisms of stereochemical control came with the discovery of bridged metallocene precatalysts (*ansa*-catalysts) first presented by Kaminsky[14, 15] and Brintzinger,[16] which restricted the otherwise facile Cp ligand rotation. Introducing rigidity to the single-site CP catalyst by forming a bridge between the two Cp rings (or Cp like substituents) has provided great insight into how the metal-ligand geometry effects the tactic nature of the polymer chains.[15] Common bridging groups are $SiMe_2$ and short chain alkyls.[17] Since their original discovery in the early 1980s, *ansa*-metallocene-based complexes have been reported by many for the successful polymerization of olefins with varying degrees of activity and stereoselectivity.[18]

1.4. Mechanism of Chain Propagation

There are two general steps involved in the single-site CP polymerization mechanism of α-olefins with an active, cationic initiator. The first is coordination of the monomer to the open coordination site on the metal center. The second is 1,2-migratory insertion of the pi-bond through the formation of a 4-membered cyclic ring. Although the initiator is referred to as single-site owing to only one polymer chain per metal center, the mechanism by which propagation occurs is considered a two-site

system because the location of the active-site and the growing polymer chain interconvert their positions as a result of the 1,2-migratory insertion step, Scheme 1.3. The mechanism proposed in Scheme 1.3 matches closely to the mechanism proposed by Cossee for heterogeneous CP.[10]

Scheme 1.3: General mechanism for CP polymerization.

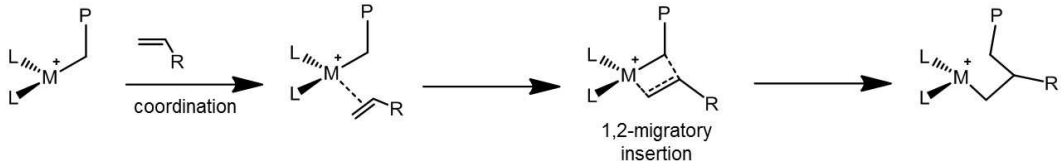

There two additional proposed mechanisms for olefin CP that are worth mentioning: 1) the modified Green-Rooney and 2) the transition state agnostic mechanisms;[44f] both are similar in coordination and insertion to the Cossee mechanism but include also agostic interactions, Scheme 1.4. All three mechanisms proposed for early transition metal single-site initiators have been deemed reasonable, and experimental and computational experiments have shown evidence supporting propagation both with and without agostic interactions as a function of initiator type and environmental conditions. The specific mechanism is not always known for a given system but it is agreed that even small changes in environmental conditions and to catalyst design influence polymerization.[19]

Scheme 1.4: General mechanism for CP polymerization with agostic interactions.

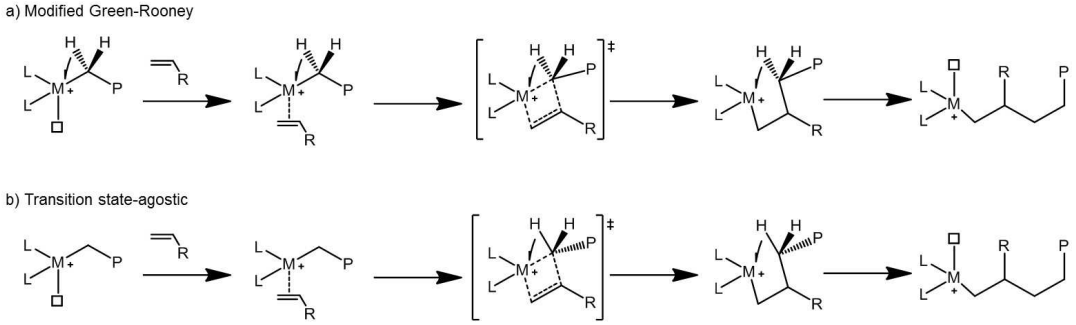

Irregular 2,1-migratory insertion, as opposed to traditional 1,2-insertion, is also possible but occurs to a much lesser extent for early transition metal complexes, often due to sterics. 2,1-migratory insertion is referred to as regioirregular insertion whereas 1,2-insertion is referred to as regioregular. The rate of insertion for a new monomer following a 2,1-misinsertion is much slower compared to the rate for consecutive regioregular insertions. Further, if a 2,1-misinsertion does occur, then isomerization of the last inserted monomer may also occur, which results in what looks like a 3,1-insertion; a 2,1-misinsertion may also cause polymerization deactivation. Scheme 1.5 provides a visual example of the modes of regioselectivity.

Scheme 1.5: 1,2-insertion vs. 2,1-insertion with 3,1-isomerization.

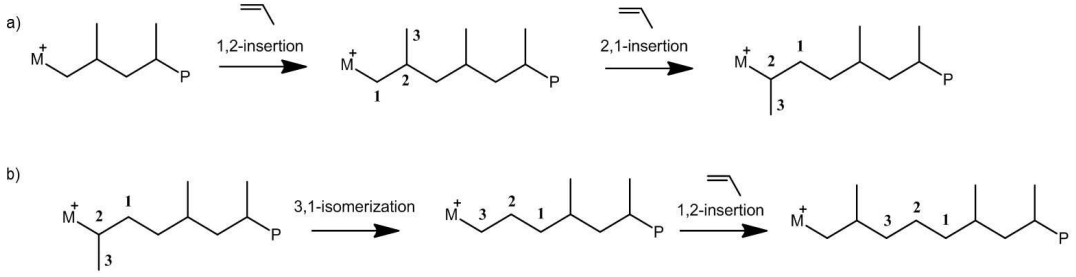

1.5. Stereoselectivity

It was previously stated that propene and higher alkenes are prochiral, that is, following propagation, each repeating unit possesses a chiral center with two possible configurations relative to the adjacent monomer units. If two consecutive monomer units have the same configuration then it is labeled as *meso* or '*m*' for short. On the other hand, if two adjacent monomer units have opposite configuration, then they are referred to as racemic (*rac*), or '*r*'. The degree of stereoselectivity (tacticity) can be determined by examining the number of consecutive *m* configurations. For example, a high percentage of *mmmm* pentads (i.e. five repeating units in a row with the same '*m*' configuration) is highly stereoselective and is denoted as isotactic. There are at least three additional maximum-order microstructures worth noting: Atactic: where the '*m*' and '*r*' configurations are randomly distributed along the polymer backbone. Syndiotactic: where the configuration consistently alternates sides leading to a high percentage of *rrrr* pentads. Hemiisotactic: every other pendant group is on the same side, but the configuration of the middle pendant group can be either on the same side as the adjacent pendant groups or on the opposite side. It is necessary to note that microstructure analysis can generally be evaluated by NMR. Figure 1.1 provides a representation of each of the four types of maximum order microstructure (the four microstructures can be reduced to two primary forms: isotactic and syndiotactic, because atactic and hemiisotactic are technically microstructures that can be found at some point in between isotactic and syndiotactic).

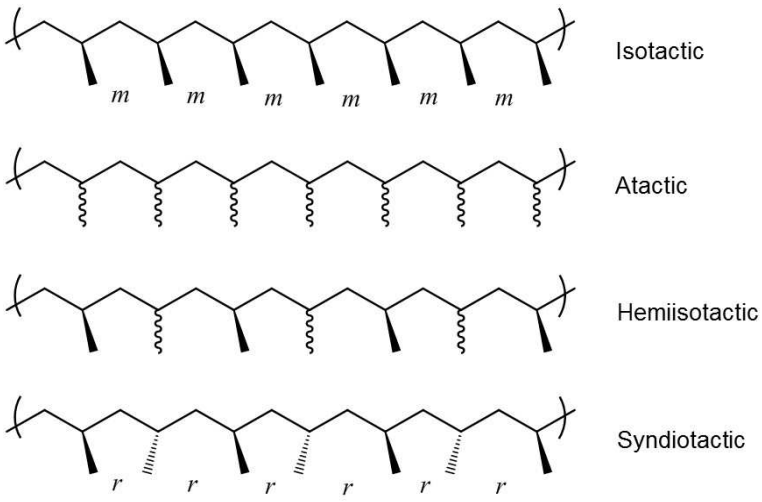

Figure 1.1: Common polypropylene microstructures.

The polymer's microstructure is known to be controlled by one of two ways, chain-end control or enantiomorphic site control. The stereoselectivity for polymerizations that proceed *via* chain-end control are governed by the orientation of the last inserted monomer relative to the ligand framework on the active metal center. Since the stereochemistry of the last inserted monomer directs the orientation of the incoming monomer then any stereoerror that occurs will permanently change the direction of the new incoming monomers until a new stereoerror occurs, that is, if a chain was originally propagating with *re* insertions and a stereoerror occurs (*si* insertion) forming an *r* configuration, then the polymer chain will continue to propagate with *si* insertion until a new stereoerror occurs, Figure 1.2 (bottom). On the other hand, the stereoselectivity for polymerizations that proceed through enantiomorphic site control is dictated by the geometry of the catalyst. Therefore, if enantiomorphic site control is the predominant mechanism for a given polymerization exhibiting isoselectivity, then each stereoerror will give rise to a pentad with a

minimum of two *r* configurations (i.e. *mrrm*). In this regard, when the catalyst geometry directs the face of the incoming monomer the mechanism is self-correcting, Figure 1.2 (top).

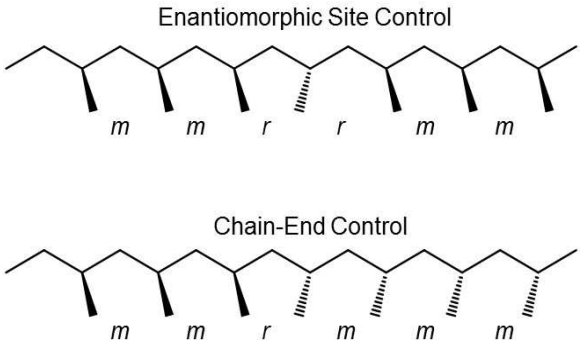

Figure 1.2: Mechanisms of stereocontrol.

When considering propagation through the enantiomorphic site control mechanism there are five general types, or classes, of metal-ligand architectures that are responsible for the stereospecific enchainment (coordination/propagation) of propene and higher α-olefins. Class I and class II with respective C_{2v} and C_s-symmetric geometry both give rise to atactic polymers. Stereoregularity observed with these catalyst geometries are either controlled by chain-end control (monomer dependent) and/or are carried out at extremely low temperatures (≤ -45 °C).[13] In general, class III catalysts with C_2 symmetry result in isotactic polymers.[20] Catalysts with class IV (C_s) geometry are notable for producing syndiotactic polymers.[21] Lastly, C_1-symmetric, class V catalysts can be classified as a 'wild-card' – reproducible predictions for stereocontrol have not been clearly established for C_1-symmetric systems, that is, all tactic types have been observed with Class V

complexes.[3] An example of the unpredictability seen with C_1-symmetric complexes is noted in Chapter 2 where the use of two different C_1-symmetric catalysts results in two distinct polymers with very different stereoselectivity. Despite the significant advancements seen with the CP of olefins, especially with respect to catalyst activity and stereospecificity, there still remain key issues to be resolved such as the development of 'living' polymerization systems and the formation of polyolefins that are capable of exhibiting higher glass transition temperatures compared to PE and PP, *vide infara*.

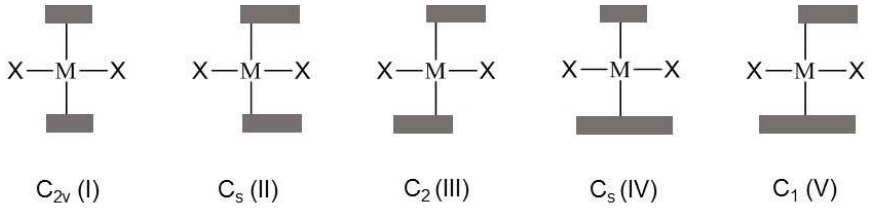

Figure 1.3: Classes of metal-ligand geometry.

When considering the stereochemical control of C_1-symmetric complexes the isoselectivity is thought to be attributed to one of two mechanisms. 1) site epimerization, and 2) the alternating mechanism. While the site epimerization mechanism is more commonly reported as the likely source of stereocontrol, there have been claims for both.[22, 23] In both cases it is agreed that there are two active sites but because they are diastereotopic; one site (the more stereoselective α-site) is favored over the other (less stereoselective β-site) for monomer coordination. The mechanism (epimerization vs. alternating) by which the more favorable active site becomes available for propagation is still debated. In the case for site epimerization it is argued that through a unimolecular, metal-centered epimerization process, the

growing polymer chain is shifted to the β-site allowing the incoming monomer to coordinate at the more favored α-site. On the other hand, the alternative mechanism makes use of both active coordination sites (α- and β-site) similarly to the CP mechanism presented in Scheme 1.3. However, following initial coordination of the monomer, the transition state for monomer insertion involves a location shift of the growing polymer chain to the β-site freeing up the original α-site for insertion. The primary difference between the two mechanisms which allow repetitive insertions at the α-site is that the alternating process occurs in concert and the site epimerization process occurs sequentially. An example of these two mechanisms are presented in Scheme 1.6 based on the work completed by Bercaw and coworkers.[22]

Scheme 1.6: Site epimerization vs. alternating stereocontrol mechanisms from work completed by Bercaw and coworkers.[22]

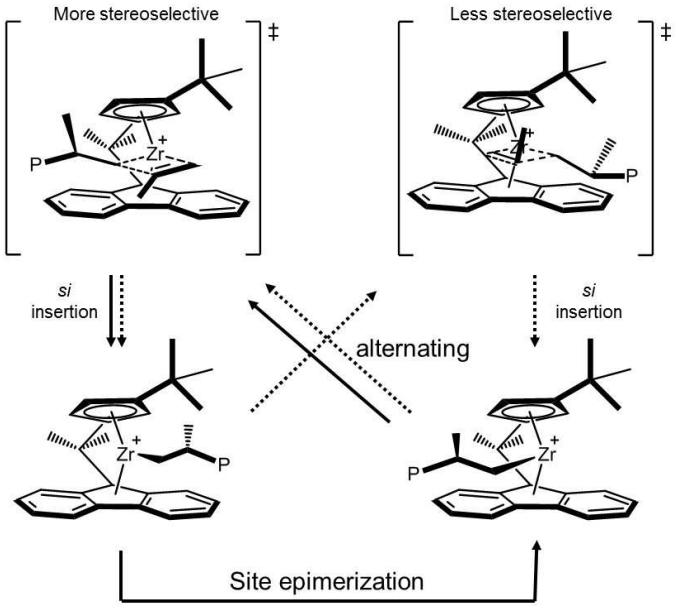

1.6. Glass Transition Temperature

It is worthwhile to briefly introduce glass transition temperature. The glass transition temperature (T_g) is the temperature at which a polymer material transitions from a glassy state to a rubber-like state. The glass transition is considered the single most important property of a polymer when selecting its application.[24] Polymers that have low T_g's (at or below room temperature) are sometimes referred to as elastomers, whereas a polymer that has a T_g near or higher than 100 °C is often referred to a thermoplastic. In the second case, the polymer is processed above its T_g and then cooled into a glassy solid. Although polymers both with, and without, the ability to crystallize can exhibit a T_g, it is important to note that a glass is an amorphous solid. Thus, the glass transition pertains only to amorphous polymers, or the amorphous regions of crystalline (semi-crystalline) polymers. There are several factors that contribute to the temperature at which the glass transition occurs. Perhaps the most influential characteristic is backbone flexibility of the polymer chain. The more flexible the backbone the lower the T_g tends to be. This trend is observed because polymer chains that are more flexible generally correlate with a lower energy barrier between available configurations. Thus, some variation in T_g is expected for a polymer as a function of tacticity (the T_g for atactic polypropylene tends to be 15 °C – 25 °C lower than isotactic polypropylene). Another factor to consider is the intermolecular interaction strength. Polymer's that exhibit strong intermolecular interactions such as hydrogen bonding tend to have higher T_g's. For example, polypropylene has a T_g between 0 °C and -25 °C depending on the tacticity and molecular weight.[25] If the pendent CH_3 groups are replaced with OH groups

(poly(vinyl alcohol)), the glass transition increases to around 85 °C.[25] It is also important to account for the polymer's molecular weight. The T_g of a polymer can increase somewhat (on the order of a 10 °C deviation) with increasing molecular weight.[24]

Polyolefins tend to exhibit glass transitions at lower temperatures. For example, polyethylene has a T_g near -80 °C, polypropylene has a T_g between 0 °C and -25 °C, poly(1-hexene) has a T_g around -45 °C. There are polyolefins that have high T_g's (here 'high T_g' includes temperatures ≥ 100 °C) such as polynorbornene, which has a T_g over 200 °C,[24] or other cyclic olefins.[26] However, the polymerization of these bulky monomers is often cumbersome (harsh reaction conditions) and the resulting high T_g polymers (referred to as engineering thermoplastics when ≥ ca. 200 °C) are expensive.[24] Therefore, it is of interest to develop high T_g polyolefins that possess glass transitions ≥ 100 °C (desired for industrial processing) and that can be polymerized easily from olefin monomer without harsh reaction conditions. In the following sections topics such as living coordination polymerization and cyclopolymerization may provide the components that are necessary for higher T_g polyolefins from straightforward and achievable methods.

1.7. Living Coordination Polymerization, LCP

There has been a great deal of debate over the past several decades as to what constitutes a 'living' polymerization system.[27, 28] Whether or not a given system is living is an important factor as they generally encompass key qualities such as narrow polydispersity, complete conversion of monomer, unique chain architectures such as

star- and block copolymers, and end functionalization for post polymerization modification. Researchers have attempted to define their polymerization systems by using terms such as 'living', 'controlled', 'quasi-living' and 'immortal'. Unfortunately, these terms are used even when not all of the polymerization characteristics suggest living polymerization (see list of living criteria below), and wading through these polymerization systems can be confusing when trying to decipher which systems truly proceed in a living fashion. Thus, in an effort to clarify which polymerization systems can be deemed 'living', a set of criteria have been established. In general, living polymerizations encompass negligible irreversible termination and chain transfer (it is important to note that reversible termination and chain transfer can still give rise to living polymerization systems provided that the rate of reversible termination and/or chain transfer occurs on a time scale that is much faster than the rate of chain propagation). All active sites should remain active throughout the duration of the polymerization (i.e. the concentration of active site remains constant during polymerization) and chain propagation should continue to occur so long as monomer is present. Reiterated and additional criteria are provided below as a bulleted list:[27, 28] Ideally, a truly living system will encompass all of these characteristics, that is, no single criterion can be used to term a system living; multiple, if not all the criterion must be present.

1) The degree of polymerization (DP) must increase linearly with monomer conversion ($DP = [M]_o/[I]_o$; where $[M]_o$ and $[I]_o$ are the initial monomer and initiator concentration).
2) The concentration of active initiator species, [I], must remain constant.

3) The rate of initiation is much faster than the rate of propagation ($k_i >> k_p$).
4) The active species is stable in the absence of monomer.
5) Polymerization will restart with the addition of more monomer.
6) If criteria 1-5 are true, then polydispersity will remain narrow ($Đ \leq 1.1$).
7) If criteria 1-5 are true, then well-defined block copolymers and end functionalization should be achieved readily.

The first living polymerization was reported by Szwarc in 1956 for the anionic polymerization of styrene,[29] which was immediately followed by the report of a polystyrene-polyisoprene block copolymer[30] (refer to Section 1.11 for an introduction to block copolymers). Living polymerization is now well documented for many different polymerization techniques including radical,[31, 32] cationic,[33, 34] atom transfer,[32, 35] and ring-opening polymerizations.[34, 36] The living polymerization of olefins using coordination polymerization was first reported by Doi[37] and coworkers in 1979 using an astereospecific vanadium precatalyst activated by $AlEt_2Cl$. Despite slow activation (a criterion for living polymerization would ideally encompass fast insertion; $k_i > k_p$), the polydispersity was relatively narrow ($Đ \leq 1.2$) at cold temperatures ($\leq$ -65 °C). The first group 4 transition metal complexes to participate in living coordination polymerization (LCP) were discovered in the 1990s for the non-stereospecific polymerization of olefins by several groups such as McConville,[38] Schrock,[39] Fujita,[40] and Coates,[27] and Kol.[41] LCP of olefins to afford highly stereoselective polyolefins were not achieved until 2000 by Sita[42, 43] (see Section 1.8). Since that time, new reports for stereoselective LCP have been established, some of

which have been discussed in reviews such as the ones by Fujita.[44] and Schellenberg.[45]

1.8. Sita Group Precatalysts

Over the past 15 years the Sita group has developed a number of group 4 transition metal dimethyl-monocyclopentadienyl acetamidinate complexes that were found to catalyze the polymerization of olefins such as ethylene, propene and higher alkenes upon activation with a cocatalyst. The precatalysts encompass the general formula (η^5-C_5R_5)-M(Me_2)[N(R^1)C(R^3)N(R^2)] (**I**) where M = Ti, Zr or Hf, R = Me or H, and R^1, R^2 and R^3 = various alkyl substituents such as Me (CH_3), Et (CH_2CH_3), *i*-Pr ($CH(CH_3)_2$), *t*-Bu ($C(CH_3)_3$) and Cy (C_6H_{11}). The cocatalysts most often employed are boron derivatives such as N,N-dimethylanilinium tetrakis(pentafluorophenyl)-borate ([$PhNMe_2H$][$B(C_6F_5)_4$]) (**II**).

Presented here is a summary of the Sita group polymerization catalysts, note that some of the precatalyst derivatives discussed in this section were also applied to the thesis research that is showcased in the proceeding chapters. These catalysts are labeled in numerical order according to their use. Other precatalyst derivatives discussed in this section, but not employed in the current thesis research, will also be given numerical values but may not be presented in numerical order. Upon activation with a designated cocatalyst the newly generated catalyst/initiator (the terms catalyst and initiator will be used interchangeably henceforth and refer to the activated forms of the precatalysts) will retain the same numerical labeling value assigned to the precatalyst, but will adorn the letter '**a**' (e.g. precatalyst **1** will correspond to initiator **1a** upon activation with a given cocatalyst).

Sita catalysts can be easily synthesized from a two-step, one-pot synthesis according to Scheme 1.7. In general, working in an inert atmosphere, a given Cp^*MCl_3 complex is dissolved in diethylether then cooled to -78 °C prior to the dropwise addition of a given carbodiimide ligand followed by the dropwise addition of methyl lithium. The reaction is allowed to warm to 25 °C prior to purification and crystallization.

Scheme 1.7: General synthesis for Sita catalysts.

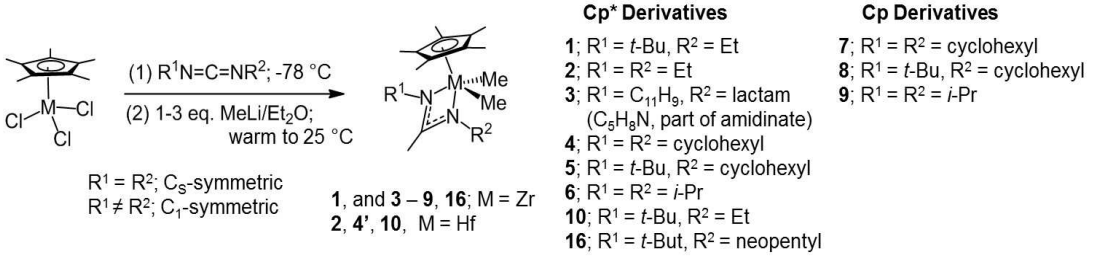

A particularly significant contribution was the discovery presented in 2000 by Kumudini,[43] which stands as the first living coordination polymerization (LCP) of 1-hexene to proceed in a highly active and living fashion for the production of isotactic poly(1-hexene) (*i*-PH) with tunable molecular weight and extremely narrow polydispersity ($Đ$ = 1.03) (previous reports produced either isotactic polyolefins with non-living systems or atactic polyolefins with living systems). The precatalyst responsible for the exceptional finding is a C_1-symmetric complex with the formula: Cp^*ZrMe_2[N(Et)C(Me)N(*t*-Bu)] (**1**) where $Cp^* = \eta^5$-C_5Me_5. **1** was fully activated with a stoichiometric amount of **II** for the formation of cationic Cp^*ZrMe[N(Et)C(Me)N(*t*-Bu)][$B(C_6F_5)_4$] (**1a**; it is worth noting that initiator **1a** is one of three primary catalysts employed throughout the remaining thesis chapters,

and **1a** is the staple Sita catalyst to which all other Sita initiators are compared). Also presented in the original report by Kumudini is the successful LCP of 1-hexene using C_S-symmetric Cp*$ZrMe_2$-[N(Cy)C(Me)N(Cy)] (**4**) activated by **II** for the formation of active cationic initiator **4a**; however, the resulting PH product lacks stereoregularity and is atactic. The work discussed in Kumudini's report with respect to both **1** and **4** revealed that polydispersity decreased with decreasing polymerization temperature. Optimal reaction conditions were reported using chlorobenzene (PhCl) as solvent with a reaction temperature of -10 °C, Scheme 1.8. According to the accompanying kinetic analysis of 1-hexene polymerization with **1a**, the reaction reached near 100 % completion after only 60 minutes, Figure 1.4.

Scheme 1.8: LCP of 1-hexene from using Sita catalyst **1**.

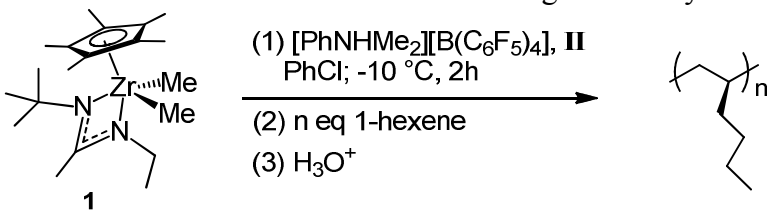

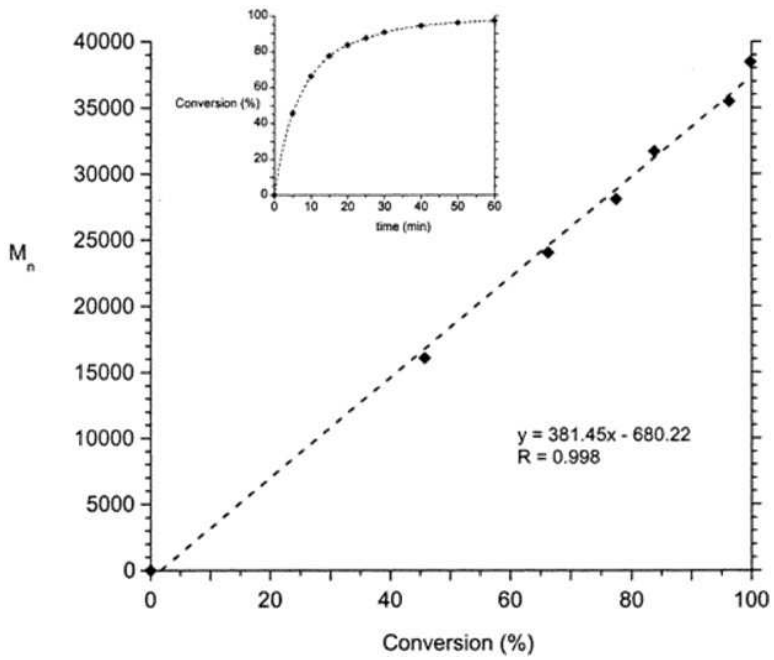

Figure 1.4: Plot of M_n vs. % conv. of 1-hexene (1.97 M 1-hexene; 50 μmol **1a**). Work completed by Kumudini and coworkers.[43]

Following the initial report by Kumudini in 2000, numerous subsequent studies have been carried out by the Sita group to better understand the mechanism by which polymerization proceeds through the use of **1** as well as with derivatives of **1** (**I**). As a direct result of these studies, a great deal of insight has been realized regarding various Sita precatalysts over the past several years. Details of these results are summarized here in a more-or-less chronological fashion.

Shortly following the debut of the first stereoselective LCP discussed above, Kumudini and coworkers expanded the use of **1** and **4**, and introduced a third precatalyst with formula: Cp*$ZrMe_2$-[N(*t*-Bu)C(Me)N(Cy)] (**5**) for the cyclopolymerization of 1,5-hexadiene resulting in the formation of poly(methylene-1,3-cyclopentane) (PMCP).[42] It was discovered that that **1**, **4**, and **5**, when activated by **II** to form cationic **1a**, **4a**, and **5a**, are efficient catalysts for the LCP of 1,5-hexadiene with ≥ 98 % cyclization selectivity.

Further, it was found that *trans* ring selectivity increased with increasing steric bulk of the initiator; 64 %, 78 % and 82 % respectively for **1a**, **4a**, and **5a** (Section 1.9 provides a detailed introduction to cyclopolymerization). Due to the living nature of these polymerization systems, block copolymers of PMCP and PH were formed resulting in the first report of a polyolefin block copolymer synthesized *via* LCP to exhibit microphase separation (see Section 1.11 for an introduction to block copolymers), Figure 1.5.

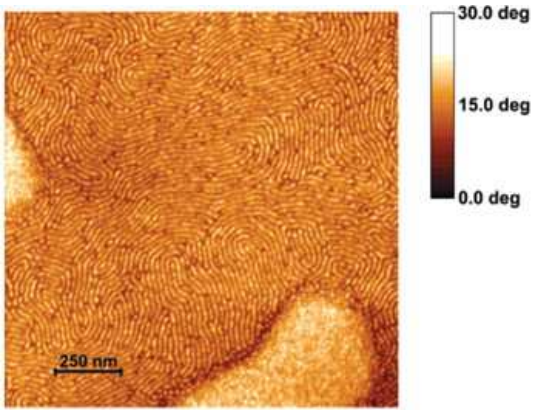

Figure 1.5: AFM phase map for PH:PMCP:PH triblock copolymer; film thickness 220 nm. Reproduced here from work by Kumudini and coworkers.[42]

Additional studies using **1** and derivatives of **1** such as Cp*ZrMe$_2$-[N(*i*-Pr)C(Me)N(*i*-Pr)] (**6**) revealed that upon activation with **II** the cationic initiator exists as a dicationic dimer in the solid state.[46, 47] Further, the cationic initiators (mono-cationic in solution or di-cationic in solid state) exhibit exceptionally slow amidinate ring-flipping on the NMR time scale to the extent that any epimerization that may occur is negligible during polymerization. It has been observed, however, that Sita catalysts exist as a racemic mixture (both R and S manifolds are present) as a results of the facile amidinate ring-flipping that occurs in the neutral, dormant state.

Specifically, calculations have revealed that several hundred ring-flips take place per second. The low energy barrier (10.9 kcal/mol at 223 K) for epimerization can be used as an advantage under conditions involving partial precatalyst activation during polymerization, which gives rise to degenerative methyl group transfer.[48] A more detailed discussion of this phenomena, including related literature, is saved for Section 1.10.

Bulkier monomers such as vinylcyclohexane (VCH) can also be polymerized via LCP forming stereospecific poly(VCH) (PVCH) using, **7**, **8**, and **9**, the less sterically encumbered Cp derivatives of **4**, **5**, and **6** respectively (where Cp = η^5-C_5H_5). Living character for PVCH was verified through the formation of an ABA triblock copolymer with PH as the mid-segment, narrow polydispersities ($Đ \leq 1.1$), and a linear conversion of monomer vs. time providing expected M_n (DP = $[M]_o/[I]_o$), Figure 1.6.[49] Interestingly, the PVCH that results from both C_S-symmetric initiators **7** and **9** (in addition to C_1-symmetric **8**) is highly isospecific (> 95 % selective for *mmmm* pentad). The rational for an isospecific polymer with an achiral initiator is that chain-end control is dominant over enantiomorphic site-control.

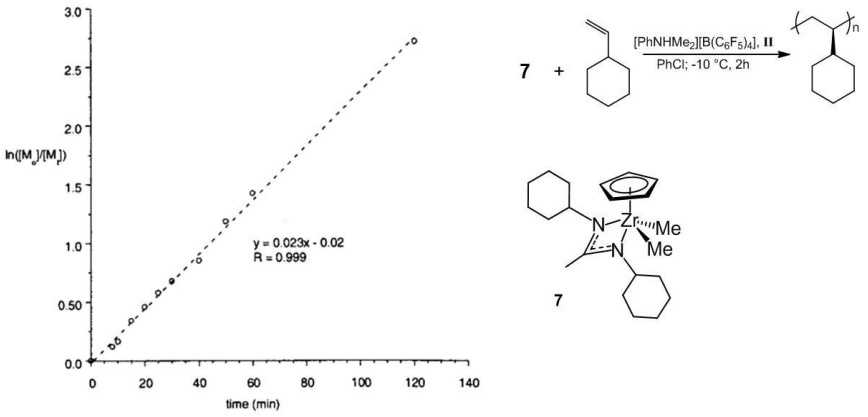

Figure 1.6: Kinetic analysis: LCP of VCH using **7** activated by **II**. Work completed by Keaton and coworkers [49]

Initiator **1a** was used for the polymerization of cyclopentene for the formation of *cis*-poly(1,3-cyclopentene), instead of the anticipated *cis*-poly(1,2-cyclopentene). NMR analysis of 1-2 equiv. of 5-methylcyclopentene with **1a** suggests that structural isomerization occurs readily above -30 °C (-10 °C is the standard LCP reaction temperature with Sita catalysts), Scheme 1.9.[49b]

Scheme 1.9: Representation of structural isomerization of 5-methylcyclopentene with **1a**.[49b]

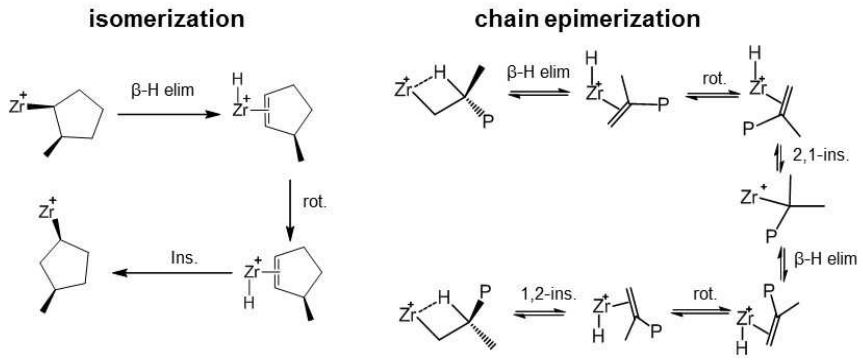

Numerous other studies have been carried out by the Sita group using derivatives of **1** including: 1) CP with **1** on a solid support, 2) how substitution at the distal position of the amidinate ligand might improve CP, identifying the effect of 'loose' vs. 'tight' ion pairs, 3) the effect of binuclear initiators on polymerization, 4) employing living chain transfer polymerization using main group metal alkyls, and 5) living degenerative group transfer. Described briefly below are a few examples of these studies. A discussion on living degenerative group transfer and binuclear Sita catalysts is saved for Section 1.10.

LCP was carried out using solid-supported **1** (**17**) using commercially available chloromethylated polystyrene beads (Figure 1.7) for the formation of isotactic PH with narrow polydispersity ($Đ \leq 1.10$) and tunable M_n. Isotactic PH-*b*-poly(1-octene) diblock copolymers were also formed by this method as a display of the living polymerization character.[50]

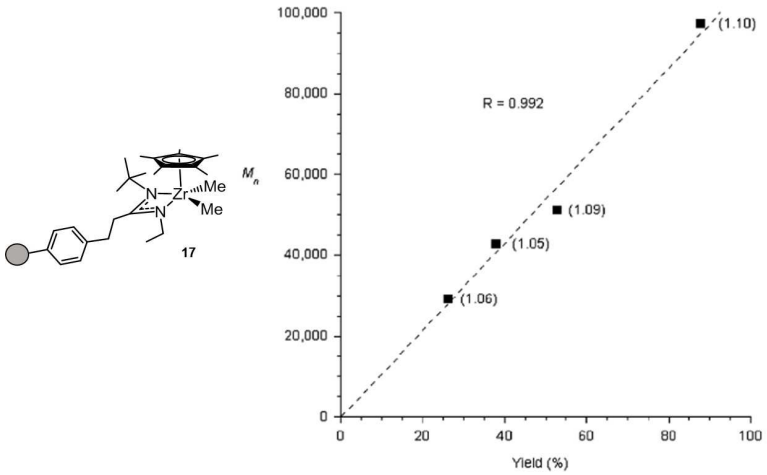

Figure 1.7: Solid supported derivative of **1** (**17**) and M_n vs. yield plot of LCP of 1-hexene with **17** activated by **II**. Work completed by Zhang and coworkers.[50]

Additional derivatives of **1** were achieved by substituting the distal methyl group of the amidinate ligand with either smaller (hydrogen; **18**) or larger (phenyl; **19**, *t*-Bu; **20**) substituents in an effort to determine their effect on the LCP of 1-hexene, Figure 1.8. Interestingly, it was observed that only the original catalyst, **1**, gave highly isotactic PH. Precatalyst **19** with a distal phenyl group gave the second most isotactic PH when activated by **II**. Polymerization with **18** (hydrogen) resulted in atactic PH with a broad polydispersity and low yield ($Đ$ = 1.59, 45 % yield) when activated by **II**. Complex **20** (*t*-Bu substituent) was not active for polymerization. The variety of results observed are likely attributed to buttressing effects induced by the steric bulk of the distal ligand group.[51]

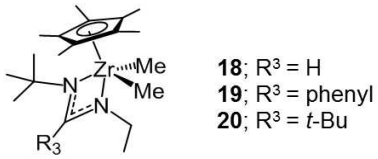

Figure 1.8: Derivatives of **1** formed by substitution at the distal position of the amidinate ligand (precatalysts **18**, **19**, and **20**).[51]

Living coordinative chain transfer polymerization with **2** using main group alkyls such as diethylzinc ($ZnEt_2$) have been established for the polymerization of propene, ethylene, 1-hexene and non-conjugated dienes.[52, 53] The reversible chain transfer between active **2a** and non-propagating, surrogate $ZnEt_2$ (or other main group metal alkyls such as AlR_3) allow for the production of large quantities of low M_n polyolefins with vary narrow polydispersities ($Đ \leq 1.10$), Figure 1.9.

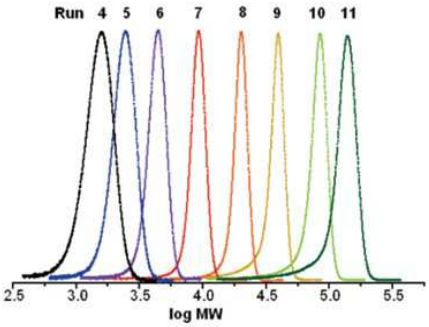

Run	2 (μmol)	$ZnEt_2$ (eq.)	Yield (g)	M_n (kDa)	D
1	20	20	6.02	12.6	1.03
2	20	20	7.92	15.9	1.03
3	20	20	1.63	3.63	1.05
4	20	200	4.99	1.45	1.08
5	20	100	4.93	2.28	1.06
6	20	50	4.94	4.18	1.04
7	20	20	4.18	8.75	1.04
8	20	10	4.78	18.7	1.04
9	20	5	4.85	33.3	1.09
10	10	10	10.1	71.9	1.09
11	10	5	9.64	111	1.15

Figure 1.9: LCCTP of propene using **2**. Left: SEC traces; right: respective SEC data.[52]

LCCTP has also been employed to investigate the effect of 'loose' vs. 'tight' ion pairs through the use of either **II** ($[PhHNMe_2][B(C_6F_5)_4]$; loose) or **III** ($B(C_6F_5)_3$, which forms $[MeB(C_6F_5)_3]^-$ following demethylation of neutral precatalysts **I**). It was found that under LCCTP conditions for ethylene, precatalysts **2** and **4'** (**4'** = **4** with tethered polymer chain), when independently activated by **II** have higher activity and comonomer incorporation compared to activation by **III** under otherwise similar conditions (comonomer = 1-hexene). It is suggested that, due to the smaller counter anion size formed from **III**, $[MeB(C_6F_5)_3]^-$ interacts more strongly with cationic **2a** and **4'a**, thus hampering the active site, and limiting polymerizability.[54]

The above review on the development of and use Sita catalysts over the past several years provides unequivocal evidence that these complexes have been well tested and are excellent candidates for use in the LCP of a wide range of olefins including ethylene, propene, 1-hexene, higher terminal alkenes. One area of interest that has yet to be thoroughly studied using Sita catalysts is the LCP of α,ω-non-

conjugated dienes for high T_g polyolefins. Reviewed previously in Section 1.6, the T_g of a polymer is a key property that must be considered when evaluating the appropriate materials application. In general, the T_g of polyolefins produced from linear alkenes such as ethylene, propene and 1,5-hexadiene have low T_g's and thus have limited application (the T_g is a determinant in the upper service temperature of a polymer). Preliminary work by our group has shown that Sita catalysts are efficient initiators for the cyclopolymerization of 1,5-hexadiene, which exhibit relatively low T_g (-20 °C to 10 °C based on M_n, diastereoselectivity and degree of crystallinity). However, by further increasing the rigidity of the polymer backbone, higher T_g's may be obtained. Therefore, it is of interest to apply Sita catalysts for the polymerization of higher non-conjugated dienes such as 1,6-heptadiene to identify if 1) Sita catalysts are active toward the living polymerization higher non-conjugated dienes, and 2) if the resulting materials display an increase in T_g. Therefore, upon completion of Chapter 1, the remaining Chapters (2 – 6) are dedicated to a discussion of the synthesis and cyclopolymerization of non-conjugated dienes using Sita catalysts.

1.9. Cyclopolymerization

The intramolecular coordination cyclopolymerization of non-conjugated dienes to form poly(methylenecycloalkane)s have garnered increased attention in recent years for their unique chemical microstructures. Specifically, the cyclopolymerization of α,ω-olefins give rise to four possible maximum-order microstructures, *cis*-isotactic, *trans*-isotactic, *cis*-syndiotactic and *trans*-syndiotactic, owing to a marked increase in microstructure intricacy when compared to the two

maximum-order microstructures, isotactic and syndiotactic, observed for the linear-acyclic coordination polymerization of α-olefins, Figure 1.10.

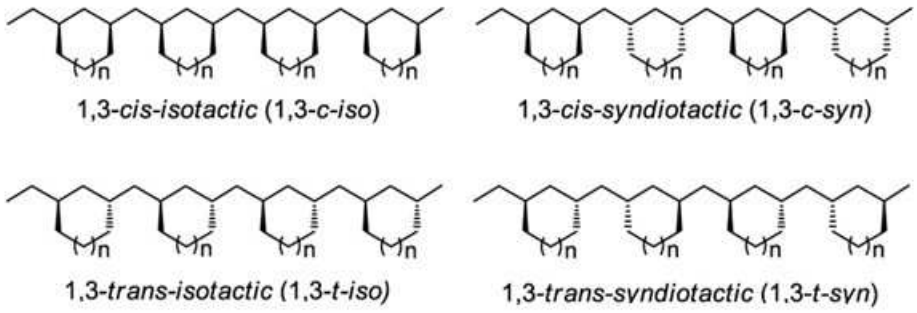

Figure 1.10: Maximum order microstructures for the cyclopolymerization of non-conjugated dienes (n is equal to 0, 1 or 2).

The increase in microstructure complexity for poly(methylenecycloalkane)s can be attributed to: 1) the enantiofacial (homo- or hetero-facial) 1,2-insertion (1,2-addition) of the α,ω-olefin into the metal center, which governs the polymer's tacticity, and 2) the pseudo ring conformation that occurs during secondary 1,2-insertion (cyclization) allowing for *cis/trans* diastereoselectivity. Together, these two components give rise to the aforementioned cyclic microstructures of maximum-order.[55] However, the four possible maximum-order microstructures described for poly(methylenecycloalkane)s are permitted only on the bases that intramolecular cyclization is complete (high cyclization selectivity). If cyclization is not completed prior to the next 1,2-addition of monomer then pendant vinyl groups will form allowing the opportunity for crosslinking *via* subsequent intermolecular insertion into an adjacent active site. Maximum ring size for each repeating unit is achieved with

consistent regio-regular primary and secondary 1,2-insertions. For example, 1,2-addition followed by 1,2-cyclization of 1,6-HD gives rise to the formation of 6-membered rings (likewise, 1,5-HD will give 5-membered rings and 1,7-OD will give 7-membered rings). However, a smaller ring size will form upon 2,1-primary insertion (2,1-addition) followed by 1,2-cyclization (i.e., the monomers 1,6-HD, 1,5-HD and 1,7-OD will give rise to 5-, 4- and 6- membered rings respectively), Scheme 1.10. In contrast to primary additions, 2,1-secondary insertions (cyclization) are not generally observed due to sterics from the limited alkyl chain length.[55]

Scheme 1.10: Modes of insertion during the cyclopolymerization 1,6-HD.

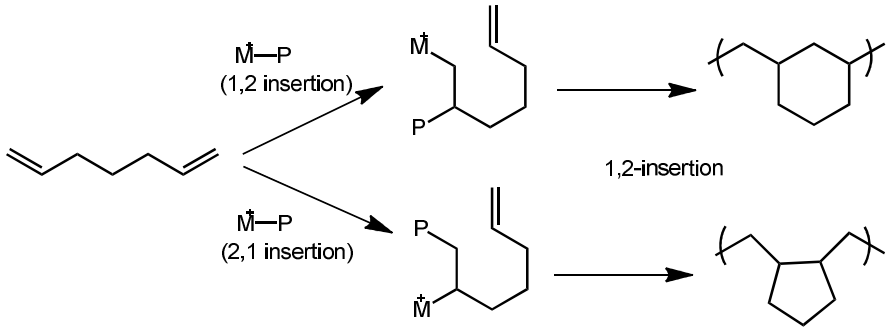

The degree of intramolecular cyclization (cyclization selectivity) for a given non-conjugated diene results from the competing rate of cyclization vs. 1,2-addition (intermolecular propagation). For example, immediately following 1,2-addition there will either be a second primary 1,2-addition leaving a pendant vinyl group (from the previously inserted monomer), or an occurrence of 1,2-cyclization. The rates of reaction for intermolecular propagation and intramolecular cyclization have been studied for 1,5-HD under the assumption that intermolecular propagation follows a

Markovian process and intramolecular cyclization follows a Bernoullian process.[56] Taking note that the rate of 1,2-addition (k_p) is dependent on concentration (bimolecular) and that the rate of cyclization (k_c) is independent of concentration (unimolecular), the following equations (1 – 3) can be used to describe the respective rates of reaction for 1,5-HD:

$$v_{pp} = k_{pp}[M_p^*][M] \qquad (1)$$

$$v_{cp} = k_{cp}[M_c^*][M] \qquad (2)$$

$$v_c = k_c[M_p^*] \qquad (3)$$

where $[M_p^*]$ = number of propagating chain ends of 1,2-addition units (P), $[M_c^*]$ = number of propagating chain ends of cyclized units (C), [M] = monomer concentration, k_{pp} = rate constant of 1,2-addition for a second monomer following a previous 1,2-addition (no cyclization), k_{cp} = rate constant of 1,2-addition for a second monomer following cyclization, and k_c = rate constant of cyclization. The ratio of v_{pp}/v_c can be simplified to show how the selectivity for cyclization is affected by monomer concentration, equation 4.

$$v_{pp}/v_c = (k_{pp}/k_c)[M] \qquad (4)$$

Since the reaction rate for intermolecular propagation (1,2-addition) increases with increasing monomer concentration, contrary to the rate of cyclization (v_c), the selectivity for cyclization is decreased with increasing monomer concentration. Therefore, intramolecular cyclization has the opportunity to occur more readily under dilute conditions. Cyclization selectivity is also dependent on temperature, which has been shown to either increase or decrease at a given temperature depending on the

structure of the catalyst. Scheme 1.11 provides an example of intramolecular cyclization vs. intermolecular 1,2-addition.

Scheme 1.11: Intramolecular cyclization vs. intermolecular 1,2-addition.

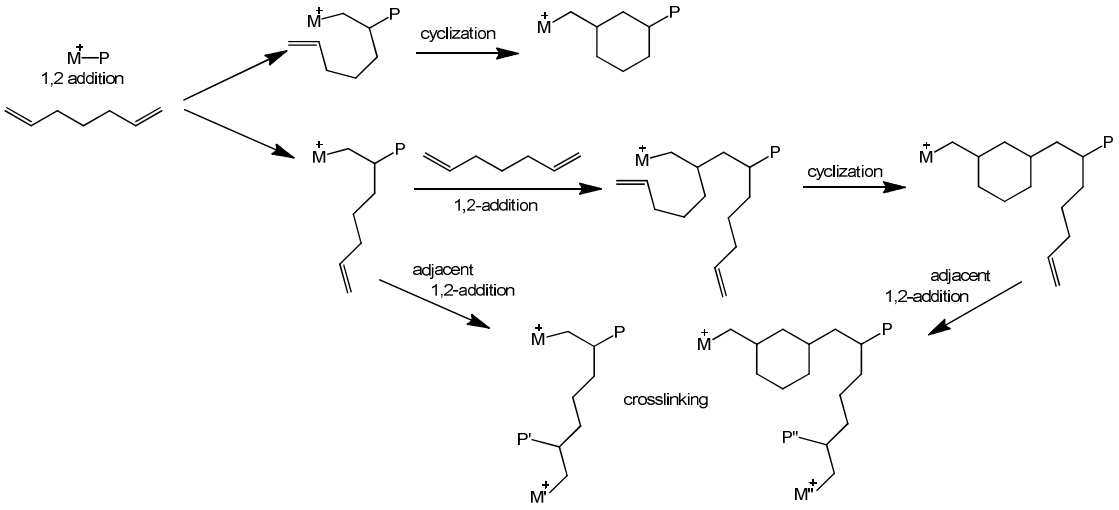

1.9.1. Cyclopolymerization: Related Literature

The stereochemical complexity and modes of pi-bond insertion for non-conjugated dienes have prompted researchers to put forth tremendous efforts toward the development of coordination catalysts, which can control both the polymer's tacticity as well as the diastereoselectivity. Considered here are the poly(methylenecycloalkane)s that result from the coordination cyclopolymerization of the non-conjugated dienes: 1,5-hexadiene, 1,6-heptadiene, and 1,7-octadiene (1,5-HD, 1,6-HD and 1,7-OD respectively). 1,5-HD, the most intensely studied of the three monomers, is most notably known for having a high degree of crystallinity upon cyclopolymerization, regardless of the tacticity or *cis/trans* content, to form

poly(methylene-1,3-cyclopentane), PMCP. A brief overview on a few key PMCP reports are highlighted here. The first report of PMCP came through the use of a Ziegler-Natta catalyst by Marvel in 1958.[57] The PMCP-type product was reported as a hard, rubbery, white solid with ca. 40 % solubility in benzene. The polymerization was carried out at room temperature with a 3:1 ratio of triisobutylaluminum to titanium tetrachloride. It was noted that the best results were obtained using dilute conditions. The polymer product was analyzed by infrared spectroscopy (FT-IR), which indicated a 5 – 8 % presence of pendant vinyl groups as result of incomplete cyclization. Several years later, in 1990 Waymouth[58] and coworkers reported on the full structural characterization of PMCP with high diastereoselectivity confirmed by ^{13}C NMR. Polymerizations were carried out using Ziegler-Natta derivatives of the form Cp_2ZrX_2 (where Cp = η-C_5H_5, and X = methyl or chloro), activated by methylaluminoxane (MAO) using toluene as a solvent. Their report concludes that a high *trans* diastereoselectivity was observed at room temperature with Cp_2ZrX_2, and high *cis* confirmations were observed when polymerizations were carried out at colder temperatures (-22 °C) or with the use of more sterically encumbered Cp* complexes (Cp* = η-C_5Me_5). Shortly thereafter, in 1991 through 1993 Waymouth[59, 60] and coworkers reported on the development of chiral, and thus optically active, PMCP materials using a series of chiral metallocene based catalysts for cyclopolymerization, Figure 1.11. PMCP materials were reported having 58 – 91 % *trans* ring content, and degree of intramolecular cyclization between 68 and > 99 % depending on the reaction conditions and initiator employed. The T_g values for these PMCP materials were not reported. The calculated M_n range from 300 Da up to

30 kDa, all with very broad polydispersities ($2 \leq Đ \leq 6$), indicative of a non-living system.

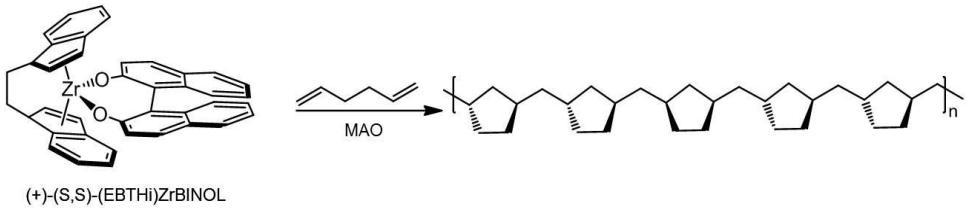

Figure 1.11: Chiral catalyst precursors used by Waymouth and coworkers for the production of optically active PMCP. Some stereoerror present.[59, 60]

Previously, our group reported on the synthesis of PMCP with the presence of pendant vinyl groups as low as 1 – 2 %, and a high degree of tacticity and up to 64 % *trans* diastereoselectivity from the living coordination cyclopolymerization of 1,5-HD with group 4 transition metal monocyclopentadienyl amidinate complex **1** activated by (**II**) ($[PhNMe_2H][B(C_6F_5)_4]$), Scheme 1.12.[42] Since the polymerization methods used here are living, the M_n can be finely tuned as needed and have narrow polydispersities ($Đ \leq 1.1$). In a few cases, PMCP has also been reported to display liquid crystalline properties.[61] Numerous other reports have provided details on the synthesis of PMCP copolymers with monomers such as ethylene,[62, 63] propylene,[64] styrene,[63] 4-methyl-1-pentene,[45] and 1-hexene.[45, 65]

Scheme 1.12: Reaction of **1** activated by **II** for cyclopolymerization of 1,5-HD.

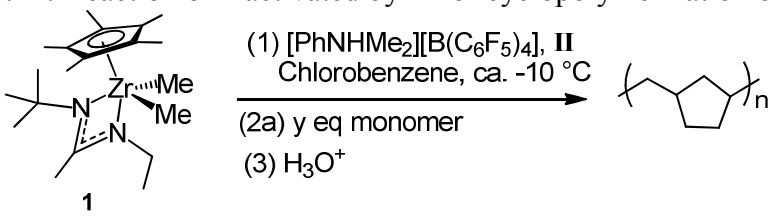

In contrast, the cyclopolymerization of 1,7-OD has been reported to a lesser extent. The increased degrees of freedom associated with the longer alkyl chain decreases the probability of intramolecular cyclization for 1,7-OD thus allowing for the increased likelihood of crosslinking through intermolecular insertion of a pendant vinyl moiety into an adjacent metal center.[66, 67] Shi[68] and coworkers reported on the non-living homopolymerization of 1,7-OD using a dimethylpyridylamidohafnium catalyst. Their report confirmed the formation of crosslinking for their samples and noted an increase in crosslinking with increased 1,7-OD concentration (similar to the trends observed for 1,5-HD). After separating the homopolymer from the insoluble crosslinked material, they were able to determine M_n, $Đ$ and T_g for two samples: 1) M_n = 2.68 kDa, $Đ$ = 2.44, T_g = 45 °C, and 2) M_n 1.33 kDa, $Đ$ = 2.79, T_g = 51 °C. No melting temperature was observed but 100 % *cis* ring formation for both samples was verified by NMR. Naga[66, 69] and coworkers carried out a detailed analysis on the polymerization of 1,7-OD with three separate non-living polymerization catalysts activated by MAO: **A**) isospecific *rac*-dimethylsilylenebis-(indenyl) zirconium dichloride, **B**) syndiospecific-diphenylmethylene(cyclopentadienyl)-(9-fluorenyl) zirconium dichloride, and **C**) aspecific Cp_2ZrCl_2. An increase in cyclized content was observed with increasing temperature (40 °C > 0 °C > -20 °C) and with lower monomer concentrations. A trend in the degree of cyclization was also observed with

catalyst type (**A** > **C** > **B**). M_n values were reported for poly(1,7-OD) from **A** and **B**, and range from 700 Da up to 1.9 kDa with broad polydispersities ($Đ$ = 1.7 – 6.4). As anticipated the T_g decreases with increasing pendant vinyl group concentration. The observed T_g at a pendant vinyl group concentration of 42 mol % is 13.9 °C and increases up to 51.4 °C with a pendant vinyl group concentration as low as 7.6 mol %; similar to that reported by Shi. Waymouth[60] and Coates reported the non-living cyclopolymerization of 1,7-OD with up to 78 % *cis* ring content using an ethylenebis(tetrahydroindenyl) zirconium binaphtholate catalyst ($EIn_2ZrNapth_2$); however, no further characterization of the polymer was provided. 1,7-OD has been successfully polymerized with a high degree of cyclization (low crosslinking) most notably as a copolymer at low concentrations with ethylene,[66, 70, 71] propylene,[72] styrene,[71] and 1,-octene.[73]

Despite the striking contrast between 1,5-HD's ease of crystallization and high degree of cyclization, and 1,7-OD's markedly low degree of cyclization, reports on the coordination cyclopolymerization of 1,6-HD are extremely limited. Summarized here are the only known reports regarding the cyclopolymerization of 1,6-HD as a homopolymer. The first cyclopolymerization of 1,6-HD was reported by Marvel in 1958 through the use of a Ziegler-Natta type catalyst prepared by reduction of titanium tetrachloride with triisobutylaluminum. The resulting material was described as being a tough polymer, that, when dried, appears as a transparent film with a capillary melting temperature between 210 °C – 230 °C. Detailed chemical analysis was not preformed beyond characterization *via* detection of C-C and C-H stretching observed by FT-IR.[57] Several years later in 1992, Waymouth and Coates

presented the synthesis of two separate poly(methylene-1,3-cyclohexane) (PMCH) materials using the Zeigler-Natta catalysts. The first synthesis, carried out at room temperature with Cp_2ZrCl_2, resulted in a 50:50 *cis*:*trans* poly(cycloalkane) consisting of 6-membered rings. The result suggests a consistent 1,2-secondary insertion with a lack of diastereoselectivity during the cyclization step. The second synthesis was carried out with more sterically encumbered $Cp^*_2ZrCl_2$ at -25 °C yielding 6-membered rings with 84 % *cis* conformation suggesting a higher degree of homo-facial 1,2-secondary insertions. Their report does not discuss the stereoselectivity of the first insertion step, nor does it provide characterization data. Finally, their report suggests that the cyclopolymerization of longer chain α,ω-dienes give rise to a greater selectivity for *cis* ring formation. As an example of this claim, the catalyst $EIn_2ZrNapth_2$ was used for the cyclopolymerization of 1,5-HD, 1,6-HD and 1,7-OD to afford polymers with 34 %, 50 % and 78 % *cis* rings, respectively.[60]

A decade later, in 2002, Coates and coworkers reported two new non-living cyclopolymerization catalysts for 1,6-HD. The first synthesis was carried out with *rac*-ethylene-bis(indenyl) zirconium dichloride (**D**) activated with MAO to afford complete cyclization forming 6-membered rings with a 50:50 ratio of *cis/trans* diastereoselectivity. The second synthesis was carried out with a pentafluro-dichloride titanium catalyst (**E**) activated by MAO to afford complete cyclization of 1,6-HD resulting in the formation of a mixture of both 5- and 6-membered poly(methylenecycloalkane)s.[27, 74] Additional characterization beyond ^{13}C NMR was not reported for this system. The ^{13}C NMR spectra for these two compounds are provided in Figure 1.12.

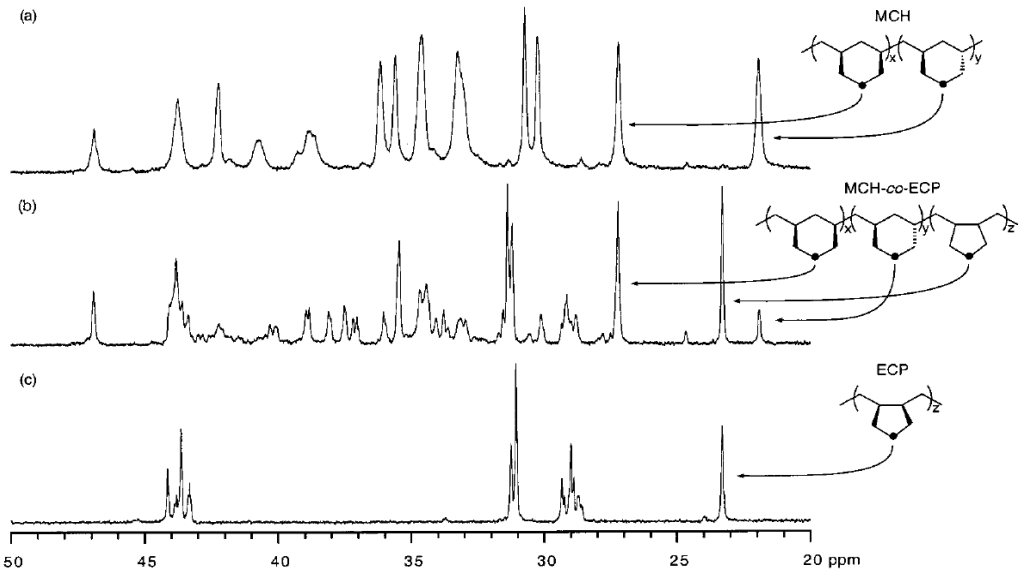

Figure 1.12: Cyclopolymerization of 1,6-HD with catalysts **D** (top) and **E** (middle); ^{13}C NMR reproduced from reference.[74]

Takeuchi and coworkers have developed a series of non-living late transition metal, Fe, Co, and Ni bis(imino)pyridine complexes for the cyclopolymerization of various 1,6-heptadienes, including 1,6-HD. Careful characterization has revealed a series of 5-membered ring poly(methylenecycloalkane)s with complete cyclization in all cases. The Fe complexes give rise to poly(1,6-HD) with a varied mixture of *cis* and *trans* 5-membered rings depending on the bulkiness of the ligand. Cyclopolymerization with the Co complex gives rise to only *cis* diastereoselectivity. The average M_n for these poly(cycloalkane) materials range between 3 kDa – 14 kDa with relatively broad polydispersities ($Đ$ = 1.7 – 2.4).[75, 76] The ^{13}C NMR from these poly(methylenecycloalkane)s from the Fe and Co complexes are provided in Figure 1.13.

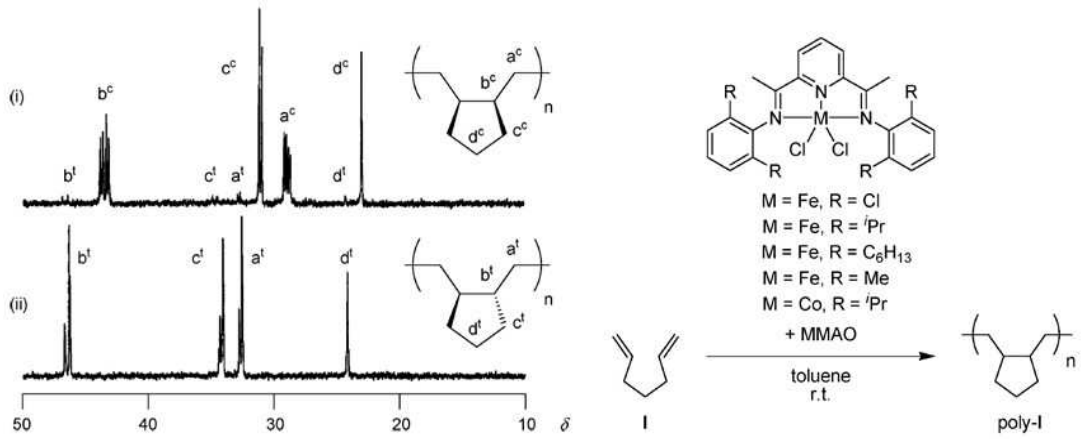

Figure 1.13: ^{13}C NMR spectra and catalyst types used by Takeuchi for the polymerization of 1,6-HD.[76]

In 2009, Coates and coworkers reported the use of a tridentate phenoxyamine hafnium complex (**F**) for the synthesis of *cis*-enriched (> 97% *cis*) isotactic PMCH with a M_n of 87 kDa ($Đ = 1.38$), T_m and T_g of 179 °C and 103.9 °C, respectively.[77] This report is the first presentation of *cis*-isotactic PMCH supported with characterization data, Figure 1.14. However, there was no discussion regarding the living character of the reported cyclopolymerization. Finally, it is important to note that while co-polymerizations with 1,6-HD are not the focus of this thesis project, there are a few literature examples that report on the incorporation of 1,6-HD as a copolymer with ethylene,[78] isoprene,[79] and styrene.[78]

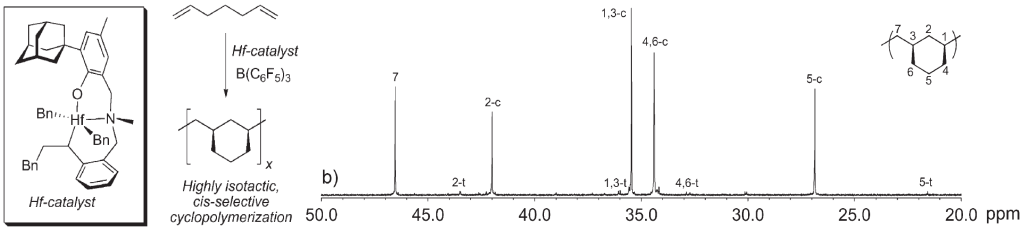

Figure 1.14: Cyclopolymerization of 1,6-HD with complex **F**, and resulting ^{13}C NMR spectra. Figure recreated from report by Coates.[77]

As evidenced by the aforementioned literature, the highly regio- and stereo-specific living coordination cyclopolymerization of 1,6-HD for the formation of poly(methylene-1,3-cyclohexane), PMCH, has remained elusive. Therefore, it is of interest to expand the use of Sita catalysts to include the coordination polymerization of 1,6-HD. While it is anticipated that some reaction will occur, it is unclear if the polymerization will proceed in a living fashion or what the degree of cyclization selectivity will be. The polymerization of 1,6-HD using Sita precatalysts **1**, **2**, and **3** activated with a stoichiometric amount of **II** (Scheme 1.13) is the primary focus of Chapter 2.[80]

Scheme 1.13: Reaction of Precatalyst (**1**, **2**, or **3**) activated by **II** for cyclopolymerization of 1,6-HD.[80]

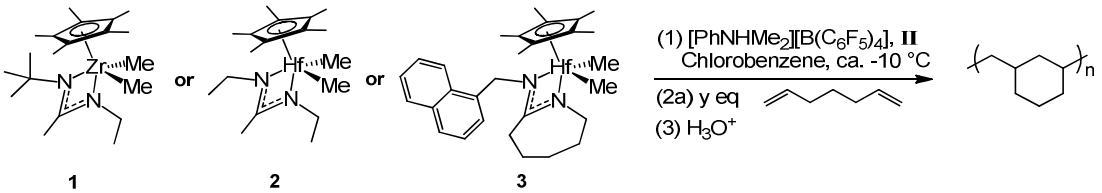

1.10. Degenerative Methyl Group Transfer using Sita Catalysts

The Sita group has previously shown that precatalyst **1** is configurationally unstable as a result of facile 'ring-flipping' of the amidinate ligand.[48] Monodemethylation of **1** with **II** to form cationic **1a** provides a highly active initiator toward the living coordination polymerization (LCP) of α-olefins[42, 49, 81, 82] and α,ω-olefins.[42, 80, 83] It has also been shown that **1a** exists in the solid state as a dimeric dication with bridging methyl groups[46] and that, in solution, rapid methyl group exchange occurs between **1a** and **1** or an otherwise structurally related initiator.[84] These combined observations prompted the Sita group to investigate the possibility of reversible deactivation by degenerative transfer (DT), wherein methyl group exchange between an active, cationic initiator (**1a**) and a dormant, neutral species (**1**). In order to maintain LCP under these conditions (determined in part by narrow $Đ$, and expected molecular weights etc.) methyl group exchange must be readily reversible and occur at a rate (v_{ex}) that is much faster than the rate of propagation (v_p), that is, $k_{ex} >> k_p$, where k_{ex} and k_p are the rate constants for methyl group exchange and propagation respectively.

It was found that degenerative methyl group transfer between active, cationic **1a**, and neutral, dormant **1** (made possible through the subactivation of **1** by **II**), results in a living polymerization system for the coordination polymerization of 1-hexene for the formation of poly(1-hexene) (PH), which exhibits similar expected M_n and $Đ$ values observed under non-DT conditions.[48] Interestingly, the PH produced under DT conditions appears atactic (confirmed by $^{13}C\{^1H\}$ NMR), whereas the PH produced under non-DT conditions with the same initiator is highly isotactic, Figure

1.15. The loss of stereocontrol under DT was confirmed to be attributed to the rapid metal-centered epimerization (ring-flipping) observed for **1**.

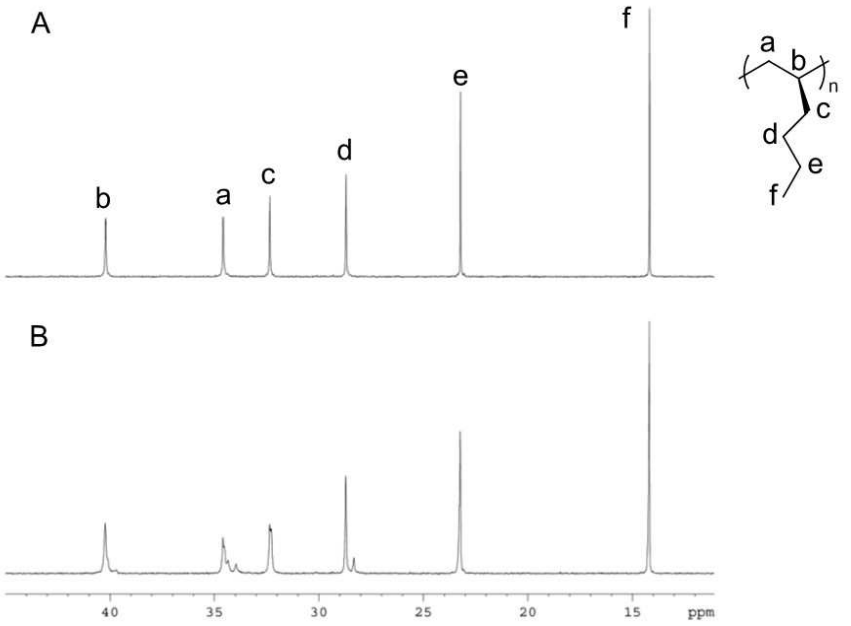

Figure 1.15: $^{13}C\{^{1}H\}$ NMR of PH completed by Zhang. A) [**II**]/[**1**] = 1.0. B) [**II**]/[**1**] = 0.5; 100 MHz, chloroform-d_1 25 °C.[48]

As discussed in Section 1.8, initiator **1a**, under complete activation conditions, exists as a racemic mixture of R- and S-manifolds. The R-manifold forms an R isotactic chain, and the S-manifold forms an S isotactic chain. While it has been shown that epimerization of cationic **1a** does not occur on a time scale competitive with propagation (i.e. it is negligible), neutral **1** readily epimerizes. For example, consider an R-manifold of cationic **1a** (R-**1a**). When R-**1a** undergoes bridging methyl group exchange, generating newly formed **1** (with tethered polymer chain intact), ring-flipping of the amidinate ligand readily occurs until the next methyl group exchange takes place re-generating an isospecific active propagating species of **1a**,

which forms either R-**1a** or S-**1a** irrespective of the manifold present prior to the preceding methyl group exchange. If the same R-manifold re-forms, then propagation will continue without the any stereoerror. On the other hand, if the S-manifold forms, then propagation will still continue in an isospecific fashion but there will a stereoerror at the point of re-activation due to switching between the two enantiomeric forms. By increasing the concentration of **1** during polymerization, the likelihood of forming a stereoerror increases, thus giving rise to a polymer chain that approaches an atactic microstructure. Therefore, it must hold true that the rate of metal-centered epimerization (ν_{epi}) be faster than ν_{ex} such that $k_{epi} > k_{ex} >> k_p$ where k_{epi} is the rate constant for metal-centered epimerization, Scheme 1.14.[48]

Scheme 1.14: Reversible deactivation *via* degenerative methyl group transfer.

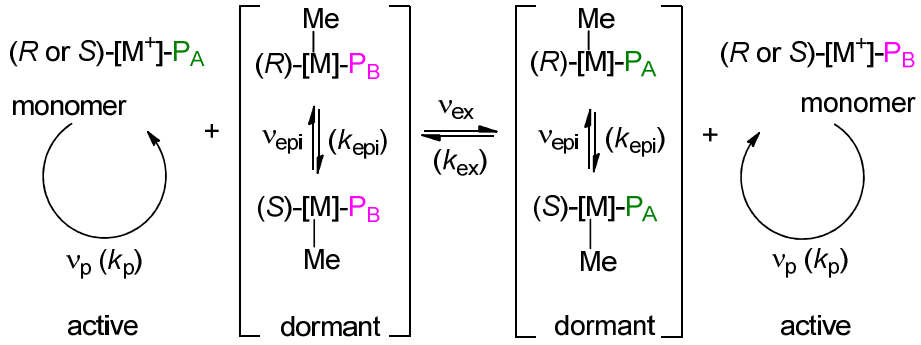

To date, the Sita group has successfully extended the mechanism of facile reversible deactivation by degenerative group transfer to include the hafnium analog of precatalyst **1** (**10**), the diisobutyl (in place of dimethyl) analog of **10** (**11**), as well

as the DT of Cl in a chloride, isobutyl (in place of dimethyl) analog of **1** (**12**), Figure 1.16.[84, 85]

Further, the Sita group also developed bimetallic derivatives of **1** (**13**, **14**, and **15**) with the formula: [(Cp*Zr(Me)$_2$)$_2$][N(*t*-Bu)C(Me)N-(CH$_2$)$_n$-NC(Me)N(*t*-Bu)] where n = 4 (**13**), n = 6 (**14**), and n = 8 (**15**). When using precatalysts **13**, **14**, and **15** for the polymerization of propene, it was observed that while overall stereoselectivity decreased slightly with decreasing alkyl chain length of the tethering unit, the frequency of stereoerror under DT conditions was seen to decrease with decreasing alkyl chain length of the tethering unit. The higher control of stereoselectivity observed in the latter case is likely due to a higher energy barrier for metal-centered epimerization as a result of sterics that arise from the close proximity of the tethered active sites, Figure 1.17.[83]

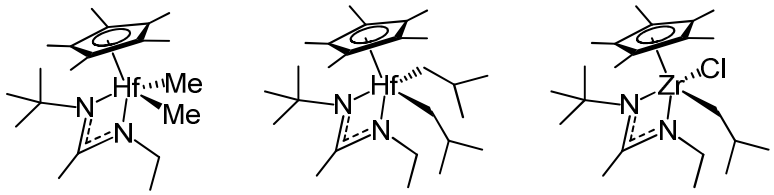

10 **11** **12**

Figure 1.16: Precatalysts **10**, **11**, and **12**.[84, 85]

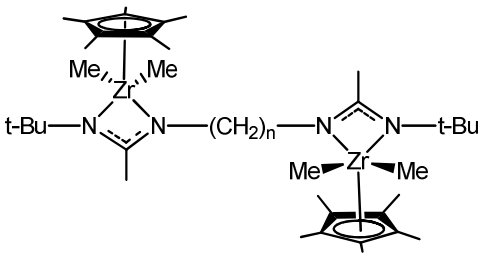

Figure 1.17: Bimetallic zirconium precatalysts **13** (n = 4), **14** (n = 6), and **15** (n = 8).[83]

The fast and reversible degenerative methyl group transfer mechanism was also successfully utilized for the formation of stereogradient PP through the modulated subactivation of **1** by **II**.[86] First, a series of polymerizations were carried out at various degrees of activation, namely, [**II**]/[**1**] = 1.0, 0.95, 0.925, 0.90, 0.85 and 0.50. The $^{13}C\{^{1}H\}$ NMR analysis for each PP sample clearly indicates an increase in the number of stereoerrors as the percent activation of **1** is decreased. Partial $^{13}C\{^{1}H\}$ NMR spectra for each sample has been reproduced in Figure 1.18.

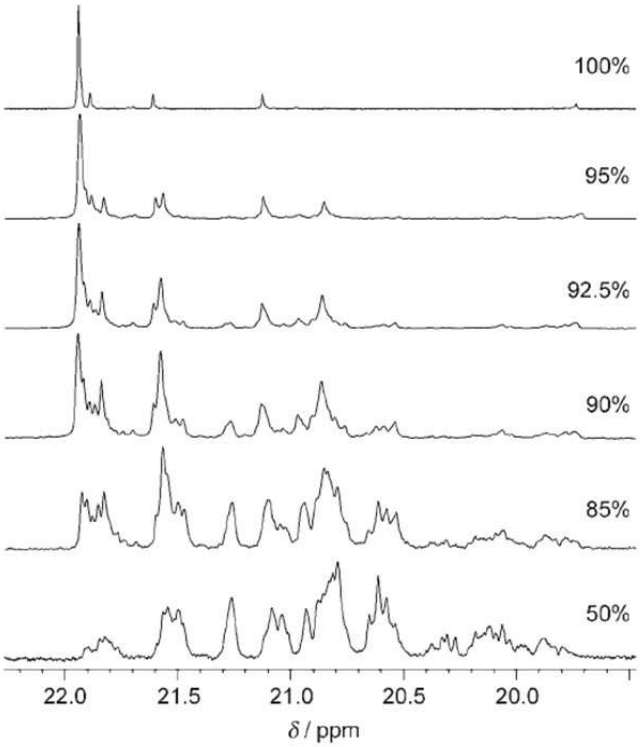

Figure 1.18: $^{13}C\{^{1}H\}$ NMR completed by Harney. DT polymerization of PP; 125 MHz, TCE-d_2, 70 °C.[86]

Based on the successful stereomodulation of PP through the subactivation of **1**, the next polymerization was initiated using **1** at 60 % activation (i.e. [**II**]/[**1**] = 0.60) (standard conditions: -10 °C, in PhCl with a propene flow rate of 5 psi). After the first 30 minutes of polymerization, a syringe pump was used to systematically increase the activation level to 90 % over the course of 3 hours. This method of synthesis for stereogradient PP was successful as depicted by the observed increase in stereoregularity in the $^{13}C\{^{1}H\}$ NMR spectra taken at various time points during the polymerization (30 min, 90 min, 150 min and 180 min). The methyl regions of the $^{13}C\{^{1}H\}$ NMR spectra were compared to difference spectra taken from a separate experiment (not shown) using ^{13}C(99%)-labeled methyl end groups. The analysis

clearly show an increase in stereoregularity throughout the duration of the polymerization.

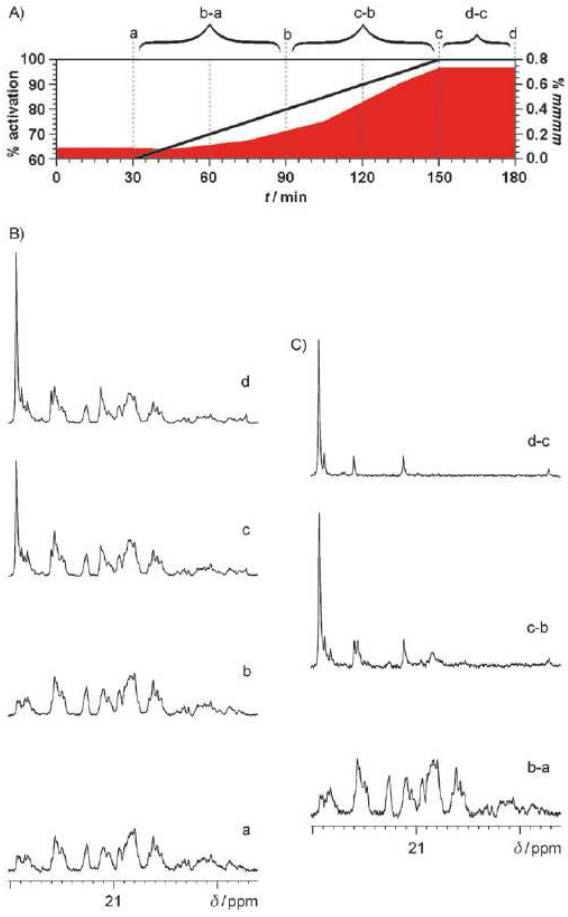

Figure 1.19: A) stereogradient map. B) $^{13}C\{^{1}H\}$ NMR spectra of the methyl region at time points a, b, c and d. C) The corresponding difference spectra taken from a separate experiment using ^{13}C(99%)-labeled methyl end groups; 125 MHz, TCE-d_2, 70 °C.[86]

Finally, reversible deactivation by DT for LCP provides the opportunity for the development of stereoblock polyolefins. The formation of well-defined stereoblocks can be achieved by systematically turning DT "on" and "off" throughout the duration of a given polymerization. The formation of molecularly discrete, well-

defined stereoblock-PP (sb-PP) is of great interest for high impact materials such as thermoplastic elastomers, TPEs (a further discussion of polyolefin-based TPEs from ABA triblock copolymers is presented in Chapter 6). In this regard, the Sita group was able to successfully apply DT for the design of discrete multiblock atactic-isotactic sb-PP with narrow *Đ* and tunable molecular weight.[81, 86-88] The challenge here was with the method by which the isospecificity during polymerization can be reversibly turned "on" and "off" on demand. To solve this challenge a derivative of **1**, (Cp*$ZrMe_2$-[N(*t*-Bu)C(Me)N(neopentyl)]; **16**) which can undergo irreversible methyl group transfer, yet is inactive toward polymerization under the applied reaction conditions, was employed to convert the active propagating species **1a** to the configurationally unstable dormant **1** for a given polymerization time prior to re-activating with additional **II**. Alternating between additions of **16** and **II** during

Scheme 1.15: Irreversible methyl group transfer between **1a** and **13**.

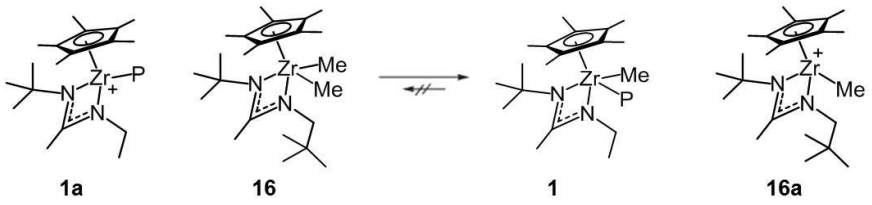

polymerization provides atactic and isotactic stereoblocks, respectively. Three different sb-PP samples were reported; an atactic-isotactic diblock (abbreviated *a*-*i*-PP with 60:40 *a*:*i* ratio), an *a*-*i*-*a*-PP triblock (30:40:30) and an *a*-*i*-*a*-*i*-PP tetrablock (30:20:30:20). The block copolymer sb-PP samples have M_n values of 164 kDa, 167 kDa and 172 kDa respectively (*Đ* = 1.19 for each). sb-PP has long been sought

after as a potentially new class of thermoplastic elastomer. Therefore, the elastomeric properties of the sb-PP materials synthesized by the method described above were analyzed using tensile and cycling tests, Figure 1.20. The triblock sb-PP had the longest extension at break (1530 % strain), followed by an increase in tensile strength but shorter extension at break for the diblock sb-PP (1325 % strain) and tetrablock sb-PP (1227 % strain). Cycling tests were also performed *via* 10 extension cycles to 300 % strain. An example of the cycling test, which indicates ca. 70% recovery after the first cycle for the tetrablock sb-PP, is also provided in Figure 1.20.

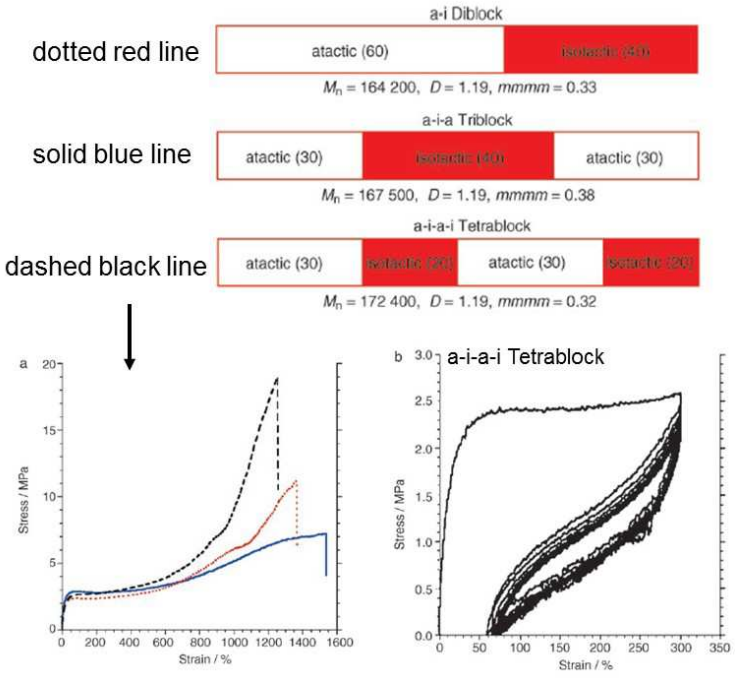

Figure 1.20: Top: representation of sb-PP block copolymers. Bottom: corresponding tensile testing (left) and cycling test (right).[81]

Previously, our group also reported on the synthesis and mechanical properties of a series of triblock isotactic-atactic-isotactic (*i*-*a*-*i*) stereoblock PP elastomers by modulating the length of the isotactic end-blocks by degenerative transfer with **16** to afford crystalline regions ranging from 1 % to 20 % isotacticity (by NMR) relative to the atactic middle block. M_n values varied from 195 kDa to 385 kDa with polydispersities ≤ 1.33. The *i*-*a*-*i*-PP materials were electrospun into fibrous mats and then evaluated for elasticity using tensile testing. It was found that ultimate tensile strengths ranged from 2.78 MPa to 15.82 MPa with maximum strain between 405 % and 2671 %.[88] It was determined that the elastomeric properties decreased with increasing isotactic content, Figure 1.21.

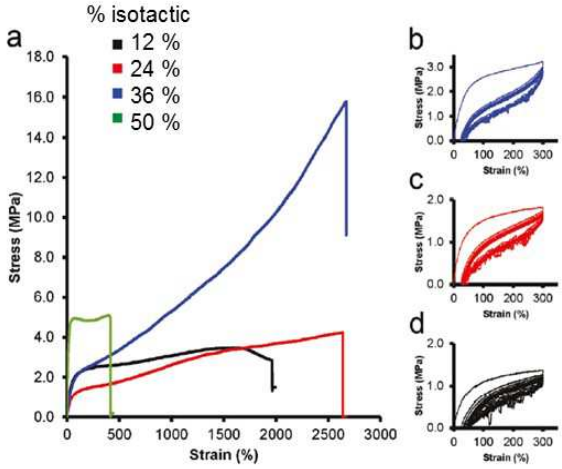

Figure 1.21: Stress v. strain plots for *i*-*a*-*i*-PP completed by Giller and coworkers.[88]

1.11. Block Copolymers

Diblock copolymer materials have been heavily studied over the past several decades. A literature search conducted in February 2015 revealed nearly 20,000 peer-reviewed journal articles, dating as far back as the 1960s, which cover a wide range of topics from biodegradable materials and drug delivery vehicles,[89] to electronic devices,[90] directed self-assembly,[91] lithography,[92, 93] composite materials and blends.[94] A more general search of 'block copolymers' revealed over 70,000 peer-reviewed articles (not including patents). At least 300 journal articles on diblock copolymers have already been reported for the current 2015 calendar year (this number does not include other types of BCPs such as star- and triblock copolymers).

The high impact and versatility of diblock copolymers can be attributed to the often facile self-assembly of the *A* and *B* segments into respective *A*-rich and *B*-rich domains, which give rise to unique physical and chemical properties with respect to their homopolymer counterparts. The synergistic behavior of the combined polymer segments present an important step forward in the synthesis of new materials. There are several books and detailed review articles on the topic of block copolymers.[95, 96] Provided here is a summarized introduction to linear BCPs with AB diblock copolymer configuration.

To start, a block copolymer (BCP) refers to a polymer chain that is composed of two or more segments (blocks) of different chemical composition. An interesting feature of BCPs is their ability to self-assemble into ordered morphologies on the nanometer scale (ca. 10-100 nm), and their inability to macrophase separate due to the chemical connectivity of the block segments. The propensity of BCPs to undergo

microphase separation rely on the interplay between two competing thermodynamic contributions, enthalpy and entropy. For example, as temperature decreases the enthalpic process of demixing is favored. However, the process of demixing comes with an entropic penalty. Thus, the overall 'strength' of microphase separation, degree of long range ordering, and type of morphology observed for a particular system are influenced by a number of contributing factors such as chemical structure, segment lengths, crystallization, the overall degree of polymerization (*N*), and environmental conditions such as temperature.

The entropic-enthalpic balance for BCPs can be described as χN where χ is the Flory-Huggins interaction parameter and *N* is the degree of polymerization. χ is inversely proportional to temperature and is often approximated by equation 5:

$$\chi = A + \frac{B}{T} \qquad (5)$$

where A and B are contributing entropic and enthalpic terms respectively, and T is the absolute temperature. Based on the inverse relationship between χ and T, the degree of phase separation can be predicted as a function of temperature (and block ratio). At sufficiently high temperatures χ becomes small resulting in the two block segments, *A* and *B*, to favor mixing over phase separation, Figure 1.22. Furthermore, the type of ordered morphology can be predicted from the plot of χN as a function of block ratio. For example, as seen in Figure 1.22 (right) the *A:B* block ratio is conveyed on the x-axis as the volume fraction of segment *A* in an *A-B* diblock copolymer. As the fraction of *A* approaches either maximum (*f* = 0 or 1) mixing is favored and no phase separation is observed. Similarly, at sufficiently low *N* the block copolymer remains in the disordered phase. The phase boundary (dashed line in

Figure 1.22) is the order to disorder transition (ODT). For a symmetric diblock copolymer ($A = B = 0.5$) the product, χN, at the ODT is ca. 10.5 representing the weak segregation limit (WSL; weakly phase separated). The ODT is often measured using rheology and small angle x-ray scattering (SAXS). The type of microphase-separated morphology observed changes as a function of block ratio. The most straightforward morphological arrangement consists of alternating layers between the incompatible *AB* block segments (lamella; L) and occurs readily in symmetric diblock copolymers with sufficient χN. As the fraction of *A* deviates from 0.5 the BCP transitions to alternative microphase-separated morphologies with increasing curvature are observed. Phase boundaries between different types of phase morphologies without entering a disordered state are referred to as order to order transitions (OOT). Hexagonally packed cylindrical (Cyl.) morphology is the second most commonly observed morphology, followed by spheres with body-centered cubic ordering (BCC), Scheme 1.16. Additional (more ambiguous) microphase-separated morphologies have also been observed; bicontinuous, gyroid and 'perforated layer' phases.

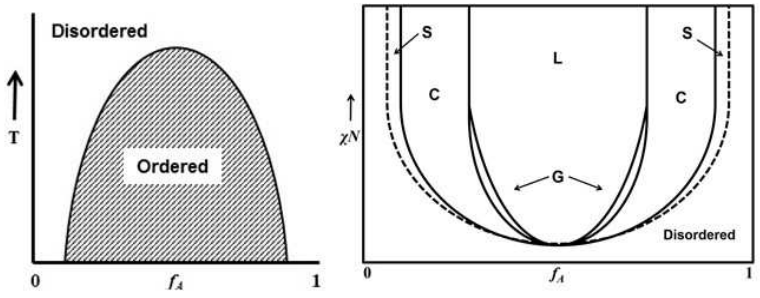

Figure 1.22: Left: mixing of AB BCP as a function of temperature and asymmetric block ratio. Right: Theoretical phase diagram of diblock copolymer system.

Scheme 1.16: Common diblock copolymer phase-separated morphologies.

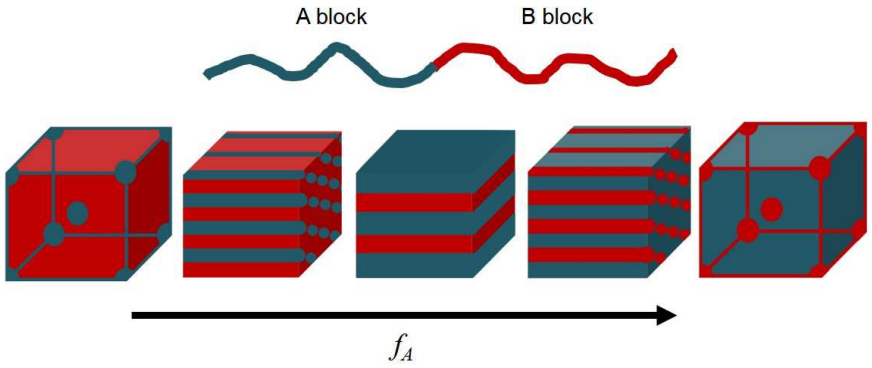

1.11.1. Pure Polyolefin Block Copolymers

While reports on BCPs, in general, are many, there are far fewer reports on BCPs composed of purely polyolefin segments. Two reasons for the dearth on olefin block copolymers (OBCs) could be the limited number of living polymerization initiators capable of producing OBCs, and that once the OBCs are formed, crystallization driven macrophase separation tends to dominate over microphase separation. When considering OBCs it is common to refer to the block segments as being either 'hard' or 'soft'. The hard blocks are composed of crystallizable or glassy segments and the soft blocks are most often low T_g, amorphous polymer segments.

The most common method for developing polyolefin-like BCPs is through post polymerization hydrogenation of styrenic block copolymers (SBCs). SBCs are generally composed of di-, tri- or multi-block with combinations of polystyrene (PS), polybutadiene (PB), polyisoprene (PI) or other similar unsaturated polymer, and are by far the most predominate type of BCP. PS has a high T_g (ca. 100 °C) and is denoted as the hard segment compared to low T_g, amorphous PB or PI. SBCs were originally developed by the Shell Chemical Co. in the 1950s, most notability as PS-*b*-

(PB or PI)-*b*-PS formally known as Kraton.[97] Kraton is an excellent thermoplastic elastomer (TPE); TPEs are the focus of Chapter 6 and will be discussed in more detail there. One of the major challenges with controlling the microphase separation of hydrogenated SBCs is their propensity to crystallize upon saturation (once hydrogenated (H), SBCs resemble C-*b*-(PE-*alt*-PP)-*b*-C or similar configuration (C = poly(methylenecyclohexane), PE = polyethylene, PP = polypropylene). The fully (or partially) saturated, semi-crystalline SBCs have been heavily studied by Bates[92, 96] and coworkers, and by Register[98-100] and coworkers. The most common phase morphology observed for the H-SBCs is crystallization driven lamella, bicontinuous or otherwise more complex phases. For example, a recent study carried out by Bates examines the phase separation and mechanical properties of tetrablock and heptablock H-SBC systems synthesized using anionic polymerization.[101] The tetrablocks and heptablocks are composed of C-*b*-PE-*b*-C-*b*-PP (CECP, XP) and CECPCEC (XPX). The segment fractions are ca. 0.25 for C and E and ca. 0.50 for P. The six listed samples have the following M_n: XPX-2a = 59 kDa, XPX-2b = 79 kDa, XPX-2c = 114 kDa, XPX-2d = 133 kDa, XPX-de = 195 kDa, and XP-2 = 86 kDa. In each case complex microstructures were observed (by TEM) and the BCPs exhibit high stress values at break (up to 35 MPa) but due to crystallization and/or ill-defined microphase separated morphologies, the elasticity is limited (elongation strain at break $\leq$ 750 %), Figure 1.23.

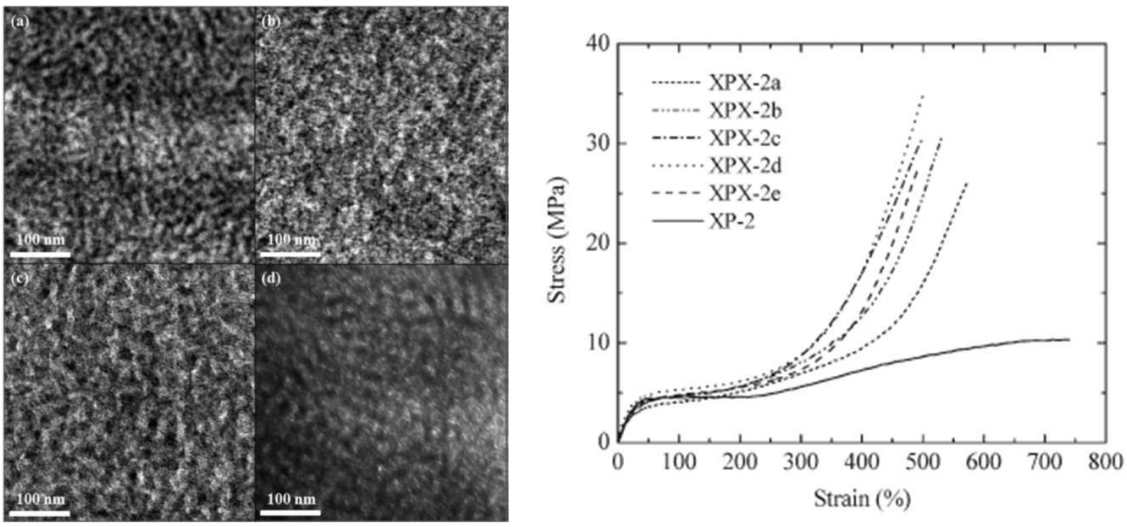

Figure 1.23: Figure reproduced from work by Bates. (Left) TEM micrographs of a) XPX-2a, b) XPX-2d, c) XPX-2e, d) XP-2. (Right) stress v. strain curve for H-SBCs.[101]

In another example, Register and coworkers employ living ring opening metathesis polymerization (ROMP) and subsequent hydrogenation for the synthesis of tri- and penta-block copolymers with the following respective configurations: crystalline-rubbery-crystalline (CRC) and crystalline-glassy-rubbery-glassy-crystalline (CGRGC), where C = polynorbornene (hPN), G = polymethyltetracyclododecene (hPMTD) and R = poly(5-hexylnorbornene) (hPHN), Figure 1.24.[100] M_n values ranged between 128 kDa to 250 kDa each with narrow polydispersity ($Đ \leq 1.1$). In all cases the rubbery block makes up a majority of the BCPs. Although the polyolefin-like BCPs possess unique chemical architectures, no microphase separation was observed and the tensile measurements are lower compared to the previous example. The maximum stress at break is ca. 15 MPa with maximum elongation at break equal to < 550 % strain, Figure 1.24.

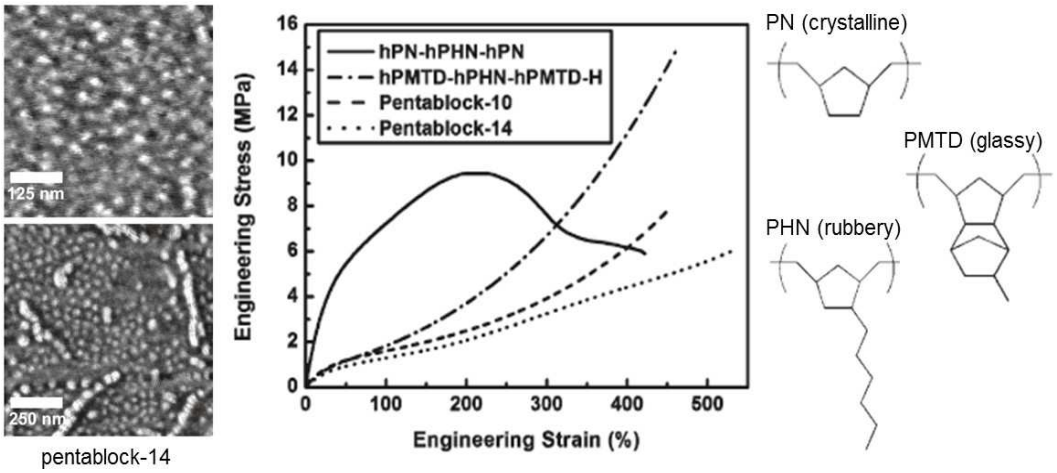

Figure 1.24: Figure reproduced from Register and coworkers. (Left) AFM phase maps before (top) and after (bottom) annealing. (Right) stress v. strain curve for BCPs.[100]

Efforts to mitigate crystallization of polyolefin block segments has also been studied in detail.[99, 102, 103] Here, coordination polymerization (CP) is employed for the synthesis of blocky copolymer – BCPs using α-olefins such as ethylene, propene and higher alkenes. There are two primary BCP configurations that represent these blocky structures. The first is stereoblock polyolefin (most notably as sb-PP; see Section 1.10 for examples reported by the Sita group). In this case, differences in the stereochemical microstructure within a single polymer chain gives rise to block structures such as iPP-aPP-iPP (polypropylene with alternating isotactic and atactic segments). Although the number of reports on sb-PP and its role as a TPE have increased in the past several years, there are two specific examples noted here in addition to the previously described reports by our group (Section 1.10). Coates and Waymouth[104] reported a series of atactic-isotactic sb-PP elastomers using oscillatory stereocontrol with single-sight coordination polymerization. While the report is limiting with respect to the discussion of the observed mechanical properties, one

particular sample was presented as having an ultimate tensile strength and maximum strain at break of 462 psi (3.19 MPa) and 1210 %, respectively (M_w 330 kDa; 16.1 % isotactic content). Auriemma[105] and co-workers reported significant improvement on the tensile strength of atactic-isotactic sb-PP (ca. 130 MPa - 180 MPa) albeit at the cost of maximum tensile strain (ca. 280 % - 950 %), by increasing the percent isotacticity (M_w 200 kDa - 220 kDa; up to 44 % isotactic content).

The second configuration type consists of a single homopolymer such as PE with segments of copolymer (i.e. PE-copolymer with varying ratios of copolymer from one end of the polymer chain to the other). The more copolymer added in each segment the lower the crystallizability of the 'crystalline' segment. An example of this are the blocky PE/PolyO BCPs (PolyO = polyoctene) introduced by the Dow Chemical Co. in 2006.[106] Numerous other reports of PE-polyolefin blocky copolymers have also been reported.[103, 107, 108] Although the formation of well-defined block segments in these blocky BCPs has been clearly established, microphase separation beyond crystallization driven lamella or other complex morphologies have not been well reported.

In addition to the two primary BCP configurations described above, studies on polyolefin-hybrid BCPs have been reported wherein two separate polymerization methods are utilized to form polyolefin-*graft*-polymer BCPs. The non-polyolefin segment may be polystyrene, polyacrylates, or other polymers of interest.[108, 109] Graft BCPs (as well as blocky copolymers and stereoblocks) are not part of the thesis research and will not be discussed further.

To date, pure polyolefin BCPs that readily exhibit microphase separation without the presence of crystallization have yet to be reported. Thus, there is a need to better understand the microphase separation behavior of well-defined pure polyolefin BCPs. To this end, preliminary results on the microphase separation of amorphous, glassy-rubbery AB diblock polyolefin copolymers constructed using Sita catalysts will be the central focus of the research presented in Chapter 5. Further, details regarding the first ABA triblock copolymer that employs glassy poly(methylene-1,3-cyclohexane) as the A segments and the inherent elastomeric properties will be discussed in Chapter 6.

The research presented in the subsequent Chapters serve as the first report of the living cyclopolymerization of 1,6-HD for the formation of *cis*-poly(methylene-1,3-cyclohexane) and its subsequent use in degenerative methyl group transfer, and block copolymers. This work has led to the publication of two first author reports in peer-reviewed journals with additional reports in preparation.

1.12. References

1. http://marketsandmarkets.com/PressReleases/polyolefins.asp. Polyolefins Market. Accessed 02252015.
2. Pruitt, M. E.; Baggett, J. M. Catalysts for the polymerization of olefin oxides. US2706181, 1955.
3. Kuran, W., *Principles of Coordination Polymerisation*. John Wiley & Sons: 2001; p 544 pp.
4. Ziegler, K.; Holzkamp, E.; Breil, H.; Martin, H., *Angew. Chem.* **1955**, *67*, 426.

5. Ziegler, K., *Angew. Chem.* **1964**, *76* (13), 545-553.

6. Natta, G.; Pino, P.; Corradini, P.; Danusso, F.; Mantica, E.; Mazzanti, G.; Moraglio, G., *J. Am. Chem. Soc.* **1955**, *77*, 1708-1710.

7. Natta, G., *J. Polym. Sci.* **1959**, *34* (127), 531-549.

8. Natta, G.; Pasquon, I.; Zambelli, A., *J. Am. Chem. Soc.* **1962**, *84*, 1488-1490.

9. Arlman, E. J.; Cossee, P., *J. Catal.* **1964,** *3* (1), 99-104.

10. Cossee, P., *J. Catal.* **1964,** *3* (1), 80-88.

11. Breslow, D. S.; Newburg, N. R., *J. Am. Chem. Soc.* **1957**, *79*, 5072-5073.

12. a) Andresen, A.; Cordes, H. G.; Herwig, J.; Kaminsky, W.; Merck, A.; Mottweiler, R.; Pein, J.; Sinn, H.; Vollmer, H. J., *Angew. Chem.* **1976**, *88* (20), 689-690.; b) Sinn, H.; Kaminsky, W.; Vollmer, H. J.; Woldt, R., *Angew. Chem.* **1980**, *92* (5), 396-402.; c) Sinn, H.; Kaminsky, W., *Adv. Organomet. Chem.* **1980**, *18*, 99-149.; d) Kaminsky, W.; Miri, M.; Sinn, H.; Woldt, R., *Makromol. Chem., Rapid Commun.* **1983**, *4* (6), 417-421.

13. Ewen, J. A., *J. Am. Chem. Soc.* **1984**, *106* (21), 6355-6364.

14. Kaminsky, W.; Buschermoehle, M., *NATO ASI Ser., Ser. C* **1987,** *215* (Recent Adv. Mech. Synth. Aspects Polym.), 503-514.

15. Kaminsky, W.; Kuelper, K.; Brintzinger, H. H.; Wild, F. R. W. P., *Angew. Chem. Int. Ed.* **1985**, *97* (6), 507-508.

16. a) Smith, J. A.; Brintzinger, H. H., *J. Organomet. Chem.* **1981**, *218* (2), 159-167.; b) Wild, F. R. W. P.; Zsolnai, L.; Huttner, G.; Brintzinger, H. H., *J. Organomet. Chem.* **1982**, *232* (3), 233-247.

17. Smith, J. A.; Von Seyerl, J.; Huttner, G.; Brintzinger, H. H., *J. Organomet. Chem.* **1979**, *173* (2), 175-185.

18. Raith, A.; Altmann, P.; Cokoja, M.; Herrmann, W. A.; Kuehn, F. E., *Coord. Chem. Rev.* **2010**, *254* (5-6), 608-634; McKnight, A. L.; Waymouth, R. M., *Chem. Rev.* **1998**, *98* (7), 2587-2598.

19. Baugh, L. S.; Canich, J. A. M.; Editors, *Stereoselective Polymerization with Single-Site Catalysts*. CRC Press LLC: 2008; pp. 677.

20. Antberg, M.; Dolle, V.; Haftka, S.; Rohrmann, J.; Spaleck, W.; Winter, A.; Zimmermann, H. J., *Makromol. Chem., Macromol. Symp.* **1991**, *48-49*, 333-347.

21. Ewen, J. A.; Jones, R. L.; Razavi, A.; Ferrara, J. D., *J. Am. Chem. Soc.* **1988**, *110* (18), 6255-6256.

22. Miller, S. A.; Bercaw, J. E., *Organometallics* **2006**, *25* (15), 3576-3592.

23. a) Veghini, D.; Henling, L. M.; Burkhardt, T. J.; Bercaw, J. E., *J. Am. Chem. Soc.* **1999**, *121* (3), 564-573.; b) Keaton, R. J.; Sita, L. R., *J. Am. Chem. Soc.* **2002**, *124* (31), 9070-9071.; c) Price, C. J.; Irwin, L. J.; Aubry, D. A.; Miller, S. A. In *Fluorenyl-containing catalysts for stereoselective propylene polymerization*, CRC Press LLC: 2008; pp 37-82.

24. Hiemenz, P. C.; Lodge, T. P., *Polymer Chemistry*. 2nd ed.; Wiley: Boca Raton, FL, 2007; p 465-500.

25. Drobny, J. G., *Handbook of Thermoplastic Elastomers*. William Andrew Publications: New York, NY, 2007; p 1-8.

26. Henschke, O.; Koller, F.; Arnold, M., *Macromol. Rapid Commun.* **1997**, *18* (7), 617-623.

27. Coates, G.; Hustad, P.; Reinartz, S., *Angew. Chem. Int. Ed.* **2002**, *41* (13), 2236-2257.

28. Domski, G. J.; Rose, J. M.; Coates, G. W.; Bolig, A. D.; Brookhart, M., *Prog. Polym. Sci.* **2007**, *32* (1), 30-92.

29. Szwarc, M., *Nature* **1956**, *178*, 1168-1169.

30. Szwarc, M.; Levy, M.; Milkovich, R., *J. Am. Chem. Soc.* **1956**, *78*, 2656-2567.

31. a) Kato, M.; Kamigaito, M.; Sawamoto, M.; Higashimura, T., *Macromolecules* **1995**, *28* (5), 1721-1723.; b) Matyjaszewski, K.; Gaynor, S.; Greszta, D.; Mardare, D.; Shigemoto, T., *J. Phys. Org. Chem.* **1995**, *8* (4), 306-315.; c) Mueller, A. H. E.; Zhuang, R.; Yan, D.; Litvinenko, G., *Macromolecules* **1995**, *28* (12), 4326-4333.; d) Chiefari, J.; Chong, Y. K.; Ercole, F.; Krstina, J.; Jeffery, J.; Le, T. P. T.; Mayadunne, R. T. A.; Meijs, G. F.; Moad, C. L.; Moad, G.; Rizzardo, E.; Thang, S. H., *Macromolecules* **1998**, *31* (16), 5559-5562.; e) Kamigaito, M.; Ando, T.; Sawamoto, M., *Chem. Rev.* **2001**, *101* (12), 3689-3745.

32. Wang, J.-S.; Matyjaszewski, K., *J. Am. Chem. Soc.* **1995**, *117* (20), 5614-515; Wang, J.-S.; Matyjaszewski, K., *Macromolecules* **1995**, *28* (23), 7901-7910.

33. Webster, O. W., *Science* **1991**, *251* (4996), 887-893.

34. Jordan, R.; Ulman, A., *J. Am. Chem. Soc.* **1998**, *120* (2), 243-247.

35. Braunecker, W. A.; Matyjaszewski, K., *Prog. Polym. Sci.* **2007**, *32* (1), 93-146.

36. a) Lynn, D. M.; Kanaoka, S.; Grubbs, R. H., *J. Am. Chem. Soc.* **1996**, *118* (4), 784-790.; b) Connor, E. F.; Nyce, G. W.; Myers, M.; Moeck, A.; Hedrick, J. L., *J. Am. Chem. Soc.* **2002**, *124* (6), 914-915.

37. Doi, Y.; Ueki, S.; Keii, T., *Macromolecules* **1979**, *12* (5), 814-821.

38. a) Scollard, J. D.; McConville, D. H., *J. Am. Chem. Soc.* **1996**, *118* (41), 10008-10009.; b) Liang, L.-C.; Schrock, R. R.; Davis, W. M.; McConville, D. H., *J. Am. Chem. Soc.* **1999**, *121* (24), 5797-5798.

39. Knight, K. S.; Wang, D.; Waymouth, R. M.; Ziller, J., *J. Am. Chem. Soc.* **1994**, *116* (5), 1845-1854.

40. a) Matsui, S.; Mitani, M.; Saito, J.; Tohi, Y.; Makio, H.; Tanaka, H.; Fujita, T., *Chem. Lett.* **1999**, (12), 1263-1264.; b) Mitani, M.; Mohri, J.; Yoshida, Y.; Saito, J.; c) Ishii, S.; Tsuru, K.; Matsui, S.; Furuyama, R.; Nakano, T.; Tanaka, H.; Kojoh, S.-i.; Matsugi, T.; Kashiwa, N.; Fujita, T., *J. Am. Chem. Soc.* **2002**, *124* (13), 3327-3336.

41. Tshuva, E. Y.; Goldberg, I.; Kol, M.; Goldschmidt, Z., *Inorg. Chem. Commun.* **2000**, *3* (11), 611-614.

42. Jayaratne, K. C.; Keaton, R. J.; Henningsen, D. A.; Sita, L. R., *J. Am. Chem. Soc.* **2000**, *122* (42), 10490-10491.

43. Jayaratne, K. C.; Sita, L. R., *J. Am. Chem. Soc.* **2000**, *122* (5), 958-959.

44. a) Hagihara, H.; Shiono, T.; Ikeda, T., *Macromolecules* **1998**, *31* (10), 3184-3188.; b) Hasan, T.; Ioku, A.; Nishii, K.; Shiono, T.; Ikeda, T., *Macromolecules* **2001**, *34* (10), 3142-3145.; c) Hasan, T.; Ioku, A.; Nishii, K.; Shiono, T.; Ikeda, T., *Macromolecules* **2001**, *34* (17), 6152.; d) Nishii, K.; Shiono, T.; Ikeda, T., *Macromol.*

Rapid Commun. **2004**, *25* (10), 1029-1032.; e) Makio, H.; Kashiwa, N.; Fujita, T., *Adv. Synth. Catal.* **2002**, *344* (5), 477-493.; f) Makio, H.; Fujita, T. In *Stereoselective propylene polymerization with early and late transition metal catalysts*, CRC Press LLC: 2008; pp 157-168.; g) Schellenberg, J., *Prog. Polym. Sci.* **2009**, *34* (8), 688-718.; h) Terao, H.; Nagai, N.; Fujita, T., *Yuki Gosei Kagaku Kyokaishi* **2008**, *66* (5), 444-457.

45. Yeori, A.; Goldberg, I.; Shuster, M.; Kol, M., *J. Am. Chem. Soc.* **2006**, *128* (40), 13062-13063.

46. Keaton, R. J.; Jayaratne, K. C.; Fettinger, J. C.; Sita, L. R., *J. Am. Chem. Soc.* **2000,** *122* (51), 12909-12910.

47. Jayaratne, K. C.; Sita, L. R., *J. Am. Chem. Soc.* **2001**, *123* (43), 10754-10755.

48. Zhang, Y.; Keaton, R. J.; Sita, L. R., *J. Am. Chem. Soc.* **2003**, *125* (30), 9062-9069.

49. Keaton, R. J.; Jayaratne, K. C.; Henningsen, D. A.; Koterwas, L. A.; Sita, L. R., *J. Am. Chem. Soc.* **2001**, *123* (25), 6197-6198.

50. Zhang, Y.; Sita, L. R., *Chem. Commun.* **2003**, (18), 2358-2359.

51. Zhang, Y.; Reeder, E. K.; Keaton, R. J.; Sita, L. R., *Organometallics* **2004**, *23* (14), 3512-3520.

52. Zhang, W.; Sita, L. R., *J. Am. Chem. Soc.* **2008**, *130* (2), 442-443.

53. a) Zhang, W.; Wei, J.; Sita, L. R., *Macromolecules* **2008**, *41* (21), 7829-7833.; b) Wei, J.; Zhang, W.; Sita, L. R., *Angew. Chem., Int. Ed.* **2010,** *49* (10), 1768-1772.

54. Wei, J.; Zhang, W.; Wickham, R.; Sita, L. R., *Angew. Chem., Int. Ed.* **2010**, *49* (48), 9140-9144.

55. Kim, I. In *Tactic nonconjugated diene cyclopolymerization and cyclocopolymerization*, CRC Press LLC: 2008; pp 489-507.

56. Kim, I.; Shin, Y. S.; Lee, J. K.; Won, M.-S., *J. Polym. Sci. A1* **2000**, *38* (9), 1520-1527.

57. Marvel, C. S.; Stille, J. K., *J. Am. Chem. Soc.* **1958**, *80* (7), 1740-1744.

58. Resconi, L.; Waymouth, R. M., *J. Am. Chem. Soc.* **1990**, *112* (12), 4953-4954.

59. a) Resconi, L.; Coates, G. W.; Mogstad, A.; Waymouth, R. M., *J. Macromol. Sci. Chem.* **1991**, *A28* (11-12), 1225-1234.; b) Coates, G. W.; Waymouth, R. M., *J. Am. Chem. Soc.* **1993**, *115* (1), 91-98.

60. Coates, G. W.; Waymouth, R. M., *J. Mol. Catal.* **1992**, *76* (1-3), 189-194.

61. a) Naga, N.; Yabe, T.; Sawaguchi, A.; Sone, M.; Noguchi, K.; Murase, S., *Macromolecules* **2008**, *41* (20), 7448-7452.; b) Naga, N.; Shimura, H.; Sone, M., *Macromolecules* **2009**, *42* (20), 7631-7633.

62. Han, S.; Yao, E.; Qin, W.; Zhang, S.; Ma, Y., *Macromolecules* **2012**, *45* (10), 4054-4059.

63. Sernetz, F. G.; Muelhaupt, R.; Waymouth, R. M., *Polym. Bull.* **1997**, *38* (2), 141-148.

64. a) Doi, Y.; Tokuhiro, N.; Soga, K., *Makromol. Chem.* **1989**, *190* (3), 643-651.; b) Jeong, H. M.; Song, J. H.; Chi, K. W.; Kim, I.; Kim, K. T., *Polym. Int.* **2002**, *51* (4), 275-280.

65. Pan, Y.; Xu, T.; Ge, Y.-S.; Lu, X.-B., *Organometallics* **2011**, *30* (21), 5687-5694.

66. Naga, N.; Toyota, A., *Macromol. Rapid Commun.* **2004**, *25* (18), 1623-1627.

67. Takeuchi, D.; Osakada, K., *Polymer* **2008**, *49* (23), 4911-4924.

68. Shi, X.-c.; Wang, Y.-x.; Liu, J.-y.; Cui, D.-m.; Men, Y.-f.; Li, Y.-s., *Macromolecules* **2011**, *44* (4), 1062-1065.

69. Naga, N.; Shiono, T.; Ikeda, T., *Macromol. Chem. Phys.* **1999**, *200* (6), 1466-1472.

70. a) Pietikainen, P.; Vaananen, T.; Seppala, J. V., *Eur. Poly. J.* **1999**, *35* (6), 1047-1055.; b) Pietikainen, P.; Seppala, J. V.; Ahjopalo, L.; Pietila, L. O., *Eur. Polym. J.* **2000**, *36* (1), 183-192.; c) Naga, N.; Imanishi, Y., *Macromol. Chem. Phys.* **2002**, *203* (15), 2155-2162.; d) Williamson, A.; Fink, G., *Macromol. Chem. Physic.* **2003**, *204* (9), 1178-1190.; e) Marques, M. D. V.; Ramos, D.; Rego, J. D., *Eur. Polym. J.* **2004**, *40* (11), 2583-2589.; f) Naga, N.; Okada, S.; Imanishi, Y., *Polymer* **2004**, *45* (1), 117-124.; g) Sarzotti, D. M.; Narayan, A.; Whitney, P. M.; Simon, L. C.; Soares, J. B. P., *Macromol. Mater. Eng.* **2005**, *290* (6), 584-591.; h) Park, E. S., *J. Appl. Polym. Sci.* **2008**, *109* (6), 3631-3638.

71. Apisuk, W.; Nomura, K., *Macromol. Chem. Physic.* **2014**, *215* (18), 1785-1791.

72. a) Naga, N.; Shiono, T.; Ikeda, T., *Macromolecules* **1999**, *32* (5), 1348-1355.; b) Arnold, M.; Bornemann, S.; Knorr, J.; Schimmel, T. In *Metallocene catalyzed copolymerization of propene with mono- and diolefins*, Springer-Verlag: 2001; pp 353-364.; c) Song, F.; Pappalardo, D.; Johnson, A. F.; Rieger, B.; Bochmann, M., *J. Polym. Sci. A1* **2002**, *40* (10), 1484-1497.; d) Paavola, S.; Saarinen, T.; Lofgren, B.; Pitkanen, P., *Polymer* **2004**, *45* (7), 2099-2110.; e) Ye, Z. B.; AlObaidi, F.; Zhu, S. P., *Industrial & Engineering Chemistry Research* **2004**, *43* (11), 2860-2870.; f) Lima,

A.; Azeredo, A. P.; Nele, M.; Liberman, S.; Pinto, J. C., *Macromol. Symp.* **2014**, *344* (1), 86-93.

73. Nomura, K.; Liu, J.; Fujiki, M.; Takemoto, A., *J. Am. Chem. Soc.* **2007**, *129* (46), 14170-14170.

74. Hustad, P. D.; Tian, J.; Coates, G. W., *J. Am. Chem. Soc.* **2002**, *124* (14), 3614-3621.

75. a) Takeuchi, D.; Matsuura, R.; Fukuda, Y.; Osakada, K., *Dalton T.* **2009**, (41), 8955-8962.; b) Takeuchi, D., *Macromol. Chem. Physic* **2011**, *212* (15), 1545-1551.

76. Takeuchi, D.; Matsuura, R.; Park, S.; Osakada, K., *J. Am. Chem. Soc.* **2007**, *129* (22), 7002-7004.

77. Edson, J. B.; Coates, G. W., *Macromol. Rapid Commun.* **2009**, *30* (22), 1900-1906.

78. a) Guo, F.; Nishiura, M.; Li, Y.; Hou, Z. M., *Sci. China Ser. B.* **2014**, *57* (8), 1150-1156.; b) Guo, F.; Nishiura, M.; Koshino, H.; Hou, Z. M., *Macromolecules* **2011**, *44* (8), 2400-2403.

79. Guo, F.; Nishiura, M.; Li, Y.; Hou, Z. M., *Chem.-Asian J.* **2013**, *8* (10), 2471-2482.

80. Crawford, K. E.; Sita, L. R., *J. Am. Chem. Soc.* **2013**, *135* (24), 8778-8781.

81. Harney, M. B.; Zhang, Y.; Sita, L. R., *Angew. Chem., Int. Ed.* **2006**, *45* (15), 2400-2404.

82. a) Harney, M. B.; Keaton, R. J.; Fettinger, J. C.; Sita, L. R., *J. Am. Chem. Soc.* **2006**, *128* (10), 3420-3432.; b) Kissounko, D. A.; Fettinger, J. C.; Sita, L. R., *Inorg. Chim. Acta* **2003**, *345*, 121-129.

83. Zhang, W.; Sita, L. R., *Adv. Synth. Catal.* **2008**, *350* (3), 439-447.

84. Kissounko, D. A.; Zhang, Y.; Harney, M. B.; Sita, L. R., *Adv. Synth. Catal.* **2005**, *347* (2), 426-432.

85. Zhang, Y.; Sita, L. R., *J. Am. Chem. Soc.* **2004**, *126* (25), 7776-7777.

86. Harney, M. B.; Zhang, Y.; Sita, L. R., *Angew. Chem., Int. Ed.* **2006**, *45* (37), 6140-6144.

87. Sita, L. R., *Angew. Chem., Int. Ed.* **2009**, *48* (14), 2464-2472.

88. Giller, C.; Gururajan, G.; Wei, J.; Zhang, W.; Hwang, W.; Chase, D. B.; Rabolt, J. F.; Sita, L. R., *Macromolecules* **2011**, *44* (3), 471-482.

89. Gref, R.; Domb, A.; Quellec, P.; Blunk, T.; Mueller, R. H.; Verbavatz, J. M.; Langer, R., *Adv. Drug Delivery Rev.* **1995**, *16* (2,3), 215-233.

90. Segalman, R. A.; Yokoyama, H.; Kramer, E. J., *Adv. Mater.* **2001**, *13* (15), 1152-1155.

91. a) Lin, Y.; Boeker, A.; He, J.; Sill, K.; Xiang, H.; Abetz, C.; Li, X.; Wang, J.; Emrick, T.; Long, S.; Wang, Q.; Balazs, A.; Russell, T. P., *Nature* **2005**, *434* (7029), 55-59.; b) Stoykovich, M. P.; Mueller, M.; Kim, S. O.; Solak, H. H.; Edwards, E. W.; de Pablo, J. J.; Nealey, P. F., *Science* **2005**, *308* (5727), 1442-1446.

92. Park, M.; Harrison, C.; Chaikin, P. M.; Register, R. A.; Adamson, D. H., *Science* **1997**, *276* (5317), 1401-1404.

93. Evens, G. G.; Pijpers, E. M. J., *MMI Press Symp. Ser.* **1983**, *4* (Transition Met. Catal. Polym.: Alkens Dienes, Pt. A), 245-264.

94. a) Xie, H.-Q.; Liu, D.-G.; Xie, D.; Guan, J.-G., *J. Appl. Polym. Sci.* **2006**, *99* (4), 1887-1894.; b) Pascault, J. P.; Girard-Reydet, E., *Polym. Prepr. (Am. Chem. Soc., Div. Polym. Chem.)* **1999**, *40* (2), 1092-1093.

95. a) Shin, J.; Kim, Y.-W.; Kim, G.-J., *Kongop Hwahak* **2014**, *25* (2), 121-133.; b) Ramanathan, M.; Tseng, Y.-C.; Ariga, K.; Darling, S. B., *J. Mater. Chem. C* **2013**, *1* (11), 2080-2091.; c) Hillmyer, M., *Curr. Opin. Solid State Mater. Sci.* **2000**, *4* (6), 559-564.; d) Bates, F. S.; Fredrickson, G. H., *Phys. Today* **1999**, *52* (2), 32-38.; e) Bates, F. S.; Fredrickson, G. H., *Annu. Rev. Phys. Chem.* **1990**, *41*, 525-557.; e) Diaz, R. H.; Ferguson, A. P.; Editors, *Block Copolymers: Phase Morphology, Material Applications and Future Challenges*. Nova Science Publishers, Inc.: 2014; p 188.; f) Takenaka, M.; Hasegawa, H.; Editors, *Self-Assembly of Block Copolymers: Its Science and Technology*. Shi Emu Shi Shuppan Co., Ltd.: 2013; p 231.

96. Bates, F. S., *Science* **1991**, *251* (4996), 898-905.

97. Drobny, J. G., *Handbook of Thermoplastic Elastomers*. William Andrew Pub.: New York, 2007.

98. a) Harada, T.; Bates, F. S.; Lodge, T. P., *Macromolecules* **2003**, *36* (15), 5440-5442.; b) Xu, J. J.; Nguyen, B. T.; Bates, F. S.; Hahn, S. F.; Hudack, M. L., *J. Polym. Sci., Part B: Polym. Phys.* **2003**, *41* (7), 725-735.; c) Xu, J. J.; Bates, F. S., *Macromolecules* **2003**, *36* (14), 5432-5434.; d) Meuler, A. J.; Hillmyer, M. A.; Bates, F. S., *Polym. Prepr. (Am. Chem. Soc., Div. Polym. Chem.)* **2007**, *48* (2), 417-418.; e) Alfonzo, C. G.; Fleury, G.; Chaffin, K. A.; Bates, F. S., *Macromolecules* **2010**, *43*

(12), 5295-5305.; f) Mansour, A. S.; Lodge, T. P.; Bates, F. S., *J. Polym. Sci., Part B: Polym. Phys.* **2012**, *50* (10), 706-717.; g) Lee, I.; Panthani, T. R.; Bates, F. S., *Macromolecules* **2013**, *46* (18), 7387-7398.; h) Lee, I.; Bates, F. S., *Macromolecules* **2013**, *46* (11), 4529-4539.; i) Rangarajan, P.; Register, R. A.; Fetters, L. J.; Bras, W.; Naylor, S.; Ryan, A. J., *Macromolecules* **1995**, *28* (14), 4932-4938.; j) Angelescu, D. E.; Waller, J. H.; Adamson, D. H.; Deshpande, P.; Chou, S. Y.; Register, R. A.; Chaikin, P. M., *Adv. Mater.* **2004**, *16* (19), 1736-1740.; k) Adams, J. L.; Quiram, D. J.; Graessley, W. W.; Register, R. A.; Marchand, G. R., *Macromolecules* **1996**, *29* (8), 2929-2938.; l) Adams, J. L.; Graessley, W. W.; Register, R. A., *Macromolecules* **1994**, *27* (21), 6026-6032.; m) Sebastian, J. M.; Graessley, W. W.; Register, R. A., *J. Rheol.* **2002**, *46* (4), 863-879; Hatjopoulos, J. D.; Register, R. A., *Macromolecules* **2005**, *38* (24), 10320-10322.

99. a) Mori, Y.; Lim, L. S.; Bates, F. S., *Macromolecules* **2003**, *36* (26), 9879-9888.; b) Lim, L. S.; Harada, T.; Hillmyer, M. A.; Bates, F. S., *Macromolecules* **2004**, *37* (16), 5847-5850.; c) Koo, C. M.; Wu, L.; Lim, L. S.; Mahanthappa, M. K.; Hillmyer, M. A.; Bates, F. S., *Macromolecules* **2005**, *38* (14), 6090-6098.; d) Phatak, A.; Lim, L. S.; Reaves, C. K.; Bates, F. S., *Macromolecules* **2006**, *39* (18), 6221-6228.; e) Myers, S. B.; Register, R. A., *Macromolecules* **2009**, *42* (17), 6665-6670.

100. Bishop, J. P.; Register, R. A., *Macromolecules* **2010**, *43* (11), 4954-4960.

101. Zuo, F.; Alfonzo, C. G.; Bates, F. S., *Macromolecules* **2011**, *44* (20), 8143-8153.

102. a) Chung, T. C.; Xu, G.; Lu, Y.; Hu, Y., *Macromolecules* **2001**, *34* (23), 8040-8050.; b) Coates, G. W.; Hustad, P. D.; Reinartz, S., *Angew. Chem., Int. Ed.* **2002**, *41*

(13), 2236-2257.; c) Ver Strate, G.; Cozewith, C.; West, R. K.; Davis, W. M.; Capone, G. A., *Macromolecules* **1999**, *32* (12), 3837-3850.; d) Wardhaugh, L. T.; Williams, M. C., *Polym. Eng. Sci.* **1995**, *35* (1), 18-27.

103. Chung, T. C. M., *Macromolecules* **2013**, *46* (17), 6671-6698.

104. Coates, G. W.; Waymouth, R. M., *Science* **1995**, *267* (5195), 217-219.

105. Auriemma, F.; De Rosa, C.; Corradi, M., *Adv. Mater.* **2007**, *19* (6), 871-874.

106. a) Arriola, D.; Carnahan, E.; Hustad, P.; Kuhlman, R.; Wenzel, T., *Science* **2006**, *312* (5774), 714-719.; b) Hotta, A.; Cochran, E.; Ruokolainen, J.; Khanna, V.; Fredrickson, G. H.; Kramer, E. J.; Shin, Y.-W.; Shimizu, F.; Cherian, A. E.; Hustad, P. D.; Rose, J. M.; Coates, G. W., *Proc. Natl. Acad. Sci. U. S. A.* **2006**, *103* (42), 15327-15332.

107. a) Jones, T. D.; Macosko, C. W.; Moon, B.; Hoye, T. R., *Polymer* **2004**, *45* (12), 4189-4201.; b) Xiao, A.; Zhou, S.; Liu, Q., *Polym.-Plast. Technol. Eng.* **2014**, *53* (17), 1832-1837.; c) Ye, Z.; Xu, L.; Dong, Z.; Xiang, P., *Chem. Commun.* **2013**, *49* (56), 6235-6255.

108. Zhao, Y.; Shi, X.; Gao, H.; Zhang, L.; Zhu, F.; Wu, Q., *J. Mater. Chem.* **2012**, *22* (12), 5737-5745.

109. a) Kuo, J.-C.; Lin, W.-F.; Yu, C.-H.; Tsai, J.-C.; Wang, T.-C.; Chung, T.-M.; Ho, R.-M., *Macromolecules* **2008**, *41* (21), 7967-7977.; b) Boardman, B. M.; Bazan, G. C., *Acc. Chem. Res.* **2009**, *42* (10), 1597-1606.; c) Chung, T. C. M., *Adv. Polym. Sci.* **2013**, *258* (Polyolefins: 50 Years after Ziegler and Natta II), 233-278.; d) Hong, S. C.; Jia, S.; Teodorescu, M.; Kowalewski, T.; Matyjaszewski, K.; Gottfried, A. C.; Brookhart, M., *J. Polym. Sci., Part A: Polym. Chem.* **2002**, *40* (16), 2736-2749.; e)

Stehling, U. M.; Malmstroem, E. E.; Waymouth, R. M.; Hawker, C. J., *Macromolecules* **1998**, *31* (13), 4396-4398.

110. Fontaine, P. P.; Epshteyn, A.; Zavalij, P. Y.; Sita, L. R., *J. Organomet. Chem.* **2007**, *692* (21), 4683-4689.

Chapter 2

Living Coordination Cyclopolymerization of Non-Conjugated Dienes

2.1. Introduction

Polyolefins have become ubiquitous in everyday life, yet surprisingly their use remains limited by the inherently low glass transition temperature (T_g) observed with common polyolefin materials. The T_g is an important bulk property that is a limiting factor when considering service temperature of a polymer. Recalling from Chapter 1; Section 1.6, restricting movement of the polymer backbone by introducing cyclic structures will increase the T_g and thus will further expand the number of available applications for polyolefins. Briefly, the glass transition is the temperature at which a polymer material transitions from a glassy to a rubber-like state (when decreasing from high to low temperature). Polymer's with glass transitions near 100 °C are considered thermoplastics. Commodity thermoplastics such as polystyrene (PS), poly(methyl methacrylate) (PMMA) and polycarbonate (PC) are widely used materials due in-part to their inherent glass transitions (which are near 100 °C). The approximate T_g's for these polymers are: PS = 100 °C, PMMA = 110 °C and PC = 145 °C.[1] It is of interest to develop a pure polyolefin that also exhibits a T_g near 100 °C. One method to achieve this may be through the living coordination of non-conjugated dienes. For examples, the cyclopolymerization of 1,5-hexadiene gives

poly(methylene-1,3-cyclopentane) (PMCP) with a T_g around -20 °C - 10 °C. Coates and coworkers reported the non-living cyclopolymerization of 1,6-heptadiene to afford poly(methylene-1,3-cyclohexane) (PMCH) with a glass transition of 103.9 °C.[2] Preliminary work by the Sita group for the cyclopolymerization of 1,5-hexadiene by Sita catalysts **1** and **2**, when activated by **II**, has been shown to be successful; however, additional studies are warranted.

Therefore, the current Chapter provides a discussion regarding the experimental results from the cyclopolymerization of 1,6-HD using precatalysts **1**, **2**, and **3** activated by **II**, Scheme 2.1. Experimental details regarding the cyclopolymerization of 1,5-HD and 1,7-OD will also be presented, but to a much lesser extent as these later two monomers have already been reported extensively and were thus not the primary focus of this work. The work presented in this chapter was completed by Crawford unless otherwise noted. There are sections of this chapter, particularly figures and experimental details that have been reproduced from the following published work: Crawford, K. E. and Sita, L. R. *J. Am. Chem. Soc.* **2013**, *135*, 8778-8781.[3]

Scheme 2.1: Reaction of Precatalyst (**1**, **2** or **3**) activated by **II** for cyclopolymerization of 1,6-HD.[3]

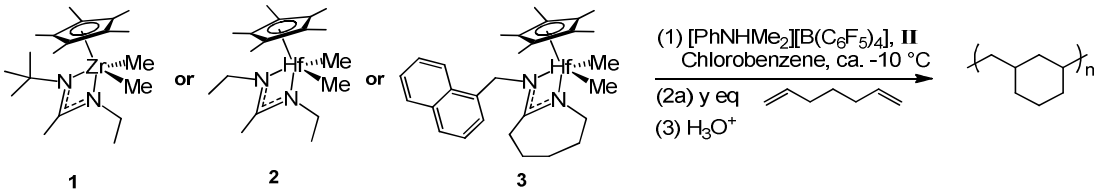

2.2. Cyclopolymerization of 1,6-Heptadiene, 1,6-HD

The PMCH material that results from the cyclopolymerization of 1,6-HD with **1a** is an opaque powder while PMCH from cationic initiators **2a** and **3a** are transparent and have the consistency of a rigid glass. In all cases the product yields were near quantitative, a notable result considering the limited success reported for the cyclopolymerization of 1,6-HD with other systems. Each sample was carefully analyzed using SEC, NMR, DSC, TGA, and WAXD. The results from these characterization methods are discussed here. PMCH samples that were polymerized using **1**, **2**, or **3** (activated by **II** to form **1a**, **2a** and **3a** respectively) will be denoted as samples 1, 2 and 3. Sample 1 was only sparingly soluble in organic solvents used for SEC analysis (xylenes and THF). Samples 2 and 3 were easily soluble in organic solvents. The M_n and $Đ$ for samples 1, 2 and 3 was determined to be: 8.2 kDa, 16.8 kDa and 12 kDa, and 1.08, 1.02 and 1.04, respectively, Figure 2.1. The M_n are similar to the expected values based on a single-site LCP system.

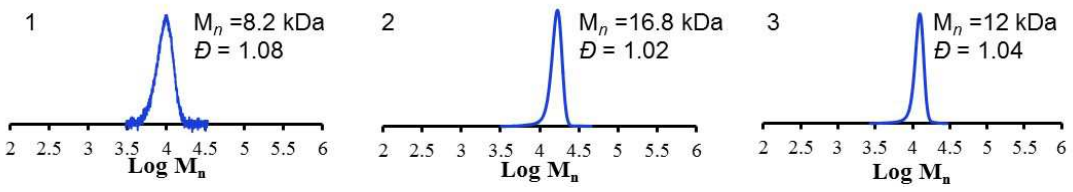

Figure 2.1: SEC plots for PMCH synthesized from: (left) **1**, (middle) **2**, and (right) **3**.

The high yield and sufficiently narrow polydisperisities for samples 1, 2, and 3 suggest a LCP system. Further validation of a living mechanism for these systems

was achieved through analysis of ^{1}H NMR (NMR conditions: 600 MHz, with TCE-d_2 as solvent at 110 °C). Specifically, the presence of vinyl resonances (4.5 ppm – 6.0 ppm) that would result from irreversible β-hydride elimination were confirmed to be absent in all cases, indeed suggesting a living coordination cyclopolymerization system for 1,6-HD with cationic initiators **1a**, **2a**, and **3a**, Figure 2.2. The lack of vinyl resonances in the ^{1}H NMR spectra for these materials also suggest complete intramolecular cyclization, *vide infara*.

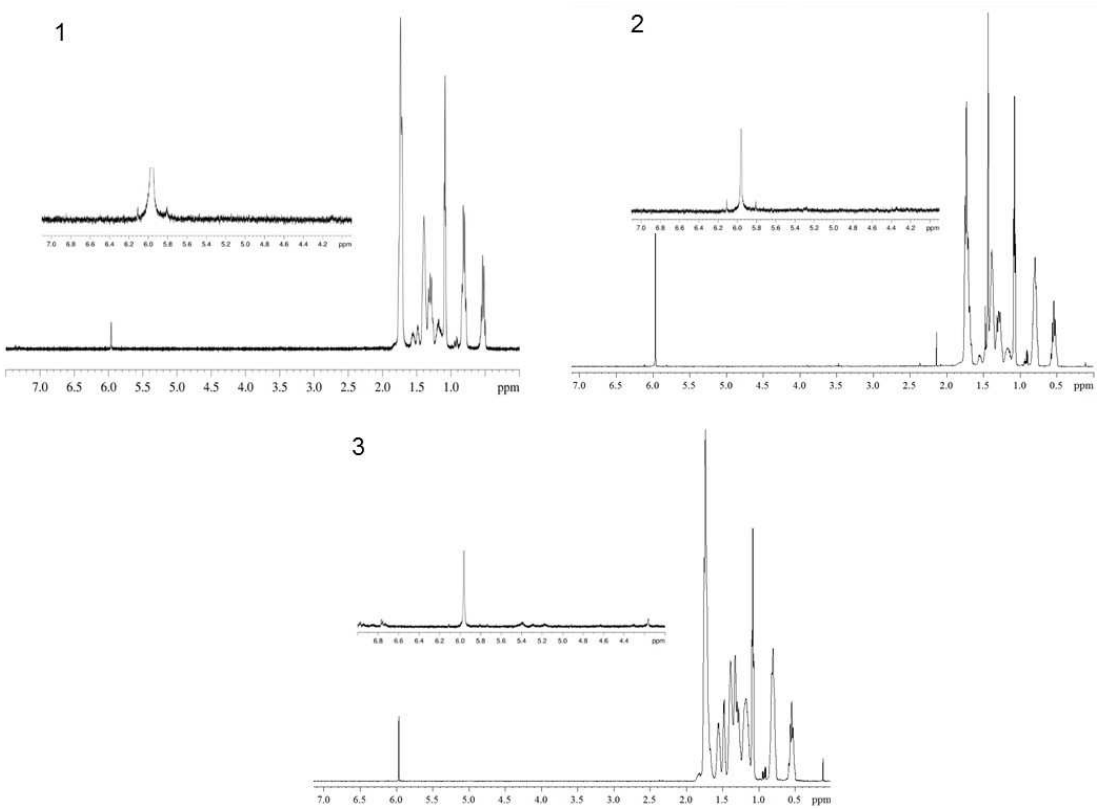

Figure 2.2: ^{1}H NMR spectra for PMCH synthesized from cationic initiators **1a** (left), **2a** (right), and **3a** (bottom); 600 MHz, 110 °C, in TCE-d_2.

With the M_n, $Đ$ and the living nature of the system realized, next it was of interest to determine the chemical microstructure. An important question to answer considering the severely limited literature available for PMCH. Fortunately, the

microstructure can likely be determined through the use of $^{13}C\{^{1}H\}$ NMR and was thus employed here as a means to elucidate the microstructure for PMCH samples 1, 2 and 3. It is important to emphasize that prior to $^{13}C\{^{1}H\}$ NMR analysis, it was uncertain if the polymer chains contained 5-membered rings (2,1-primary insertion with 1,2-secondary insertion) or 6-membered rings (repeated 1,2-primary and 1,2-secondary insertions). It was also unclear if the LCP with **1**, **2**, and **3**, when activated by **II** produced stereoselective PMCH or if there was any degree of diastereoselectivity towards *cis* or *trans* rings. The $^{13}C\{^{1}H\}$ NMR experiments (carried out with a resonance frequency of 150 MHz in TCE-d_2 at 110 °C) indeed reveal a range of stereoregularity and diastereoselectivity among samples 1-3. For example, PMCH sample 1 has a very high degree of regio- and stereo-selectivity with the formation of 6-membered rings consisting of almost entirely *cis*-isotactic selectivity (*c*-iso-PMCH). The $^{13}C\{^{1}H\}$ NMR spectra for sample 1 (Figure 2.3) consists of five major peaks at 26.4 ppm, 34 ppm, 35 ppm, 41.5 ppm and 46 ppm, there are lesser peaks, which may be attributed to a small degree of *trans*-isotactic selectivity (resonances as ca. 21 ppm, 32 ppm, 35.5 ppm and 43 ppm). Sample 2 also consist entirely of 6-membered rings with high *cis* conformation, albeit with a loss of stereoselectivity. The atacticity observed for PMCH sample 2 was anticipated based on the C_S-symmetric nature of **2**. The new resonances at ca. 34 ppm, 35 ppm, and 42 ppm represent the introduction of stereoerror upon primary insertion (random enantiofacial insertion). Finally, sample 3, synthesized from **3a**, had the least stereocontrol and *cis* selectivity as evidenced by a significant increase in the number of resonances in the $^{13}C\{^{1}H\}$ NMR, Figure 2.3. Although C_1-symmetric initiators

may allow for highly stereospecific polymer microstructures (as seen with **1**), it is not a given that high stereospecificity or diastereoselectivity will be observed. Here, the loss of stereocontrol and *cis/trans* selectivity may be attributed to the increased steric hindrance generated by the large amidinate ligand framework. Further, after reviewing the ^{1}H NMR spectrum for sample 3 (Figure 2.2, region 4 ppm - 6 ppm) there may be some small degree of incomplete cyclization for sample 3 (ca. 1 % by NMR) although no crosslinking is observed, and the high yield and narrow polydispersity suggest that the minute vinyl resonances are not due to irreversible β-hydride elimination.

Based on the highly regio-regular *cis* 6-membered ring microstructures revealed by ^{13}C{^{1}H} NMR for PMCH, a general mechanism based on other reports for coordination cyclopolymerization with **1a**, **2a** and **3a** is proposed, Scheme 2.2. In each case primary 1,2-addition occurs more readily than 2,1-addition as evidenced by the 6-membered rings and living characteristics. In the case of **1a**, both the repeated regio-regular 1,2-addition and the 1,2-secondary insertion (cyclization) occur on the same face giving rise to highly *cis* isotactic PMCH with very little *trans* content. Initiator **2a** yields highly regio-regular PMCH, but the enantiofacial insertion of 1,2-additions occur randomly with no preference for homo- vs. hetero-facial insertion. Regardless of mode of primary insertion, the cyclization step occurs on the same face as the primary 1,2-addition, thus yielding highly *cis* atactic PMCH. Finally, in the case of cyclopolymerization with **3a**, there appears to be very little selectivity for homo- or hetero-facial 1,2-additions and only moderate selectivity for homo-facial secondary insertion (cyclization) resulting in highly regio-regular atactic PMCH with

a mixture of *cis:trans* ring content (calculated from ^{1}H NMR data to be 75:25 *cis:trans*, respectively).

Scheme 2.2: General cyclopolymerization mechanism; x = 1 carbon for 1,6-HD (x = 0 or 2 carbons for 1,5-HD and 1,7-OD, *vide infara*).

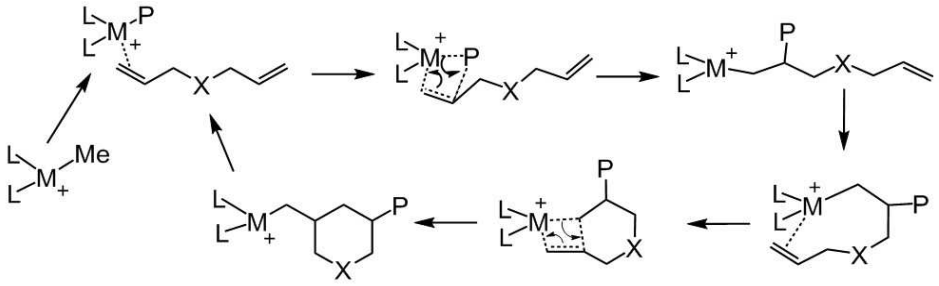

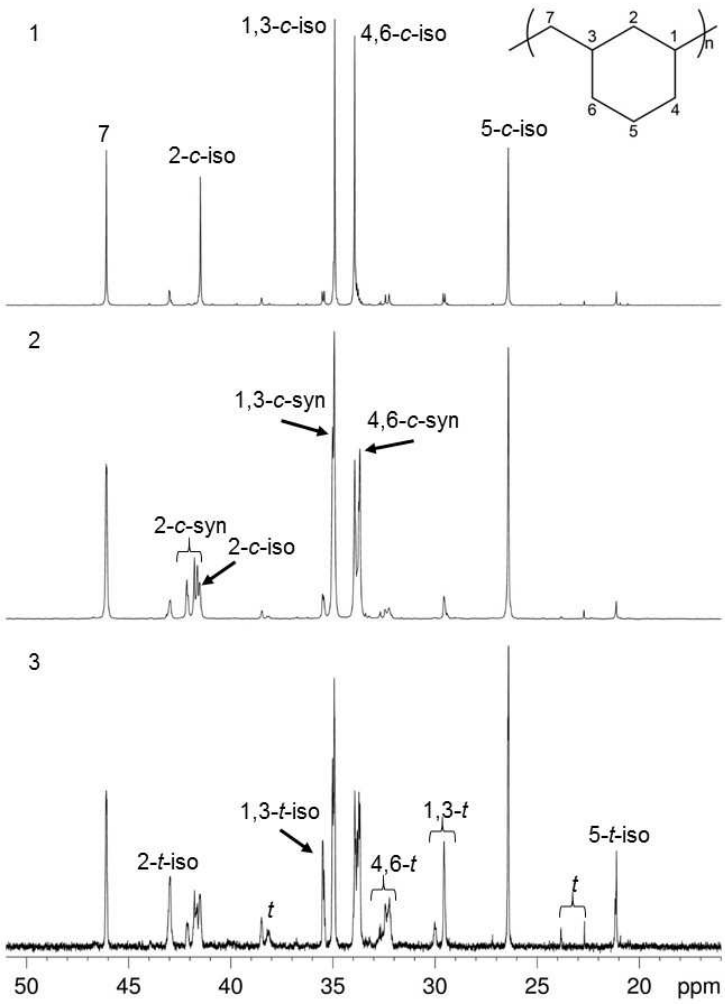

Figure 2.3: $^{13}C\{^{1}H\}$ NMR spectra for PMCH samples 1 (top), 2 (middle), and 3 (bottom) synthesized from **1a**, **2a**, and **3a** respectively; 150 MHz, TCE-d_2, 110 °C.

Next it is necessary to verify if the PMCH samples are crystalline. The propensity for a material to crystallize plays an important role in identifying a suitable materials application. Therefore, the PMCH samples 1-3 were analyzed by WAXD. Sample 1 indeed shows some degree of crystalline behavior with one sharper peak with domain spacing (*d*-spacing) = 4.3 Å and a second smaller peak at a *d*-spacing of 5.2 Å. Samples 2 and 3 do not display any significant peaks in the WAXD plots to suggest crystallization and are thus concluded to be non-crystalline. This work serves

as the first WAXD report on any PMCH material. The WAXD plots were not investigated further due to the limited availability of crystallization data for these materials.

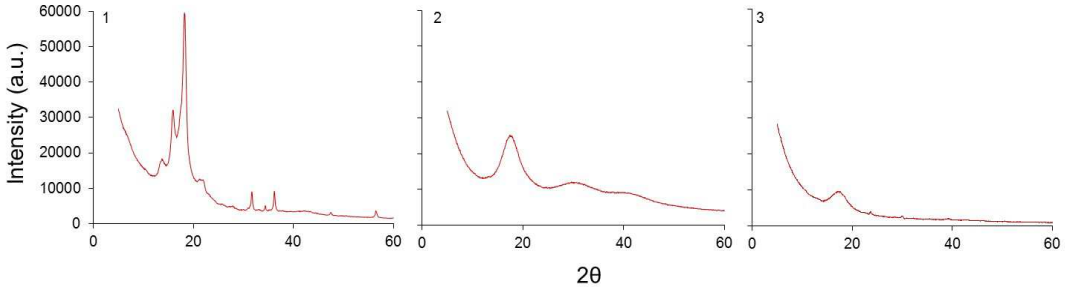

Figure 2.4: WAXD plots for PMCH samples 1 (left), 2 (middle), and 3 (right) synthesized from **1a**, **2a**, and **3a**, respectively.

The final mode of investigation for the PMCH samples was to analyze their thermal properties by thermal gravimetric analysis (TGA) and differential scanning calorimetry (DSC). Under an inert nitrogen atmosphere, sample 1 began to degrade beyond 300 °C (as evidenced by the introduction of weight loss during heating) reaching complete degradation (100 % weight loss) near 450 °C (degradation spans 445 °C ± 5 °C), Figure 2.5.

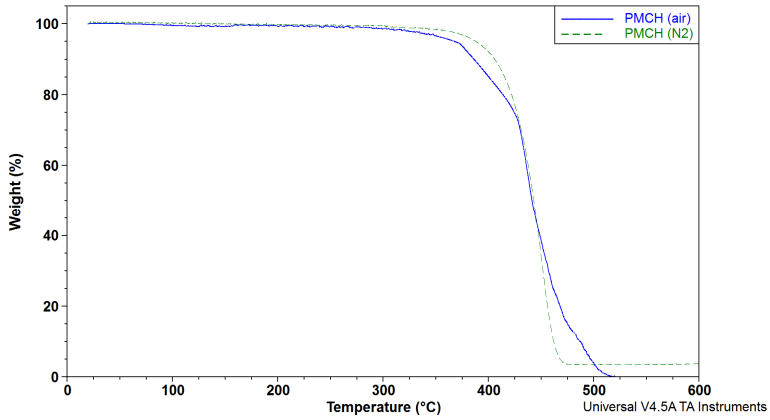

Figure 2.5: TGA plot of PMCH sample 1; N_2 (solid line), air (dashed line).

The temperature at which the onset of degradation occurs is essential to optimize the temperature program employed for DSC characterization. In that regard, the upper temperature limit for DSC thermal scans was set to ca. 250 °C, well below the onset of degradation. Based on the semi-crystalline behavior of sample 1, melting (T_m) and crystallization (T_c) temperatures are predicted. However, when initial DSC data was collected on sample 1 (ca. 8 mg sample size and 10 °C/min scan rate), no T_m or T_c was obtained. Instead, only a T_g of ca. 95 °C was observed. Reflecting on the work completed by Coates in 2009,[2] their report for *c*-iso-PMCH (M_n = 87 kDa and $Đ$ = 1.38) noted a T_m of 179 °C, but interestingly no T_c (sample size was not reported and no explanation was provided; their temperature program was 10 °C/min scan rate). It is possible that the *cis*-isotactic chain configuration thwarts efficient chain packing for crystallization. With this information in hand, alternate DSC temperature programs were investigated for sample 1 (scan rates as fast as 20 °C/min to as slow as 1 °C/min). Gratifyingly, the T_m and T_c for sample 1 can be observed using the following temperature program: four heating/cooling cycles from -70 °C to 230 °C with a 15 minute isothermal hold (230 °C) at the end of each heating cycle. The scan rate during the second heating/cooling cycles was run at 10 °C/min with all other scans run at 1 °C/min. The fourth heating and cooling cycles were used to report T_m, T_c and T_g, which are: 209 °C, 181 °C and 92 °C, Figure 2.6 and Table 2.1. The difficulty in elucidating the first order phase transitions and their relatively broad transitions indeed coincide with the WAXD conclusion for a semi-crystalline material. On the other hand, samples 2 and 3 are amorphous materials as evidenced by lack of stereoselectivity observed from $^{13}C\{^1H\}$ NMR and weak/incoherent

scattering from WAXD, and are not expected to display melting or crystallization temperatures. Using the same temperature program described above for sample 1, there was no indication of a T_m or T_c for samples 2 or 3. However, as predicted, glass transitions were easily observed for both samples 2 (72 °C) and 3 (90 °C).

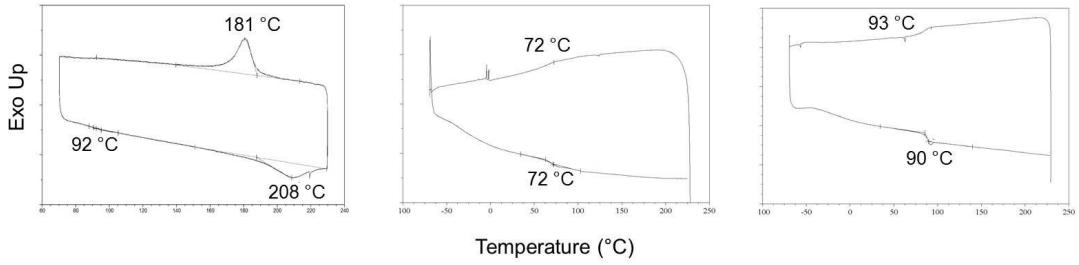

Figure 2.6: DSC plots for PMCH samples 1 (left), 2 (middle), and 3 (right) from **1a**, **2a**, and **3a** respectively.

Table 2.1: SEC and DSC data for PMCH.

Sample	Cat.	M_n (kDa)	$Đ$	T_g (°C)	T_m (°C)	T_c (°C)
1	**1**	8.2	1.08	92	209	181
2	**2**	16.8	1.02	72	-	-
3	**3**	12.0	1.04	90	-	-

In summary, 1,6-HD was successfully polymerized and fully characterized for the first time, in a living fashion, using precatalysts: **1**, **2**, and **3** to afford an array of poly(methylene-1,3-cyclohexane) (PMCH) microstructures, ranging from highly *cis*-isotactic to highly stereo-irregular with a mixture of *cis/trans* rings. An important feature of the PMCH polyolefins established here are their relatively high T_g compared to traditional acyclic polyolefins such as PE and PP providing the opportunity to expand the range of applications for polyolefin materials.

2.3. Cyclopolymerization of 1,5-Hexadiene, 1,5-HD

The cyclopolymerization of 1,5-HD using precatalyst **1** has been reported previously by our group (polymerization using **2** was also reported but under chain transfer conditions, which is not discussed here).[4] One additional poly(methylene-1,3-cyclopentane) (PMCP), synthesized from precatalyst **3**, is presented here as a comparison to PMCH. Reports for the cyclopolymerization of 1,5-HD using C_1-symmetric **3** have not been previously reported. The M_n and $Đ$ were determined by SEC to be 8.17 kDa and 1.30, respectively (sample 4). The broad polydispersity may be attributed to some degree of crosslinking that may have occurred during polymerization. ^{1}H NMR confirmed the presence of 13 mol-% pendant vinyl groups, Figure 2.7. The chemical microstructure was identified using $^{13}C\{^1H\}$ NMR was found to be largely atactic with a *cis:trans* diastereoselectivity of 56:44 (by $^{13}C\{^1H\}$ NMR). The thermal properties for sample 4 were investigated using DSC. Melting, crystallization and glass transition temperatures were easily obtained using a standard temperature program (10 °C/min; heat/cool/heat, only the second heating cycle is reported): T_m = 103 °C, T_c = 95.0 °C, and T_g = -22.2 °C.

The described properties are markedly different from not only PMCH obtained from the use of **3** (see Section 2.2), but also other PMCP materials synthesized using isospecific precatalyst **1**; the most notable difference between PMCP from **3** (sample 4) and PMCP from **1** (sample 5) is the diastereoselectivity and cyclization selectivity. The *cis* selectivity for sample 5 is lower at only ca. 35 % (*cis:trans* 35:65) compared to 56 % *cis* selectivity for sample 4 (*cis:trans* 56:44). The cyclization selectivity is higher for sample 5 at ~98 % cyclization compared to 87 %

cyclization for sample 4. Sample 5 was synthesized and characterized by colleague Wonseok Hwang and has been used here as a comparison.

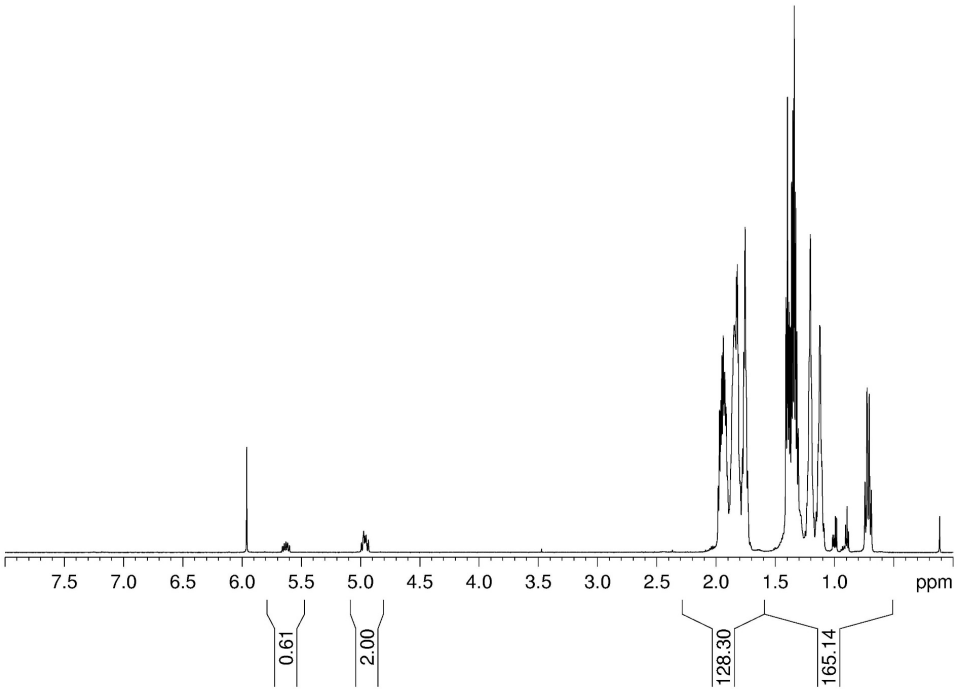

Figure 2.7: ^{1}H NMR of PMCP from **3a** (sample 4); 600 MHz, TCE-d_2, 110 °C.

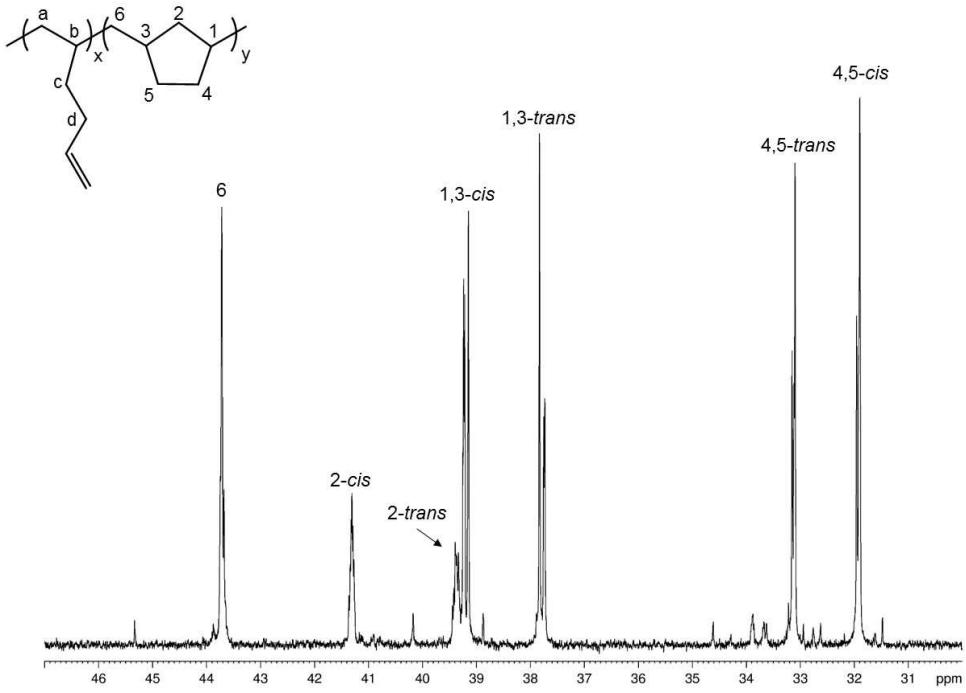

Figure 2.8: $^{13}C\{^{1}H\}$ NMR of PMCP from **3a** (sample 4); 150 MHz, TCE-d_2, 110 °C.

2.4. Cyclopolymerization of 1,7-Octadiene, 1,7-OD

The cyclopolymerization of 1,7-OD has not previously been reported by our group. Presented here, for the purposes of comparison to PMCH, are poly(methylene-1,3-cyclooctene) (PMCO) materials from the cyclopolymerization of 1,7-OD using **1** and **2** separately activated by **II**. There are three PMCO samples from **1** (samples 6 – 8) and one from **2** (sample 9). Unlike 1,5-HD and 1,5-HD (*vide supra*) all four PMCO samples have some degree of crosslinking due to incomplete intramolecular cyclization. Reflecting on Chapter 1; Section 1.9, selectivity towards cyclization was shown to improve under dilute conditions, and that cyclization selectivity is affected by temperature. Thus, the PMCO samples from **1** were carried out at two different temperatures each at a different concentration. The first PMCO was carried out at -

20 °C in PhCl for 2 hours with a monomer concentration of 85.7 mM (sample 6). The M_n for sample 6 was determined by SEC to be 9.54 kDa. The SEC trace is not monomodal suggesting that crosslinking occurred, Figure 2.9.

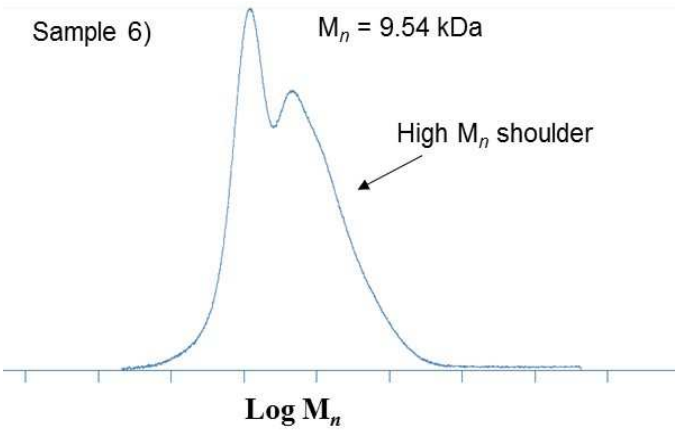

Figure 2.9: SEC trace of PMCO: sample 6.

DSC analysis was completed but thermal transitions (T_m, T_c, T_g) were not observed possibly due to the degree of crosslinking (temperature program: 10 °C/min). DEPT135 NMR displays five main peaks that coincide with a 7-membered ring; an indication that polymerization of 1,7-OD with **1** proceeds in 1,2-insertion for both primary and secondary insertion (regioregular) to afford *cis* isotactic PMCO (*cis*-i-PMCO), at least for the un-crosslinked (soluble) sections of the polymer. The DEPT135 NMR spectrum also suggests a higher mol-% of pendant vinyl units (compared to PMCP under similar conditions; Section 2.3). The resonance at ca. 25 ppm represented carbon atoms at positions 5 and 6, resonances 34 ppm correspond to carbon at positions 4 and 7, 36 ppm for carbon atoms at positions 1 and 3, 42 ppm for carbon 2, and 47 ppm for carbon at position 8. Resonances for the

uncyclized units are also present. The resonance at ca. 45 ppm represents carbon at position *a*, carbons *b*, *c* and *f* are group between 33 – 34 ppm, carbon at position *e* is at ca. 30 ppm and carbon at position *d* overlaps with the resonance for carbons 5 and 6 at 25 ppm, Figure 2.10. Assignments were made according to previously published spectra for PMCO.[5]

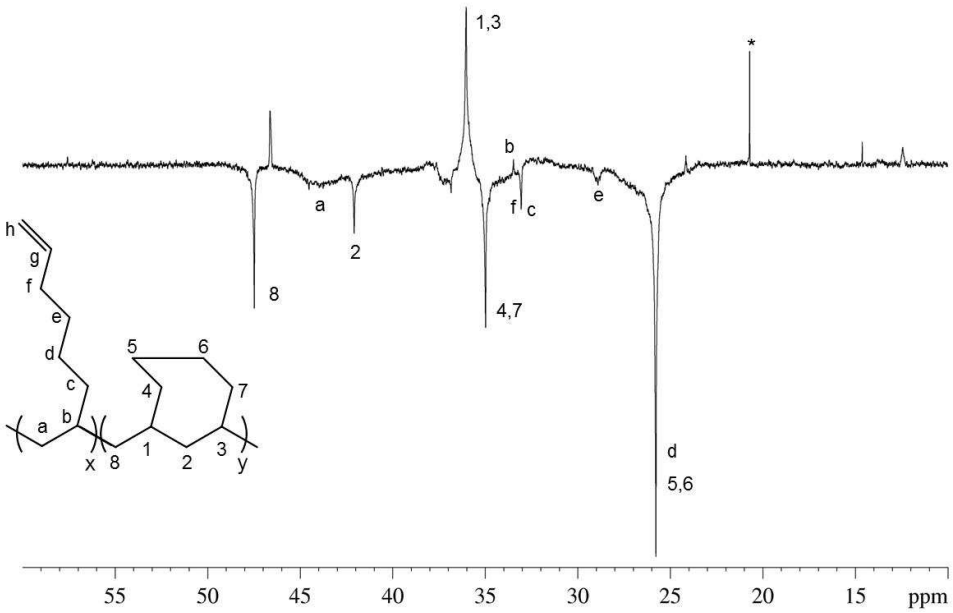

Figure 2.10: DEPT135 NMR of PMCO: sample 6 (vinyl groups not shown).

The mol-% of uncrosslinked pendant units, determined by ^{1}H NMR for sample 6 is 12 %. This value represents the pendant groups that were not involved in intermolecular 1,2-addition into an adjacent active site. The second PMCO synthesis was carried out at -10 °C with a higher monomer concentration of 150 mM (sample 7). The degree of crosslinking was much greater for sample 7 as evidenced by SEC; there are at least 4 overlapping peaks present in the SEC trace with an overall M_n of 20.8 kDa, Figure 2.11. Irrespective of the multiple peaks observed bt SEC, the DEPT135 NMR (Figure 2.12) for sample 7 is relatively clean, an indication that the

content of the polymer chains are relatively uniform, similar to those observed for sample 6 albeit with a lower mol-% of pendant vinyl groups, which was confirmed by ^{1}H NMR to be 2.2 %. The third PMCO synthesis was also carried out at -10 °C, but

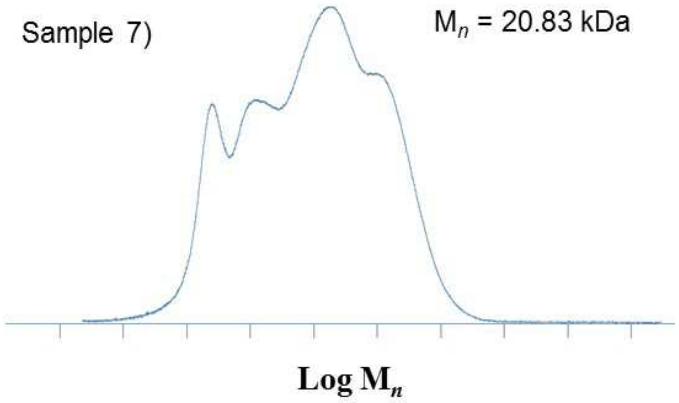

Figure 2.11: SEC trace of PMCO: sample 7.

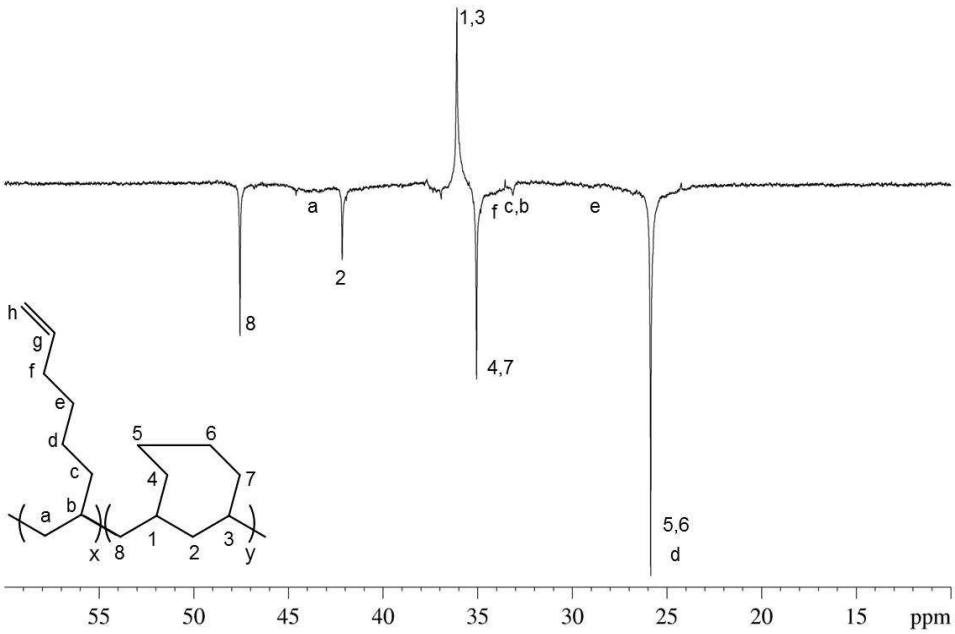

Figure 2.12: DEPT135 NMR of PMCO: sample 7 (vinyl groups not shown).

with a lower monomer concentration of 60 mM. The M_n determined by SEC is 4.9 kDa (sample 8). The SEC trace displays a high M_n shoulder commonly observed for polymer samples that contain crosslinking, Figure 2.13. NMR was not carried out for sample 8. The final PMCO sample was carried out at -10 °C at a concentration of 85.7 mM using Cs-symmetric precatalyst **2** (sample 9). Sample 9 appeared as a tough, white solid and was completely insoluble in organic solvents. Due to insolubility (from crosslinking) no further characterization was carried out for sample 9.

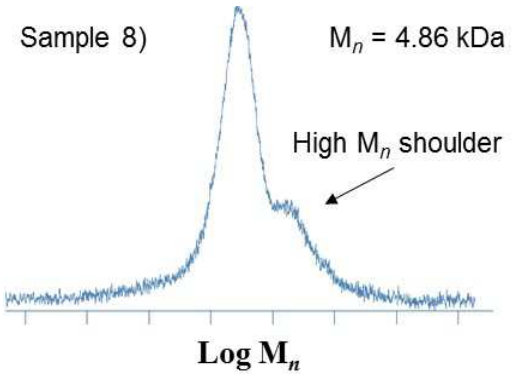

Figure 2.13: SEC trace of PMCO: sample 8.

In summary, the cyclopolymerization of 1,7-OD was carried out using precatalysts **1** and **2** with changes made to temperature and monomer concentration to form PMCO. Lower monomer concentration increased cyclization selectivity. Warmer temperatures (-20 °C vs. -10 °C) may also play a role in cyclization selectivity; further studies, holding concentration constant, are required to definitively draw this conclusion, however. Although the monomer to initiator equivalence was kept constant (100eq:1eq respectively) the M_n varied greatly. Yield and M_n decreased

with decreasing monomer concentration (lower apparent k_p under more dilute conditions). PMCO from precatalyst **2** was highly crosslinked and could not be characterized by SEC or NMR.

2.5. Conclusions

Non-conjugated dienes were successfully polymerized using living coordination polymerization to afford linear polyolefins containing cyclic repeating units (except in the case of 1,7-OD which also exhibits crosslinking). Specifically, the work presented here serves as the first report of the living coordination cyclopolymerization of 1,6-heptadiene (1,6-HD) for the formation of poly(methylene-1,3-cyclohexane) (PMCH). The materials were synthesized from cationic initiators **1a**, **2a**, and **3a**, which resulted in highly regio-regular, narrow polydispersity PMCH with varying degree of tacticity and diastereoselectivity. PMCH from **1a** (sample 1) is semi-crystalline, isotactic and has primarily *cis* diastereoselectivity with a T_g of 92 °C. PMCH from **2a** (sample 2) also has high *cis* content, but is amorphous with an atactic microstructure and T_g of 70 °C. PMCH from **3a** (sample 3) is amorphous and atactic with a 75:25 mixture of *cis:trans* ring content (90 °C). The cyclopolymerization of 1,5-hexadiene (1,5-HD), using cationic initiator **3a** results in an atactic poly(methylene-1,3-cyclopentane) (PMCP) with a 56:44 *cis:trans* ratio, 87 % cyclization selectivity, and T_m, T_c and T_g of 103 °C, 95.0 °C and -22.2 °C, respectively. The cyclopolymerization of 1,7-octadiene (1,7-OD), using cationic initiators **1a** and **2a** were also completed, which resulted in poly(methylene-1,3-cycloheptane) (PMCO) with crosslinking. In the case of PMCO from **1a**, cyclization

selectivity was improved, at the cost of yield, when dilute polymerization conditions were employed. PMCO from **2a** gave rise to highly crosslinked, insoluble material.

2.6. Experimentals

2.6.1. Synthesis of Poly(methylenecycloalkane)s

The polymerizations were carried out under an inert atmosphere of dinitrogen using a Vacuum Atmospheres glovebox. The general polymerization method for the formation of poly(methylenecycloalkane)s: PMCH, PMCP, and PMCO is as follows: 1.01 equiv. of $[PhNHMe_2][B(C_6F_5)_4]$ (**II)**, was mixed with 0.02 mmol precatalyst, **1, 2** or **3** in 1.5 mL cold (-10 °C) PhCl. The resulting bright yellow mixtures of precatalyst with **II** were then added to pre-chilled (-18 °C – -10 °C) PhCl in a 50-mL round bottomed glass reaction vessel equipped with a magnetic stir bar. The α,ω-olefin monomer (ca. 100 equiv.) was then added to the reaction mixture and allowed to stir for a given amount of time, typically 1 to 8 hours. Following a given amount of reaction time the reaction mixtures were removed from the glovebox and quenched/precipitated in a large excess of acidic methanol (300 mL – 500 mL; 10% HCl by volume). The polymers were vacuum filtered, washed with methanol, collected in a pre-weighed vial, and dried under vacuum to constant weight. Instrument parameters and source of materials information are provided in Appendices A and B, respectively.

2.7. References

1. Hiemenz, P. C.; Lodge, T. P., *Polymer Chemistry*. 2nd ed.; Wiley: Boca Raton, FL, 2007; p 465-500.

2. Edson, J. B.; Coates, G. W., *Macromol. Rapid Commun.* **2009**, *30* (22), 1900-1906.

3. Crawford, K. E.; Sita, L. R., *J. Am. Chem. Soc.* **2013**, *135* (24), 8778-8781.

4. a) Fontaine, P. P.; Epshteyn, A.; Zavalij, P. Y.; Sita, L. R., *J. Organomet. Chem.* **2007**, *692* (21), 4683-4689.; b) Jayaratne, K. C.; Keaton, R. J.; Henningsen, D. A.; Sita, L. R., *J. Am. Chem. Soc.* **2000**, *122* (42), 10490-10491.

5. Naga, N.; Shiono, T.; Ikeda, T., *Macromol. Chem. Phys.* **1999**, *200* (6), 1466-1472.

Chapter 3

Cyclopolymerization of Substituted Non-Conjugated Dienes

3.1. Introduction

The successful living coordination cyclopolymerization of 1,6-heptadiene (1,6-HD) using precatalysts **1**, **2**, and **3** for the production of PMCH (Chapter 2) has propelled interest in the study of non-conjugated dienes with substitution present at the center most atom (typically at position 4 of a given 1,6-heptadiene). The cyclopolymerization of substituted non-conjugated dienes have garnered increasing attention as a result of their interesting materials properties such as high glass transition temperature (T_g), their ability to incorporate functional groups (e.g. polarity, fluorescence), and potential for post polymerization modification. Therefore, precatalysts **1** and **2**, activated by **II**, were investigated for their catalytic activity toward the polymerization of four different non-conjugated diene monomers according to Scheme 3.1. The monomers are diallyldimethylsilane, diallylmethylphenylsilane, diallylfluorene and 1,3-diallyl-1,1,3,3-tetramethyldisiloxane. The results of this work are presented in the proceeding sections and was completed by Crawford unless noted otherwise. There are Sections in this Chapter, particularly figures and experimental details that have been reproduced from the following published work: Crawford, K. E. and Sita, L. R. *ACS Macro Lett.* **2014**, *3*, 506 – 509.[10]

Scheme 3.1: General reaction of precatalyst (**1** or **2**) activated by **II** for cyclopolymerization of non-conjugated dienes.

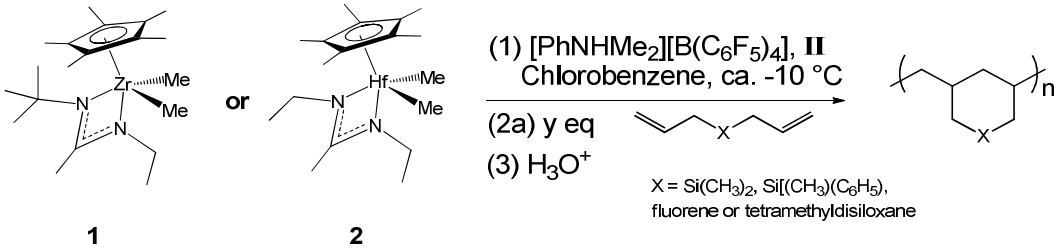

1 **2**

3.2. Cyclopolymerization of Diallylsilanes

The polymerization of diallylsilanes such as diallyldimethylsilane (DAS), diallyldiphenylsilane (DPS), and diallylmethylphenylsilane (MPS) have been studied intermittently since the mid-1950s; however, little progress has been made toward the polymerization of these monomers due to the lack of proper polymerization catalysts, which have resulted in poly(carbosilane)s with mere single unit cyclization, short chain oligomeric products (dimer, trimer etc.) or low polymer yield and broad polydispersity. In this regard, Butler and Marvel were the first to report (separately yet simultaneously) on the cyclization of DAS and DPS in 1960.[1, 2] They report using Zeigler-Natta type catalyst: $TiCl_4$ activated by triethylaluminum. Conversions were low; 7 % - 10 % for the poly(DAS) analog and up to 56 % for poly(DPS) following at least 24 hours of reaction time (60 °C – 85 °C in 5 mL – 50 mL heptane), Figure 3.1. Both reports propose cyclic 6-membered rings based on the absence of the signature C=C band (1620-1680 cm^{-1}) in infrared spectroscopy (FT-IR). Melting temperatures, determined by capillary, were 80 °C – 110 °C for poly(DAS) and from 125 °C to 155 °C for poly(DPS). M_n and $Đ$ were not determined.

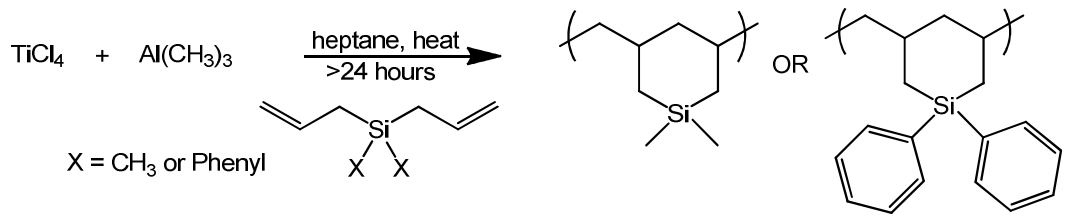

Figure 3.1: Representation of polymerization method employed by Butler and Marvel.[2, 3]

Seventeen years later, in 1977 Billingham and coworkers reported on the cyclopolymerization of various diallylsilane compounds using Ziegler-Natta catalyts.[4] Specifically, polymerizations of DAS, DPS and DMPS were catalyzed by using $TiCl_4$ activated by triethylaluminum. The Ziegler-Natta polymerizations were carried out similarly to the procedure reported by Butler and Marvel (60 °C in 7 mL heptane) albeit for a longer reaction times (48 hours). It was noted that DAS polymerized with the greatest activity although the overall reactivity for all monomers was low. M_n, $Đ$, stereoselectivity and thermal properties were not discussed for these materials. Saigo[5] and later Cragg[6] reported the use of radical and cationic polymerization of DAS, DPS and MPS using initiators benzoyl peroxide or aluminum tribromide (ca. 80 °C in benzene for radical polymerizations and -78 °C – 25 °C in toluene for cationic polymerizations, respectively). Saigo proposed the formation of 6-membered rings with *cis* diastereoselectivity for poly(DAS) and poly(MPS) based on ^{13}C NMR measurements (25.15 MHz in $CDCl_3$ at 80 °C), Figure 3.2. M_w values are low, 2.2 kDa and 2.6 kDa for poly(DAS) and poly(MPS), respectively; $Đ$ was not reported for either system. Respective T_g values were measured to be 61 °C and 74 °C for poly(DAS) and poly(MPS). Cragg reported poly(DAS) materials with M_w ca. 3.0 kDa and $Đ \cong 2$ and poly(DPS) materials encompassing M_w values ranging from 3.270 kDa

– 4.729 kDa ca. 3.0 kDa with broad polydisperisities ($1.4 \leq Đ \leq 3.2$). Details about molecular structure were not provided.

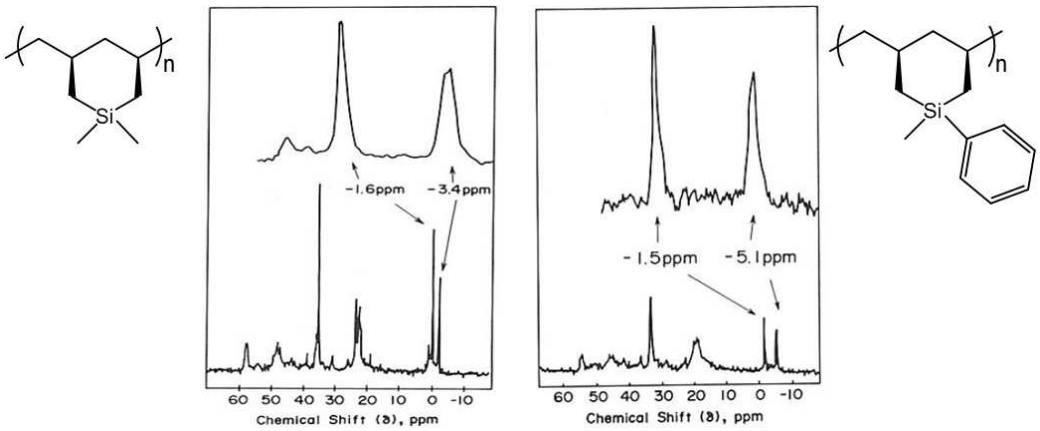

Figure 3.2: ^{13}C NMR spectra for poly(DAS) (left) and poly(MPS) (right) reproduced from reports by Saigo. Stereochemistry is not discussed. [5]

Naga used various zirconecene catalysts for the successful polymerization of diallylsilanes, wherein DAS and DPS were each incorporated separately into ethylene[7] and propylene[8] polymerizations with poly(DAS) and poly(DPS) incorporation as high as 28 mol%. Marciniec and coworkers made use of rhodium and ruthenium complexes: $RuCl_2(PPh_3)_3$, $RuHCl(CO)(PPh_3)_3$, and $RuCl(SiMe_3)(CO)(PPh_3)_2$ in the "copolymerization" of DAS and DPS with propylene; however, only acyclic dimers, trimers and short chain oligomers were achieved.[9] As evidenced by the aforementioned literature, the highly regio- and stereo-specific coordination cyclopolymerization of DAS and MPS for the formation of poly(3.5-methylene-1-1-dimethyl-silacyclohexane), PDAS, and poly(3,5-methylene-1,1-methylphenyl-silacyclohexane), PMPS have remained elusive.

3.2.1. Diallyldimethylsilane, DAS

Given that the successful cyclopolymerization of DAS has yet to be reported beyond a 3-unit oligomer or has been ill-defined in previous reports, it was unclear whether the polymerization of DAS using the same transition metal complexes, **1** and **2**, that have been successfully applied to only pure α-olefins (or α,ω-olefins), would proceed with living character, stereoselectivity, complete cyclization – or if no polymerization activity would be observed. For this reason, the polymerization conditions described in Scheme 3.1 were applied for the cyclopolymerization of DAS to form PDAS, which was subsequently recovered in 65-81% yields and appears as a white powder. PDAS material resulting from polymerization with C_1-symmetric **1** is only sparingly soluble in organic solvents. Based on this criteria we anticipated the formation of a highly *isotactic* and stereoselective product or a product that is heavily crosslinked. SEC analysis of this material revealed a M_n of 14.8 kDa with relatively broad polydispersity ($Đ$ = 1.52) (sample 1), Table 3.1 and Figure 3.3.

Table 3.1: Tabulated data for PDAS.

Run	Cat.	M_n[a]	M_w[a]	$Đ$[a]	T_g (°C)[b]	T_m (°C)[b]
1	**1**	14.8	22.5	1.52	123	264-270
2	**2**	11.8	13.3	1.13	115	-

[a]Determined by GPC; [b]Determined by DSC.

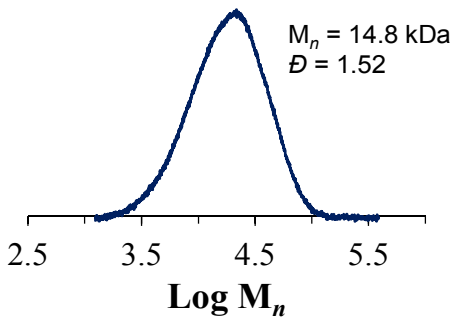

Figure 3.3: SEC trace for PDAS from **1a** (DAS-sample 1).

If the polymer had been highly crosslinked SEC would not have been viable, therefore, it is unlikely to have undergone crosslinking. Thus, to further confirm the microstructure, NMR experiments were carried out (^{1}H, ^{13}C{^{1}H}, DEPT135, HSQC, COSY and ^{29}Si NMR). ^{1}H NMR, reproduced in Figure 3.4, appears as expected for a typical hydrocarbon-based polymer obtained through coordination polymerization; however, there are small resonances in the vinylic region (ca. 4.8 ppm) suggesting possible premature chain-termination, *vide infara*. Importantly, ^{13}C{^{1}H} NMR, paired with DEPT135, confirmed the formation of highly 3,5-*cis*-isotactic-PDAS (*c*-i-PDAS).

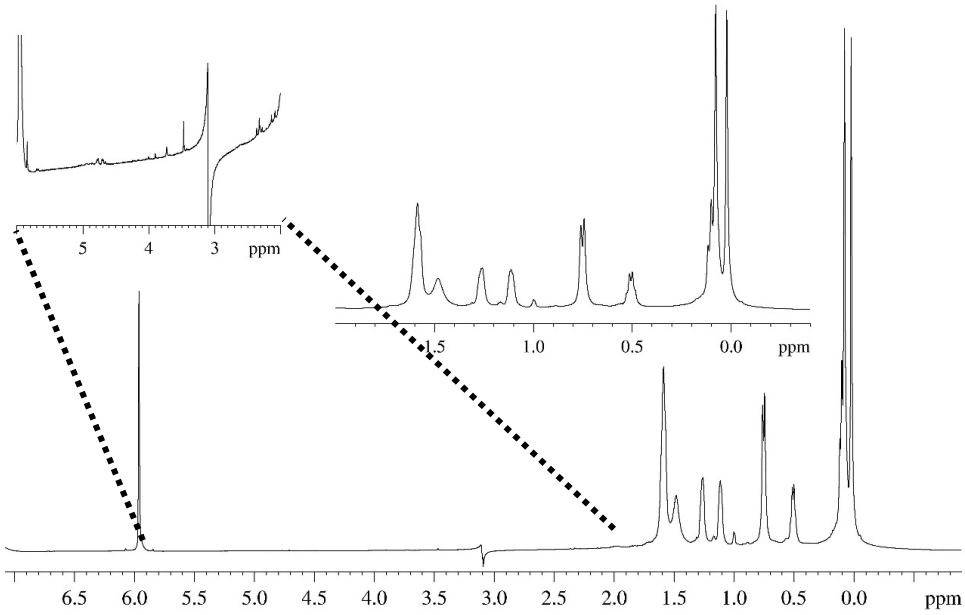

Figure 3.4: ^{1}H NMR of PDAS from **1a** (DAS-sample 1); 800 MHz NMR, 110 °C, TCE-d_2.

The proton decoupled ^{13}C NMR and DEPT135 spectra for sample 1 displays 6 sharp resonances between -5 ppm and 60 ppm, Figure 3.5 and Figure 3.6. The two resonances between -5 ppm and 0 ppm correspond to the two methyl groups bonded to the Si heteroatom. The resonance at 21.9 ppm corresponds to carbons 2 and 6 (molecular structure labels in Figure 3.5 inset). The resonance at 29.8 ppm is attributed to carbons 3 and 5. The two sharp resonances at 43.7 ppm and 54.1 ppm are attributed to carbons 4 and 7 respectively. Further, a single resonance in the ^{29}Si NMR (calibrated to tetramethylsilane, TMS-d_{12}) also suggests a highly isotactic PDAS material, Figure 3.7. Following the characterization of DAS-sample 1 via ^{13}C{^{1}H} NMR and DEPT135, HSQC was carried out in effort to determine the corresponding ^{1}H NMR peak assignments, Figure 3.8. For the ^{1}H NMR portion of the 2D HSQC NMR, the resonances between -0.6 ppm and -0.4 ppm correspond to the

two methyl groups attached to the Si heteroatom and are also correlated to a lesser extent with the carbon atoms at positions 2 and 6. The resonances between -0.1 ppm and 0.2 ppm are attributed to carbon 4. The resonances between 0.9-1.1 ppm are associated with carbons 3, 4 and 5. The resonances at 0.55 ppm and 0.7 ppm are associated with carbon 7 and the 0.2 ppm resonance corresponds with carbons 2 and 6. The combined NMR spectra for PDAS synthesized from **1a** confirm a highly *cis* isotactic microstructure.

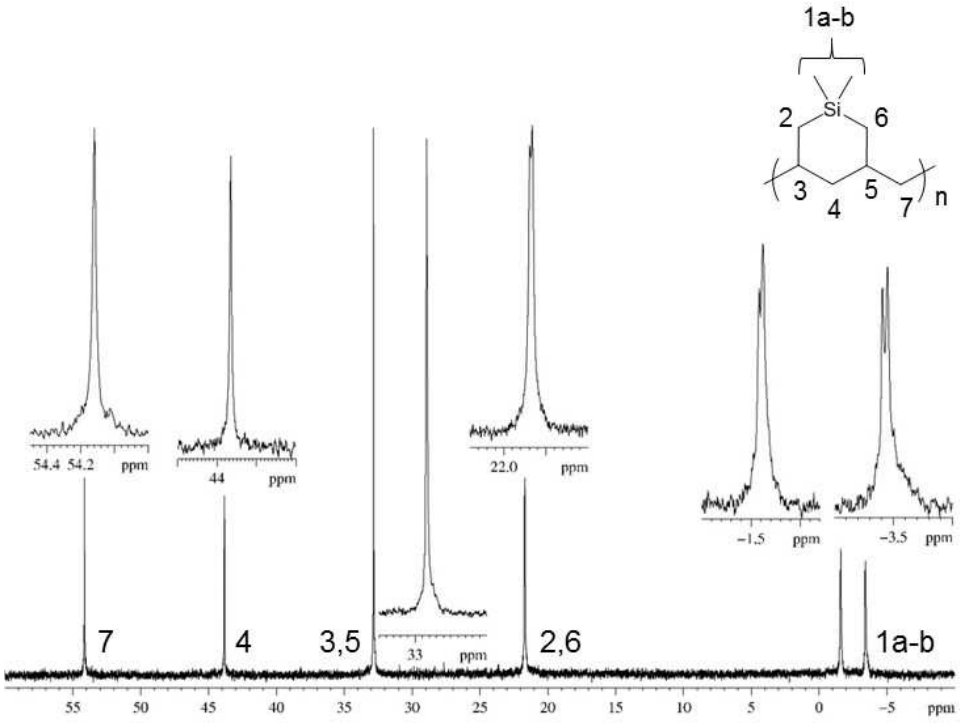

Figure 3.5: $^{13}C\{^{1}H\}$ NMR of PDAS from **1a** (DAS-sample 1); 200 MHz, 110 °C, TCE-d_2.

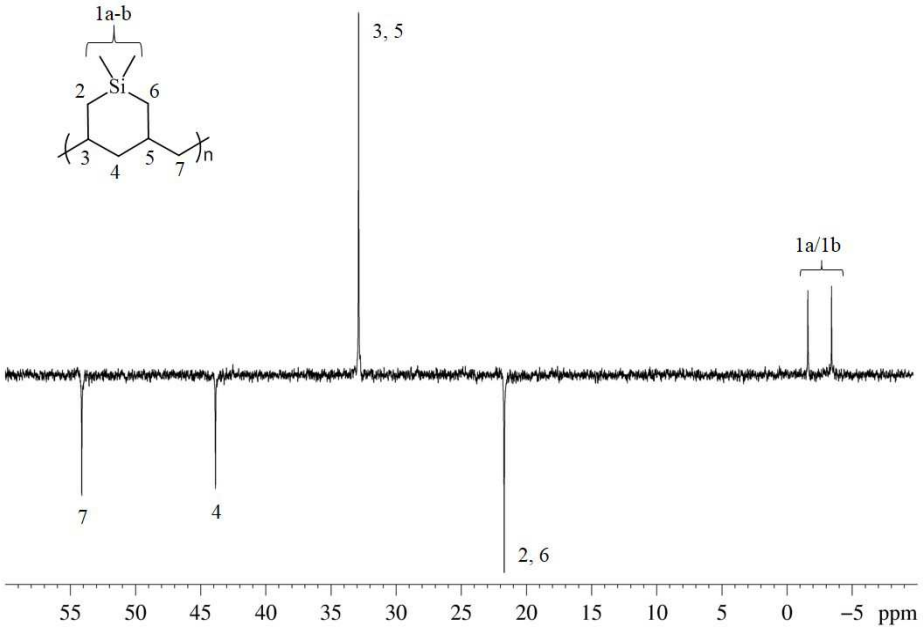

Figure 3.6: DEPT135 NMR of PDAS from **1a** (DAS-sample 1); 200 MHz, 110 °C, TCE-d_2.

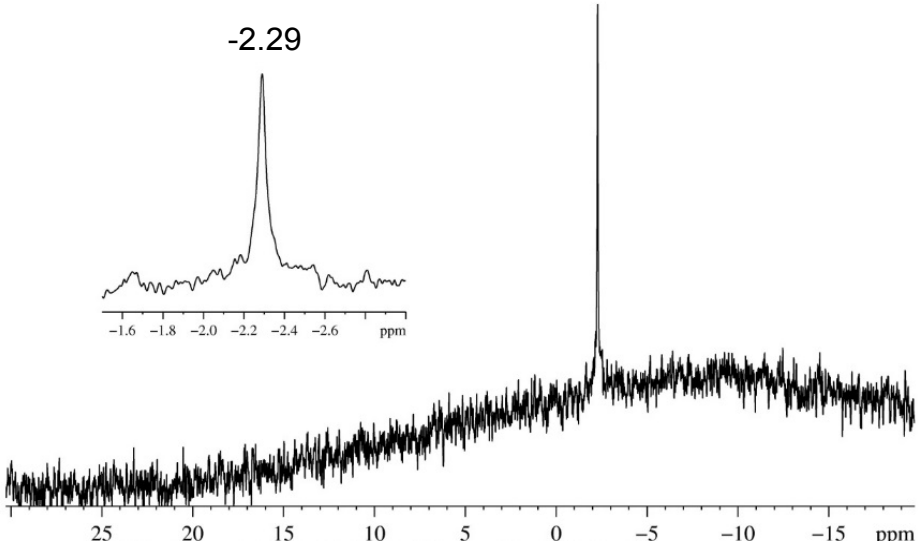

Figure 3.7: ^{29}Si NMR of PDAS from **1a** (DAS-sample 1); 100 MHz, 90 °C, TMS-d_{12}.

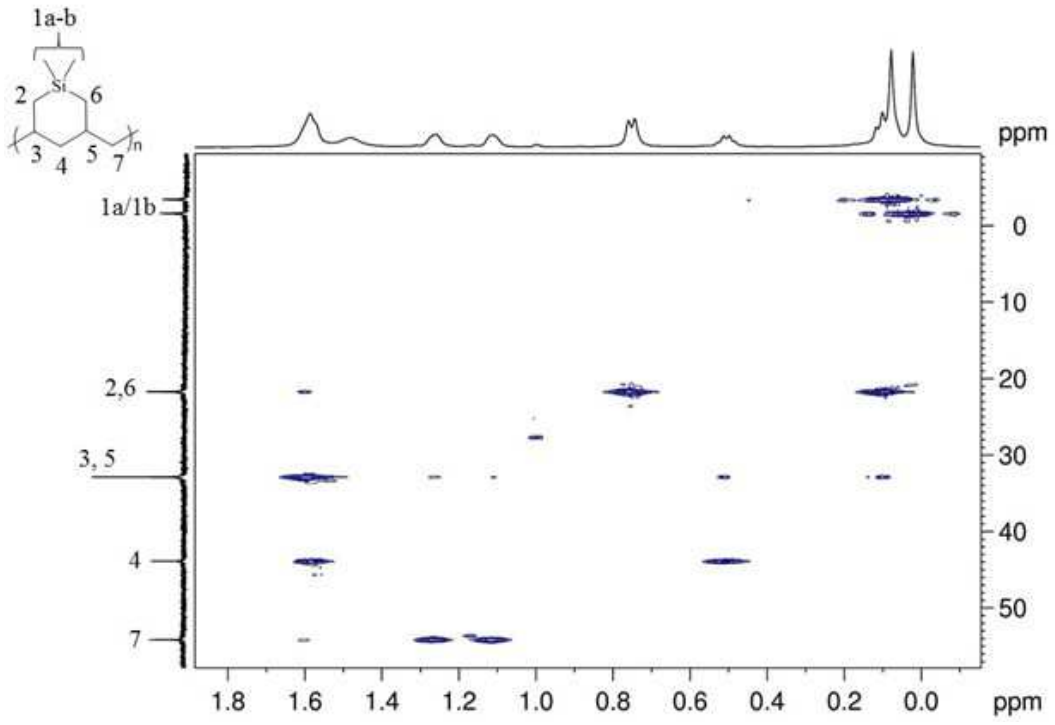

Figure 3.8: HSQC NMR of PDAS from **1a** (DAS-sample 1); 200 MHz, 110 °C, TCE-d_2.

Based on the highly isotactic nature of this material and its limited solubility in common organic solvents, it was next of interest to identify if these features correspond to any degree of crystallinity. WAXD measurements were employed to estimate the crystallinity of PDAS. It was determined that while PDAS does contain coherent scattering peaks, they are broad and weak suggesting the formation of only a semi-crystalline material, Figure 3.9. Further WAXD analysis was not carried out for these materials due to the limited availability of crystallization data for these materials. However, the semi-crystalline nature of *c*-i-PDAS suggests that a T_m and T_c may be present.

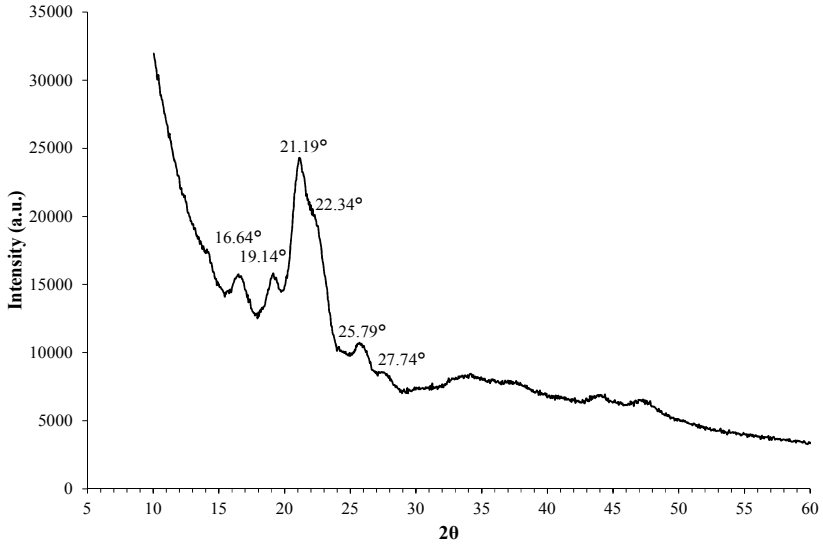

Figure 3.9: WAXD plot of PDAS from **1a** (DAS-sample 1). *d*-spacing can be calculated by using Bragg's law: $n\lambda = 2d\sin\theta$ where $n = 1$ and $\lambda = 1.54$ Å.

The thermal properties of *c*-i-PDAS were determined by thermal gravimetric analysis (TGA) and differential scanning calorimetry (DSC). First, using TGA, the onset of degradation was determined to be ca. 350 °C under a nitrogen atmosphere (as low as 270 °C under air) with full degradation at 447 ± 5 °C (82 % degradation observed under air at the same temperature), Figure 3.10. The temperature at which the onset of degradation occurs is essential to optimize the temperature program employed for DSC characterization. In that regard, the upper temperature limit for DSC thermal scans was set to 290 °C, well below the onset of degradation. Indeed, a T_m between 264 °C and 270 °C was consistently observed (fluctuation in T_m stem from changes to temperature program). The following general parameters were used for heating and cooling cycles: heat to 290 °C at 10 °C/min (not shown); isothermal hold x 30 min (not shown); cool to 0 °C at 1 °C/min; heat to 290 °C at 1 °C; cool to 0 °C at 10 °C/min; heat to 290 °C at 10 °C/min. Despite an investigation using

various temperature programs a T_c was only observed as very small change in heat flow at 258 °C, Figure 3.11.

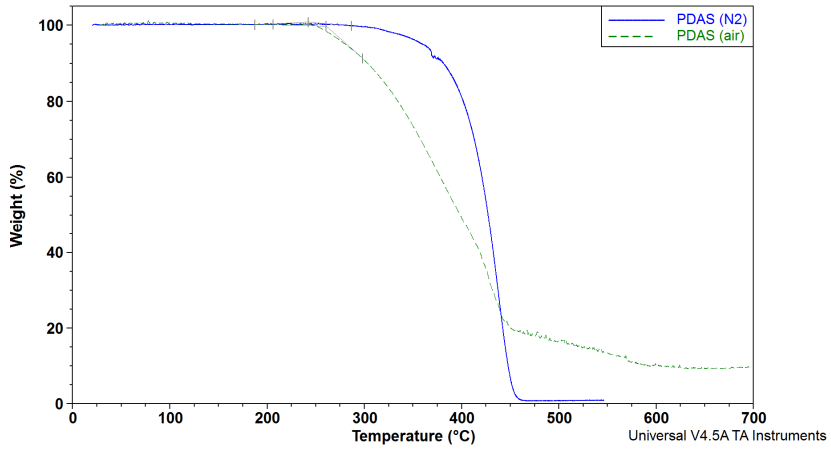

Figure 3.10: TGA plot of PDAS from **1a** (DAS-sample 1); under N_2 (solid line), under air (dashed line).

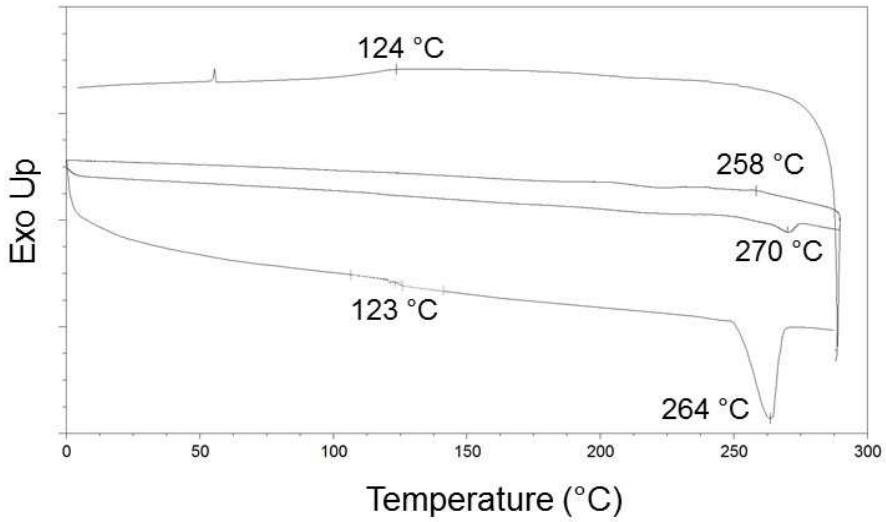

Figure 3.11: DSC of PDAS from **1a** (DAS-sample 1).

Next, it is necessary to further discuss the resonance at 4.8 ppm in the ^{1}H NMR presented earlier in Figure 3.4. While there was no evidence for vinylic resonances of the ^{1}H NMR that might arise by chain-termination of the propagating

species through β-hydrogen transfer processes, a plot of M_n vs. time (Figure 3.12) for PDAS clearly reveals a nonlinear dependence of M_n as a function of monomer conversion, as well as a steady increase in the polydispersity index ($Đ$ increases gradually throughout the duration of the polymerization from 1.08 after 5 minutes of reaction to 1.52 after 18 hours). These results are not in line with a fully living system. Upon close inspection of ^{1}H NMR (800 MHz, 110 °C, TCE-d_2) spectra of either commercially obtained or independently synthesized samples of the DAS monomer (Figure 3.13) it could be determined that these materials invariably contain 1 − 2% of isomeric 1-propenyl groups in place of the desired 2-propenyl (allyl) substituents. It has been previously established that Sita initiators (i.e. **1a – 3a**) are not catalytically active toward the polymerization of internal alkenes, and further that the presence of internal alkenes lead to catalyst deactivation. Accordingly, given the inability to purify DAS to a higher extent using conventional methods, it is likely that undesirable insertion of 1-propenyl end-groups render the initiator inactive toward polymerization.

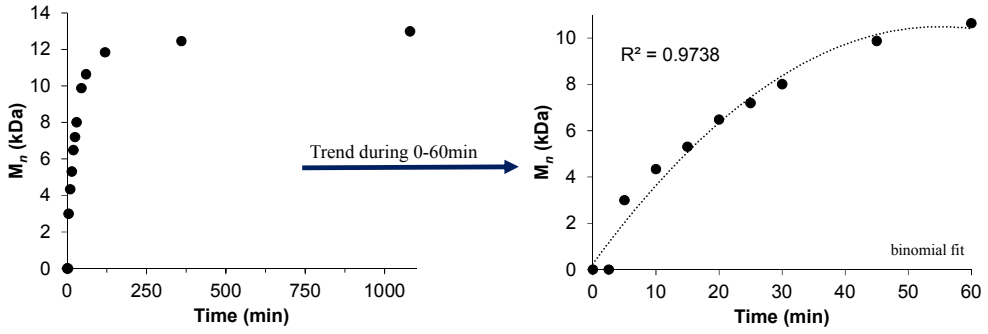

Figure 3.12: M_n vs. time for PDAS from **1a** (DAS-sample 1a). R^2 based on 1 data set only.

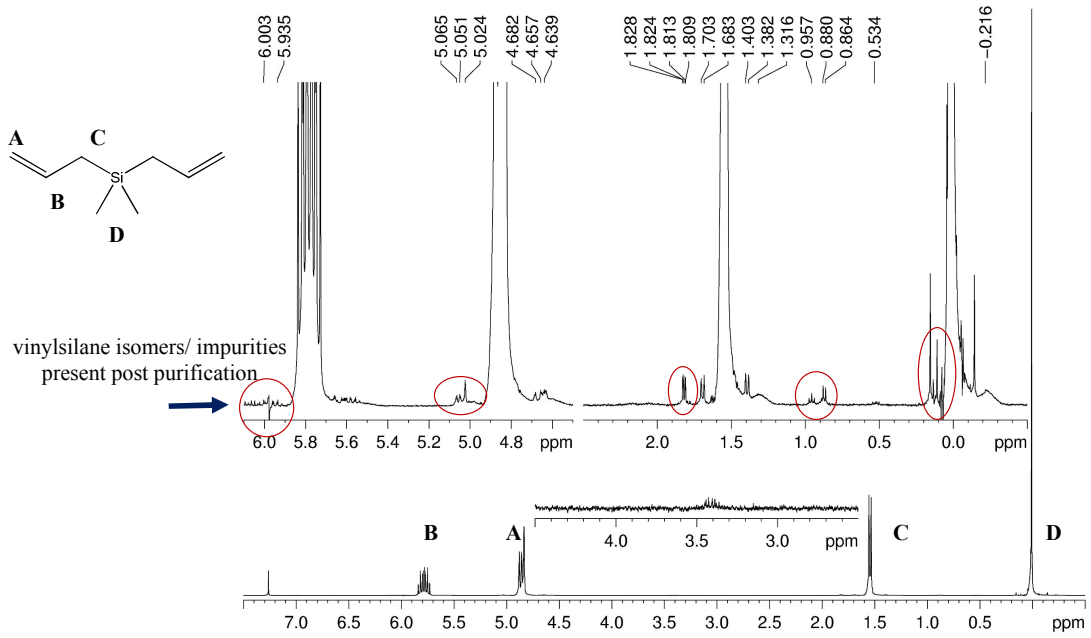

Figure 3.13: ^{1}H NMR of bis(2-propenyl)dimethylsilane (DAS) post purification with NaK; CCl_3-d_1, 400 MHz.

Kinetic results further confirm the thwarted polymerization of DAS with **1**. Two kinetic studies were carried out. Both studies were completed using GC and standard reaction conditions except for the solvent, which was switched from PhCl to toluene due to the similar boiling point of PhCl and DAS, 131 °C and 155 °C, respectively. These peaks could not be separated by GC due to the large quantity of PhCl compared to DAS and the available type of GC column. Assuming the rate of initiation (k_i) is much greater than the rate of propagation (k_p) and that k_p remains constant throughout the polymerization, as observed for living polymerizations,[11] the plot of $\ln[M_o]/[M_t]$ vs. time (where $[M_o]$ and $[M_t]$ are the monomer concentration at time zero and time, *t*, respectively) would increase linearly with time. The first study employed the same equivalence of monomer used for all standard polymerizations (i.e. DAS:**1a** = 100:1), a non-linear correlation between $\ln[M_o]/[M_t]$ and reaction time

was observed suggesting that initiator deactivation may be occurring during the polymerization. Additionally, only an 81 % monomer conversion was achieved, Figure 3.14. The second kinetic study was carried out with the awareness of the presence of DAS isomer impurity. Lowering the number of equivalence of monomer would also lower the amount of vinyl isomer impurity present with respect to the initiator concentration. In this regard, the second kinetic study was carried out using only 25 equivalence of monomer (i.e. DAS:**1a** = 25:1). As expected, the plot of $\ln[M_o]/[M_t]$ vs. time now increases linearly with reaction time, which is indicative of a constant k_p over the time scale of the experiment, and a living system. Furthermore, there was 100 % conversion of monomer with the second kinetic study, Figure 3.15.

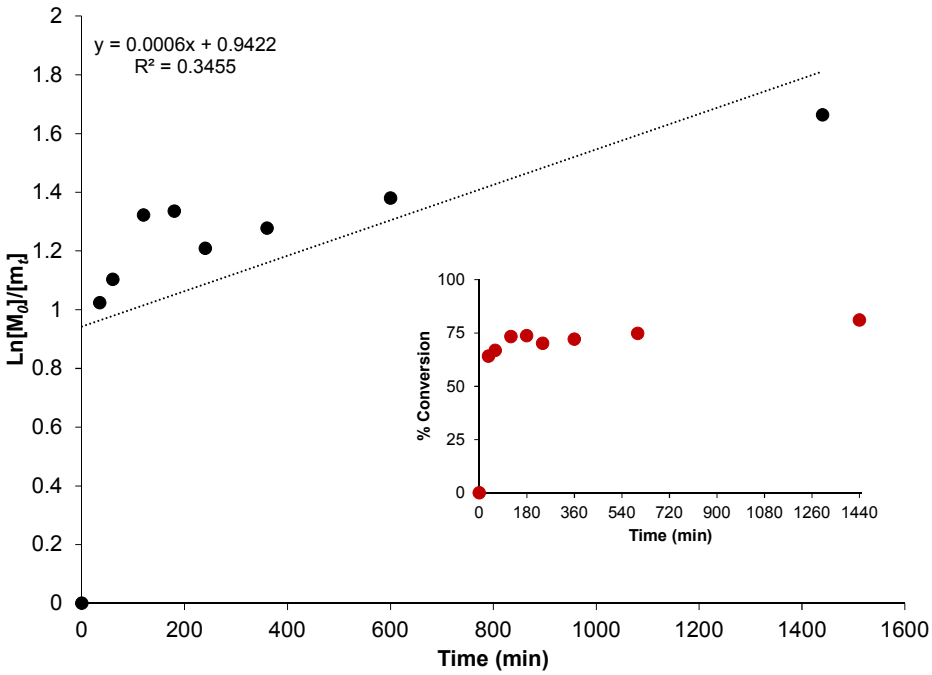

Figure 3.14: Kinetic analysis for DAS polymerization (100 equiv.). R^2 based on 1 data set only.

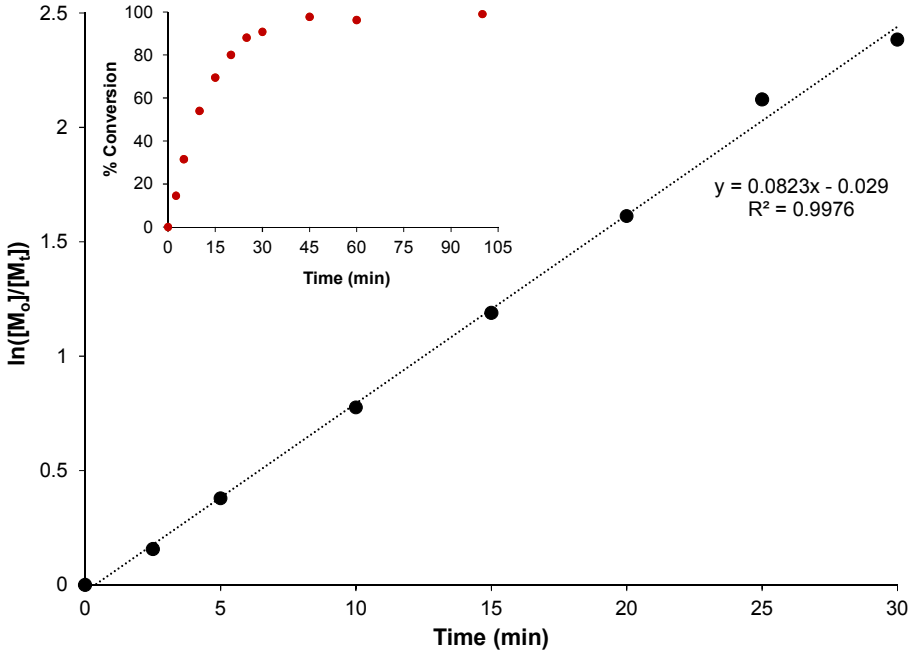

Figure 3.15: Kinetic analysis for DAS polymerization (25 equiv.). R^2 based on 1 data set only.

To summarize, DAS was successfully polymerized in a controlled fashion using precatalyst **1** activated by **II** (**1a**) for the formation of semi-crystalline, highly *cis* isotactic PDAS. M_n can be easily controlled by varying the concentration of DAS at the start of a reaction. The polydisperisty increases with polymerization time but is not observed to be greater than $Đ = 1.52$, despite a longer reaction time (18 hours). The highly regio- and stereospecific PDAS exhibits a T_m between 264 °C – 270 °C depending on the DSC temperature program employed. The T_g is 123 °C, which is approximately 20 °C higher compared to polyolefins with similar structure, such as PMCH (Chapter 2).

The successful controlled polymerization of DAS with **1** prompted a study on how the same DAS monomer would behave in the presence of **2** activated by **II** (**2a**). Thus, the polymerization conditions described earlier in Scheme 3.1 were applied for

the cyclopolymerization of DAS to form PDAS, which could be recovered in 65 % - 80 % yield and has the appearance of a transparent glassy material. PDAS material resulting from polymerization with C_s-symmetric **2** is easily soluble in organic solvents and is predicted to have formed an amorphous atactic PDAS material. SEC analysis of this material revealed a M_n of 11.8 kDa and relatively narrow polydispersity ($Đ$ = 1.13) (DAS-sample 2), Table 3.1 and Figure 3.16.

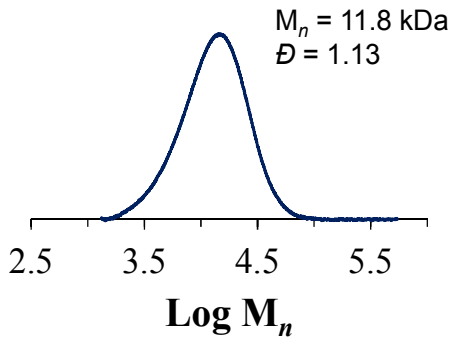

Figure 3.16: SEC trace for PDAS from **2a** (DAS-sample 2).

A *cis* atactic PDAS microstructure was indeed confirmed by $^{13}C\{^1H\}$ NMR. The $^{13}C\{^1H\}$ NMR for sample 2 displayed 5 groups of resonances between -5 ppm and 60 ppm, Figure 3.17. The resonances between -5 ppm and 0 ppm correspond to the two methyl groups bonded to the Si heteroatom. The resonances at near 22 ppm correspond to carbons atoms at positions 2 and 6 (molecular structure labels in Figure 3.17 inset). The resonances at ca. 30 ppm are attributed to carbon atoms at positions 3 and 5. The resonances between 43.5 ppm and 44 ppm are attributed to carbon 4, and the final resonance at ca. 54 ppm corresponds to carbon 7. Analysis of PDAS using ^{29}Si NMR, Figure 3.18, which exhibit three distinct, yet broad resonances (-2.0 ppm –

-2.28 ppm), further confirms the aspecific stereochemical microstructures suggested by $^{13}C\{^{1}H\}$ NMR.

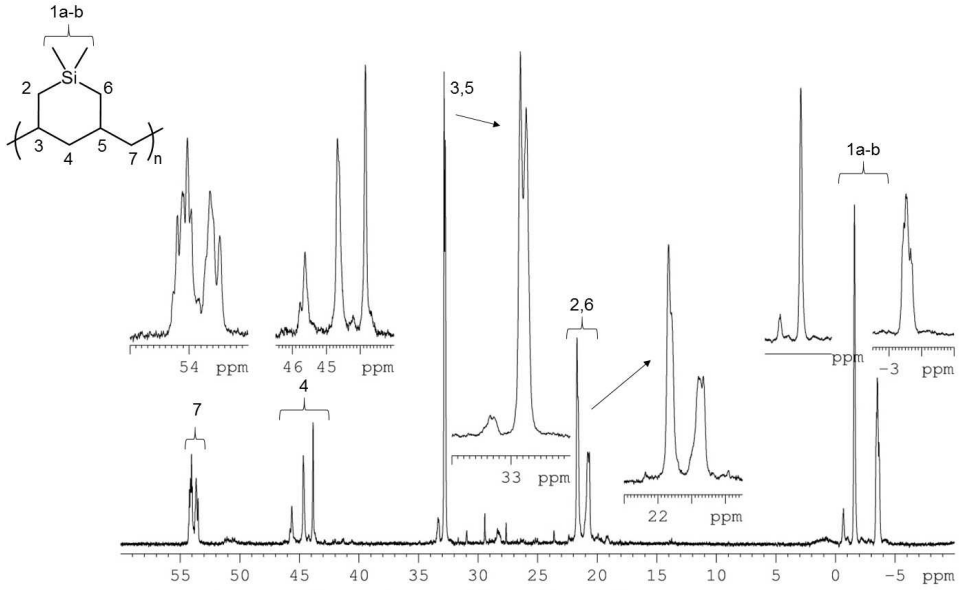

Figure 3.17: $^{13}C\{^{1}H\}$ NMR of PDAS from **2a** (DAS-sample 2); 200 MHz, 110 °C, TCE-d_2.

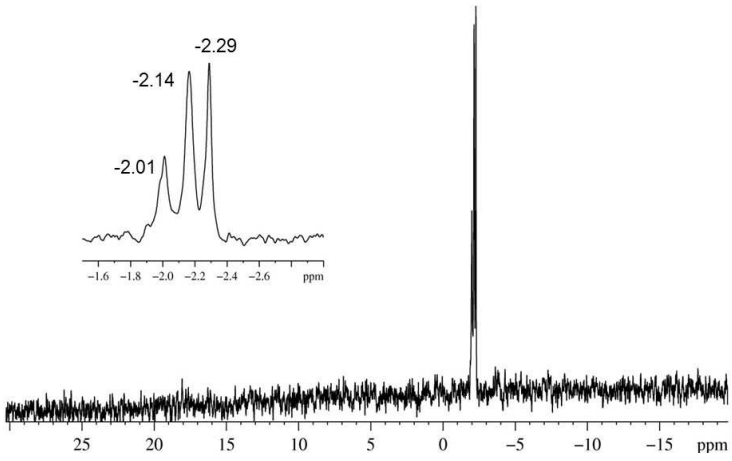

Figure 3.18: ^{29}Si NMR of PDAS from **2a** (DAS-sample 2); 100 MHz, 90 °C, TMS-d_{12}.

DSC measurements for DAS-sample 2 were carried out using the similar parameters described above for DAS-sample 1. Briefly, the temperature program was as follows: heat to 300 °C at 10 °C/min; isothermal hold x 30 min; cool to 70 °C at 10 °C/min; heat to 300 °C at 10 °C/min; cool to 70 °C at 10 °C/min. Shown: final cool cycle, final heat cycle. As anticipated based on the atactic nature of the material, no T_m or T_c was observed, only a T_g of 115 °C, Figure 3.19. The ^{1}H NMR for DAS-sample 2 exhibited vinyl resonances similar to those observed for DAS-sample 1. These small vinylic peaks, combined with the less than quantitative yields may be attributed to the same 1 % - 2 % isomer impurity hindering sample 1. Thus, for the time being, this system, the cyclopolymerization of DAS with cationic **2a**, has been designated as a controlled, rather than a strictly living, polymerization.

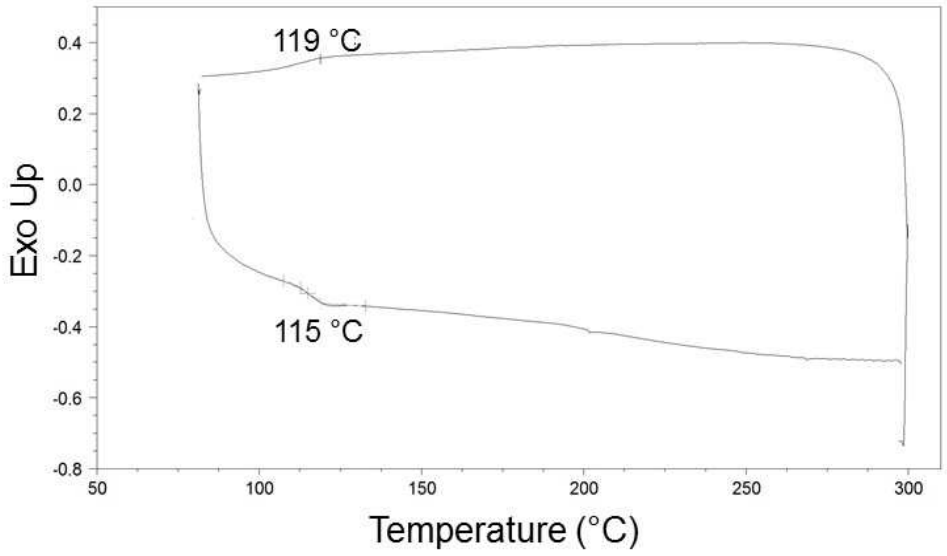

Figure 3.19: DSC trace of PDAS from **2a** (DAS-sample 2).

In summary, DAS was successfully cyclopolymerized, in a controlled fashion, to produce PDAS with two distinct stereochemical forms as a function of the type of

initiator employed. Cationic initiator **1a** produces a highly *cis* isotactic PDAS with T_m and T_g of ca. 264 °C and 124 °C, respectively (DAS-sample 1). Cationic initiator **2a** yields an atactic PDAS structure, yet is still highly regio-selective towards *cis* diastereoselectivity. The T_g for sample 2 is 115 °C, no T_m is observed.

3.2.2. Diallylmethylphenylsilane, MPS

Prior to the polymerization of DAS (diallyldimethylsilane) to afford PAS, initiators **1** and **2** had only previously been investigated using pure hydrocarbon α-olefins[12] and to a much lesser extent α,ω-olefins.[13] Therefore, it is of interest to 'stretch' the pool of monomers available for polymerization with precatalysts **1** and **2** (activated by **II** to form **1a** and **2a** respectively). In this regard, following the successful cyclopolymerization of DAS, MPS (diallylmethylphenylsilane) was also pursued as a potential monomer for cyclopolymerization using **1a** and **2a**. Similar reaction conditions used previously for DAS (outlined in Scheme 3.1) were applied for the cyclopolymerization of MPS. The resulting transparent, glassy polymers were obtained in lower than expected yields (40 % - 66 %), and are easily soluble in common organic solvents. The poly(3,5-methylene-1,1-methylphenyl-silacyclohexane) (PMPS) that results from cationic initiator **1a** has an M_n of 45.1 kDa and broad polydispersity ($Đ$ = 2.08) as determined by SEC, Figure 3.20.

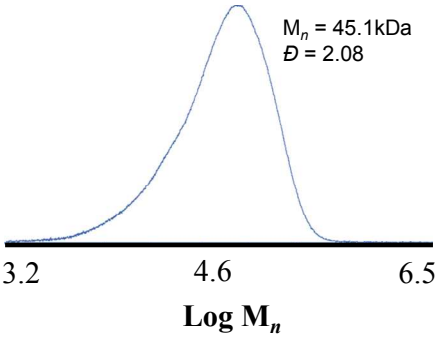

Figure 3.20: SEC trace of PMPS from **1a** (MPS-sample 3).

The M_n is much higher than the theoretical molecular weight predicted for a living, single-site catalyst polymerization. The higher M_n and broad *Đ* is an indication that initiator deactivation occurs during polymerization. This indication, along with the low yields suggest a non-living system under the polymerization conditions used. Nevertheless, the polymer that is produced from cationic initiator **1a** is expected to be highly isotactic, and the polymer produced from cationic initiator **2a** is expected to be atactic. *Cis* diastereoselectivity is anticipated for both PMPS materials. Interestingly, the DEPT135 NMR spectra obtained from polymerization of MPS using cationic **1a** (sample 3) does not resemble a highly isotactic material, that is, the spectra do not have 6 sharp resonances as seen with *c*-i-PDAS (Figure 3.5). Instead, there are 5 groups of overlapping resonances between -10 ppm and 60 ppm, plus the aromatic resonances (125 ppm – 135 ppm, not shown); however, the ring formation remains selective towards a *cis* conformation, Figure 3.21. The two resonances between -5 ppm and 0 ppm correspond to the methyl group bonded to the Si heteroatom. The resonances at near 20 ppm correspond to carbon atoms at positions 2 and 6 (molecular structure labels in Figure 3.21 inset). The resonances at ca. 32 ppm are

attributed to carbon atoms at positions 3 and 5. The resonances between 43 ppm and 44 ppm are attributed to carbon 4, and the final resonance at ca. 54 ppm corresponds to carbon 7. Analysis of PDAS using ^{29}Si NMR, Figure 3.22, which exhibit several overlapping resonances (-7.0 ppm – -7.0 ppm), further confirms the aspecific stereochemical microstructures suggested by $^{13}C\{^{1}H\}$ NMR

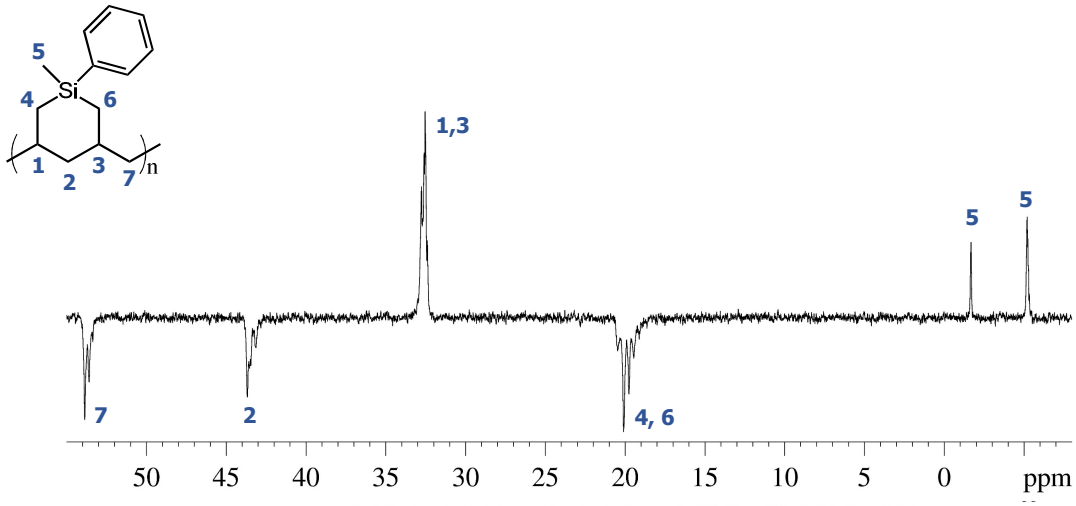

Figure 3.21: DEPT135 NMR of PMPS from **1a** (MPS-sample 3); 100 MHz, 90 °C, TCE-d_2.

The increase in the number of NMR resonances may be explained by the inherent monomer asymmetry, which stem from the unique pendant groups bonded to the Si atom: -CH_3 (methyl) and –C_6H_5 (phenyl). Although it is anticipated that the cationic initiator **1a**, retains enantiofacial stereoselectivity and *cis* diastereoselectivity, there is no control over which of the two allyl groups bonded to Si coordinate to the active site on the metal center first, Scheme 3.2.

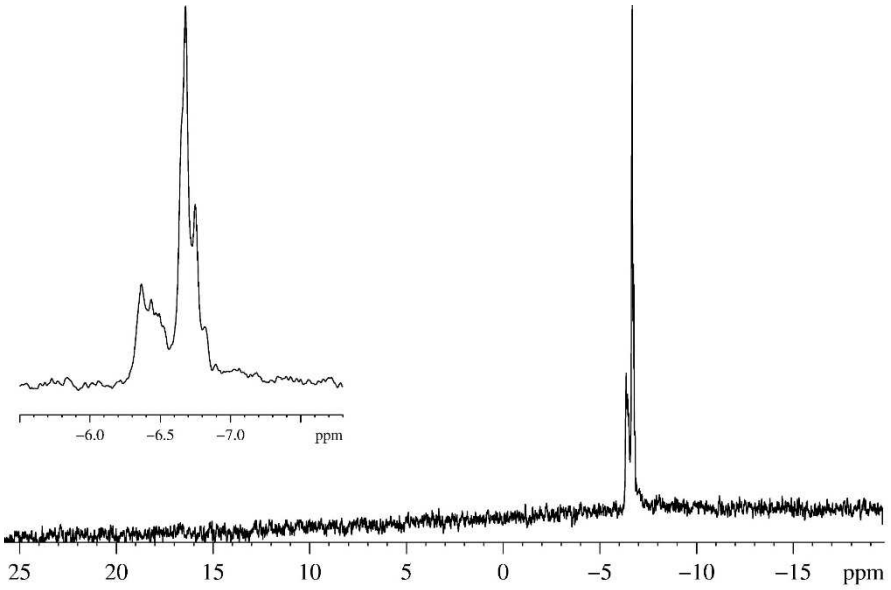

Figure 3.22: ^{29}Si NMR of PMPS from **1a** (MPS-sample 3); 100 MHz, 90 °C, TMS-d_{12}.

Scheme 3.2: Schematic of allyl group coordination for cyclopolymerization.

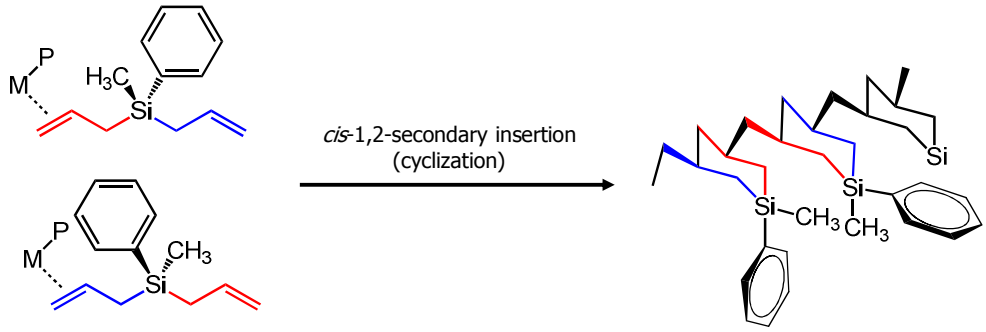

Next, it was of interest to determine the thermal properties for sample 3. While a melting temperature is not expected for this material based on the confirmed microstructure, a T_g is expected; further the T_g is anticipated to be higher than that observed for the PDAS materials due to the increased bulkiness of the cyclic repeating unit. Indeed, following DSC analysis using a standard temperature program:

heat/cool/heat at 10 °C/min from 0 °C to 290 °C, a T_g of 155 ± 2 °C was observed (no T_m), Figure 3.23.

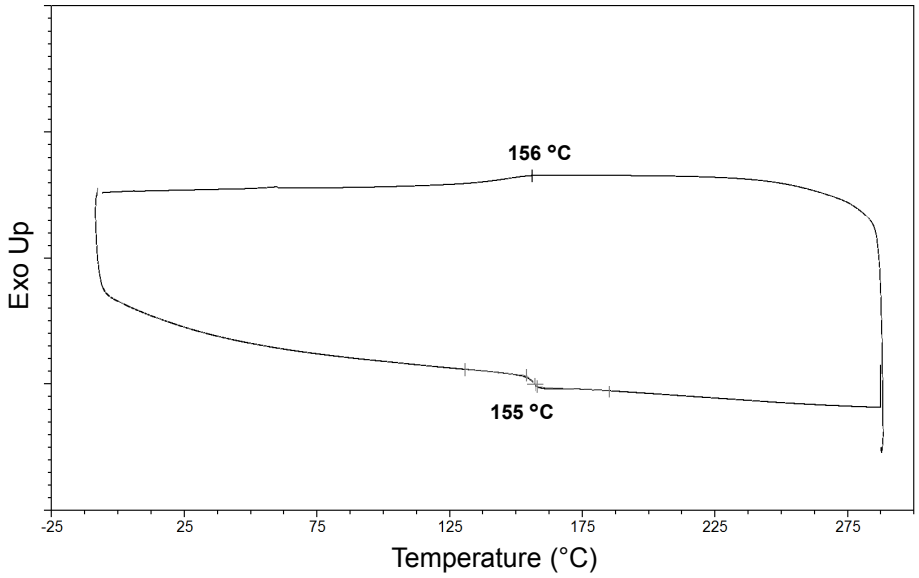

Figure 3.23: DSC trace for PMPS from **1a** (MPS-sample 3).

Similar results are observed for the cyclopolymerization of MPS with cationic initiator **2a** (sample 4), albeit the DEPT135 NMR resonances are more broad, which is indicative of greater aspecificity within the microstructure, Figure 3.24. The T_g is also slightly lower (150 ± 2 °C) compared to PMPS from **1a** (sample 3). The M_n is 31.1 kDa with broad polydispersity, $Đ = 1.94$. The molecular weight is higher than the theoretical M_n predicted for a living, single-site coordination polymerization. This result, combined with low yields (40 % - 60 %), suggest a non-living polymerization under the tested conditions.

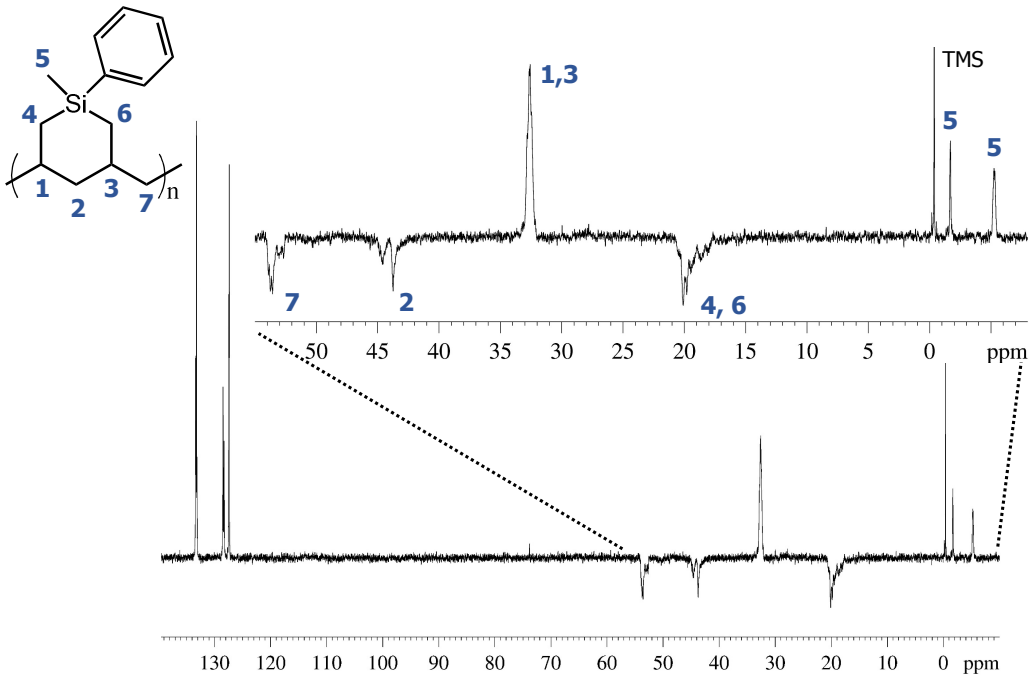

Figure 3.24: DEPT135 NMR of PMPS from **2a** (MPS-sample 4); 100 MHz, 90 °C, TCE-d_2.

In summary, MPS was successfully polymerized, in a controlled fashion, through the use of precatalysts **1** and **2** when activated by **II** for the formation of cationic **1a** and **2a**. The PMPS materials have high selectivity for cyclization (no pendant vinyl groups observed), are easily soluble in organic solvents, and have high T_g's (≥ 150 °C).

3.3. Cyclopolymerization of 9,9-Diallylfluorene, DAF

9,9-Diallylfluorene (DAF) can be synthesized from fluorene and subsequently used for cyclopolymerization. While few reports currently exist regarding the cyclopolymerization of DAF there is a great interest in developing poly(9,9-

diallylfluorene) (PDAF) materials for their potential use as conductive materials capable of electron-transport and as an emission source.[14] Both characteristics would be permissible through pi-stacking effects that may arise from well-defined PDAF materials. Takeuchi and coworkers have investigated an array of polymerization catalysts for the production of PDAF.[15] Specifically, they used various Ni, Pd, Fe and Co diimine complexes (**G** – **J**) activated by either modified methylaluminoxane (MMAO) or NaBARF ($[B\{C_6H_3(CF_3)_2\text{-}3,5\}_4^-]$) for the production of PDAF consisting of a wide range of stereochemical microstructures with both 5- and 6-membered rings as well as selectivity towards *cis* or *trans* diastereoselectivity depending on the catalyst employed, Figure 3.25.

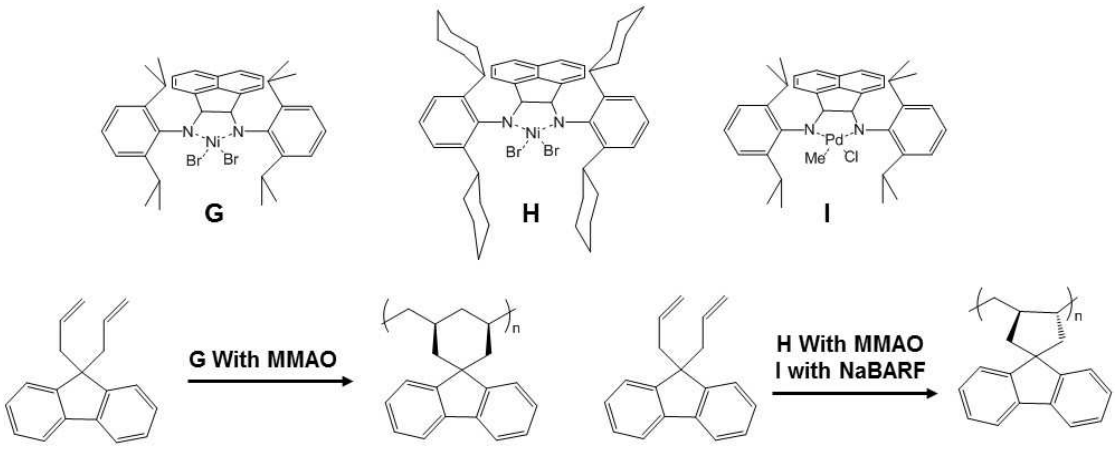

Figure 3.25: Catalysts for polymerization of DAF used by Takeuchi and coworkers.[15]

Molecular weights for these PDAF materials ranged between 6.1 kDa to 23.9 kDa with relatively broad polydisperisities ($Đ$ = 1.35 – 2.40). Interestingly, their reports do not discuss potential for emission or electron transport. Naga was successful with the incorporation of DAF as a comonomer for copolymerization with either ethylene or propylene[16] Higher cyclization selectivity was reported for copolymerization with propylene compared to ethylene; however, both copolymers consist of some degree of acyclic pendant groups, which contributed to crosslinking, in some cases severely. PDAF incorporation into either polyethylene (PE) or polypropylene (PP) was reported between 0 % and 20.8 %. The catalyst types and proposed polymerization products are shown in Figure 3.26. Their report provides UV-vis and photoluminescence spectroscopy data indicating that absorbance (ca. 270 nm) and emission (ca. 315 nm) intensities increase with increasing PDAF content in the PP copolymer.

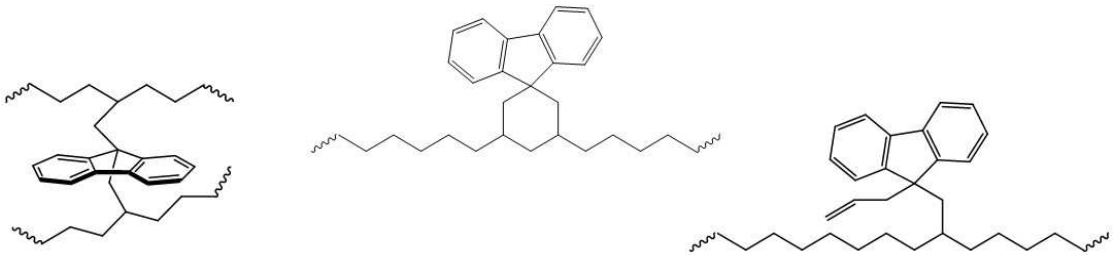

Figure 3.26: PDAF related products reported by Naga.[16]

It may be feasible to use Sita precatalysts **1** and **2** for the cyclopolymerization of DAF to form PDAF. In this regard, DAF was successfully synthesized from fluorene through the stepwise deprotonation of the weakly acidic protons at the C9-position using n-butyl lithium as a Lewis base followed by nucleophilic attack of the

anionic florenyl intermediate on allyl-bromide, Scheme 3.3. The DAF product was confirmed by ^{1}H NMR, which revealed a small amount of the mono-allyl fluorene derivative and an even lesser quantity of the fluorene starting material, Figure 3.27.

Scheme 3.3: Reaction scheme for the synthesis of DAF from fluorene.

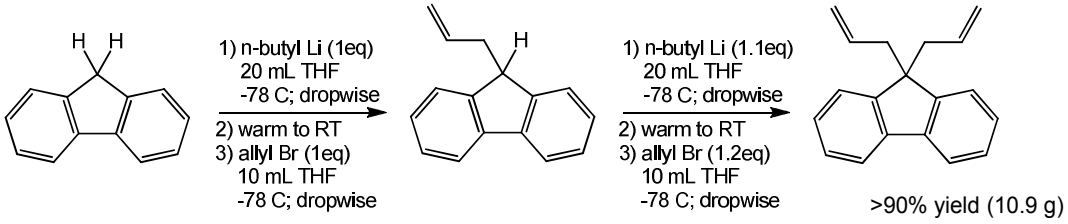

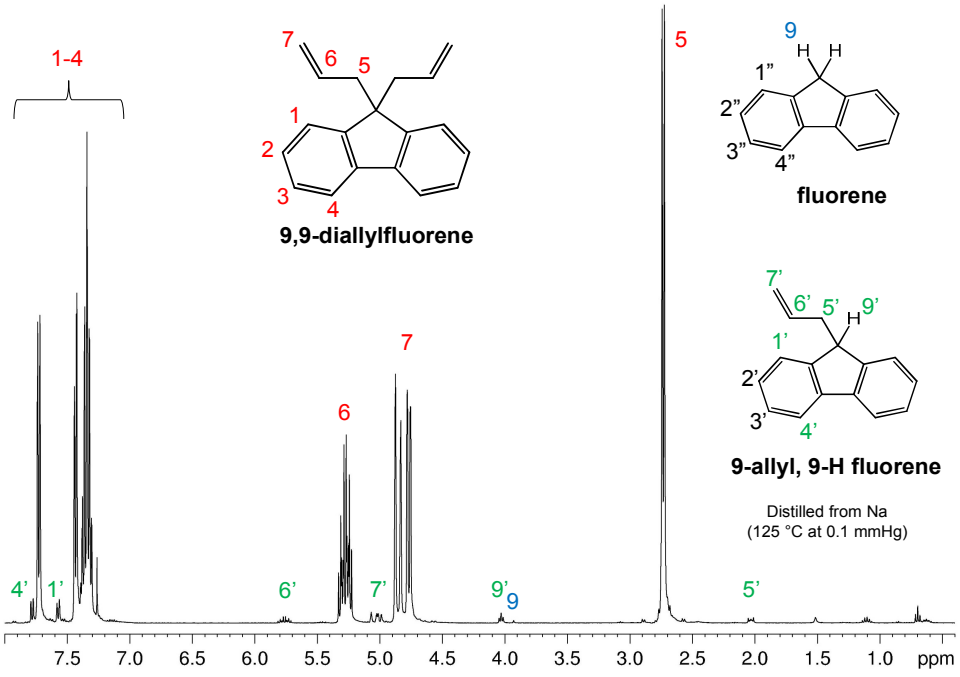

Figure 3.27: ^{1}H NMR of 9,9-diallylfluorene; 400 MHz, CCl3-d_1, 25 °C.

Polymerizations of DAF were attempted using standard polymerization conditions (refer to Scheme 3.1). Unfortunately, despite repeated attempts, cationic

initiators **1a** and **2a** were not successful in catalyzing the polymerization of DAF. Three possibilities are considered: 1) the acidic proton(s) located at the C9-position for the mono-allyl fluorene derivative and fluorene starting material could have competed with allyl insertion into the active-site on metal center causing deactivation toward polymerization. 2) Coordination of the fluorene substituent to the initiator complex may have inhibited polymerization. 3) Monomer bulkiness may have greatly hindered facile coordination and subsequent insertion/propagation. The first consideration can likely be ruled out as the DAF product depicted in Figure 3.27 was re-allylated, thus largely removing the remaining mono-allyl fluorene derivative and starting material but was still inactive for polymerization. Further investigation regarding the thwarted polymerization of DAF with **1a**, and **2a**, including its incorporation as a comonomer for copolymerizations, were not pursued.

3.4. Cyclopolymerization of Diallyl-tetramethyl-disiloxane, AMS

Carbosiloxane homopolymers have received considerable attention due to the versatility of the siloxane moiety. In general, siloxanes exhibit good gas permeability, low temperature flexibility and thermal stability.[17] The primary polymerization method for 1,3-diallyl-1,1,3,3-tetramethyldisiloxane (AMS) is through acyclic diene metathesis (ADMET).[18] To date, the cyclopolymerization of AMS has not been successful. However, there have been several successful reports on the single-unit cyclization of AMS resulting in a cyclic siloxane structure.[19] It is well known that group 4 transition metal catalysts for coordination polymerization, such as precatalysts **1** and **2** (activated by **II** to afford **1a** and **2a** respectively), are unable to polymerize olefins containing polar functional groups. However, cationic initiators **1a**

and **2a** are active for the cyclopolymerization of dienes containing silane functionality (see Section 3.2). While oxygen containing monomers are not generally considered for coordination polymerization with early transition metals, a well-protected oxygen atom may help to mitigate the deactivating effects of oxygen. In that regard, the four methyl substituents on the AMS monomer may serve to hinder catalyst deactivation. For this reason, AMS was synthesized and subsequently employed for polymerization using precatalysts **1** and **2**. Briefly, synthesis of AMS was carried out by the addition of 2.1 equivalence of magnesium allyl-bromide to 1.0 equivalence of 1,3-dichloro-1,1,3,3-tetramethyldisiloxane, Scheme 3.4. The reaction resulted in 18.6 g of AMS (95 % yield), whose molecular structure was confirmed by ^{1}H NMR, Figure 3.28.

Scheme 3.4: Reaction scheme for the synthesis of AMS.

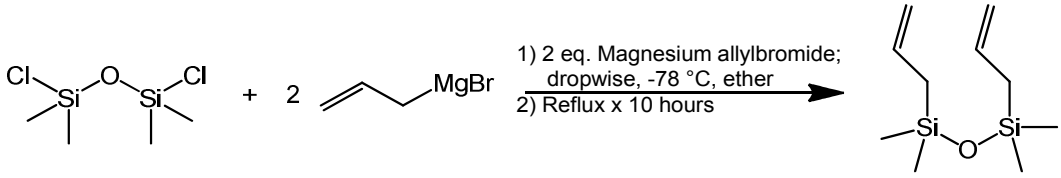

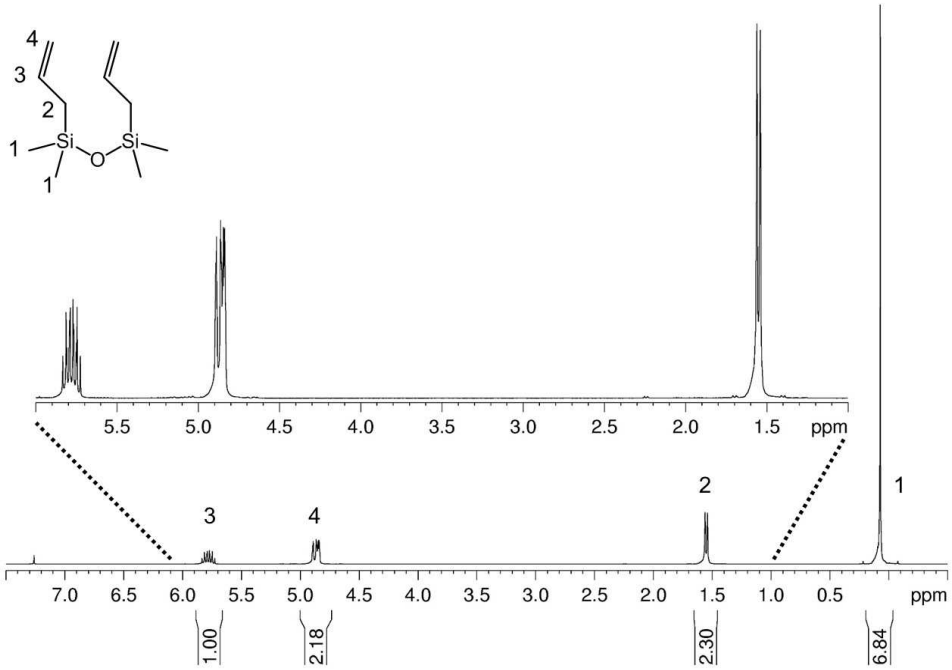

Figure 3.28: ^{1}H NMR of purified AMS; 400 MHz, 25 °C, CCl_3-d_1.

Polymerizations of AMS were attempted using standard polymerization conditions (refer to Scheme 3.1). Unfortunately, despite repeated attempts, cationic initiators **1a** and **2a** were not successful in catalyzing the polymerization of AMS. The reason for lack of polymer is likely due to initiator deactivation as a result of the competing coordination of the oxygen vs. coordination of the pi-electrons from the allyl groups. Polymerization of AMS was not pursued further.

3.5. Conclusions

Cationic group 4 transition metal complexes, developed previously by the Sita group, with the general formula: (η^5-C_5R_5)M[N(R^1)C(R^2)N(R^3)](Me_2) (M = Zr, Hf, R = alkyl, Me = methyl, Et = ethyl) were applied, for the first time, to a series of substituted non-conjugated dienes. Specifically, **1** ((η^5-C_5Me_5)Zr[N(t-

butyl)C(Me)N(Ethyl)](Me$_2$)), and **2** ((η^5-C$_5$Me$_5$)Hf[N(Et)C(Me)N(Et)](Me$_2$)), were activated by **II** ([PhHNMe$_2$][B(C$_6$F$_5$)$_4$]) to catalyze the polymerization of monomers: diallyldimethylsilane (DAS), diallylmethylphenylsilane (MPS), 9,9-diallylfluorene (DAF), and 1,3-diallyl-1,1,3,3-tetramethyldisiloxane (AMS), using standard polymerization conditions (ca. -10 °C – -15 °C, 2-8 hours in chlorobenzene or toluene as solvent). Cyclopolymerizations were successful for DAS and, to a lesser extent, for MPS. The controlled cyclopolymerization of DAS with precatalyst **1** resulted in highly regio- and stereospecific *cis* isotactic poly(3,5-methylene-1,1-dimethylsilacyclohexane) (PDAS) with high glass transition and melting temperatures, 124 °C and 264 °C – 270 °C, respectively. The controlled cyclopolymerization of DAS with precatalyst **2** resulted in highly regio-regular, *cis*, atactic PDAS with a T_g of 115 °C and no T_m. The controlled cyclopolymerization of MPS with precatalysts **1** and **2** gave amorphous poly(3,5-methylene-1-methyl-1-phenylsilacyclohexane) (PMPS) in part due to the asymmetry of the Si atom substituents (methyl and phenyl), which likely disrupt effective packing for crystallization. The PMPS materials have T_g values of 155 ± 3 °C and 150 ± 3 °C for PMPS from precatalysts **1** and **2**, respectively. Melting temperatures were not observed for either material. Polymerizations of DAF and AMS with precatalysts **1** and **2** were unsuccessful.

3.6. Experimentals

3.6.1. General Polymer Synthesis Procedure

The polymerizations were carried out under an inert atmosphere of dinitrogen using a Vacuum Atmospheres glovebox. The general polymerization method is as follows: 1.01 equiv. of cocatalyst $[PhNHMe_2][B(C_6F_5)_4]$ (**II)**, was mixed with 0.02 mmol precatalyst, **1** or **2** in 1.5 mL cold PhCl. The resulting bright yellow mixtures of precatalyst with **II** were then added to pre-chilled (-18 °C – -10 °C) PhCl in a 50-mL round bottomed glass reaction vessel equipped with a magnetic stir bar. The α,ω-olefin monomer (ca. 100 equiv.) was then added to the reaction mixture and allowed to stir for a given amount of time, typically 1 to 8 hours. Following a given amount of reaction time the reaction mixtures were removed from the glovebox and quenched/precipitated in a large excess of acidic methanol (300 mL – 500 mL; 10% HCl by volume). The polymers were vacuum filtered, washed with methanol, collected in a pre-weighed vial, and dried under vacuum until constant weight. Instrument parameters and source of materials information are provided in Appendices A and B.

3.7. References

1. Butler, G. B.; Stackman, R. W., *J. Org. Chem.* **1960**, *25*, 1643-1644.
2. Marvel, C. S.; Woolford, R. G., *J. Org. Chem.* **1960**, *25*, 1641-1643.
3. Berlin, K. D.; Butler, G. B., *J. Am. Chem. Soc.* **1960**, *82*, 2712-2714.
4. Billingham, N. C.; Jenkins, A. D.; Kronfli, E. B.; Walton, D. R. M., *J. Polym. Sci.* **1977**, *15* (3), 675-681.

5. Saigo, K.; Tateishi, K.; Adachi, H., *J. Polym. Sci. A1* **1988**, *26* (8), 2085-2097.

6. Cragg, R. H.; Jones, R. G.; Swain, A. C., *Eur. Polym. J.* **1991**, *27* (8), 785-788.

7. Naga, N., *Macromol. Chem. Phys.* **2005**, *206* (19), 1959-1966.

8. Naga, N., *J. Polym. Sci. A1* **2006**, *44* (20), 6083-6093.

9. Marciniec, B.; Lewandowski, M.; Kwiatkowska, E., *J. Polym. Sci. A1* **1997**, *35* (15), 3299-3304.

10. Crawford, K. E.; Sita, L. R., *ACS Macro Lett.* **2014**, *3* (6), 506-509.

11. Matyjaszewski, K., *J. Phys. Org. Chem.* **1995**, *8* (4), 197-207.

12. a) Harney, M. B.; Zhang, Y.; Sita, L. R., *Angew. Chem., Int. Ed.* **2006**, *45* (15), 2400-2404.; b) Harney, M. B.; Keaton, R. J.; Fettinger, J. C.; Sita, L. R., *J. Am. Chem. Soc.* **2006**, *128* (10), 3420-3432.; c) Kissounko, D. A.; Fettinger, J. C.; Sita, L. R., *Inorg. Chim. Acta* **2003**, *345*, 121-129.; d) Keaton, R. J.; Jayaratne, K. C.; Henningsen, D. A.; Koterwas, L. A.; Sita, L. R., *J. Am. Chem. Soc.* **2001**, *123* (25), 6197-6198.; e) Jayaratne, K. C.; Sita, L. R., *J. Am. Chem. Soc.* **2000**, *122* (5), 958-959.

13. a) Crawford, K. E.; Sita, L. R., *J. Am. Chem. Soc.* **2013**, *135* (24), 8778-8781.; b) Zhang, W.; Sita, L. R., *J. Am. Chem. Soc.* **2008**, *130* (2), 442-443.; c) Jayaratne, K. C.; Keaton, R. J.; Henningsen, D. A.; Sita, L. R., *J. Am. Chem. Soc.* **2000**, *122* (42), 10490-10491.

14. a) Egelhaaf, H.-J.; Holder, E.; Herman, P.; Mayer, H. A.; Oelkrug, D.; Lindner, E., *J. Mater. Chem.* **2001**, *11* (10), 2445-2452.; b) Rathore, R.; Abdelwahed, S. H.; Guzei, I. A., *J. Am. Chem. Soc.* **2003**, *125* (29), 8712-8713.

15. a) Takeuchi, D.; Fukuda, Y.; Park, S.; Osakada, K., *Macromolecules* **2009**, *42* (16), 5909-5912.; b) Takeuchi, D.; Matsuura, R.; Fukuda, Y.; Osakada, K., *Dalton T.* **2009**, (41), 8955-8962.

16. Naga, N.; Sakai, H.; Usui, C.; Tomoda, H., *J. Polym. Sci. A1* **2010**, *48* (16), 3542-3552.

17. Brook, M. A., *In Silicon in Organic Organometallic, and Polymer Chemistry*. Wiley-VCH Verlag: 2000; p 405.

18. Smith, D. W., Jr.; Wagener, K. B., *Macromolecules* **1993**, *26* (7), 1633-1642.

19. Pun, D.; Knobloch, D. J.; Lobkovsky, E.; Chirik, P. J., *Dalton T.* **2011**, *40* (30), 7737-7747.

Chapter 4

Degenerative Methyl Group Transfer Polymerization

4.1. Introduction

As shown in Chapters 2 and 3 precatalyst **1** (Cp*ZrMe$_2$[N(Et)C(Me)N(*t*-Bu)]) is an effective isoselective polymerization catalyst following complete activation by addition of a stoichiometric amount of cocatalyst **II** ([PhHNMe$_2$][B(C$_6$F$_5$)$_4$]) (forming cationic **1a**: Cp*ZrMe[N(Et)C(Me)N(*t*-Bu)][B(C$_6$F$_5$)$_4$]) toward the living and controlled cyclopolymerization of 1,6-heptadiene (1,6-HD) and diallyldimethylsilane (DAS) monomers, respectively.[1, 2] Precatalyst **1** has also been shown to be an efficient isoselective, living coordination polymerization (LCP) catalyst upon activation by a stoichiometric amount of **II** for the polymerization of α-olefins such as propene and higher alkenes.[3, 4] Further, it is known that C$_1$-symmetric **1**, in the neutral state, exists as a racemic mixture of the R- and S-manifolds as a result of rapid epimerization (amidinate ring-flipping has a low energy barrier; $\Delta G^{\ddagger}$ 10.9 kcal/mol at 223 K).[5] Once activated by cocatalyst **II**, however, the energy barrier for ring-flipping is much higher causing the rate of epimerization to be extremely slow and is considered negligible on the NMR and polymerization time scales. That is, once complete activation of **1** by cocatalyst **II** has taken place, the amidinate ligand on the now cationic **1a** is 'locked in place' and thus produces isoselective polyolefins with a 50:50 mixture of polymer chains with all R- or all S-configuration. The Sita group has also shown that with the partial activation of **1** by substoichiometric amounts of **II**

results in rapid and reversible methyl group exchange between the cationic initiator **1a** and neutral **1**, Scheme 4.1. Here the rate of epimerization of **1** in the neutral state is much faster than the rate of methyl group exchange between **1** and **1a**, which is in turn occurs faster than the rate of propagation (i.e. $k_{epi} >> k_{ex} > k_p$, where k_{epi}, k_{ex} and k_p are the rate constants for epimerization, exchange and propagation).

Scheme 4.1: Reversible deactivation *via* degenerative methyl group transfer.

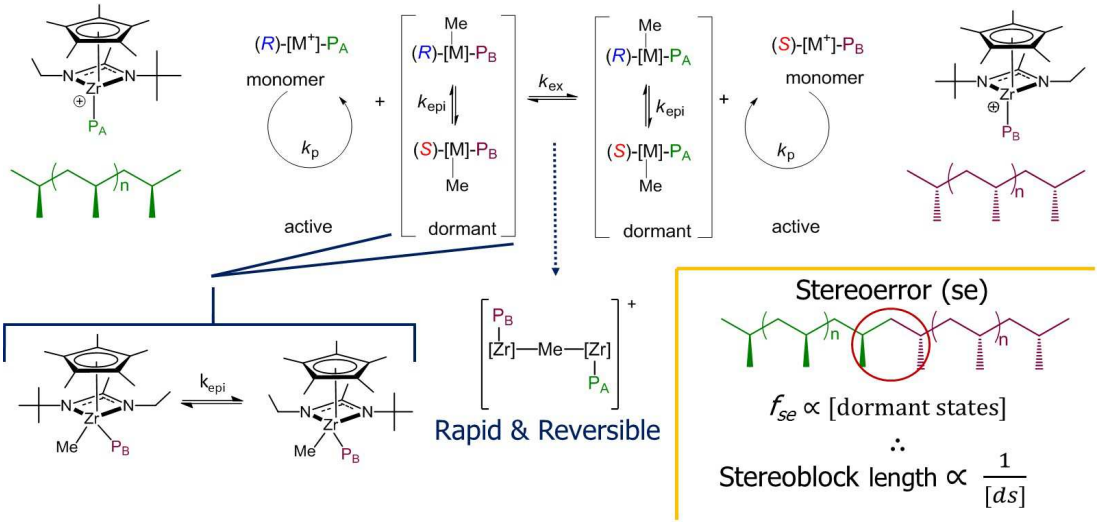

As a result of this effect the polymer that is produced under these conditions appears atactic. Although loss of stereocontrol under degenerative methyl group transfer seems apparent, it is important to point out that the initiator still propagates in an isoselective fashion but when the initiator is in the dormant state (appears as **1** with a tethered polymer chain) epimerization occurs. When further exchange of the bridging methyl group occurs, **1a** is reformed as either the R- or S-manifold. If the handedness of the initiator changed at point of re-activation, then propagation continues in an isoselective manor albeit with opposite configuration. The higher the concentration of [**1**] (i.e. [**1a**]:[**1**] → 0) during polymerization, the higher the

probability of epimerization at the point of re-activation following degenerative methyl group transfer (stereoengineering).

Although the scenario above has been shown to efficiently stereoengineer polyolefins such as poly(1-hexene) (PH)[5-7] and polypropene (PP),[4, 8] in living fashion, through the subactivation of **1** by **II** (i.e. [**II**]/[**1**] < 1.0), it is not a given that the stereoengineering technique can be successfully applied during the cyclopolymerization of 1,6-heptadiene (1,6-HD) to afford stereomodulated PMCH. For example, if v_{ex} decreases as a result of cyclopolymerization with respect to v_p then the molecular weight distribution will become broad (e.g. $Đ$ > 1.1; recall from Chapter 1: $Đ \cong 1 + k_p/k_{ex}$).[9] Marks and coworkers[10] observed a broadening of molecular weight distribution under DT conditions for their non-living polymerizations with 1-hexene, styrene and ethylene. Further, Schrock and coworkers[11] found that their living system exhibited deactivation with the use of DT for the polymerization of 1-hexene and 2-heptenes. Therefore, the current Chapter focuses on the degenerative methyl group transfer (stereoengineering) cyclopolymerization of non-conjugated diene monomers: 1,6-heptadiene (1,6-HD) and diallyldimethylsilane (DAS). The work presented in this chapter was completed by Crawford unless otherwise noted. Figures, schemes and experimental details for the presented work may have been reproduced from the following published articles: Crawford, K. E. and Sita, L. R. *J. Am. Chem. Soc.* **2013**, *135*, 8778 – 7871,[1] and Crawford, K. E. and Sita, L. R. *ACS Macro Lett.* **2014**, *3*, 506 – 509.[2]

4.2. Stereoengineering of Poly(methylene-1,3-cyclohexane), PMCH

1,6-HD was polymerized using cationic **1a** with the following degrees of subactivation by **II**: [**II**]/[**1**] = 1.0, 0.95, 0.90, 0.87, 0.85, 0.80, 0.75 and 0.50, denoted here as sample runs 1a – 1h respectively (where PMCH-sample 1a is PMCH-sample 1 the from Chapter 2: Section 2.2: *cis*-*i*-PMCH; the sample has been re-provided here for comparison), Scheme 4.2. In all cases the product yields were near quantitative. Samples 1c – 1h are transparent glassy materials and are easily soluble in organic solvents. Samples 1a and 1b are opaque powders and are only sparingly soluble in organic solvents. Each sample was carefully analyzed using SEC, NMR, DSC, TGA, and WAXD. The M_n for 1a - 1h range between 8.2 kDa and 13 kDa each with a narrow polydisperisty ($Đ \leq 1.12$), Table 4.1 and Figure 4.1. The narrow $Đ$ and high polymer yield suggest that the rate of exchange (k_{ex}) is much greater than the rate of propagation (k_p) ($Đ \triangleq 1 + k_p/k_{ex}$).[9] This result indicates that although **1a** is present at a low concentration, coordination polymerization still proceeds in a living manner and is not affected by the rapid and reversible methyl group transfer between the active and dormant species.

Scheme 4.2: General polymerization scheme for DT.

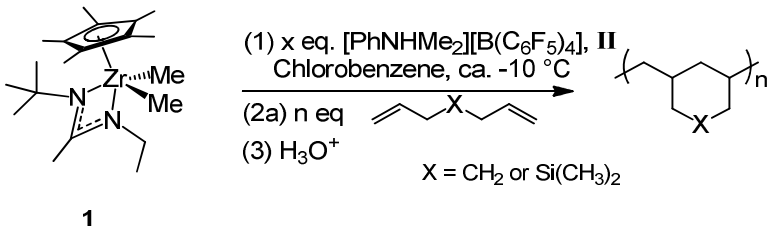

1

Table 4.1: SEC and DSC data for stereoengineering PMCH from [**II**]/[**1**] ≤ 1.0.

Sample	[II]/[I]	M_n (kDa)	$Đ$	T_g (°C)	T_m (°C)	T_c (°C)
1a	1.0	8.2	1.08	92	209	181
1b	.95	8.6	1.12	97	202	170
1c	.90	11.6	1.08	99	-	-
1d	.87	12.8	1.08	100	-	-
1e	.85	12.9	1.09	100	-	-
1f	.80	13.0	1.06	101	-	-
1g	.75	12.8	1.07	99	-	-
1h	.50	11.2	1.03	94	-	-

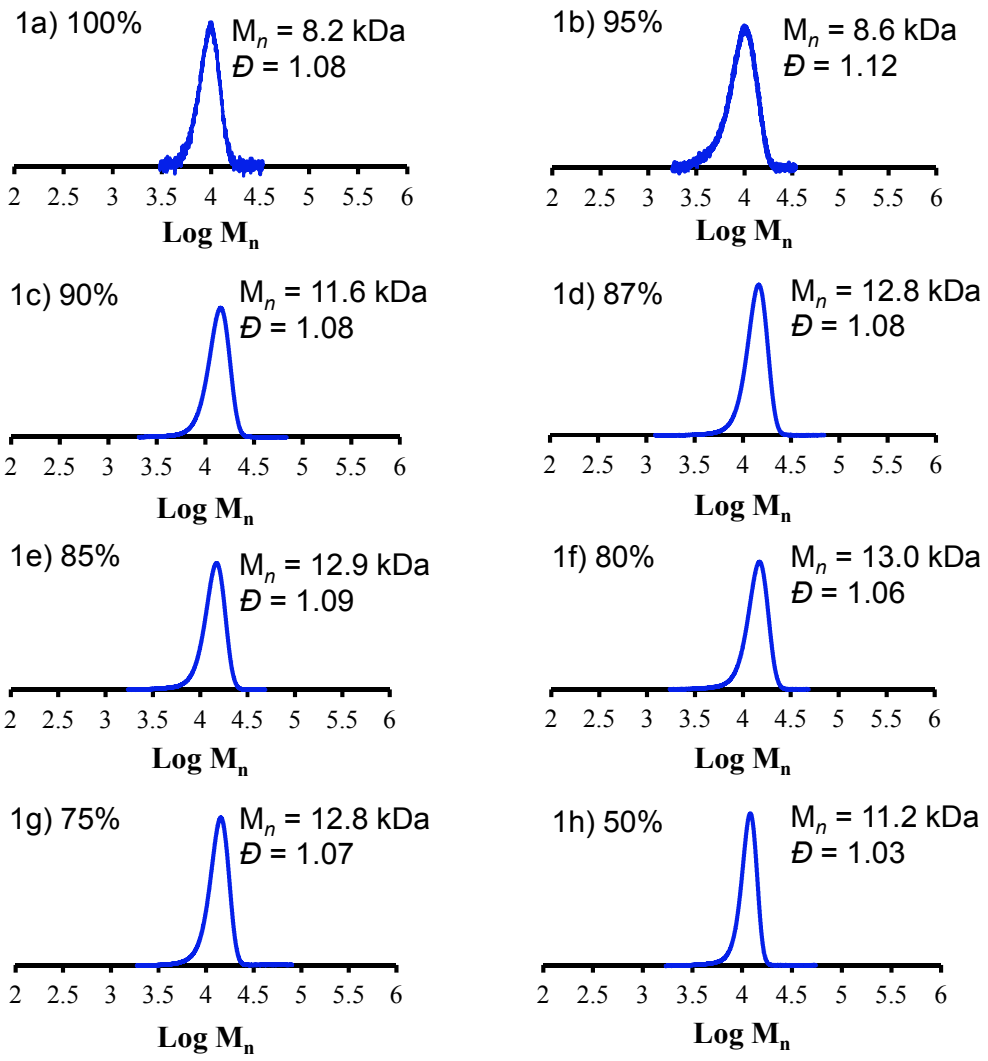

Figure 4.1. SEC plots for stereoengineered PMCH from [**II**]/[**1**] ≤ 1.0.

The thermal properties of PMCH materials 1a – 1h were investigated using DSC. It was previously determined that PMCH begins to degrade under a nitrogen atmosphere just above 300 °C followed by complete degradation 445 ± 5 °C, (see Chapter 2). Degradation temperatures were considered when developing the temperature parameters for DSC. The upper temperature was set to 230 °C, well below the onset of degradation. The general temperature program employed for 1a and 1b was: four heating/cooling cycles up to 230 °C with a 15 minute isothermal hold (230 °C) at the end of each heating cycle. The scan rate during the second heating/cooling cycles was run at 10 °C/min with all other scans run at 1 °C/min. Use of this temperature program reveal a T_m (202 °C), T_c (170 °C) and T_g (96.5 °C) for sample 1b (recall that sample 1a exhibits a T_m of 209 °C, T_c 181 °C and T_g of 92.2 °C). The temperature program for samples 1c – 1h are somewhat different; the third heating and second cooling cycle are presented, where during the second cooling cycle (after first heating, first cooling and second heating) the temperature was held isothermal for 5 minutes at 230 °C before decreasing the temperature at a rate of 5 °C/min. T_g values for samples 1a - 1h were observed to be between 92.2 °C and 101 °C, Table 4.1 and Figure 4.1. There is some variation in the T_g for the PMCH samples 1a - 1h. Although there may be a trend corresponding to the degree of stereoregularity and T_g, a clear conclusion cannot be drawn at this point as these differences may also be influenced by other factors such as variations in M_n and $Đ$, sample size (6 - 9 mg) or fluctuations in purge gas quality and flow rate. In order to definitively conclude a trend in T_g as a function of stereoregularity a separate investigation would need to be conducted. More importantly, all the of T_g values are

high (above 90 °C) compared to polyolefins produced by simple α-olefins such as PE (ca. -80 °C)[12] or PP (ca. -25 °C - 0 °C),[13] which was a motivating factor in pursuing cyclopolymerization with 1,6-HD.

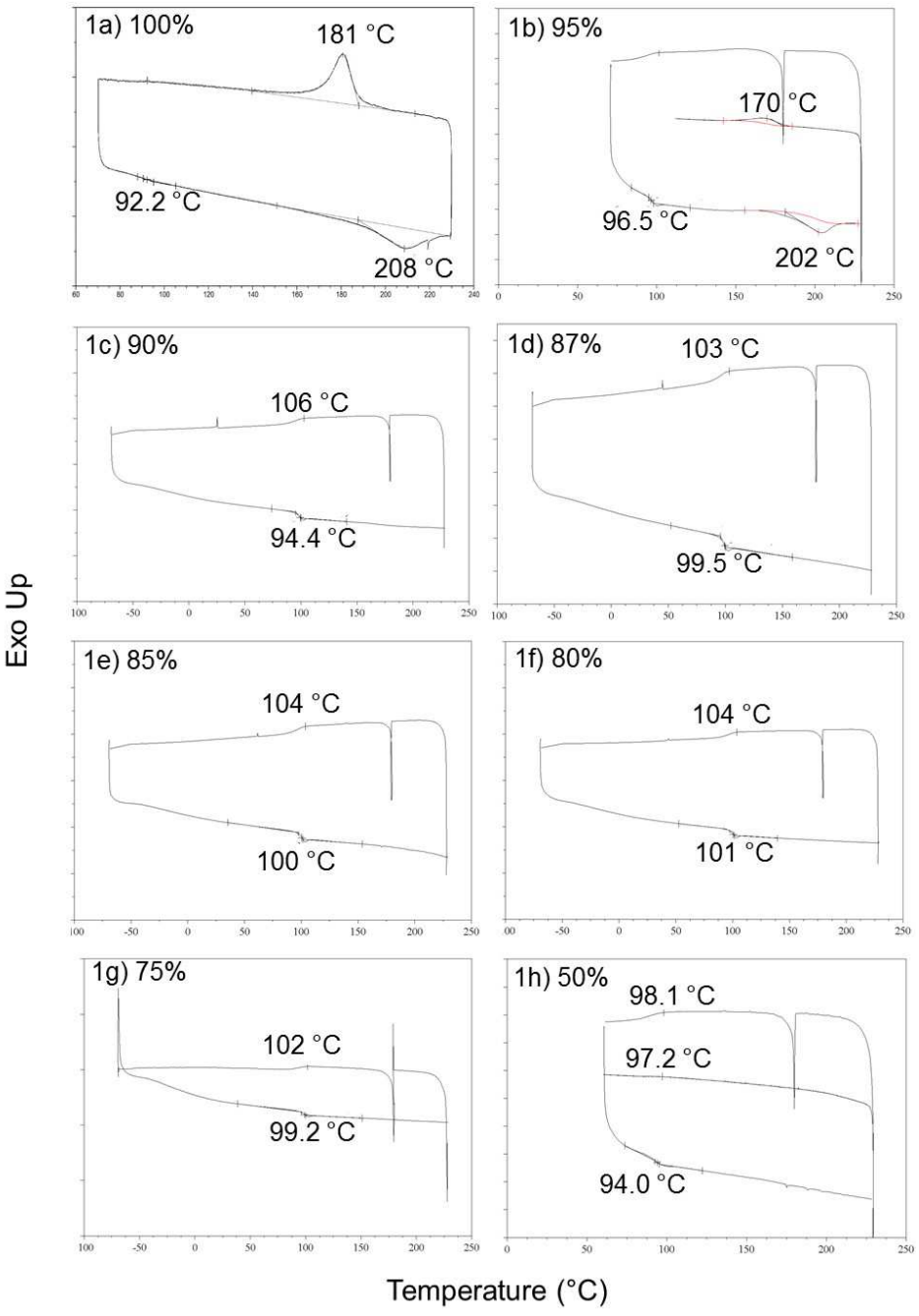

Figure 4.2: DSC plot for PMCH samples 1a – 1h.

It is of interest to determine how stereoengineering affects stereoregularity. Our group has previously shown partial loss of stereocontrol with the presence of even a small concentration (5 %) of the dormant initiator species during the polymerization of PP and poly(1-hexene).[4, 5, 7] In an effort to better understand how DT contributes to stereoregularity for the cyclized PMCH products, $^{13}C\{^{1}H\}$ NMR was employed to discern the microstructure for each sample. The resulting trend is quite striking. Beginning with the highly *c*-iso-PMCH (1a) obtained from the complete activation of **1** (i.e. [**II**]/[**1**] = 1.0) there is a distinct decrease in stereoblock length with decreasing concentration of **1a** as evidenced by the increase in resonances within the $^{13}C\{^{1}H\}$ NMR spectra. The most notable increase in resonances are associated with carbon atoms at positions 2, 4 and 6; partial $^{13}C\{^{1}H\}$ NMR spectra for select degenerative transfer ratios have been reproduced in Figure 4.3. The $^{13}C\{^{1}H\}$ NMR for PMCH samples 1a - 1h clearly show an increase in the loss of stereocontrol with increasing subactivation of initiator. This phenomena may be explained by the previously described amidinate ring-flipping that takes place when the otherwise active, stable initiators are in a dormant, configurationally unstable state.[5] Interestingly, the diastereoselectivity remains selective for *cis* rings despite the modulation of stereoregularity. There are at least two reasonable explanations that allow diastereoselectivity to remain intact during living degenerative transfer polymerization. 1) Steric hindrance from the ligand framework along with the limited degrees of freedom available to the monomer may cause the formation of the *trans* ring conformation to be disfavored. 2) The rate of intramolecular cyclization (k_c) may occur faster than the rate of exchange (k_{ex}). For this second explanation to hold true

during living degenerative transfer k_{ex} must be >> than k_p, therefore, k_c must also be >> k_p. The source for diastereoselectivity under DT conditions was not further pursued.

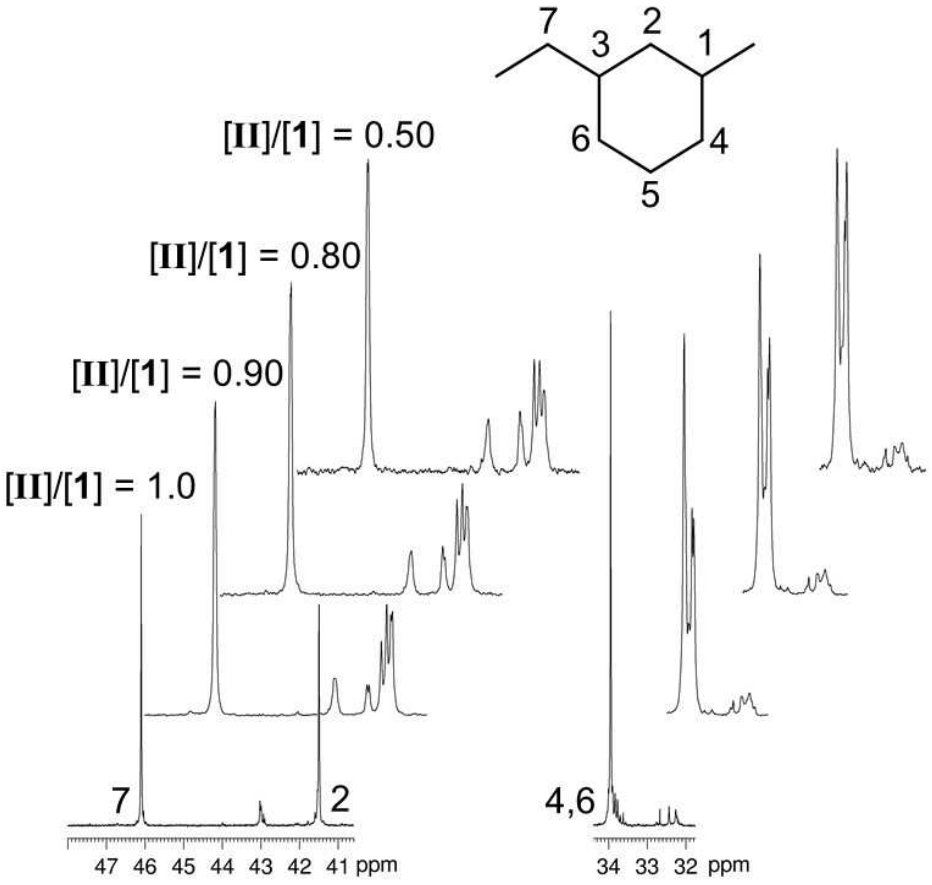

Figure 4.3: Partial $^{13}C\{^1H\}$ NMR spectra for PMCH samples (bottom to top): 1a, 1c, 1f and 1h; 150 MHz, TCE-d_2, 110 °C.[1]

Next, it is of interest to determine if the stereoengineered PMCH samples are crystalline, an important factor in identifying the appropriate materials application. The presence of crystallinity within PMCH samples 1c – 1h is not expected due to the absence of melting and crystallization peaks in upon DSC analysis. To confirm their

amorphous nature the PMCH samples 1c - 1h were analyzed by WAXD. Sample 1a was discussed in Chapter 2 and has been reproduced in Figure 4.4 (top-left). Briefly, sample 1a indeed shows some degree of crystalline behavior with one sharper peak with *d*-spacing = 4.4 Å and a second smaller peak with *d*-spacing = 5.2 Å. The remaining samples, however, do not display any peak sharpness in the WAXD plots to suggest crystallization and are thus concluded to be non-crystalline. Representative plots for select PMCH samples obtained from living degenerative transfer at percent activation levels of 90 %, 80 %, and 50 % are provided in Figure 4.4. This work serves as the first WAXD report on PMCH materials with modulated stereoselectivity. Due to the limited information available on PMCH the WAXD plots were not investigated further.

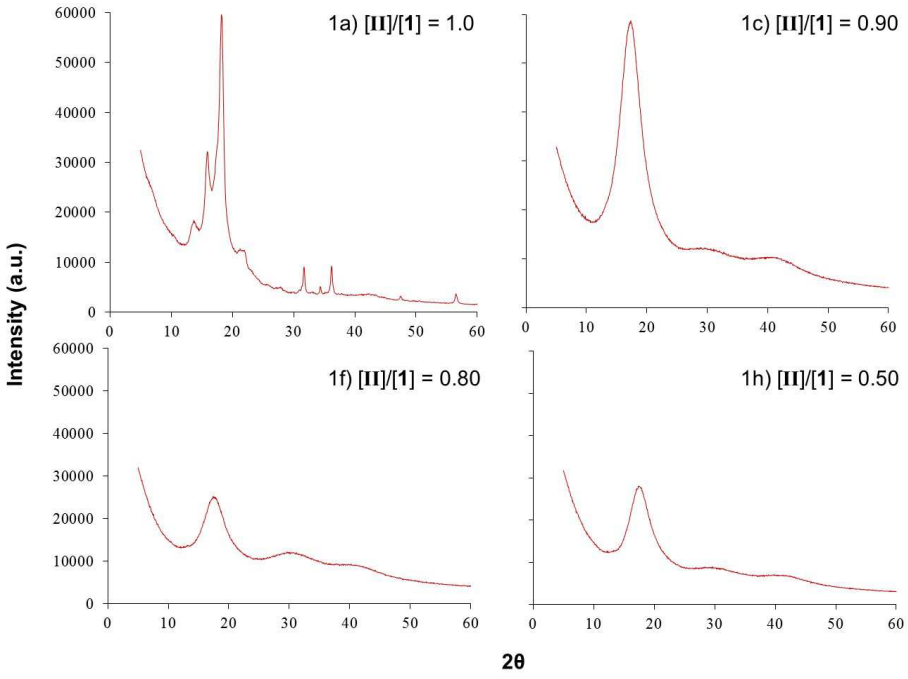

Figure 4.4: WAXD measurements for PMCH samples: Top (left) 1a, (right) 1c; Bottom (left) 1f, and (right) 1h. *d*-spacing can be calculated by using Bragg's law: $n\lambda = 2d\sin\theta$ where n = 1 and λ = 1.54 Å

In short, stereoengineering was applied, for the first time, toward the cyclopolymerization of 1,6-HD for the formation of highly regio-regular PMCH. It was not a given that degenerative methyl group transfer would occur in a living fashion, and further the contribution of intramolecular cyclization was not apparent. It was determined that the stereospecificity of the *cis*-PMCH materials can be finely tuned by adjusting the activation of **1** by **II**. With increasing concentration of **[1]** with respect to **[1a]** there is an increase in the number of stereoerrors and thus a decrease in the stereoregularity of the PMCH materials. Despite loss of tacticity, T_g values remains high (≥ 93 °C), an important consideration for use in complex materials such as block copolymers (see Chapter 5).

4.3. Stereoengineering of Poly(3,5-methylene-1,1-silacyclohexane), PDAS

Section 4.2 provided evidence of successful stereoengineering for PMCH by means of a "two-state" LCP system, wherein the introduction of diastereotopic stereoerror throughout the main-chain backbone could be fine-tuned with increased substoichiometric use of [**II**] (*i.e.,* [**II**]/[**1**] < 1.0).[1] As a result of the high stereoregularity, slow crystallization kinetics and limited solubility of 3,5-*c*-*iso*-PDAS (poly(3,5-methylene-1,1-dimethylsilacyclohexane); Chapter 3), it is of great interest to apply the stereoengineering phenomena realized with PMCH to the newly discovered PDAS. Therefore, multiple polymerizations were carried out with increasing substoichiometric concentrations of [**II**]. Specifically, [**II**]/[**1**] = 1.0, 0.75, 0.65, 0.50 and 0.30 denoted here as PDAS-samples 2a – 2e (where PDAS-sample 2a is PDAS-sample 1 the from Chapter 3, Section 3.2.1; *cis*-i-PDAS; the sample has been re-provided here for comparison). It is important to note that the same DAS

starting material that was applied for the synthesis of PDAS-sample 2a in Chapter 3 was also used here, which means the same vinyl-isomer impurity was present across both research projects (refer to Figure 3.13). Thus, although stereoengineering appears to have been successfully applied to PDAS, *vide infara*, there is still some degree of catalyst deactivation expected during polymer synthesis. M_n values, determined by SEC range from 13.6 kDa to 18.5 kDa with somewhat broad polydisperisities compared to stereoengineering PMCH samples ($Đ \leq 1.5$), Figure 4.5. It is interesting to note that polydispersity appears to decrease with increasing concentration of [**1**], that is, as the percent of precatalyst activation decreases, $Đ$ also decreases, Table 4.2. Although the exact reasoning for this trend is unknown at this time, it is possible that the decrease in $Đ$ may originate from a proportional decrease in the affective rate of propagation (v_p) with increasing ratio of [**1**]:[**1a**] ($Đ \cong 1 + k_p/k_{ex}$).[5, 9]

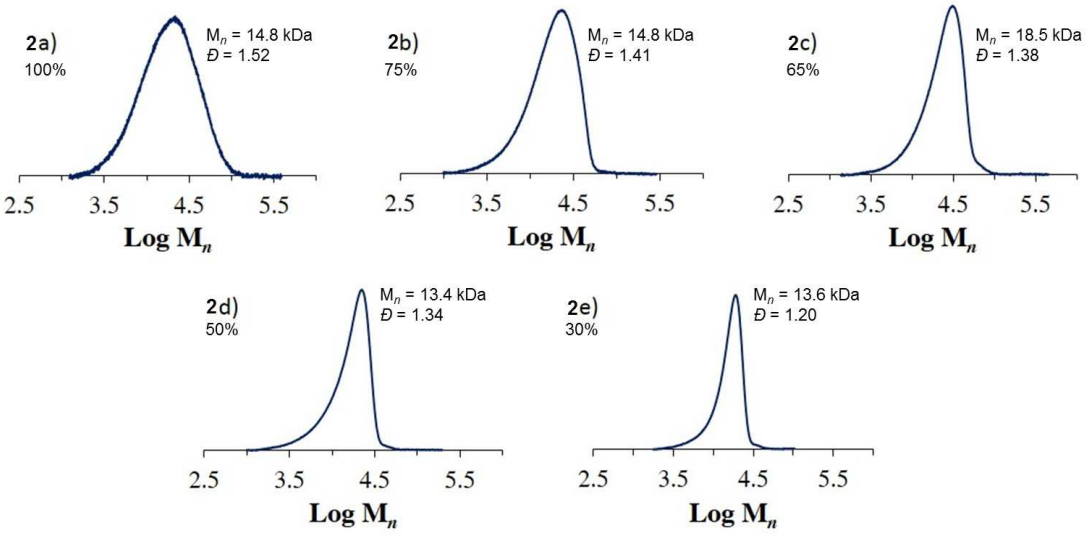

Figure 4.5: SEC plots for stereoengineered PDAS from [**II**]/[**1**] ≤ 1.0.

Table 4.2: SEC and DSC data for stereoengineering PDAS from [**II**]/[**1**] ≤ 1.0.

Run	[II]/[1]	M_n (kDa)	*Đ*	T_g (°C)	T_m (°C)[c]
2a	1.0	14.8	1.52	123	264
2b	0.75	14.8	1.41	125	-
2c	0.65	18.5	1.38	125	-
2d	0.50	13.4	1.34	126	-
2e	0.30	13.6	1.20	127	-

To determine the thermal properties of *c*-i-PDAS TGA and DSC analysis was performed. First, using TGA, the onset of degradation was determined to be ca. 350 ± 4 °C with full degradation at 447 ± 4 °C, Figure 4.6. The temperature at which the onset of degradation occurs is essential to optimize the temperature program employed for DSC characterization. In that regard, the upper temperature limit for DSC thermal scans was set to 290 °C, well below the onset of degradation. Importantly, while T_m endotherms and T_c exotherms of PDAS 2b – 2e were not observed under various DSC temperature programs, the high T_g originally identified for 3,5-*c*-i-PDAS (2a) remains ever-present with values ranging from 123 °C to 127 °C, Figure 4.7. The following general parameters were used for heating and cooling cycles: heat to 290 °C at 10 °C/min (not shown); isothermal hold x 30 min (not shown); cool to 0 °C at 1 °C/min; heat to 290 °C at 1 °C; cool to 0 °C at 10 °C/min; heat to 290 °C at 10 °C/min.

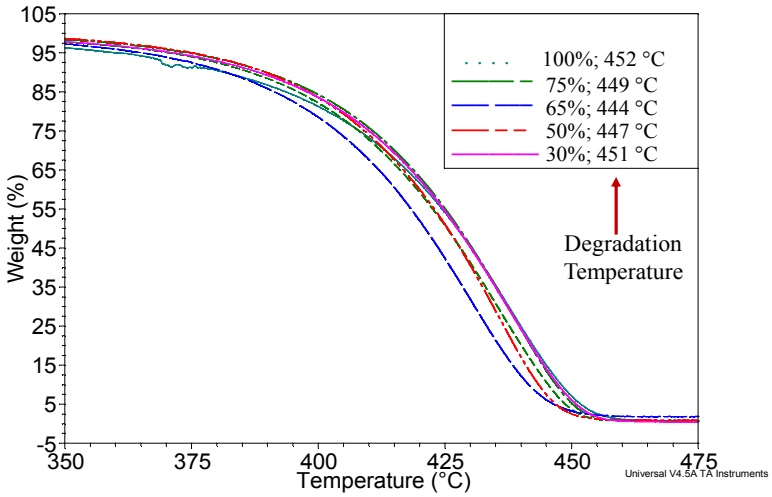

Figure 4.6: TGA plot for PDAS samples 2a – 2e (degradation temp. = 447 ± 4 °C).

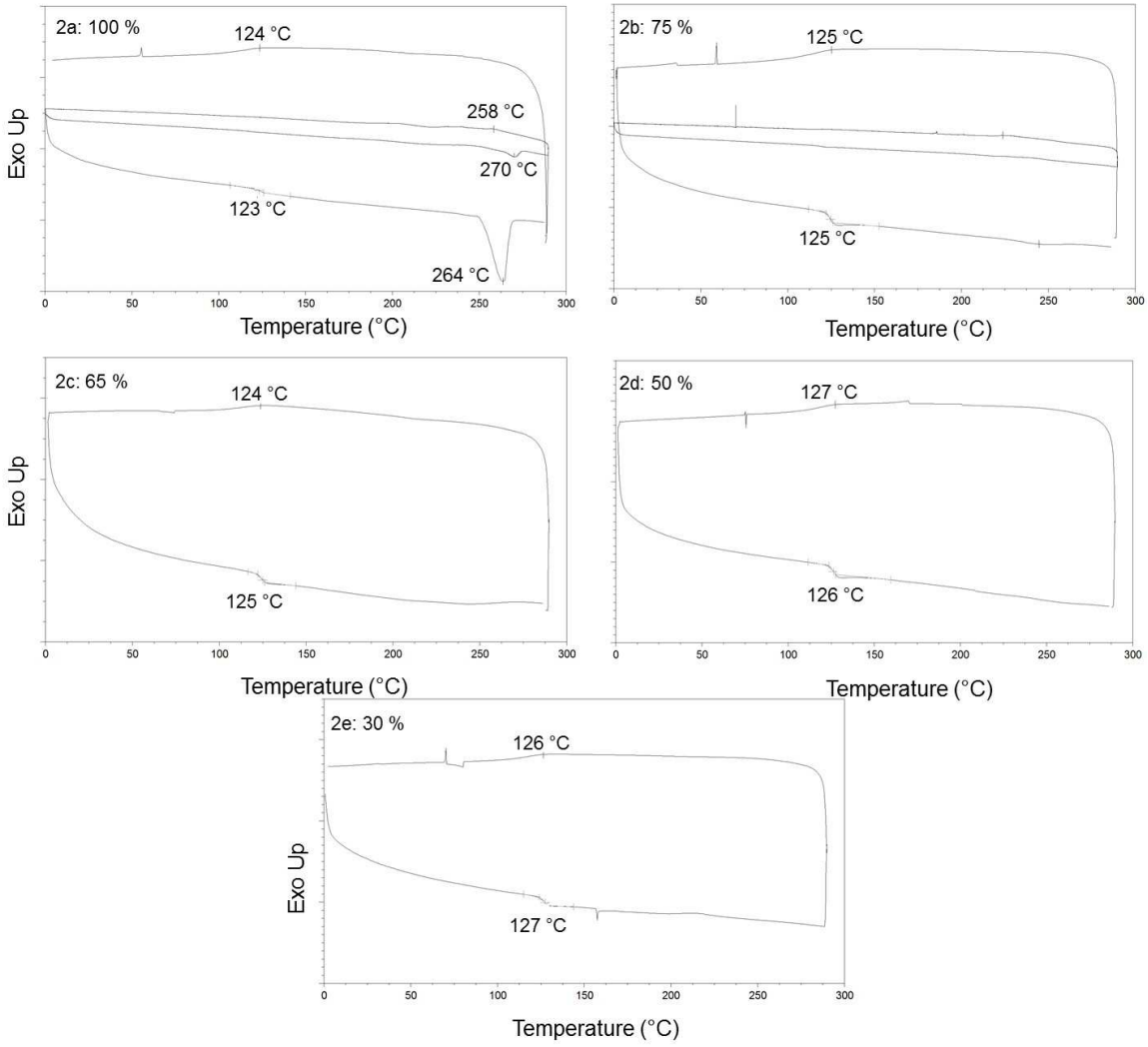

Figure 4.7: DSC plots for PDAS-samples 2a – 2e.

WAXD measurements are consistent with DSC analysis, which support the amorphous character of PDAS samples 2b – 2e; the scattering peaks are broad and weak suggesting little coherence and thus, are considered amorphous, Figure 4.8. Further WAXD analysis was not carried out for these materials.

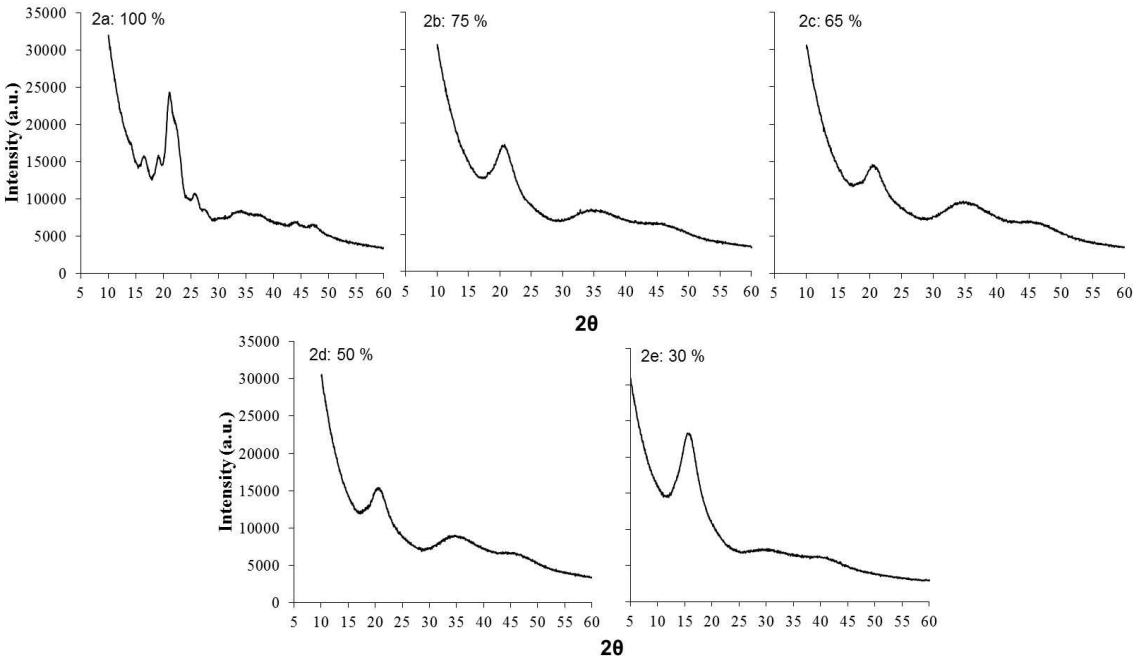

Figure 4.8: WAXD plots of PDAS-samples 2a – 2e.

Next it is of interest to determine the microstructure of each PDAS material (2b – 2e) by ^{29}Si and ^{13}C{^{1}H} NMR to investigate the any correlation of stereoerror as a function of [**1**]. Gratifyingly, it was found that the stereoengineering methods applied previously to PMCH do in-fact extend to PDAS. The ^{29}Si NMR spectra (100 MHz, 90 °C, TCE-d_2) support an increase in stereoerror within the polymer main-chain in keeping with the increasing concentration of configurationally unstable, dormant species. While PDAS-sample 2a ([**II**]/[**1**] = 1.0) resulted in an ^{29}Si NMR spectrum with only a single resonance at -2.29 ppm, PDAS samples 2b – 2e ([**II**]/[**1**] < 1.0) depict ^{29}Si NMR spectra with multiple resonances near -2.29 ppm; each with increasing intensity as [**II**]/[**1**] approaches zero, Figure 4.9. A similar correlation was observed upon analysis of ^{13}C{^{1}H} NMR. Specifically, as the concentration of configurationally unstable species increased, the stereoblock length

decreased respectively with 2a > 2b > 2c > 2d > 2e. There are five groups of resonances in the $^{13}C\{^{1}H\}$ spectra. The two resonances between -3.5 ppm and -1.5 ppm correspond to the two methyl groups bonded to the Si heteroatom. The resonances between 20 ppm and 22 ppm correspond to carbons 2 and 6 (molecular structure labels in Figure 4.10 inset). The resonances around 33 ppm are attributed to carbons 3 and 5. The group of resonances between 43 ppm and 46 ppm correspond to carbon atoms at position 4. The final group of resonances between 53 ppm and 55 ppm are attributed to carbon atoms at position 7, Figure 4.10. A partial $^{13}C\{^{1}H\}$ NMR exhibiting the decrease in stereoblock length from 2a to 2e for the carbon atom at position 4 is also provided in Figure 4.9. There are minute resonances in the vinyl region ca. 150 ppm with one small resonances also at 120 ppm ($^{13}C\{^{1}H\}$ NMR vinyl resonances not shown), which correspond to the small concentration of vinyl groups *vide supra*.

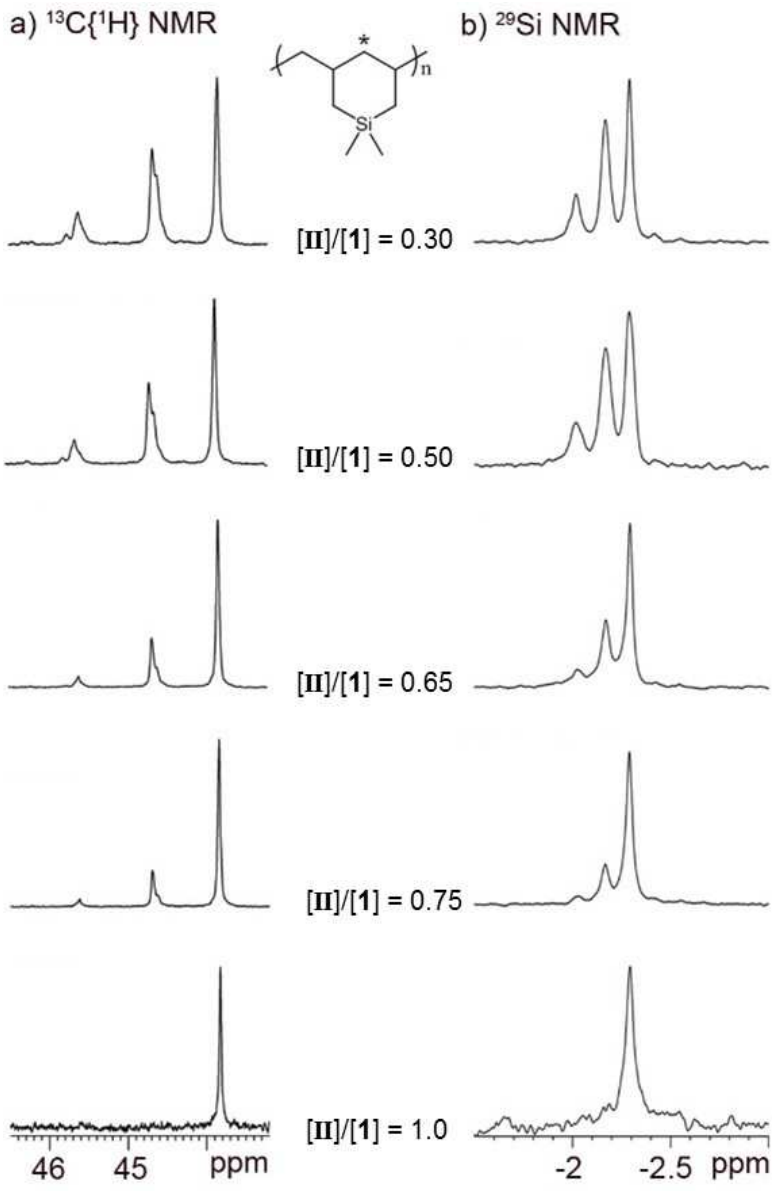

Figure 4.9: PDAS-samples 2a – 2e. Left: partial $^{13}C\{^1H\}$ NMR, resonances correspond to carbon at position 4, highlighted with an asterisk (*); 200 MHz, 110 °C, TCE-d_2. Right: ^{29}Si NMR spectra; 100 MHz, 90 °C, TMS-d_{12}.

It is noteworthy to discuss the two diastereotopic methyl groups bonded to the Si atom. The designated resonance for each methyl group suggests that the pseudo chair confirmations of the cyclic repeating units are not easily interconverted (at least not on the NMR time scale under the conditions probed). The 'rigid' structures likely

contribute to the observed increase in T_g for PDAS compared to PMCH. Moreover, the methyl resonances at -3.5 for PDAS sample 2a is sharp (appears as two sharp overlapping peaks) but with decreasing stereoblock length (from 2b to 2e) the peak becomes broad and appears as numerous overlapping resonances. An increase in the number of resonances is expected as the iso-rich character of a polymer decreases; however, the resonance for the second methyl group at -1.5 ppm remains sharp despite the overall observed decrease in stereoblock length. The integrity of the sharp resonance at -1.5 ppm suggests that the second methyl group is directed toward the equatorial position within the pseudo *cis* chair conformation and is thus less effected by configuration (stereoselectivity) between repeating units.

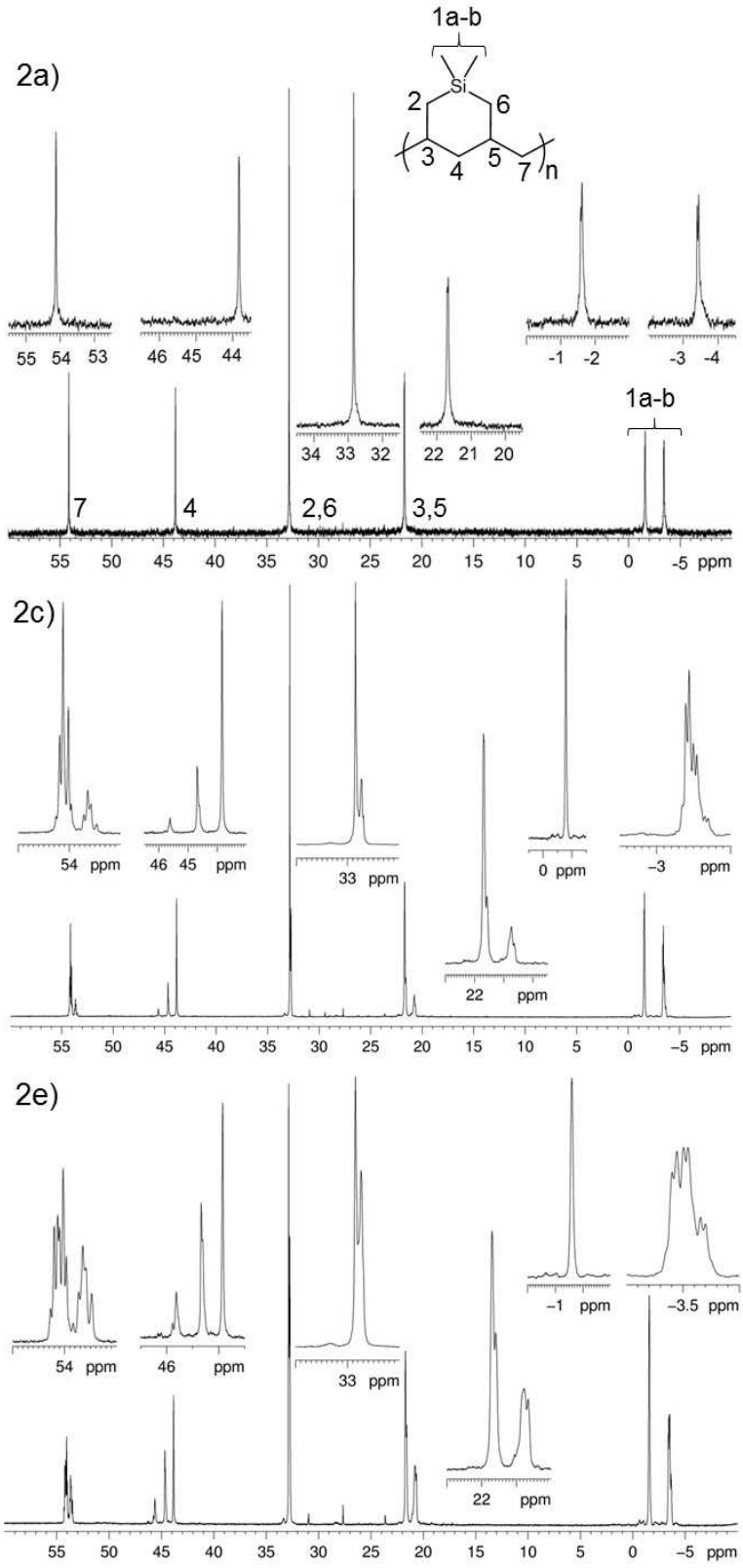

Figure 4.10: $^{13}C\{^{1}H\}$ NMR spectra for PDAS samples 2a: 100 % (top), 2c: 65 % (middle), and 2e: 30 % (bottom); 200 MHz, 110 °C, TCE-d_2.

In short, stereoengineering was applied, for the first time, toward the cyclopolymerization of DAS for the formation of highly regio-regular PDAS. It was not a given that degenerative methyl group transfer would occur in a controlled fashion, and further the contribution of intramolecular cyclization was not previously apparent. It was determined that the stereospecificity of the *cis*-PDAS materials can be finely tuned by adjusting the activation of **1** by **II**. With increasing concentration of **1** with respect to **1a** there is an increase in the number of stereoerrors and thus a decrease in the stereoregularity of the PDAS materials. Despite loss of isotacticity, T_g values for PDAS remain relatively high (≥ 123 °C).

4.4. Conclusions

This work serves as the first documentation of the stereoengineering of PMCH and PDAS. It was found that stereoregularity can be finely tuned with increasing substoichiometric additions of **II** while maintaining high selectivity for cyclization, regio-selectivity and glass transition temperature. The use of degenerative methyl group transfer did not adversely impact the living (for PMCH) and controlled (for PDAS) nature of polymerization with precatalyst **1** suggesting that bridging methyl group exchange between cationic species **1a** is rapid and reversible allowing for a living/controlled 'two-state' coordination polymerization mechanism where the rate of methyl group exchange (k_{ex}) is much faster than the rate of propagation (k_p) ($k_{ex} >> k_p$).

4.5. Experimentals

4.5.1. Synthesis of PMCH and PDAS

The polymerizations were carried out under an inert atmosphere of dinitrogen using a Vacuum Atmospheres glovebox. The general polymerization method for the formation of PMCH and PDAS are as follows: substoichiometric amounts of cocatalyst $[PhNHMe_2][B(C_6F_5)_4]$ (**II**), was mixed with 20 – 30 μmol precatalyst **1** in 1.5 mL cold PhCl. The resulting bright yellow mixtures of **1** with **II** were then added to pre-chilled (-18 °C – -10 °C) PhCl in a 50-mL round bottomed glass reaction vessel equipped with a magnetic stir bar. Monomer (100 equiv.) was then added to the reaction mixture and allowed to stir for a given amount of time, typically 1 to 8 hours. Following a given amount of reaction time the reaction mixtures were removed from the glovebox and quenched/precipitated in a large excess of acidic methanol (300 mL – 500 mL; 10% HCl by volume). The polymers were vacuum filtered, washed with methanol, collected in a pre-weighed vial, and dried under vacuum until constant weight. Instrument parameters and source of materials information are provided in Appendices A and B.

4.6. References

1. Crawford, K. E.; Sita, L. R., *J. Am. Chem. Soc.* **2013**, *135* (24), 8778-8781.

2. Crawford, K. E.; Sita, L. R., *ACS Macro Lett.* **2014**, *3* (6), 506-509.

3. a) Jayaratne, K. C.; Keaton, R. J.; Henningsen, D. A.; Sita, L. R., *J. Am. Chem. Soc.* **2000**, *122* (42), 10490-10491.; b) Jayaratne, K. C.; Sita, L. R., *J. Am.*

Chem. Soc. **2000**, *122* (5), 958-959.; ca0 Zhang, Y.; Reeder, E. K.; Keaton, R. J.; Sita, L. R., *Organometallics* **2004**, *23* (14), 3512-3520.

4. Harney, M. B.; Zhang, Y.; Sita, L. R., *Angew. Chem., Int. Ed.* **2006**, *45* (37), 6140-6144.

5. Zhang, Y.; Keaton, R. J.; Sita, L. R., *J. Am. Chem. Soc.* **2003**, *125* (30), 9062-9069.

6. Jayaratne, K. C.; Sita, L. R., *J. Am. Chem. Soc.* **2001**, *123* (43), 10754-10755.

7. Zhang, Y.; Sita, L. R., *J. Am. Chem. Soc.* **2004**, *126* (25), 7776-7777.

8. Harney, M. B.; Zhang, Y.; Sita, L. R., *Angew. Chem., Int. Ed.* **2006**, *45* (15), 2400-2404; Sita, L. R., *Angew. Chem., Int. Ed.* **2009**, *48* (14), 2464-2472.

9. Mueller, A. H. E.; Zhuang, R.; Yan, D.; Litvinenko, G., *Macromolecules* **1995**, *28* (12), 4326-4333.

10. Chen, Y.-X.; Stern, C. L.; Yang, S.; Marks, T. J., *J. Am. Chem. Soc.* **1996**, *118* (49), 12451-12452.

11. Mehrkhodavandi, P.; Bonitatebus, P. J., Jr.; Schrock, R. R., *J. Am. Chem. Soc.* **2000**, *122* (32), 7841-7842.

12. White, J. L.; Choi, D. D., *Polyolefins: Processing, Structure Development, and Properties*. 1st ed.; Hanser Gardner Publications: Hanser: Cincinnati, OH, 2005; p 271.

13. Sperling, L. H., *Introduction to Physical Polymer Science*. 4th ed.; Wiley: Hoboken, NJ, 2006.

Chapter 5

Polyolefin Diblock Copolymers

5.1. Introduction

Block copolymers (BCPs) are an important class of polymer and have been highly studied and cover a wide range of topics from biodegradable materials and drug delivery vehicles,1 to electronic devices,[2] directed self-assembly,[3] lithography,[4] composite materials and blends.[5] The formation of well-defined block copolymers do not come without challenge, however. There are two primary methods for the synthesis of BCPs. The first is through the use of post polymerization functionalization wherein two end functionalized polymers with reactive functional groups become covalently tethered. The second is through the use of living polymerization methods such as living radical,[6] anionic[7] or coordination polymerization.[8] Of these methods, only living coordination polymerization (LCP) is capable of polymerizing olefins such as propene and non-conjugated dienes. Interestingly, very few reports have surfaced highlighting the successful synthesis of polyolefin-*b*-polyolefin diblock copolymers and to the best of our knowledge there is only one previous report (by the Sita group) that presents the spontaneous self-assembly and subsequent microphase separation of a pure polyolefin (PO) BCP (see Section 1.11).[8] Due to the dearth of available literature on the microphase separation of PO-BCPs using LCP it is unknown how they will behave, and the propensity of these BCPs to microphase separate has yet to be determined.

Therefore, with the first principles of BCPs in mind a series of pure PO diblock copolymers have been developed using LCP. Specifically, presented here is the synthesis and preliminary evaluation of several AB diblock copolymers with respective A and B segments composed of poly(1-hexene) (PH) and high T_g, *cis*-poly(methylene-1,3-cyclohexane) (PMCH). The PH-*b*-PMCH diblock copolymer samples were prepared under living coordination polymerization conditions using C_1-symmetric Group 4 monocyclopentadienyl amidinate precatalyst: Cp*Zr[N(Et)C(Me)N(*t*-Bu)](Me$_2$) (Cp* = η^5-C_5Me_5, Et = ethyl, Me = methyl) (**1**) activated by cocatalyst ([PhNHMe$_2$][B(C_6F_5)$_4$]) (**II**) to form cationic {Cp*Zr(Me)[N(Et)C(Me)N(*t*-Bu)][B(C_6F_5)$_4$]} (**1a**) in cold chlorobenzene (PhCl) with sequential additions of 1-hexene and 1,6-heptadiene (1,6-HD) according to Scheme 5.1.

Scheme 5.1: General synthesis method for diblock copolymers.

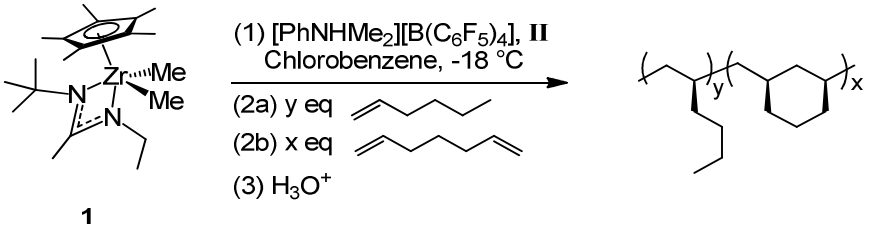

As presented in Chapter 2, the first living coordination cyclopolymerization of 1,6-HD resulting in a highly controlled spectrum of distinct *cis*-PMCH microstructures in which the relative tacticity can be modulated from highly isotactic to atactic as a function of precatalyst type was achieved.[9] Briefly, it was found that, when using a 1:1 ratio of either [**II**]:[**1**] the α,ω-nonconjugated diene (1,6-HD)

undergoes complete intramolecular cyclization with 1,2-primary insertion of the α-bond followed by an immediate 1,2-secondary insertion of the ω-bond to afford a near quantitative yield of *cis*-isotactic-PMCH (abbreviated hereafter as iPMCH).

5.2. iPH-*b*-iPMCH Diblock Copolymers

Thirteen iPH-*b*-iPMCH BCPs were synthesized and have been analyzed using a variety of characterization tools such as size exclusion chromatography (SEC), nuclear magnetic resonance (NMR), differential scanning calorimetry (DSC), wide angle x-ray diffraction (WAXD), small angle x-ray scattering (SAXS), atomic force microscopy (AFM), and rheology. The preliminary results of each are discussed below.

SEC was employed to determine both the overall M_n and polydisperisty ($Đ$) of the BCPs as well as for estimation of the individual block lengths. In the latter case, individual block length estimations are determined by analyzing, through SEC, a small aliquot of polymer A taken from the polymerization reaction just prior to the addition of the second monomer. Aliquot volumes were ca. 100 μL out of 35 mL reaction mixtures. The overall M_n values range from 15 kDa to 38 kDa, each with narrow polydisperisities ($Đ \leq 1.2$). Table 5.1 provides a list of the M_n and $Đ$ values for all BCP samples and Figure 5.1 provides representative examples of the SEC plots for block A (from aliquot) overlaid with the overall AB BCP (aliquot removed immediately following termination). The monomodal SEC traces suggest the complete formation of BCPs and successful LCP.

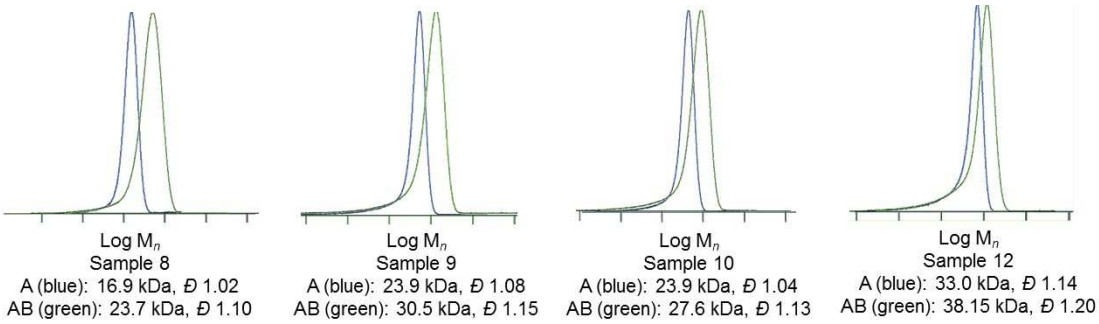

Figure 5.1: Representative SEC plots for iPH-*b*-iPMCH BCPs.

Table 5.1: SEC and mole *f* data for iPH-*b*-iPMCH BCPs.

Sample	Mn (kDa)	PDI	PMCH mole *f* by ^{1}H NMR
1	17.3	1.06	0.35
2	28.6	1.15	0.27
3	38.9	1.11	0.31
4	27.0	1.08	0.35
5	28.1	1.17	0.21
6	19.6	1.10	0.16
7	20.1	1.00	0.14
8	23.7	1.10	0.14
9	30.5	1.15	0.10
10	27.7	1.13	0.06
11	26.8	1.24	0.17
12	38.1	1.21	0.08
13	-	-	0.68

Despite the clear shift in retention volume observed between the SEC plot of the aliquot taken just prior to the addition of the second monomer (1,6-HD) and again immediately following termination of the reaction suggesting the formation of a diblock copolymer, it is not clear from this result if the block segments are discrete (i.e. pure A and B segments of respective iPH and iPMCH). It is well known that the

observed properties of polymers (e.g. melting temperature, glass transition temperature, phase separation etc.) are dependent on the polymer's microstructure, that is, the individual homopolymers for iPH[10] and iPMCH[9] of similar molecular weight and tacticity display vastly different bulk properties compared to iPH-*b*-iPMCH diblock copolymers, *vide infara*. Thus, it is important to determine the BCP microstructures. Fortunately, $^{13}C\{^{1}H\}$ NMR can be employed to confirm the formation of well-defined BCPs. Block segments that consist of either pure iPH or iPMCH will exhibit $^{13}C\{^{1}H\}$ NMR resonances resembling that of the respective homopolymers. Any new resonances different from those seen with pure iPH and iPMCH homopolymer would suggest a mixed copolymer of iPH and iPMCH as opposed to the formation of a well-defined iPH-*b*-iPMCH diblock copolymer. Gratifyingly, the $^{13}C\{^{1}H\}$ NMR spectra obtained for each BCP are consistent with the formation of molecularly discrete segments of iPH and iPMCH. Four representative $^{13}C\{^{1}H\}$ NMR spectra are provided in Figures 5.2 – 5.5 and have been selected based on various PMCH mole fractions, from very low to moderately high. As exemplified in Table 5.1, the PMCH mole fractions (*f*), determined by ^{1}H NMR, vary between 0.06 and 0.68. A representative ^{1}H NMR spectrum with a iPMCH mole *f* of 0.31 (sample 3) is provided in Figure 5.6. The $^{13}C\{^{1}H\}$ NMR spectra encompass 11 groups of resonances; six correspond to the PH segments and five to the PMCH segments. All resonances are located between 0-55 ppm. The corresponding iPH resonances are at 13.8 ppm for (carbon atoms at position F); see the inset of the $^{13}C\{^{1}H\}$ NMR Figure 5.3 – 5.5. 23 ppm (E), 28.7 ppm (D), 32.9 ppm (C), 34.9 ppm (A), and 40.8 ppm (B). The corresponding PMCH resonances are at 26.4 ppm (carbon atoms at

position 5), 34 ppm (carbons 4 and 6), 35-35.5 ppm (carbons 1 and 3), 41.5 ppm (carbon 2), and 46 ppm (carbon 7). The $^{13}C\{^{1}H\}$ NMR spectra in Figures 5.2 – 5.5 correspond to samples 3, 9, 12 and 13 with respective PMCH mole *f*'s, calculated by ^{1}H NMR, of 0.31, 0.10, 0.08 and 0.68 (PMCH mole *f* values are also tabulated in Table 5.1). The ^{1}H NMR collected for all iPH-*b*-iPMCH BCPs further suggest a living polymerization system as evidences from the lack of vinyl group resonances that would occur if β-hydride elimination had been prevalent.

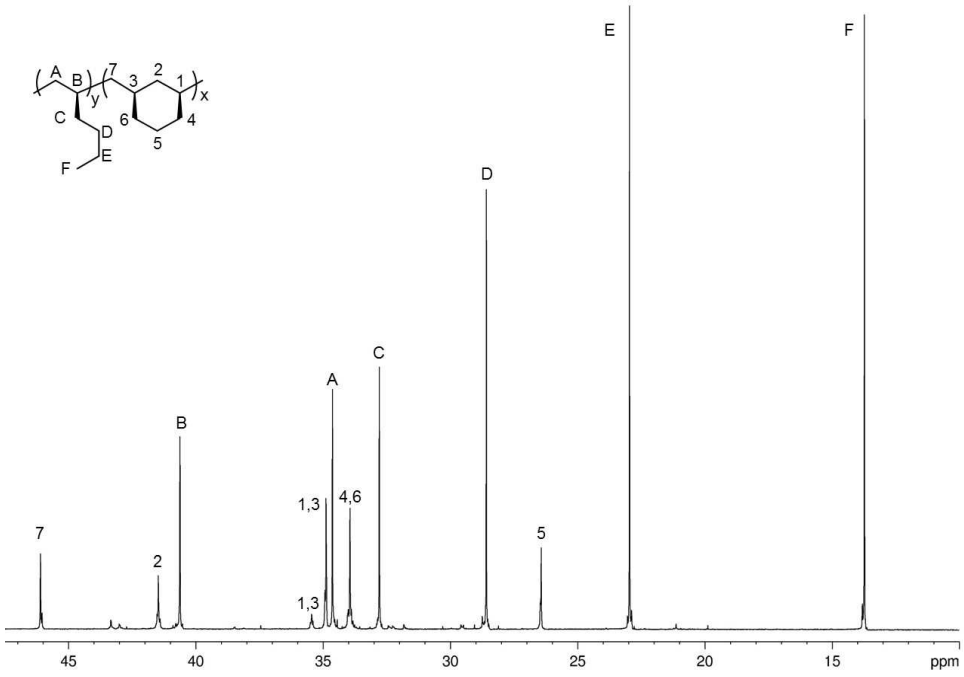

Figure 5.2: $^{13}C\{^{1}H\}$ NMR for iPH-*b*-iPMCH (BCP-sample 3); 200 MHz, 110 °C, TCE-d_2.

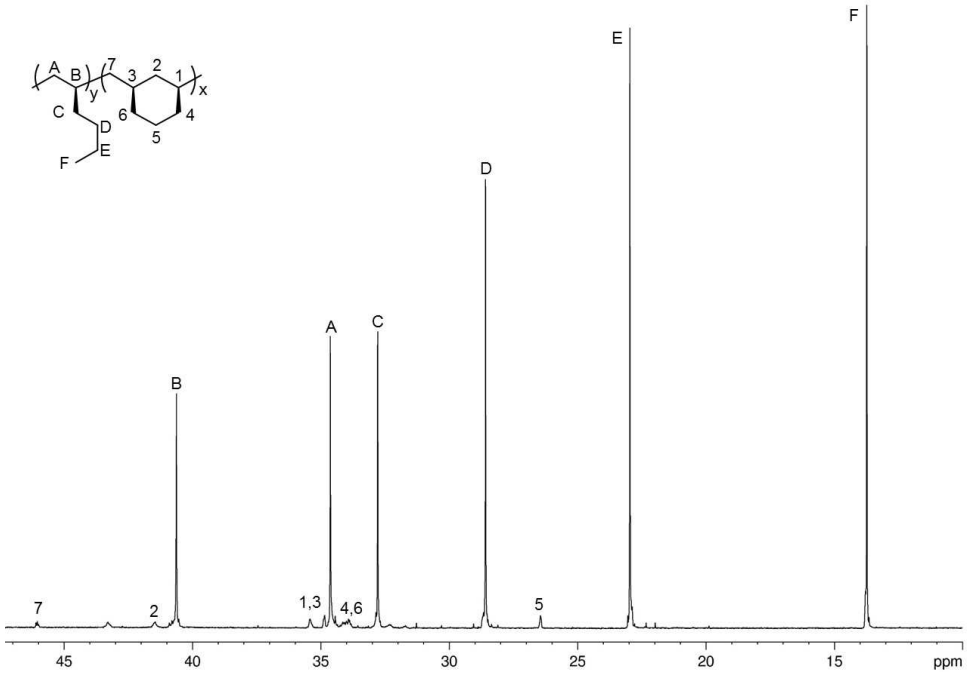

Figure 5.3: $^{13}C\{^{1}H\}$ NMR for iPH-*b*-iPMCH (BCP-sample 9); 200 MHz, 110 °C, TCE-d_2.

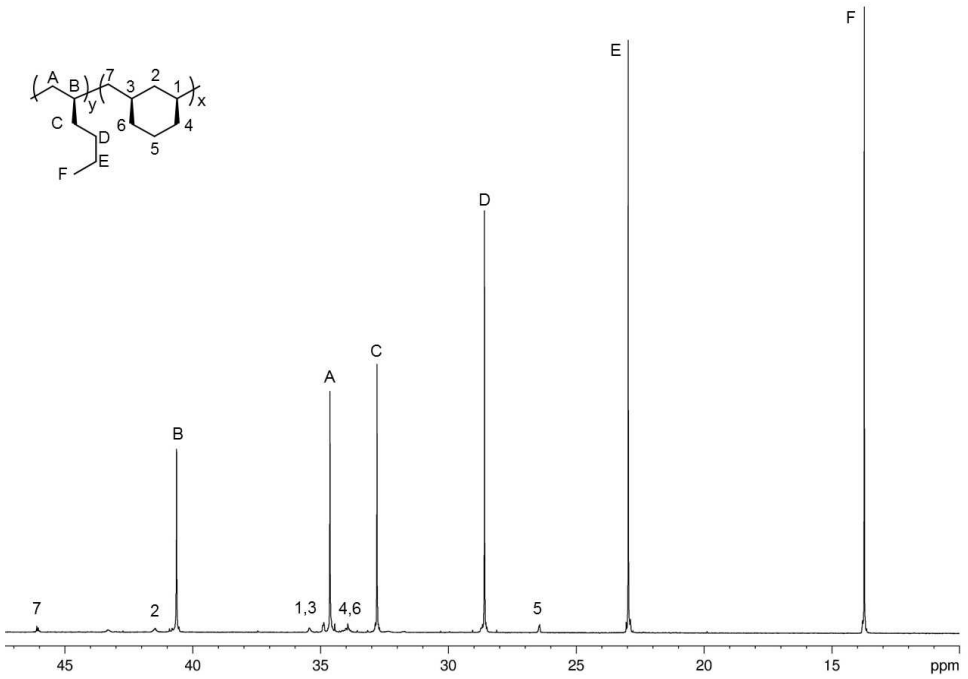

Figure 5.4: $^{13}C\{^{1}H\}$ NMR for iPH-*b*-iPMCH (BCP-sample 12); 200 MHz, 110 °C, TCE-d_2.

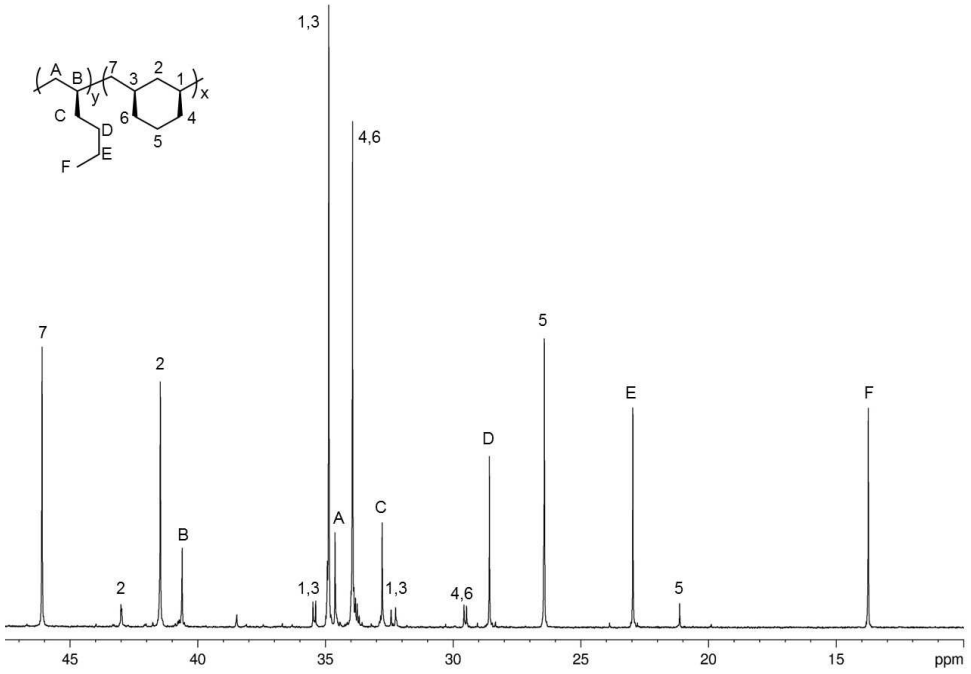

Figure 5.5: $^{13}C\{^{1}H\}$ NMR for iPH-*b*-iPMCH (BCP-sample 13); 200 MHz, 110 °C, TCE-d_2.

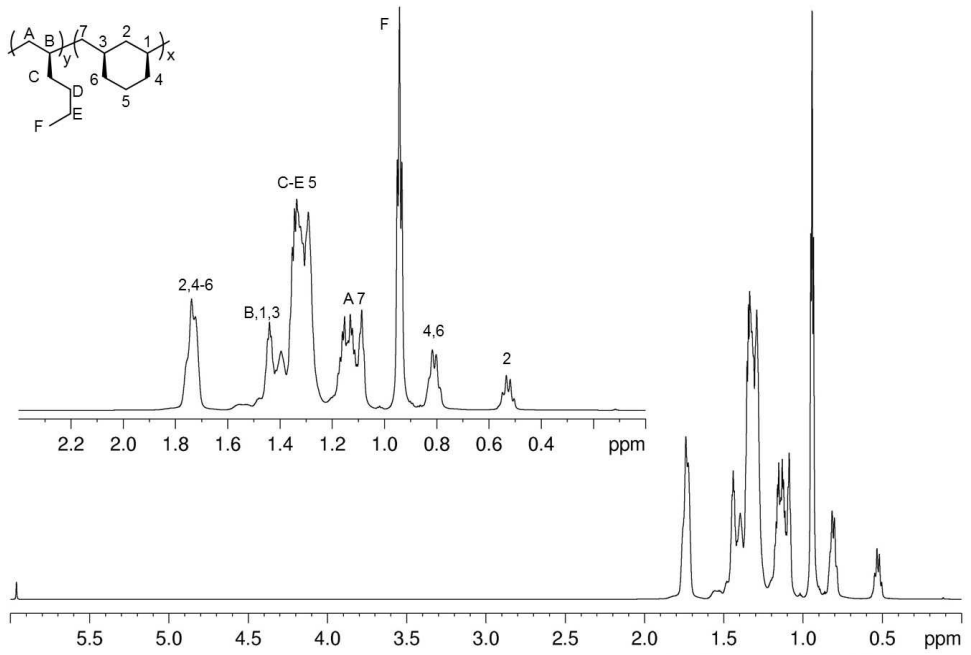

Figure 5.6: ^{1}H NMR for PH-*b*-PMCH (BCP-sample 3); 800 MHz, 110 °C, TCE-d_2.

With the M_n, $Đ$, mole *f*, and microstructures confirmed, next it was of interest to determine the thermal properties of the iPH-*b*-iPMCH BCPs. Although iPH is known to be amorphous with no melting (T_m) or crystallization (T_c), and a glass transition temperature (T_g) around -45 °C, it has been previously shown that iPMCH has a T_m around 209 °C, T_c ca. 181 °C and T_g between 92 °C and 97 °C (standard dev. ± 4 °C; see Chapter 2). DSC plots for all BCPs, however, show only one transition: a T_g that varies between -40 °C and -45 °C. No other T_m, T_c or T_g values were observed. The melting, crystallization, and glass transition temperatures normally expected for PMCH are not observed regardless of temperature program employed (shown below are the plots for heating rates of 10 °C/min), Figure 5.7. A combination of complex crystallization (with regard to the T_m and T_c), the subsequent difficulty with extracting a melting temperature for PMCH (209 °C; see Chapter 2), and the small PMCH mole fractions are the likely explanation for the absence of these thermal transitions (i.e. the change in heat flow required for these phase transitions is lower than the detectable limit rendering undiscernible transitions under the applied conditions). Wide angle x-ray diffraction (WAXD) measurements support amorphous character for all BCP samples analyzed despite the isotacticity identified for each block segment, except for sample 13 with a PMCH mole *f* of 0.68, which shows a very small sharper peak at $2\theta = 18°$. Aside from sample 13, only broad peaks are observed for all BCP samples, Figure 5.8.

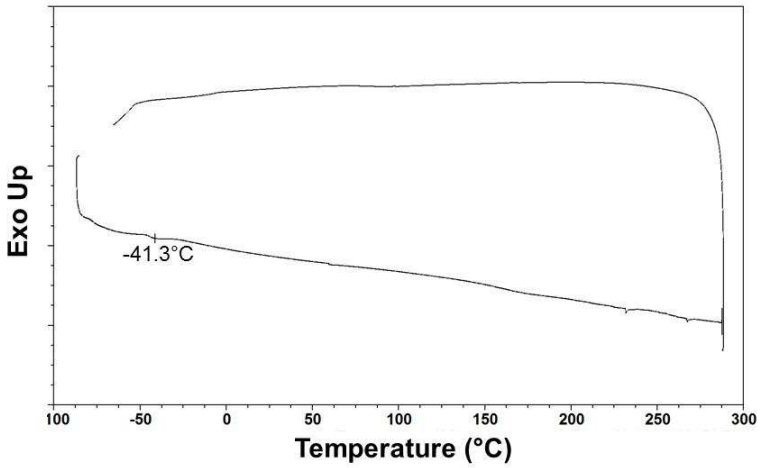

Figure 5.7: Representative DSC plot for iPH-*b*-iPMCH BCPs (BCP-sample 12).

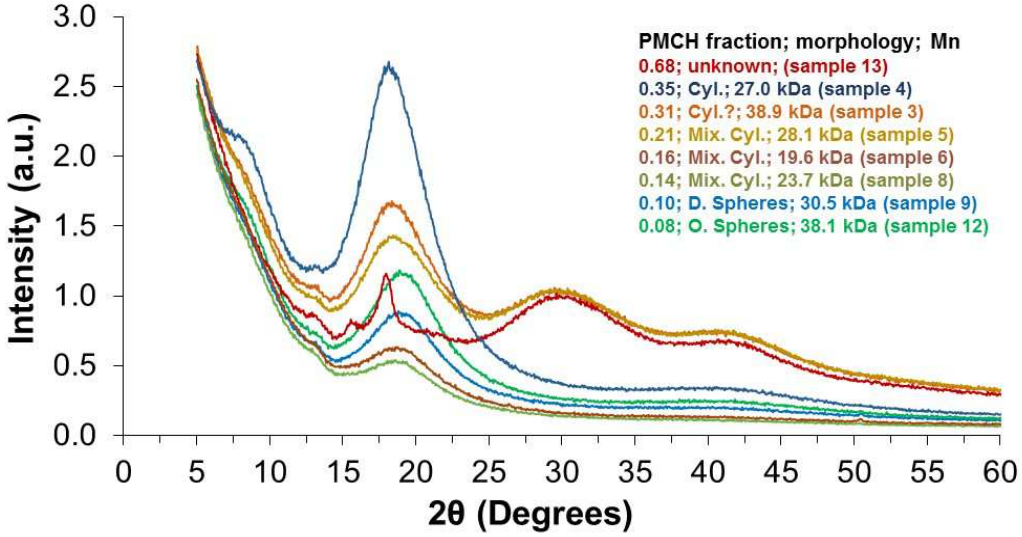

Figure 5.8: WAXD measurements for PH-*b*-PMCH BCPs. BCP-samples 1, 2, 7, 10 and 11 were not characterized *via* WAXD either due to small sample size or absence of microphase separation.

It is now known that the iPH-b-iPMCH BCPs, with M_n values ranging from 17.3 kDa to 38.9 kDa with narrow polydisperisities and PMCH mole *f*'s that vary from 0.06 to 0.68, are amorphous (aside from sample 13, which shows some WAXD

peak coherence suggesting a small degree of crystallinity) with discrete iPH and iPMCH segments. However, the propensity for these BCPs to undergo spontaneous self-assembly into microphase-separated morphologies is unclear. Thus, in an effort to determine the phase behavior of the newly formed iPH-*b*-iPMCH BCPs, AFM (tapping mode) was used in conjunction with a plot of M_n vs. PMCH mole *f* of the BCP samples 1 – 12, Figure 5.9. The plot in Figure 5.9 has been filled in with dashed lines as a prediction of the order-to-order transitions (OOT) and order-to-disorder (ODT) transitions based on preliminary analysis of AFM, SAXS and rheology data. A prediction of the morphology type has also been included based on the same preliminary results.

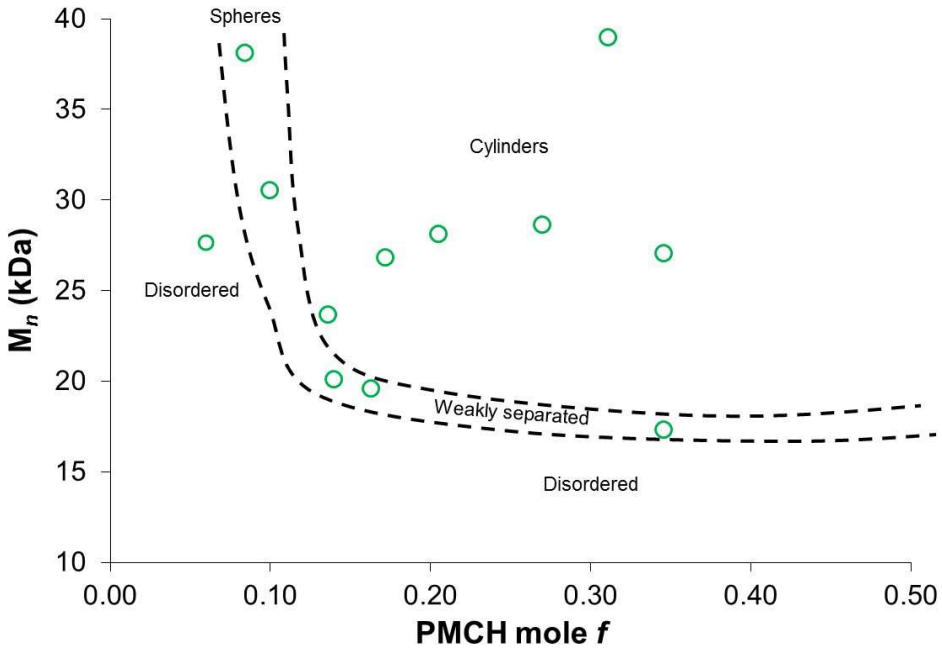

Figure 5.9: Open green circles are M_n and *f* for BCP-samples 1-12. Black dashed line and morphology labels are predictions based on first principles.

Next, AFM measurements were collected for each sample. AFM analysis was carried out on thin BCP films that were spun-cast onto 1 cm squares of silicon from 1 % toluene solutions (50 nm – 105 nm film thicknesses; annealed 12 – 18 hours at 100 °C). Microphase separation was observed in several of the BCP samples. The type of microphase separation observed have been organized into two groups: 1) BCPs with similar PMCH mole *f* but different M_n, and 2) BCPs with similar M_n but different PMCH mole *f*. The first group, with similar PMCH fractions, includes four paired samples, Table 5.2.

Pair 1: samples 1 and 4 with $f = 0.35$. Pair 2: samples 6 and 11 with $f = 0.16$ and 0.17 respectively. Pair 3: samples 7 and 8 with $f = 0.14$. Pair 4: samples 9 and 12 with $f = 0.10$ and 0.08. BCPs with similar segment fractions but different M_n values are expected to have similar phase morphology compared to BCPs with different segment fractions but similar M_n. The reasoning for this is because vertical shifts within a phase diagram (relative to M_n vs. segment fraction) are more likely to fall within the same phase domain whereas horizontal shifts in a phase diagram are more likely to cross a phase transition (OOT, ODT). This is the case observed from PMCH mole *f* Pairs 1 and 4 (BCP-samples 1 and 4, and BCP-samples 9 and 12). The AFM phase maps observed for similar fraction Pair 1 both display weak microphase separation that does not fit into a clear morphology regime. Instead, BCP-sample 1 appears to have a complex microphase morphology and BCP-sample 4 resembles cylinders with A and B segments that are oriented both perpendicular and parallel to the topological surface. The AFM phase maps observed for the similar fraction pair 4

both display spherical or hexagonally packed cylinders oriented perpendicularly to the surface. The primary difference between BCP-sample 9 and BCP-sample 12 is the degree of long range ordering. BCP-sample 12 appears to be more ordered compared to BCP-sample 9.

Table 5.2: Tabulated iPH-*b*-iPMCH sample data with similar PMCH *f*.

Pair	Sample	Mn (kDa)	PDI	PMCH mole *f* by ^{1}H NMR	Morphology (AFM)
1	1	17.3	1.06	0.35	Weakly Sep.
	4	27.0	1.08	0.35	Unknown; Cyl.
2	6	19.6	1.10	0.16	Weakly Sep.
	11	26.8	1.24	0.17	Cylinders
3	7	20.1	1.10	0.14	Weakly Sep./ No Sep.
	8	23.7	1.10	0.14	Cylinders
4	9	30.5	1.15	0.10	Disordered Spheres
	12	38.1	1.21	0.08	Ordered Spheres

In contrast to fraction Pairs 1 and 4, Pairs 2 and 3 (BCP-samples 6 and 11, and BCP-samples 7 and 8) do display clear differences in the type of microphase separation observed. In the case of Pair 2, the AFM phase map for sample 6 suggests only weakly phase separated segments and cannot be definitively assigned to a specific type of microphase separated morphology. BCP-sample 11, on the other hand, has what appears to be stronger microphase separation with cylindrical morphology. Similarly, Pair 3 also consists of one undiscernible weakly phase separated BCP (BCP-sample 7) and one with cylindrical morphology (BCP-sample 8), Figure 5.10.

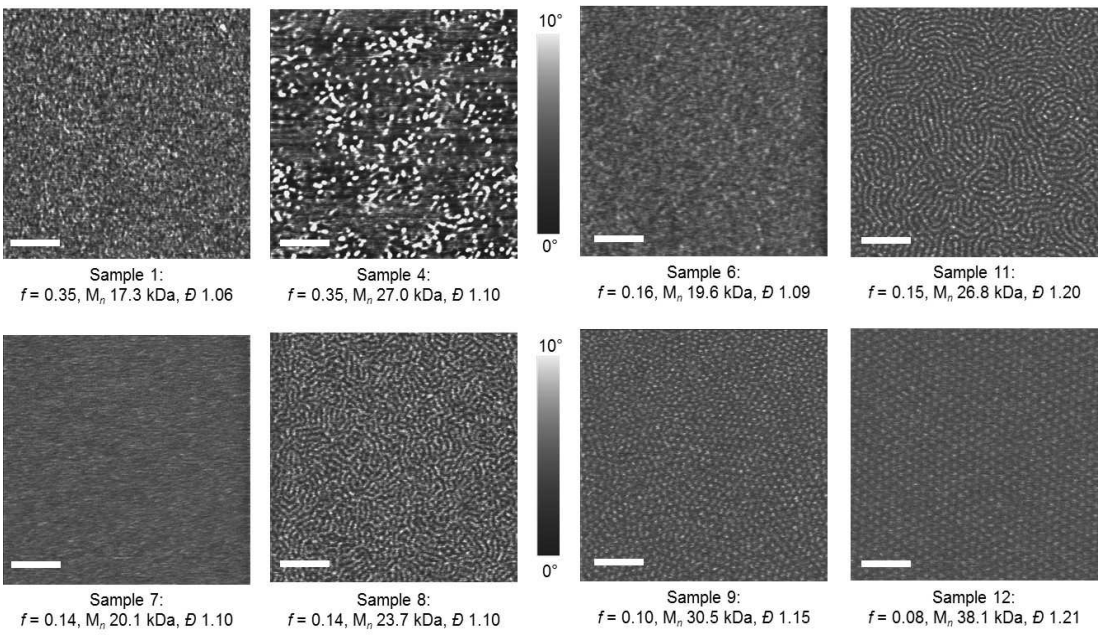

Figure 5.10: AFM images of iPH-*b*-iPMCH BCPs with similar PMCH *f*. Scale bar = 200 nm.

Group 2, BCPs with similar M_n but different PMCH mole *f*, which utilize some of the same sample discussed above can be grouped into three Pairs labeled as Pair 5 (BCP-samples 3 and 12), Pair 6 (BCP-samples 5 and 10), and Pair 7 (BCP-samples 4 and 11), Table 5.3. Each of the three M_n pairs display markedly different AFM phase maps. Pair 5 with BCP-samples 3 and 12 have respective M_n values of 38.9 kDa and 38.1 kDa. BCP-sample 3 has a higher PMCH *f* (0.31) compared to BCP-sample 12 (0.08) and appears to have cylindrical microphase separated morphology wherein the cylinders are primarily oriented parallel to the surface. On the other hand, the AFM phase map for BCP-sample 12, with a lower PMCH *f*, resembles spherical morphology. Pair 6 with BCP-samples 5 and 10 have respective M_n values of 28.1 kDa and 27.7 kDa. BCP-sample 5 has a higher PMCH *f* (0.21) compared to BCP-sample 10 (0.06) with AFM phase maps that appear complex with

low order. BCP-sample 10, however, does not exhibit microphase separation. Finally, pair 7 with BCP-samples 4 and 11 have respective M_n values of 27.0 kDa and 26.8 kDa. The AFM phase map of BCP-sample 4 (PMCH $f = 0.35$) resembles complex morphology, possibly cylinders with A and B segments that are oriented both perpendicular and parallel to the topological surface. In contrast, the AFM phase map of BCP-sample 11 (PMCH $f = 0.17$) displays what appears to be cylindrical microphase separated morphology.

Table 5.3: Tabulated iPH-*b*-iPMCH sample data with similar M_n.

Pair	Sample	Mn (kDa)	PDI	PMCH mole *f* by ^{1}H NMR	Morphology
5	3	38.9	1.11	0.31	Cylinders
	12	38.1	1.21	0.08	Ordered Spheres
6	5	28.1	1.17	0.21	Cylinders
	10	27.7	1.13	0.06	No Phase Sep.
7	4	27.0	1.08	0.35	Unknown; Cyl.
	11	26.8	1.24	0.17	Cylinders

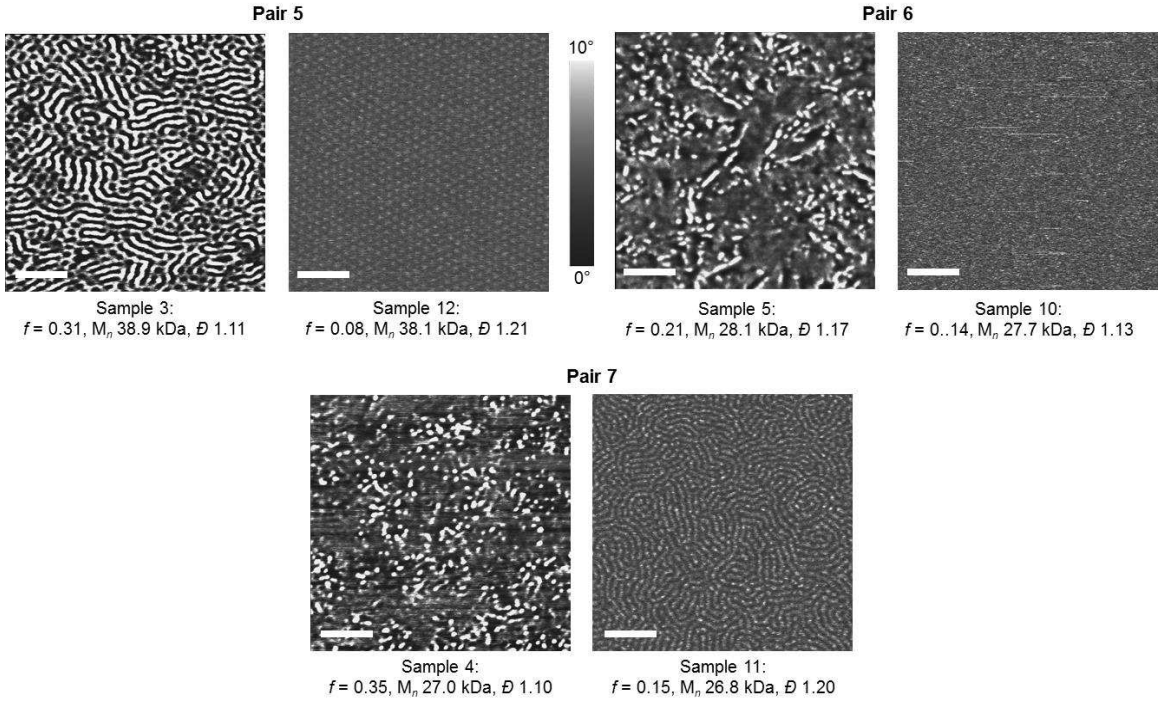

Figure 5.11: AFM images of iPH-*b*-iPMCH BCPs with similar M_n. Scale bar = 200 nm.

There are two additional samples whose AFM phase morphology has not yet been discussed, BCP-sample 2 and BCP-sample 13. BCP-sample 2 has a PMCH mole *f* of 0.27 by ^{1}H NMR and an overall M_n of 28.6 kDa. The topological morphology observed for BCP-sample 2 appears to be cylindrical with short range ordering, Figure 5.12. BCP-sample 13 has the highest PMCH mole *f*, 0.68. The BCP sample is insoluble for SEC analysis; however, the M_n obtained for the first PH block is 7.8 kDa and has a narrow polydispersity ($Đ$ = 1.04).

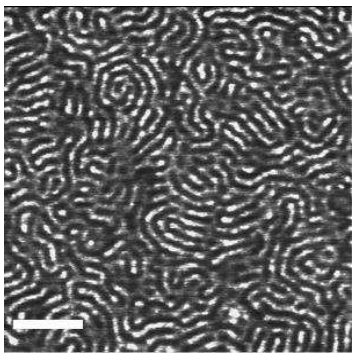

Figure 5.12: AFM images of iPH-*b*-iPMCH BCP, BCP-sample 2. Scale bar = 200 nm.

Based on the mole *f* obtained by ^{1}H NMR and the M_n of the PH block, it is estimated that the overall M_n is approximately 24.4 kDa. Also due to insolubility, BCP-sample 13 could not be prepared in thin film form for AFM analysis. Attempts to prepare a film resulting in surface dewetting. For example, three different coatings were used on the otherwise freshly cleaned silicon surface in an attempt to reduce dewetting of the higher PMCH *f* BCP. In the first attempt, the silicon surface was coated with a 3-5 nm layer of carbon prepared by electrodeposition. The second type of coating used was a layer of PH (ca. 30 nm). The third type of coating used was formed from the interaction of hexamethylsilazane with the silicon surface, which provided a hydrophobic surface for BCP deposition. Unfortunately, these methods proved unsuccessful as dewetting still occurred in each of the cases (note also that two different solvents were used without prevail, PhCl and toluene).

As a concluding discussion on the AFM carried out on these BCPs, it is necessary to measure the average domain spacing (*d*-spacing) observed for each of the phase separated materials. The *d*-spacing for BCP-samples 1 -13 are as follows. BCP-sample numbers 1, 4 – 7 and 10 exhibit only weak (BCP-samples 1, 6 and 7),

inconsistent (BCP-samples 4 and 5) or no microphase separation (BCP-sample 10) and thus the *d*-spacing was not calculated for these samples. The remaining BCPs display *d*-spacing sizes between 23 nm and 35 nm. BCP-Sample 2 (PMCH *f* 0.27, M_n 28.6 kDa, cyl.) has *d*-spacing of 35 nm ± 5 nm. BCP-sample 3 (PMCH *f* 0.31, M_n 38.9 kDa, cyl.) has *d*-spacing of 35 nm ± 4 nm. BCP-sample 8 (PMCH *f* 0.14, M_n 23.7 kDa, cyl.) has *d*-spacing of 23 nm ± 1 nm. BCP-sample 9 (PMCH *f* 0.10, M_n 30.5 kDa, disordered spheres) has *d*-spacing of 26 nm ± 1 nm. BCP-sample 11 (PMCH *f* 0.17, M_n 26.8 kDa, cyl.) has *d*-spacing of 27 nm ± 1 nm. BCP-sample 12 (PMCH *f* 0.08, M_n 38.1 kDa, spheres) has *d*-spacing of 34 nm ± 1 nm, Table 5.4.

Table 5.4: Tabulated iPH-*b*-iPMCH sample data with *d*-spacing (AFM).

Sample	Mn (kDa)	PDI	PMCH mole *f*	Morphology AFM	*d*-spacing (nm) AFM
1	17.3	1.06	0.35	Weakly Sep.	-
2	28.6	1.15	0.27	Cyl.	35 ± 5
3	38.9	1.11	0.31	Cyl.	35 ± 4
4	27.0	1.08	0.35	Unknown; Cyl.	-
5	28.1	1.17	0.21	Unknown; Cyl.	-
6	19.6	1.10	0.16	Weakly Sep.	-
7	20.1	1.10	0.14	Weakly Sep.	-
8	23.7	1.10	0.14	Cyl.	23 ± 1
9	30.5	1.15	0.10	Disordered Spheres	26 ± 1
10	27.7	1.13	0.06	No Phase Sep.	-
11	26.8	1.24	0.17	Cyl.	27 ± 1
12	38.1	1.21	0.08	Ordered Spheres	34 ± 1
13	-	-	0.68	Dewets	-

Although topological phase separation is readily observed for many of these samples by AFM there is no guarantee that the phase separation visualized at the sample surface propagates throughout the bulk of the iPH-*b*-iPMCH BCP materials.

Other characterization methods, such as SAXS, are required to confirm the bulk phase separation morphology. If a BCP sample exhibits bulk microphase separation diffraction peaks will be observed at a range of q values (q = nm^{-1}), typically between 0.01 – 1.0 nm^{-1} when analyzed by x-ray scattering. The correlation of scattering peaks for a given sample provides information about the type of phase separation present. The primary peak (q_1) can be used to determine the domain spacing (d-spacing) between microphase-separated polymer chains: *A* and *B*. Thus, SAXS measurements were carried out on three select iPH-*b*-iPMCH BCP samples (BCP-samples 3, 11 and 12) in an effort to better understand the bulk microphase separation behavior.

BCP-sample 3 with an overall M_n of 38.9 kDa and a PMCH f of 0.31 has an incident peak at 0.208 nm^{-1} (q_1). This q_1 value corresponds to a d-spacing value of 30 nm, which is slightly smaller than the d-spacing observed via AFM for the same sample (35 nm ± 5 nm). There are also two smaller peaks at 0.397 nm^{-1} (q_2) and 0.556 nm^{-1} (q_3). The ratio of peaks q_2/q_1 (1.91) and q_3/q_1 (2.64) do not coincide with the values that are expected for spherical, cylindrical or lamella. The bulk phase separation may still be cylindrical, as predicted based on the AFM phase map for sample 3, but the type of microphase separation for the bulk sample cannot be definitively confirmed based on SAXS analysis. Regardless of the type of morphology, an effort was made to determine the order-to-disorder transition (ODT) temperature. An indication of the ODT may present itself with a loss of coherence for reflection peaks q_2 and q_3. However, no change in peak coherence was observed up to 150 °C, Figure 5.13.

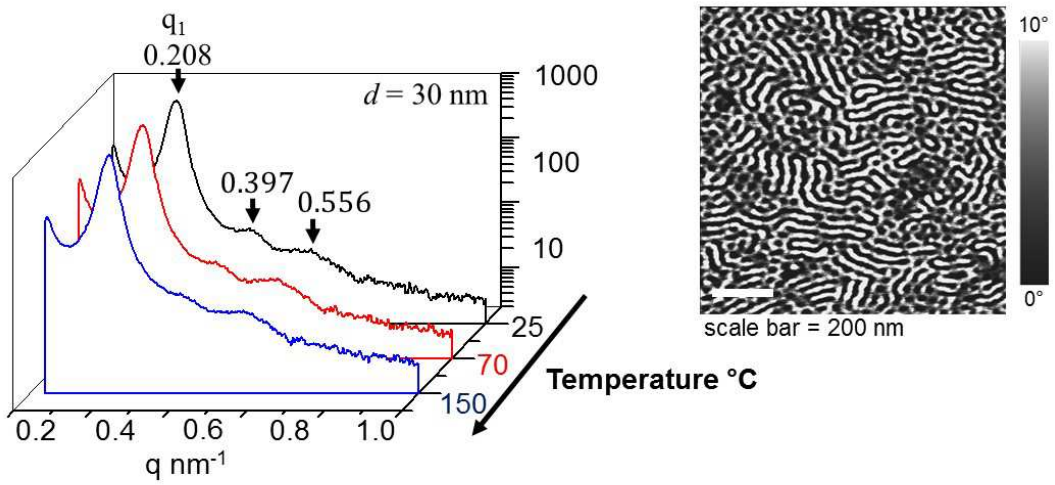

Figure 5.13: SAXS plot and corresponding AFM image for BCP-sample 3.

The second BCP analyzed using SAXS was BCP-sample 11 (overall M_n of 26.8 kDa, PMCH *f* 0.17), which has an incident peak at 0.272 (q_1). The q_1 value corresponds to a *d*-spacing of 23 nm, which is ca. 5 nm smaller than the *d*-spacing observed by AFM (27 nm ± 1 nm). There is one additional peak reflection at 0.472 nm^{-1} (q_2). The peak begins to diminish at temperatures above 60 °C and is no longer present by 75 °C. Thus, the ODT is estimated to be between 65 °C and 75 °C, Figure 5.14. The ratio of q_2/q_1 (at room temperature) is 1.73 ($\sqrt{3}$) suggesting cylindrical morphology. The AFM image presented earlier for BCP-sample 11, combined with the moderate PMCH *f*, 0.17, also coincide with microphase separated cylindrical morphology.

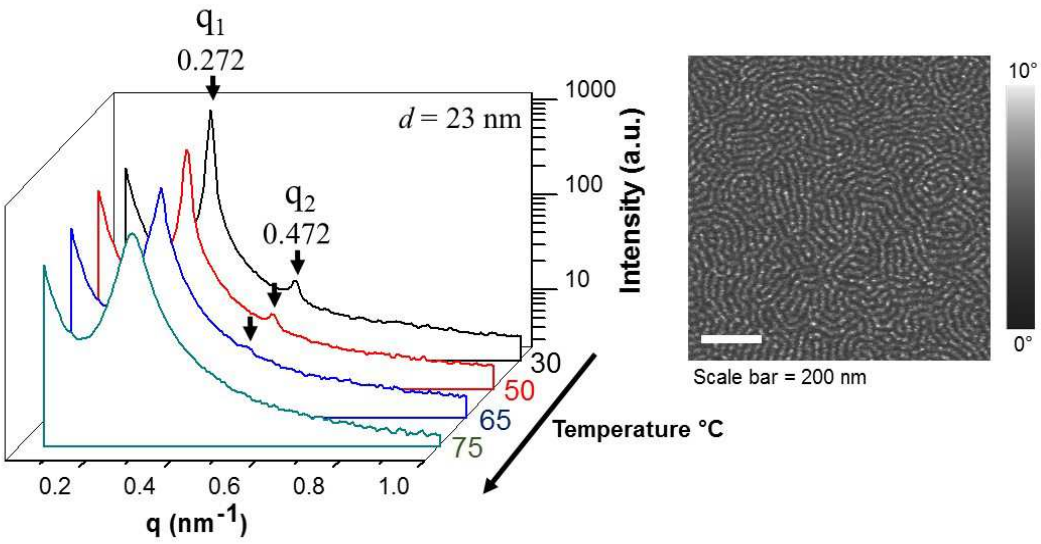

Figure 5.14: SAXS plot and corresponding AFM image for BCP-sample 11.

The third BCP analyzed by SAXS was BCP-sample 12 (M_n = 38.1 kDa, PMCH *f* 0.08). The incident peak is observed at 0.283 nm^{-1} (q_1). The calculated *d*-spacing is 22 nm, which is somewhat smaller than the value extrapolated from the AFM phase map (34 nm ± 1 nm). There is a shift in the location of the reflection peaks between 55 °C and 70 °C. Although not shown here, the shift from one broad peak at 0.489 nm^{-1} to two separate peaks at 0.349 nm^{-1} (q_2) and 0.422 nm^{-1} (q_3) was determined to occur at 58 °C (q_1^* also shifted to a slightly lower value: 0.246 nm^{-1}) . The ratio of q_2/q_1^* and q_3/q_1^* correspond to the $\sqrt{2}$ and $\sqrt{3}$ respectively suggesting spherical microphase separated morphology, which is in agreement of the AFM images. The two reflection peaks remain present through 110 °C before decreasing and finally becoming largely absent at 114 °C. Due to the observed decrease in peak coherence at this temperature, 114 °C has been assigned as the most probable temperature at which the ODT occurs. In general, temperature increments of 2 °C to 5 °C for SAXS analysis were employed with an isothermal hold of several minutes

prior to data collection up to 135 °C. Figure 5.15 provides SAXS plots for sample 12 with an overlay of intensity vs. q at various temperatures. SAXS measurements for all three samples were carried out under the supervision of colleague Wonseok Hwang. SAXS for BCP-samples 3 and 12 were obtained on the Xuess instrument at the University of Maryland. The data provided for BCP-sample 11 was obtained from the SAXS instrument at Brookhaven National Lab.

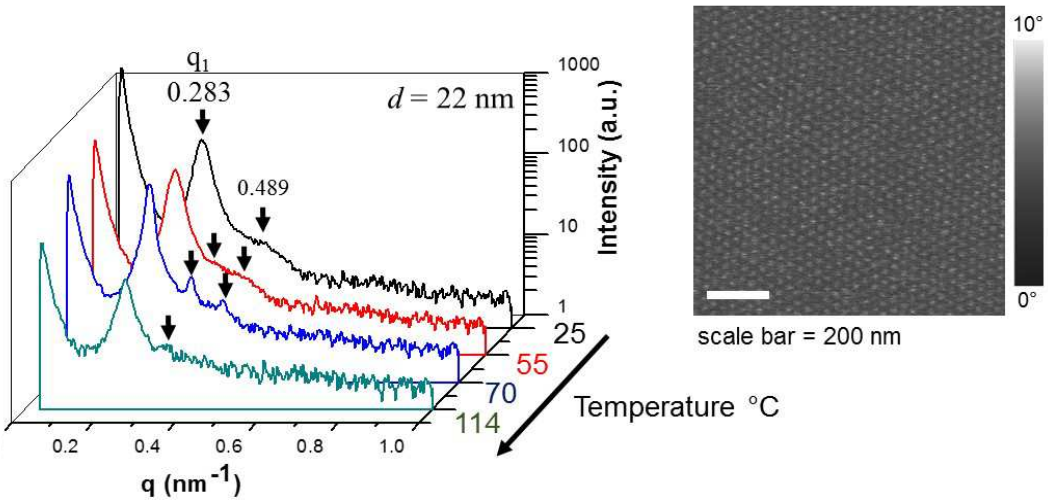

Figure 5.15: SAXS plot and corresponding AFM image for BCP-sample 12.

The viscoelastic properties of several iPH-*b*-iPMCH BCPs were measured using rheology. Samples were investigated independently as a function of strain, frequency and temperature. Temperature sweeps were carried out within the linear viscoelastic region. The linear viscoelastic region was determined using a strain sweep at constant frequency (usually 0.1 Hz) and a given temperature (varies depending on experiment). While the linear viscoelastic region often extended from 0.5 to 10 % strain, the value used to record for temperature sweeps was usually

maintained at 1 % - 2 % strain. In general, BPC samples with higher PMCH content have higher starting storage moduli (G'; Pa). BCP samples with higher PH content have lower starting G' and higher loss moduli (G" Pa). The moduli vary between 1.5e1 Pa (BCP-sample 14) to 1.0e5 Pa (BCP-sample 5) depending on the PMCH *f* and M_n. The ODT could be established for BCP-sample numbers 6 (30 °C), 8 (52 °C), 9 (48 °C), 11 (62 °C) and 12 (60 °C – 114 °C), Table 5.5. For BCP-sample 12 the ODT shifted as a function of strain; 2 % strain ODT = 60 °C, 1 % strain ODT = 82 °C and at 0.5 % strain ODT = 114 °C (The ODT at 0.5 % strain coincides with the ODT obtained by SAXS). ODT values were not observed up to 150 °C for BCP-sample numbers 2, 5 and 7. In the case of BCP-sample 7, G' and G" began decreasing rapidly from 25 °C, Figure 5.16. This characteristic, along with the weak phase separation observed from AFM, suggests an ODT very near to room temperature. On the other hand, BCP-samples 2 and 5 both have higher PMCH *f* and M_n ($0.21 \leq f \leq 0.27$ and $28.1 \text{ kD} \leq M_n \leq 28.6$ kDa). It is suspected that the ODT for these samples is > 150 °C. Figure 5.16 provides representative example plots of G' (Pa) and G" (Pa) vs. temperature (°C) for BCP-sample numbers 6 – 12 and 14. An additional sample (#14), PH homopolymer, has been included as a comparison of viscoelastic properties. As expected, BCP-sample 14 has comparatively low G' (1.5e1 Pa) and G" (7.9e2 Pa) in contrast to the BCP samples.

Table 5.5: Updated BCP data table to include rheology.

Sample	Mn (kDa)	PDI	PMCH mole *f*	Morphology AFM	*d*-spacing (nm) AFM	Log G' at 25 °C (Pa)	Log G" at 25 °C (Pa)	ODT (°C) Rheology
1	17.3	1.06	0.35	Weakly Sep.	-	-	-	-
2	28.6	1.15	0.27	Cyl.	35 ± 5	1.0e4	-	n/a
3	38.9	1.11	0.31	Cyl.	35 ± 4	3.7e3	1.7e3	-
4	27.0	1.08	0.35	Unknown; Cyl.	-	-	-	-
5	28.1	1.17	0.21	Unknown; Cyl.	-	1.0e5	-	n/a
6	19.6	1.10	0.16	Weakly Sep.	-	3.9e3	9.2e3	30
7	20.1	1.10	0.14	Weakly Sep.	-	9.6e2	3.8e3	n/a
8	23.7	1.10	0.14	Cyl.	23 ± 1	1.3e2	1.3e2	52
9	30.5	1.15	0.10	Disordered Spheres	26 ± 1	1.6e2	1.8e2	48
10	27.7	1.13	0.06	No Phase Sep.	-	6.3e2	7.3e3	-
11	26.8	1.24	0.17	Cyl.	27 ± 1	1.9e4	1.1e4	62
12	38.1	1.21	0.08	Ordered Spheres	34 ± 1	1.1e4	1.7e4	60 – 114
13	-	-	0.68	Dewets	-	-	-	-
14				No Phase Sep.	n/a	1.5e1	7.9e2	n/a

*Rheology data collected at 0.1 Hz and 1% – 2% strain (sample 8 collected at 4% strain).

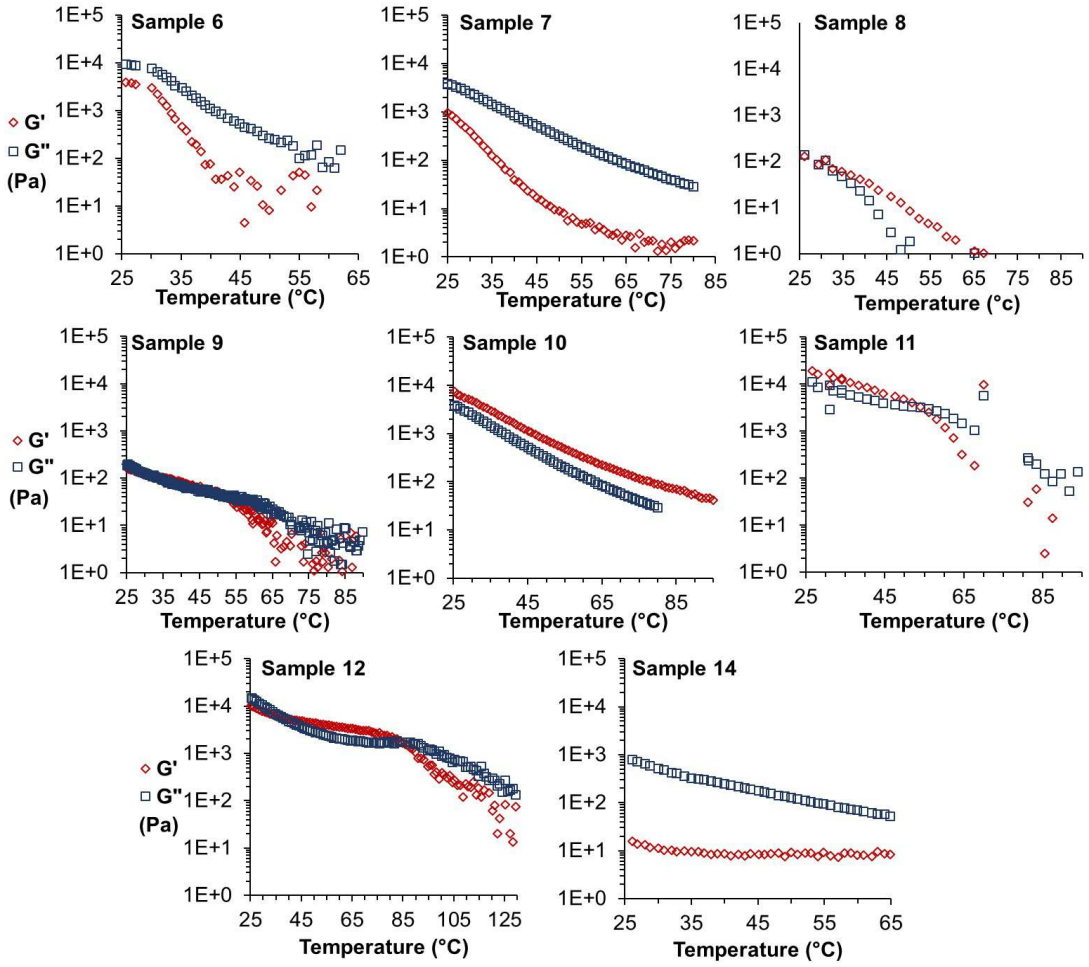

Figure 5.16: Plots of G' (Pa) and G" (Pa) vs. Temperature (°C) for select BCP samples.

5.3. Conclusions

In summary, pure polyolefin AB diblock copolymers composed of iPH (A segment) and iPMCH (B segment) were synthesized for the first time using living coordination polymerization with precatalyst **1** and were presented in this Chapter as preliminary report. The BCPs have well-defined iPH and iPMCH segments whose block ratios and overall M_n can be easily tuned by changing the ratio of 1-hexene and 1,6-HD monomers. Microphase separation (spheres, cylinders and other, undefined, complex microstructures) were observed for several of BCPs as evidenced by AFM and SAXS characterization. This exploratory work, inspired by the original BCP report of PH-*b*-poly(methylene-1,3-cyclopentene) (PMCP) originally reported by the Sita group in 2000,[8] sets a foundation from which new polyolefin based BCPs can be developed.

5.4. Experimentals

5.5. General Synthesis of Diblock Copolymers

All manipulations were carried out in an inert atmosphere of dinitrogen and with dry, oxygen-free solvents. Typical polymerizations were carried out in 50 mL round bottomed flasks equipped with magnetic stir bar with 25 mL PhCl as solvent at -18 °C. Polymerization times varied between 2-12 hours the reaction time was selected based on previously published kinetic data of poly(1-hexene) and overall targeted molecular weight.[10] A small aliquot was removed during polymerization immediately prior to the addition of the second monomer (typically 1,6-HD). Polymerization reactions were quenched with acidic methanol (10% HCl by volume). PhCl solvent was removed *in vacuo* prior to solubilizing sample in minimal toluene

for purification via column chromatography (400 mesh silica gel). Samples were collected and dried *in vacuo* until constant weight. Instrument parameters and materials information are provided in Appendices A and B.

5.6. References

1. Gref, R.; Domb, A.; Quellec, P.; Blunk, T.; Mueller, R. H.; Verbavatz, J. M.; Langer, R., *Adv. Drug Delivery Rev.* **1995**, *16* (2,3), 215-33.

2. Segalman, R. A.; Yokoyama, H.; Kramer, E. J., *Adv. Mater.* **2001**, *13* (15), 1152-1155.

3. a) Lin, Y.; Boeker, A.; He, J.; Sill, K.; Xiang, H.; Abetz, C.; Li, X.; Wang, J.; Emrick, T.; Long, S.; Wang, Q.; Balazs, A.; Russell, T. P., *Nature* **2005**, *434* (7029), 55-59.; b) Stoykovich, M. P.; Mueller, M.; Kim, S. O.; Solak, H. H.; Edwards, E. W.; de Pablo, J. J.; Nealey, P. F., *Science* **2005**, *308* (5727), 1442-1446.

4. a) Park, M.; Harrison, C.; Chaikin, P. M.; Register, R. A.; Adamson, D. H., *Science* **1997**, *276* (5317), 1401-1404.; b) Evens, G. G.; Pijpers, E. M. J., *MMI Press Symp. Ser.* **1983**, *4* (Transition Met. Catal. Polym.: Alkens Dienes, Pt. A), 245-264.

5. a) Xie, H.-Q.; Liu, D.-G.; Xie, D.; Guan, J.-G., *J. Appl. Polym. Sci.* **2006**, *99* (4), 1887-1894.; b) Pascault, J. P.; Girard-Reydet, E., *Polym. Prepr. (Am. Chem. Soc., Div. Polym. Chem.)* **1999**, *40* (2), 1092-1093.

6. Wang, J.-S.; Matyjaszewski, K., *J. Am. Chem. Soc.* **1995**, *117* (20), 5614-5615.

7. Hillmyer, M., *Curr. Opin. Solid State Mater. Sci.* **2000**, *4* (6), 559-564.

8. Jayaratne, K. C.; Keaton, R. J.; Henningsen, D. A.; Sita, L. R., *J. Am. Chem. Soc.* **2000**, *122* (42), 10490-10491.

9. Crawford, K. E.; Sita, L. R., *J. Am. Chem. Soc.* **2013**, *135* (24), 8778-8781.

10. Jayaratne, K. C.; Sita, L. R., *J. Am. Chem. Soc.* **2000**, *122* (5), 958-959.

Chapter 6

Pure Polyolefin Triblock Copolymer Thermoplastic Elastomers

6.1. Introduction

Thermoplastic elastomers (TPEs) are an important class of polymers that have garnered considerable attention over the past several decades for their unique physical properties.[1] TPEs exhibit exceptional multifaceted bulk properties, behaving both as a thermoplastic (upon heating) and a rubber (once cooled), providing the opportunity for post-consumer recycling. To date, the most widely studied TPE (Kraton) is an ABA type triblock copolymer composed of poly(styrene-butadiene-styrene), which was developed by the Shell Chemical Company in the 1950s.[1] Since then, Kraton has become a TPE archetype due to its excellent display of mechanical strength and elasticity.[1] The exemplary elastomeric properties observed with styrenic block copolymers (SBCs) are largely attributed the spherical or cylindrical microphase-separated morphologies that arise from the aggregation of the A-segments (non-covalent, physical crosslinks), and the arrangement of the confined B-segments into loops and bridges, Scheme 6.1.

Scheme 6.1: Representation of an ABA triblock copolymer network.

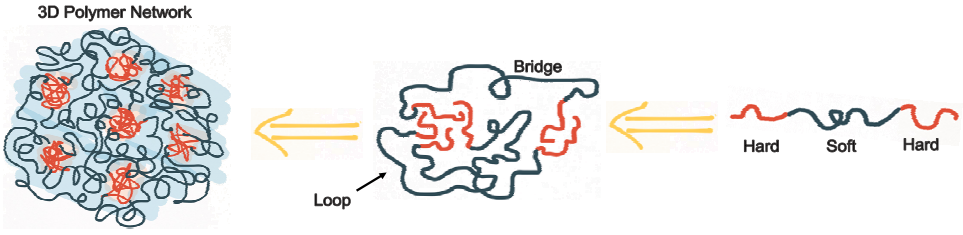

Extensive fundamental block copolymer studies carried out by Bates and coworkers,[2, 3] as well as by Register and coworkers[4] have provided a wealth of knowledge regarding the unique structure-property relationships of SBCs and their respective hydrogenated analogues.[1] The detail of work and continued efforts presented by these groups have provided a foundation from which new challenges can be addressed. Specifically, there is currently a need to further develop sustainable TPEs by using commodity olefin feedstock's such ethylene and propene. In this regard, polyolefin TPEs (PO-TPEs), are most commonly reported as stereoblock polypropene,[5] or ethylene/octene based blocky copolymers and blends (the latter was originally introduced by Dow in 2006).[3, 6] In contrast to SBCs, the physical crosslinks exhibited by PO-TPEs are attributed to crystallization. While the proclivity for certain PO segments to crystallize promotes high strength, it also hinders the formation of the spherical or cylindrical microphase separated domains that are required for high elasticity TPEs. Further, the number of polymerization methods currently available that can successfully polymerize amorphous olefins in a living fashion to afford multi-block copolymers are severely limited.[7] Therefore, it is necessary to develop PO-based, ABA type triblock copolymer elastomers that 1) readily assemble into spherical or cylindrical microphase-separated morphologies without crystallization, and 2) are capable of exhibiting a range of tensile strengths and elastomeric properties, which can be fine-tuned depending on the application of interest.

The focus of this Chapter is on the synthesis of a new family of ABA triblock copolymer thermoplastic elastomers (TPEs) using the cyclopolymerization of 1,6-

heptadiene (1,6-HD) as the A-segment and atactic polypropylene (*a*PP) as the B-segment.

6.2. PMCH-*b*-aPP-*b*-PMCH Triblock Copolymers

Presented here, for the first time, is the design and assembly of a pure PO ABA triblock copolymer elastomer with respective A and B segments composed of high T_g *cis-atactic*-poly(methylene-1,3-cyclohexane) (*cis-a*-PMCH), and low T_g *a*PP. The triblock copolymer samples were prepared under living coordination polymerization conditions using the Group 4 C_S-symmetric monocyclopentadienyl amidinate precatalyst: Cp*Hf[N(Et)C(Me)N(Et)](Me$_2$) (Cp* = η^5-C_5Me_5, Et = ethyl, Me = methyl) (**2**) activated by N,N-dimethylanilinium tetrakis (pentafluorophenyl)borate, ([PhNHMe$_2$][B(C_6F_5)$_4$]; **II**), in cold toluene with sequential additions of 1,6-HD and propene (5 psi), Scheme 6.2. As shown in Chapter 2 the first living coordination cyclopolymerization of 1,6-HD resulting in a highly controlled spectrum of distinct *cis*-PMCH microstructures in which the relative tacticity can be modulated from highly *isotactic* to *atactic* as a function of precatalyst type was achieved.[8] Briefly, it was found that, when using a 1:1 ratio of [**II**]:[**2**], the α,ω-nonconjugated diene (1,6-HD) undergoes complete intramolecular cyclization with 1,2-primary insertion of the α-bond followed by an immediate 1,2-secondary insertion of the ω-bond to afford a near quantitative yield of *cis*-atactic-PMCH (hereafter referred to PMCH in this Chapter for simplicity).

Scheme 6.2: General synthesis method for triblock copolymers using LCP.

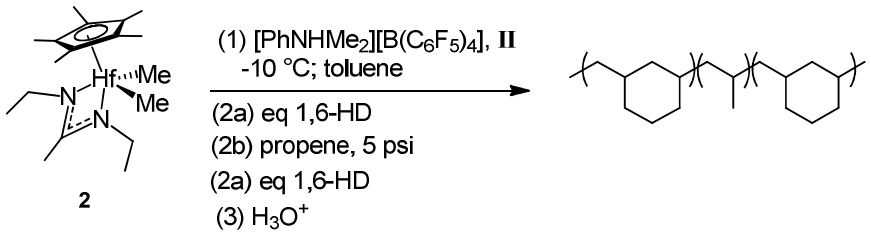

A key property of the PMCH homopolymer from cationic **2a** is the high T_g (ca. 70 °C)[8] relative to that of *a*PP (ca. 0 °C) and is considered here as a potentially suitable candidate for the 'hard' segments in a hard-soft-hard triblock copolymer with *a*PP as the high molecular weight middle 'soft' segment. Although the living coordination polymerization (LCP) with **2** when activated by **II** has been previously presented for PMCH[8] and PP homopolymers[9] it is not a given that ABA triblock copolymers consisting of PMCH and PP can be formed. Moreover, it is unclear whether the formation of PMCH-*b*-*a*PP-*b*-PMCH, ABA, triblock copolymers will behave as TPEs. Therefore, the materials presented in this report were subjected to extensive characterization techniques to allow for a more comprehensive understanding of the polymer's architecture and bulk properties. There are three PMCH-*b*-*a*PP-*b*-PMCH triblock copolymers discussed here having weight average molecular weight, M_w, values of 175 kDa, 342 kDa and 224 kDa (determined using HT-SEC) with relatively narrow polydisperisities ($Đ \leq 1.2$; determined using RT-SEC), Figure 6.1 and Table 6.1. The respective PMCH fractions are 17 %, 9.5 % and 23 % as determined by room temp SEC (RT-SEC). Figure 6.2 provides an overlay of the RT-SEC traces obtained between each block addition for samples 1 – 3. It is important to note that, according to HT-SEC, up to 4 % PMCH homopolymer is

present within the PMCH-*b*-*a*PP-*b*-PMCH matrix for samples 1 (ca. 2 %) and 3 (ca. 4 %), and come as a result of the sensitivity of block copolymer synthesis *via* LCP. These percentages were obtained from HT-SEC, the percentage is somewhat higher when considering RT-SEC for sample 3, but is overall relatively low. The independent PMCH fraction, although small, may contribute to a slight increase in tensile strength. In addition, a fourth sample, pure *a*PP, was also prepared (M_w 314 kDa and $Đ$ = 1.26; sample 4) and has been included as a benchmark comparison of mechanical properties, *vide infara*.

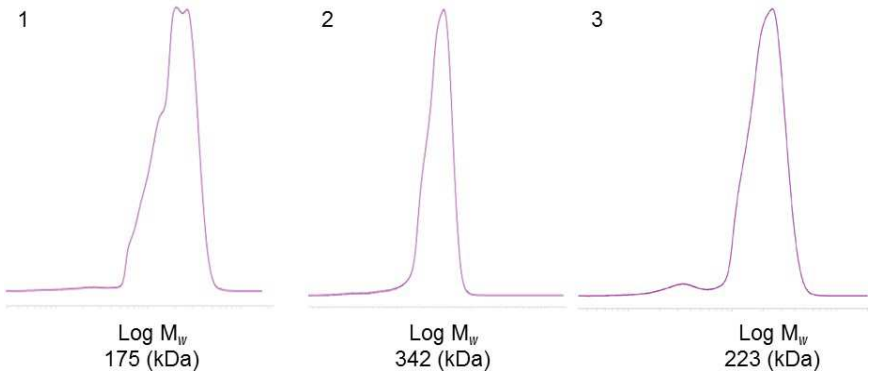

Figure 6.1: HT-SEC plots for triblock copolymer samples 1 – 3.

Table 6.1: SEC and DSC data for triblock copolymer samples 1 – 3 and aPP (sample 4).

Sample	PMCH %	M_w (kDa)	Đ	T_g (°C)[b]
1	17	175	1.03	0.86
2	9.3	342	1.18	1.50
3	23	223	1.16	1.90
4	0	314	1.26	0.53

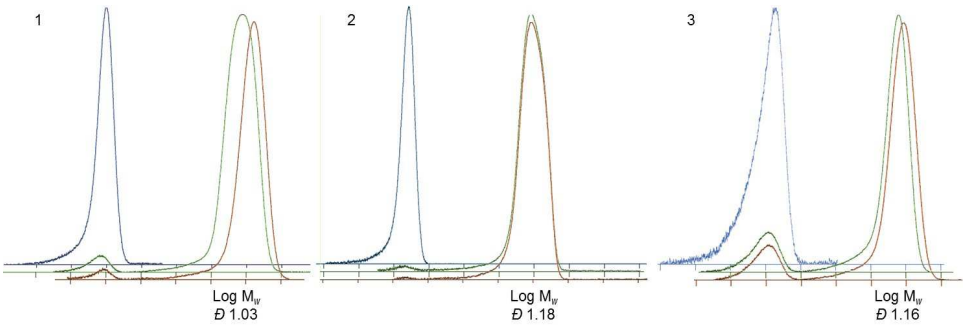

Figure 6.2: RT-SEC plots for triblock copolymer samples 1 – 3. Overlay has been offset vertically for clarity.

Also considered are the low and stand-alone T_g values for samples 1 – 3 with ranges between 0.53 °C – 1.90 °C, Figure 6.3. The thermal values reported here were determined using the second heat/cool cycle by DSC with a standard temperature program of 10 °C/min (two heat/cool cycles). Based on the overall low PMCH content compared to *a*PP (and the lower detection limit of the instrument), it is possible that the anticipated glass transition for PMCH may not be observed.

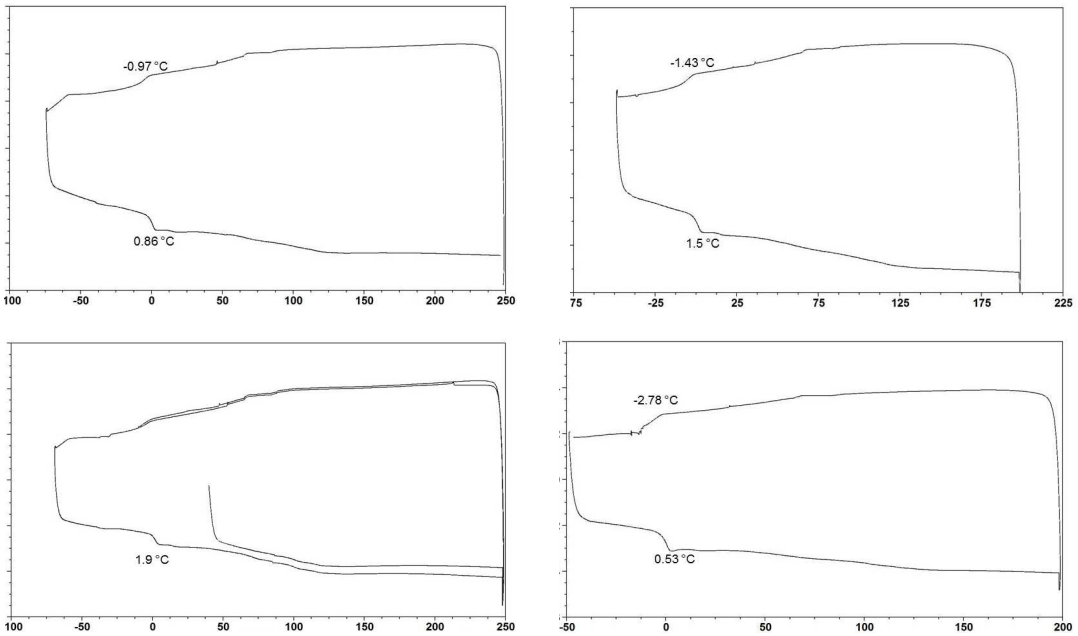

Figure 6.3: DSC plots for triblock copolymer samples 1 – 3 and aPP (sample 4).

With the confirmed synthesis of high molecular weight PMCH-*b*-*a*PP-*b*-PMCH triblock copolymers with narrow polydisperisities it is now necessary to determine if the ABA segments are *well-defined*. The formation of molecularly discrete segments is necessary for optimal aggregation of the glassy domains and subsequent confinement of the soft middle block. Segments whose microstructures consist of a mixture of A and B units will weaken the intermolecular forces required for sufficient physical crosslinking and will ultimately limit the elasticity of the material. To this end, the chemical microstructure can be realized through the use of $^{13}C\{^{1}H\}$ NMR. Block segments that are discrete from one another will display resonances with chemical shifts in the $^{13}C\{^{1}H\}$ NMR spectra of the respective homopolymers. Ill-defined segments with mixed A and B will display 'new' resonances at chemical shifts that do not match that of the homopolymers. Thus, $^{13}C\{^{1}H\}$ NMR measurements were carried out with concentrations of ca. 50 mg/mL per sample at 110 °C using 1,1,2,2-tetrachloroethane-d_2 (TCE-d_2) as solvent with a resonance frequency of 200 MHz attenuated from 800 MHz based on the gyromagnetic radius of carbon. Gratifyingly, each of the PMCH-*b*-*a*PP-*b*-PMCH triblock copolymers prepared indeed display resonances whose chemical shifts match only that of the respective PMCH and *a*PP homopolymers, Figure 6.4. There are three groups of peak resonances for *a*PP. Resonances between 19 ppm to 22 ppm correspond to the pendant methyl carbon (see Figure 6.4 inset). The sharp resonance at ca. 28 ppm corresponds to the carbon atoms at position B. The third cluster of resonances between 44 ppm and 48 ppm are attributed to the carbon atoms at position A. There are four groups of resonances for PMCH. The resonance at 26.5 ppm

corresponds to the carbon atoms at position 5 (see Figure 6.4 inset). The group of resonances between 33 ppm and 34 ppm are attributed to the carbon atoms at positions 4 and 6. The group of resonances at ca. 35 ppm corresponds to carbon atoms at positions 1 and 3. The fourth group of peak resonances are located between 41 ppm and 43 ppm and corresponds to carbon atoms at position 2. There is a fifth resonance expected at 46 ppm, which is not easily detected due to the overall low PMCH content compared to *a*PP, Figure 6.4. The absence of vinyl resonances in the ^{1}H NMR spectra for each sample further confirm LCP conditions, Figure 6.5 (representative sample 3).

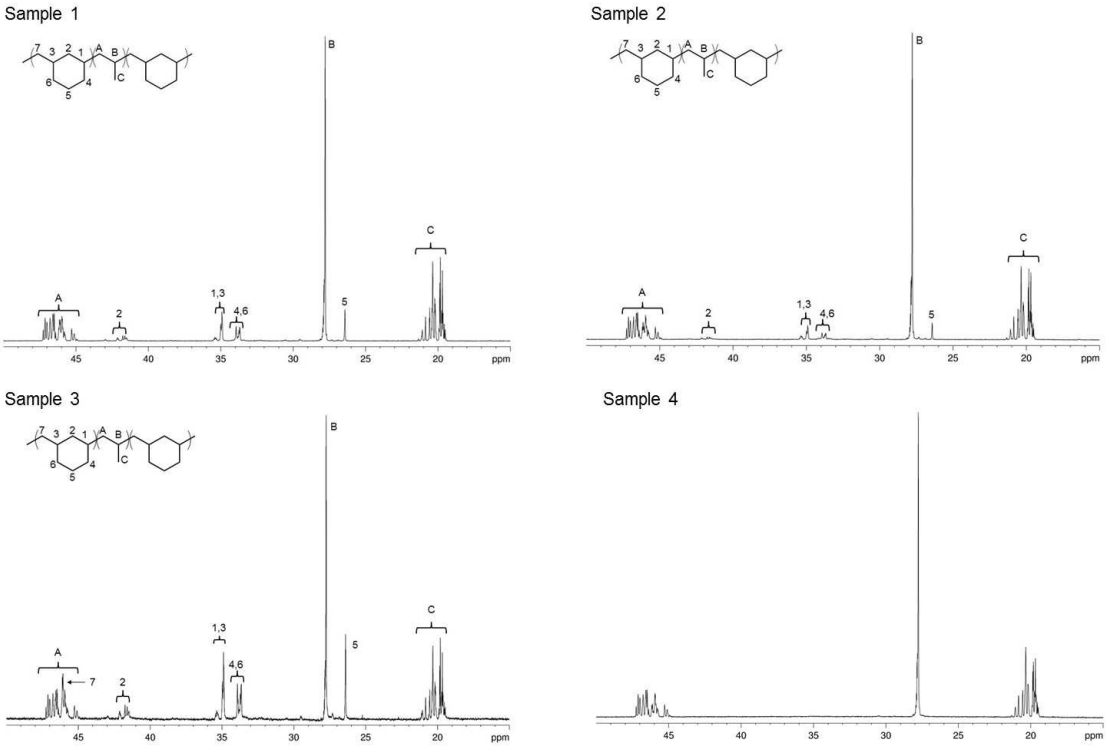

Figure 6.4: ^{13}C{^{1}H} NMR spectra for triblock copolymer samples 1 – 3 and aPP (sample 4); 200 MHz, 100 °C, TCE-d_2.

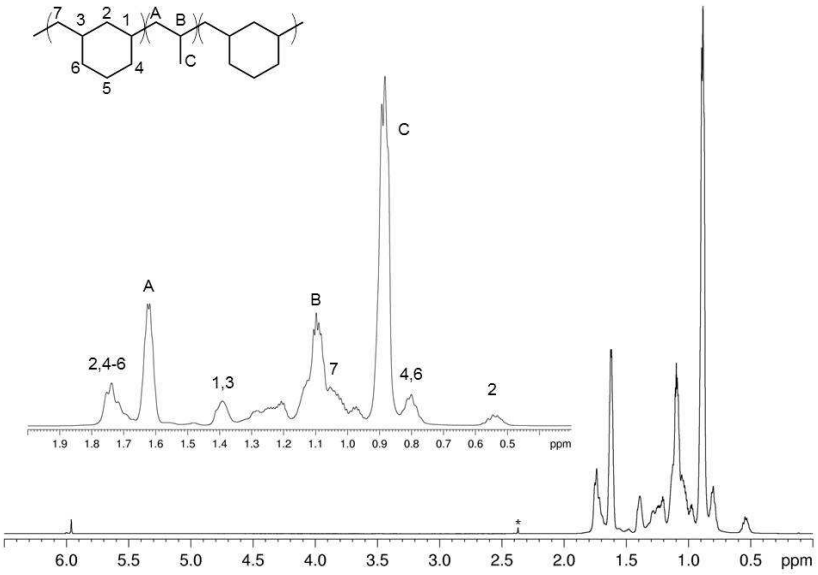

Figure 6.5: ^{1}H NMR spectrum of triblock copolymer sample 3; 800 MHz, 110 °C, TCE-d_2.

The synthesis of molecularly discrete A and B segments in the ABA triblock copolymers is a promising result in the pursuit of an elastomeric PO material. However, the presence of *well-defined* segments does not guarantee microphase separation between the A and B segments promoting the formation of physical crosslinks; nor does it provide information about the materials' contribution toward the formation of strong, elastic PO-TPEs. Therefore, additional characterization such as atomic force microscopy (AFM), transmission electron microscopy (TEM), small angle x-ray scattering (SAXS), and mechanical measurements are necessary to establish the presence of microphase separation and the subsequent elastomeric properties.

It is well known that ABA triblock copolymers exhibit similar morphological properties compared to AB diblock copolymers albeit with a much larger lamellar

region.[10] AFM analysis (tapping-mode) was performed on thin films (123 nm - 169 nm thicknesses) of annealed polymer (100 °C for 18 hours), and, to satisfaction, the AFM phase-maps for each of the triblock copolymer samples indeed exhibit microphase separation. The AFM images collected post annealing are similar in form but appear to exhibit improved topological ordering compared to the images collected prior to annealing. Each triblock copolymer sample displays a different surface topology. Sample 1, with 17 % PMCH suggests a complex morphology. Sample 2 and sample 3 depict surface topologies of spheres (9.3 % PMCH) and cylinders (23 % PMCH) respectively. The average domain spacing (*d*-spacing) increase somewhat across sample runs; 53 nm, 56 nm and 59 nm respectively for samples 1 – 3, Figure 6.6 - Figure 6.8.

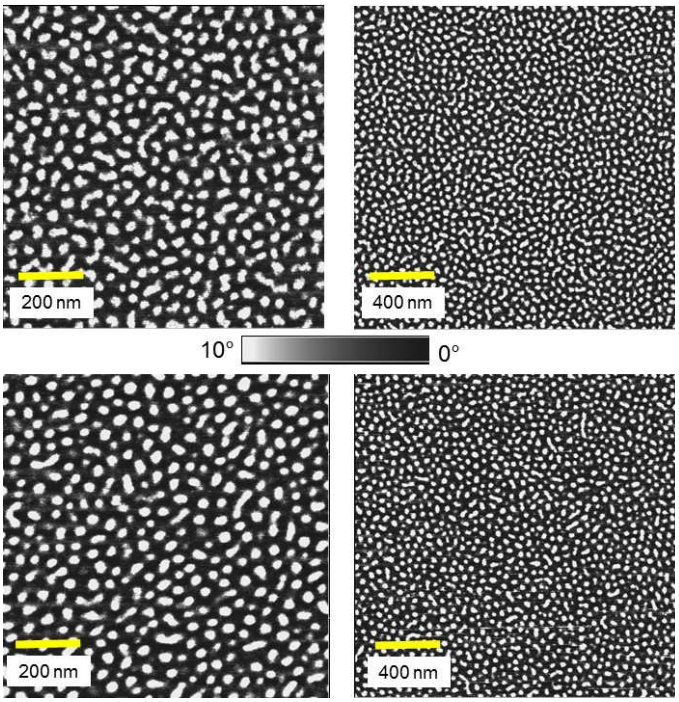

Figure 6.6: AFM images of triblock copolymer sample 1 before annealing (top) and after annealing at 100 °C for 18 hours (bottom); film thickness 123 nm.

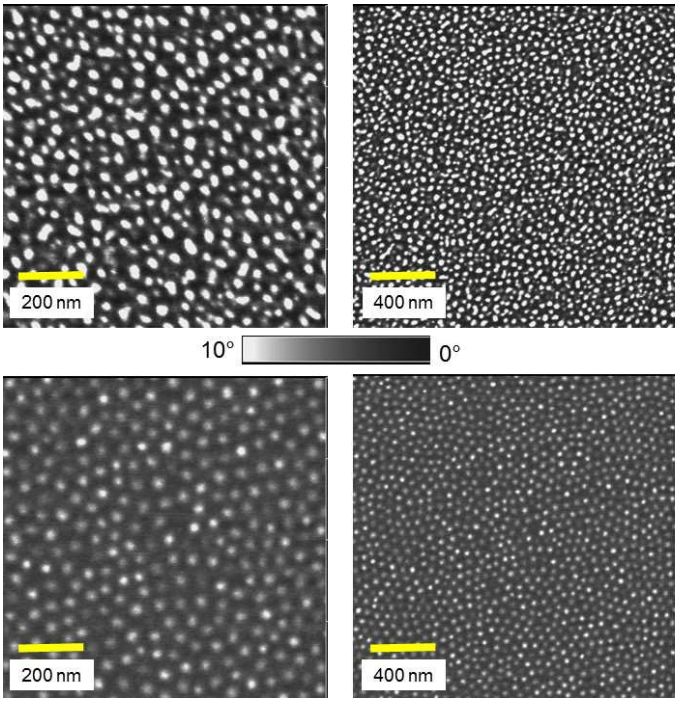

Figure 6.7: AFM images of triblock copolymer sample 2 before annealing (top) and after annealing at 100 °C for 18 hours (bottom); film thickness 160 nm.

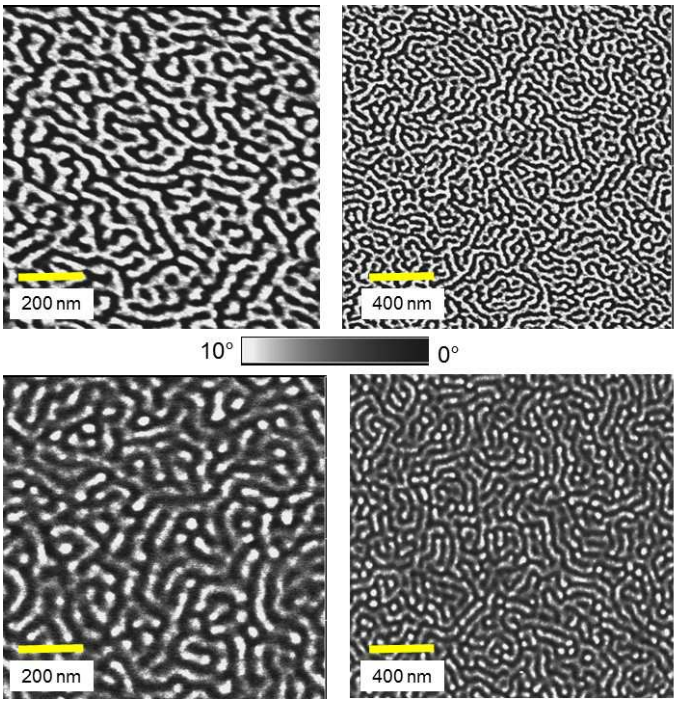

Figure 6.8: AFM images of triblock copolymer sample 3 before annealing (top) and after annealing at 100 °C for 18 hours (bottom); film thickness 169 nm.

TEM was also employed as a method to further visualize the incompatibility between the PMCH and *a*PP segments. For TEM experiments, each of the polymer samples were spun cast (average film thickness 34 nm) from toluene on to mica films and then transferred on to 400-mesh carbon coated copper grids. The prepared grids were then annealed at 100 °C for 12 hours. The TEM analysis for samples 1 – 3 reveal microphase separated morphologies that are visually consistent with the respective topological phase morphologies obtained by AFM. The *d*-spacing obtained by TEM is different compared to AFM. For TEM *d*-spacing is 56 nm for sample 1 and 50 nm for both samples 2 and 3, Figure 6.9.

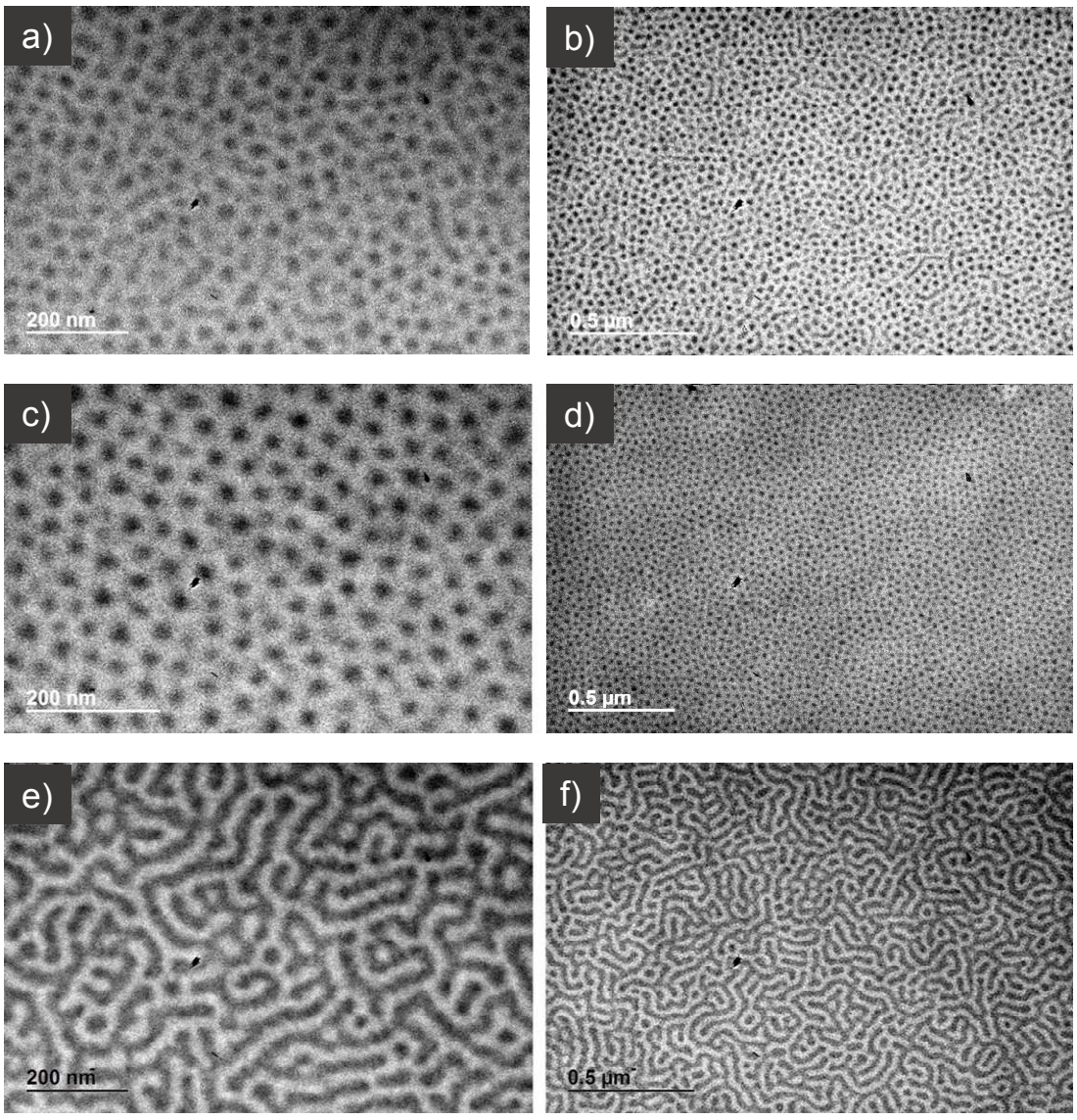

Figure 6.9: Representative TEM images for sample 1 (top; a, b), sample 2 (middle; c, d), and sample 3 (bottom; e, f). Film thickness ca. 35 nm; annealed 12h at 100 °C.

With AFM and TEM in hand, the next goal is to establish the degree of long range ordering within the microphase separated domains using SAXS, which can be a powerful tool in determining the microphase morphology of a block copolymers. First, there are several factors to consider for analysis of the scattering peaks. The low angle peak, q^*, provides information about the domain spacing ($d = 2\pi/q^*$). The

vector ratios for the Bragg peaks (that is, the subsequent peaks, q_n, divided by the low scattering angle peak) may provide details about a particular type of lattice (simple cubic, body centered cubic, one-dimensional etc.) allowing for direct correlation to different block copolymer phase morphologies (cylinders, spheres, lamellar etc.). Further, the peak broadness may elucidate information about the degree of long range ordering within a unit cell for a given morphology. However, it is possible that the Bragg peaks could be absent altogether if they coincide with a form factor minima as a result of irregularities in the size and shape the domains.[11] This latter scenario is the most likely case observed for the ABA triblock copolymers presented in this work. In an effort to understand the relationship between morphology and mechanical properties, SAXS was carried out at 25 °C using similar 'as prepared' compressed films that were employed during tensile testing, *vide infara*. The low angle peak present for sample 1 has an average *d*-spacing of 58 nm. Samples 2 and 3 have an average domain spacing of 51 nm but subsequent Bragg peaks predicted for cases of well-defined microphase separated morphologies with long range order are absent. Specifically, sample 1 consists of only a low intensity broad peak at a q_n of 0.30 nm^{-1}. Similarly, sample 2 also has a low intensity broad peak at a q_n of 0.32 nm^{-1} albeit with inclusion of a slight shoulder just after the low angle peak (0.20 nm^{-1}). Lastly, scattering for sample 3 suggests a broad shoulder at q_n equal to 0.34 nm^{-1}, Figure 6.10. Upon evaluating the AFM, TEM and SAXS measurements collectively it is reasonable to conclude that, while phase separation persists for all samples, each morphology is unique. Sample 1 indeed displays a complex morphology with a low

degree of ordering. Sample 2 has disordered spherical morphology, and sample 3 has cylindrical type microphase separation.

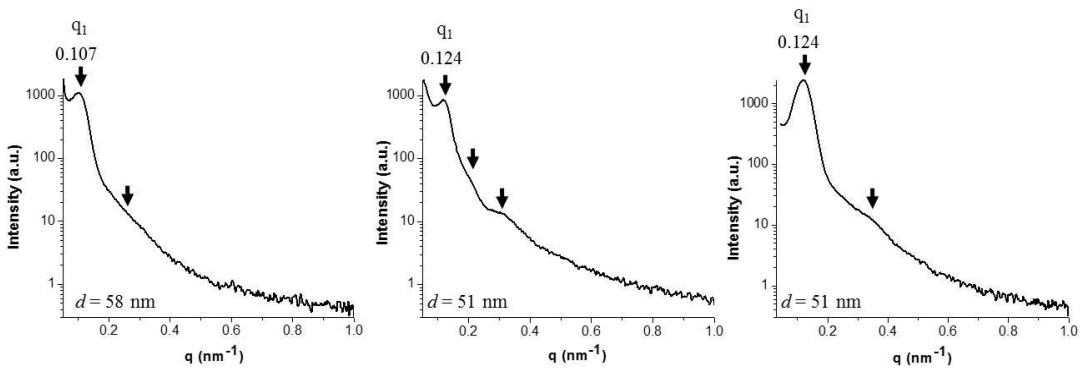

Figure 6.10: SAXS measurements from samples: 1 (left), 2 (middle), and 3 (right).

It has been shown that TPE materials exhibiting spherical morphology have better elastomeric properties compared to other domain orientations. The reason for this stems from the confined A segments within the 3D polymer network; the more secluded the aggregated A segments the stronger the crosslink. Therefore, it can be predicted that the elastomeric properties and recovery will be highest for sample 2, followed by higher strength yet lower elasticity for sample 1 as well as sample 3.

With the PMCH-*b*-*a*PP-*b*-PMCH triblock copolymer samples fully characterized, efforts were next directed toward testing the mechanical properties of the freshly assembled pure PO-TPE materials. To this end, the specimens were melt-compressed at 5 k psi at 105 °C for 45 minutes followed by slow cooling. The pressed films were further cut into dumbbell shapes with a dye-press (average testing regions measured: 10.3 x 3.5 x 0.5 mm^3; L x W x Thickness). The as prepared thin films were

then loaded into a 3345 tensile tester and elongated at a rate of 2 in/min until break, Figure 6.11.

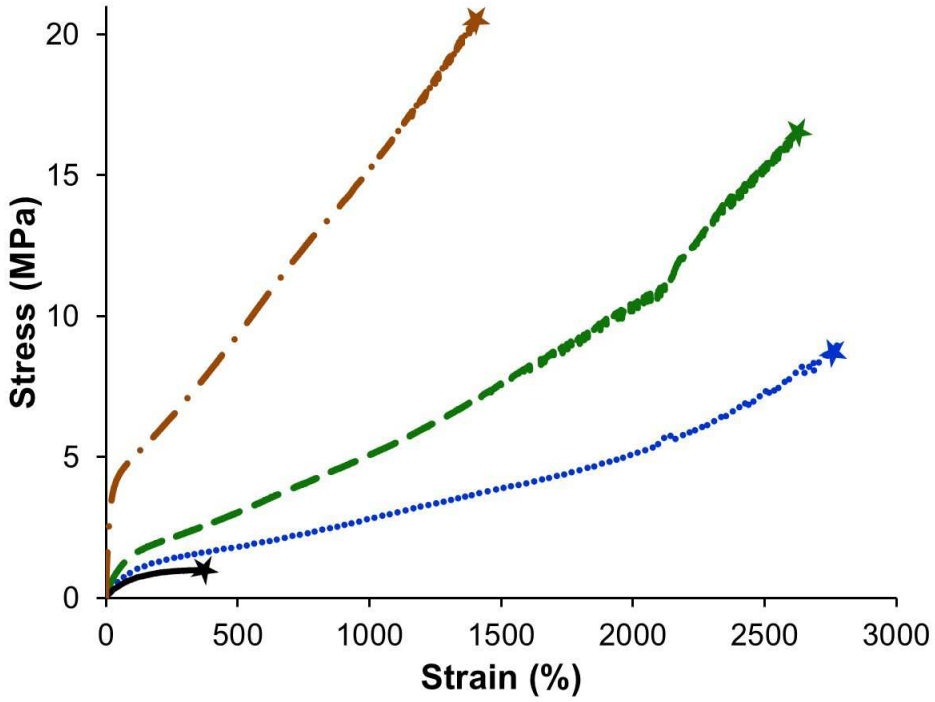

Figure 6.11: Plot of Stress v. Strain for triblock copolymer samples: 1 (green, dashed line), 2 (blue, dotted line), 3 (brown, dash-dotted line), and *a*PP (black line).

Cycling tests were also carried out and consisted of 10 elongation cycles with extensions up to 300 % strain, Figure 6.12. Sample 1, with an M_w of 175 kDa and a PMCH content of 17 % exhibits an elongation at break stress of 16.4 MPa with a strain at break reaching 2631 %. Recovery after cycling at 300 % elongation was measured to be 93 ± 1 %. Sample 2, with an M_w of 342 kDa and PMCH content 9.3 %, has a lower tensile stress (8.9 MPa) compared to sample 1, yet has a similar strain at break (2773 %). The lower stress limit for sample 2 is attributed to a higher *a*PP M_w and overall lower PMCH content. The recovery of sample 2 after cycling to

300 % elongation is 94 ± 1 %. Sample 3 has an average tensile stress of 20.3 MPa and a maximum elongation strain of 1390 % with a recovery of 72 ± 2 %, Table 6.2.

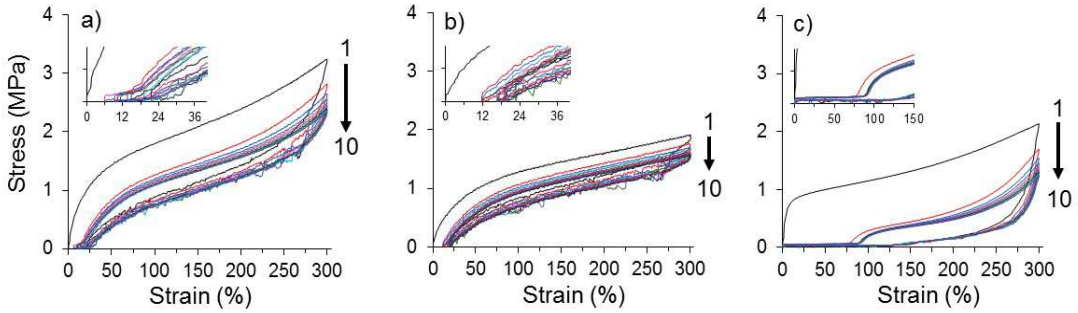

Figure 6.12: Plots reflecting cycling tests for triblock copolymers: a) sample 1, b) sample 2 and c) sample 3. Insets are expanded regions to show recovery with cycling.

Table 6.2: SEC, DSC and tensile data for triblock copolymer samples and aPP.

Sample	PMCH %	M_w (kDa)	Đ	T_g (°C)[b]	Stress (MPa)[c]	Strain %	Recovery %[d]
1	17	175	1.03	0.86	16.4	2631	93 ± 1
2	9.3	342	1.18	1.50	8.90	2773	94 ± 1
3	23	223	1.16	1.90	20.3	1390	72 ± 2
4	0	314	1.26	0.53	1.01	379	-

6.3. Conclusions

In summary, a pure polyolefin PMCH-*b*-*a*PP-*b*-PMCH triblock copolymer has been successfully synthesized, for the first time, through the use of living coordination polymerization of **2** activated by **II**. The resulting materials exhibit superior performance for use as a TPE when compared to *a*PP homopolymer.

Specifically, the addition of PMCH end blocks to *a*PP results in observed tensile strengths of nearly 20 times higher compared to *a*PP homopolymers of similar M_w. Furthermore, the observed tensile strain increases from ca. 379 % elongation at break for *a*PP to as high as 2773 % (sample 2), a nearly 8-fold increase. The overall recovery after 10 cycles with 300 % elongation is excellent with ranges between 72 ± 2 % and 94 ± 1 %. The M_w for triblock copolymer samples range from 175 kDa to 342 kDa with PMCH contents of 9.3 % to 23 %. Each of the PMCH-*b*-*a*PP-*b*-PMCH triblock copolymers readily undergo cylindrical type microphase separation with varying degrees of long rang order. Moreover, this newly established class of PO-TPE provides the foundation for an array of materials properties, which can be finely tuned based on the application of interest. Instrument parameters and materials information are provided in Appendices A and B.

6.4. Experimentals

6.4.1. General Synthesis for PMCH-*b*-aPP-*b*-PMCH Triblock Copolymers

The polymerizations were carried out under an inert atmosphere of N_2 using a Vacuum Atmospheres glovebox. The general polymerization method for the formation of triblock copolymer was as follows: $[PhNMe_2H][B(C_6F_5)_4]$ (**II**), (1.1 equiv.) was mixed with 30 μmol initiator **2** in ca. 0.5 mL cold PhCl. The resulting bright yellow mixture of **2** with **II** was then added to 50 mL cold (ca. -15 °C) toluene in a 250 mL Schlenk reaction vessel equipped with a magnetic stir bar. 1,6-heptadiene (100 equiv.) was then added to the reaction mixture and allowed to stir between 4.5-5 hours at ca. -15 °C. Following completion of the first PMCH block the

reaction vessel was charge with 5 psi propene for a given amount of time, usually between 20 min – 1 hr. The remaining propene was removed *in vacuo* prior to the start of the third block wherein 1,6-hepaiene (100 equiv.) was added and allowed to polymerize for a given amount of time (>5 h). Small aliquots (< 1/5th mL) were removed after the completion of each block for SEC analysis. The reaction was quenched with a large aliquot of acidic methanol (10% HCl by volume) prior to precipitation in copious methanol. The resulting polymer was vacuum filtered, collected in a pre-weighed vial and dried under vacuum until constant weight. Dried polymer was further purified by dissolving in toluene and passing through a column of alumina. The samples were re-collected and dried for characterization.

6.5. References

1. Drobny, J. G., *Handbook of Thermoplastic Elastomers*. William Andrew Publications: New York, NY, 2007; p 1-8.

2. a) Alfonzo, C. G.; Fleury, G.; Chaffin, K. A.; Bates, F. S., *Macromolecules* **2010**, *43* (12), 5295-5305.; b) Harada, T.; Bates, F. S.; Lodge, T. P., *Macromolecules* **2003**, *36* (15), 5440-5442.; c) Koo, C. M.; Wu, L.; Lim, L. S.; Mahanthappa, M. K.; Hillmyer, M. A.; Bates, F. S., *Macromolecules* **2005**, *38* (14), 6090-6098.; d) Lee, I.; Panthani, T. R.; Bates, F. S., *Macromolecules* **2013**, *46* (18), 7387-7398.; e) Lim, L. S.; Harada, T.; Hillmyer, M. A.; Bates, F. S., *Macromolecules* **2004**, *37* (16), 5847-5850.; f) Mansour, A. S.; Lodge, T. P.; Bates, F. S., *J. Polym. Sci., Part B: Polym. Phys.* **2012**, *50* (10), 706-717.; g) Phatak, A.; Lim, L. S.; Reaves, C. K.; Bates, F. S., *Macromolecules* **2006**, *39* (18), 6221-6228.

3. Mori, Y.; Lim, L. S.; Bates, F. S., *Macromolecules* **2003**, *36* (26), 9879-9888.

4. a) Bishop, J. P.; Register, R. A., *Macromolecules* **2010**, *43* (11), 4954-4960.; b) Hatjopoulos, J. D.; Register, R. A., *Macromolecules* **2005**, *38* (24), 10320-10322.; c) Lee, H. H.; Register, R. A.; Hajduk, D.; Gruner, S. M., *Polym. Eng. Sci.* **1996**, *36* (10), 1414-1424.; c) Loo, Y.-L.; Register, R. A.; Ryan, A. J., *Phys. Rev. Lett.* **2000**, *84* (18), 4120-4123.; d) Myers, S. B.; Register, R. A., *Macromolecules* **2009**, *42* (17), 6665-6670.; e) Sebastian, J. M.; Graessley, W. W.; Register, R. A., *J. Rheol.* **2002**, *46* (4), 863-879.

5. a) Natta, G., *J. Polym. Sci.* **1959**, *34* (127), 531-549.; b) Auriemma, F.; De Rosa, C.; Corradi, M., *Adv. Mater.* **2007**, *19* (6), 871-874.; c) Babkina, O. N.; Bravaya, N. M.; Nedorezova, P. M.; Saratovskikh, S. L.; Tsvetkova, V. I., *Kinet. Catal.* **2002**, *43* (3), 341-350.; d) Bruce, M. D.; Waymouth, R. M., *Macromolecules* **1998**, *31* (9), 2707-2715.; e) Busico, V.; Cipullo, R.; Corradini, P.; De Biasio, R., *Macromol. Chem. Phys.* **1995**, *196* (2), 491-498.; f) Cai, Z.; Nakayama, Y.; Shiono, T., *Kinet. Catal.* **2006**, *47* (2), 274-277.; g) Coates, G. W.; Mogstad, A. L.; Hauptman, E.; Bruce, M. D.; Waymouth, R. M., *Polym. Prepr. (Am. Chem. Soc., Div. Polym. Chem.)* **1995**, *36* (1), 545.; h) Coates, G. W.; Waymouth, R. M., *Science* **1995**, *267* (5195), 217-219.; i) Alfano, F.; Boone, H. W.; Busico, V.; Cipullo, R.; Stevens, J. C., *Macromolecules* **2007**, *40* (22), 7736-7738.; j) Giller, C.; Gururajan, G.; Wei, J.; Zhang, W.; Hwang, W.; Chase, D. B.; Rabolt, J. F.; Sita, L. R., *Macromolecules* **2011**, *44* (3), 471-482.; k) Harney, M. B.; Zhang, Y.; Sita, L. R., *Angew. Chem., Int. Ed.* **2006**, *45* (15), 2400-2404.; l) Lieber, S.; Brintzinger, H.-H., *Macromolecules* **2000**, *33* (25), 9192-9199.; m) Waymouth, R. M.; Hauptman, E.; Coates, G. W.

stereoblock α-olefin polymer thermoplastic elastomers, metallocene catalysts, and use of the latter to prepare the former. WO9525757A1, 1995.

6. a) Arriola, D.; Carnahan, E.; Hustad, P.; Kuhlman, R.; Wenzel, T., *Science* **2006**, *312* (5774), 714-719.; b) Jiang, G.; Wu, H.; Guo, S., *J. Macromol. Sci., Part B: Phys.* **2007**, *46* (3), 533-545.

7. Coates, G. W., *Chem. Rev.* **2000**, *100* (4), 1223-1252.

8. Crawford, K. E.; Sita, L. R., *J. Am. Chem. Soc.* **2013**, *135* (24), 8778-8781.

9. a) Zhang, W.; Sita, L. R., *J. Am. Chem. Soc.* **2008**, *130* (2), 442-443.; b) Zhang, W.; Wei, J.; Sita, L. R., *Macromolecules* **2008**, *41* (21), 7829-7833.; c) Sita, L. R., *Angew. Chem., Int. Ed.* **2009**, *48* (14), 2464-2472.; d) Wei, J.; Zhang, W.; Sita, L. R., *Angew. Chem., Int. Ed.* **2010**, *49* (10), 1768-1772.; e) Wei, J.; Zhang, W.; Wickham, R.; Sita, L. R., *Angew. Chem., Int. Ed.* **2010**, *49* (48), 9140-9144.

10. Hamley, I. W., *The Physics of Block Copolymers*. Oxford University Press: Oxford, NY, 1998; p 424.

11. a) Bates, F. S.; Fredrickson, G. H., *Annu. Rev. Phys. Chem.* **1990**, *41*, 525-557.; b) Warren, B. E., *X-Ray Diffraction*. Addison-Wesley, Inc.: Reading, MA, 1969; p 381; Martin, W. J., *Concise Encyclopedia of the Structure of Materials*. 1st ed.; Elsevier Science: Kidlington, Oxford, UK, 2007; p 512.

Appendix A: Instrumental Details

Atomic Force Microscopy (AFM): Phase-images were obtained using a Nanoscope IIIa Multimode AFM in tapping mode (ps-tm-AFM) equipped with silicon etched tip (Nanosensors: spring constant = 25-55 N/m, resonance frequency = 292 – 377 kHz) used in conjunction with Extender Electronics package (Veeco Inc., CA). Thin films of the triblock copolymers were spun cast from 1.5 wt % (in toluene) solutions onto a cleaned silicon surfaces (7:3 H_2SO_4: HNO_3 – Piranha solution: CAUTION!; wafers were rinsed with 18 mΩ deionized water and dried under dinitrogen). Film thicknesses were obtained both before and after annealing using a Gaertner optical ellipsometer.

Differential scanning calorimetry (DSC): Thermal analysis was carried out using a TA Instruments Q800 DSC. Samples were Run in sealed hermetic pans under a continuous flow of N_2 with an average sample weight of ca. 9 mg; each sample was Run alongside an empty pan for reference. General temperature program: 10 °C/min from -50 °C to 250 °C. Only the second heating/cooling cycles were used for measurement of T_g.

Nuclear Magnetic Resonance (NMR): NMR spectroscopy was carried out using one of three instruments. 1) A Bruker AVIII-800 MHz Varian spectrometer with fitted cryo-probe and Z gradient. $^{13}C\{^1H\}$ NMR spectra were obtained using the following parameters: 200 MHz; 45° pulse angle; without NOE; 2 K transients;

110 °C. 2) A Bruker AVIII-600 MHz Varian spectrometer fitted with a dual probe with Z gradient. $^{13}C\{^{1}H\}$ NMR spectra were obtained using the following parameters: 45° pulse angle; without NOE; relaxation delay 1.0 s; >9 K transients. 3) A Bruker DRX-500 MHz high resolution spectrometer. ^{29}Si spectra were obtained using the following parameters: 100 MHz; 1 K transients; 90 °C. Typical sample preparation: ca. 50 mg/mL polymer solutions calibrated to 1,1,2,2-tetrachloroethane-d_2 (TCE-d_2) or tetramethyl silane-d_{12} (TMS-d_{12}).

Size Exclusion Chromatography (SEC): Both room- and high-temperature SEC measurements were carried out on final products. For room temperature analysis, molecular weights (M_w, M_n) and polydisperisty ($Đ$) were obtained using a Malvern GPCMax equipped with 3 columns (Shodex HT-803 (x2) and HT-804) in a column oven and a differential refractometer, both maintained at 40 °C. HPLC Grade tetrahydrofuran (THF) was used as eluent with a flow rate of 1 mL/min (Sigma Aldrich). Typical sample preparation: 4 mg sample dissolved in 1.5 mL xylenes, followed by filtration through 0.2 μm Nylon filter. For high temperature analysis, molecular weights (M_w, M_n) and polydisperisty ($Đ$) were obtained using a Viscotek HT-GPC Module 350A with 3 columns (Tosoh TSKgel GMHhr-H(S) mixed bed) in a column oven maintained at 140 °C. Chromasolv® 1,2,4-trichlorobenzene (TCB) (Sigma Aldrich) was used as eluent with a flow rate of 1 mL/min. Calibration for both instruments was carried out using polystyrene standards (obtained from (1) Polymer Laboratories Inc., 580 Da – 3,150 KDa (2) Viscotek for PS standard with narrow, and broad $Đ$).

Rheology. The storage and loss moduli were followed as a function of temperature, frequency and strain using an RDA1000 and an AR2000 TA Instruments rheometer with standard 8 mm geometry. Temperatures ranged from 25 °C – 200 °C with a frequency of 0.1 Hz, strain values were selected within the linear viscoelastic region.

Small Angle X-ray Scattering (SAXS): Diffraction data was collected using a Xeuss SAXS system equipped with heating stage. Samples were prepared using stainless steel sample holders with sample diameter and height 3.9 mm and 1.0 mm respectively. Samples were protected using standard Kapton polyimide film secured with epoxy resin.

Tensile Testing: Mechanical measurements, elongation until break and cycling tests, were carried out on an Instron 3345 tensile tester. Samples were prepared by compression molding (heated to 100 °C for ca. 30 minutes at 5 k psi). The as prepared thin-films were cut into dumb-bell patterns using an ASTM certified cutter. Elongation until break experiments were carried out at an elongation rate of 2 in/min. Cycling tests were also carried out at a rate of 2 in/min with repeated elongations (10 cycles) to 300 % strain. Recovery was measured as a ratio between the 2^{nd} and 1^{st} cycles (there was little variation when the ratio of cycles 3-10 were compared with cycle 1). Due to limited sample size, measurements could be carried out at most twice.

Thermal Gravimetric Analysis (TGA): Measurements were carried out using a TA Instruments TGA Q500 system. ~2 mg samples were run under N_2 from 25 °C to 700 °C at a rate of 10 °C /min.

Transmission Electron Microscopy (TEM): Images were obtained in the NISP-lab (Nanoscale Imaging, Spectroscopy, and Properties Laboratory) using a JEM-2100 LaB6 TEM. Typical sample preparation is described as follows: thin films (ca. 30-35 nm) were spun cast on smooth mica surfaces. Polymer films were then floated on deionized water for capture with carbon coated copper TEM grids (400 mesh). Samples were annealed at 100 °C x 12 h prior to TEM analysis.

Wide Angle X-ray Diffraction (WAXD): WAXD analysis was carried out using a Bruker D8 Advanced system defractometer with LynxEye detector; source wavelength: Cu Kα = 1.54 Å; scan angle: 5 – 60° with scan step = 0.05°. WAXD analysis was carried out under ambient conditions.

Appendix B: Materials

Catalysts: The precatalysts **1** and **2** were generously provided by Precision Polyolefins LLC. Namely, {(Cp*)Zr[N(Et)C(Me)N(t-butyl)(Me_2)]} (**1**), {(Cp*)Hf[N(Et)C(Me)N(Et)(Me_2)]} (**2**). Precatalyst **3** was synthesized by previous group member Jia Wei in a similar one pot synthesis described in Chapter 1. The borate salt, [$PhNMe_2H$][$B(C_6F_5)_4$], (**II**) was purchased and used as received from Boulder Scientific.

Solvents: Two primary solvents were used in this research, toluene and chlorobenzene (PhCl). Both solvent types were purchased from Sigma Aldrich and dried/deoxygenated and collected from a two column Pure-Solv solvent system (column 1: activated alumina; column 2: gettermax-135 copper catalyst) prior to use.

Monomer: 1,6-Heptadiene was purchased from TCI America. 1-hexene, 1,5-hexadiene and 1,7-octadiene were purchased from Sigma Aldrich. Diallylsilanes were either synthesized in house *via* Grignard reactions, purchased from Sigma Aldrich or Gelest. All monomers were further purified prior to use by stirring over NaK amalgam under N_2, followed by a series of freeze-pump-thaw degassing cycles prior to collecting *via* vacuum transfer. Propene was purchased from Matheson Trigas and purified by passing through activated copper catalyst (GetterMax 135) and molecular sieves (size: 4 Å) prior to use.